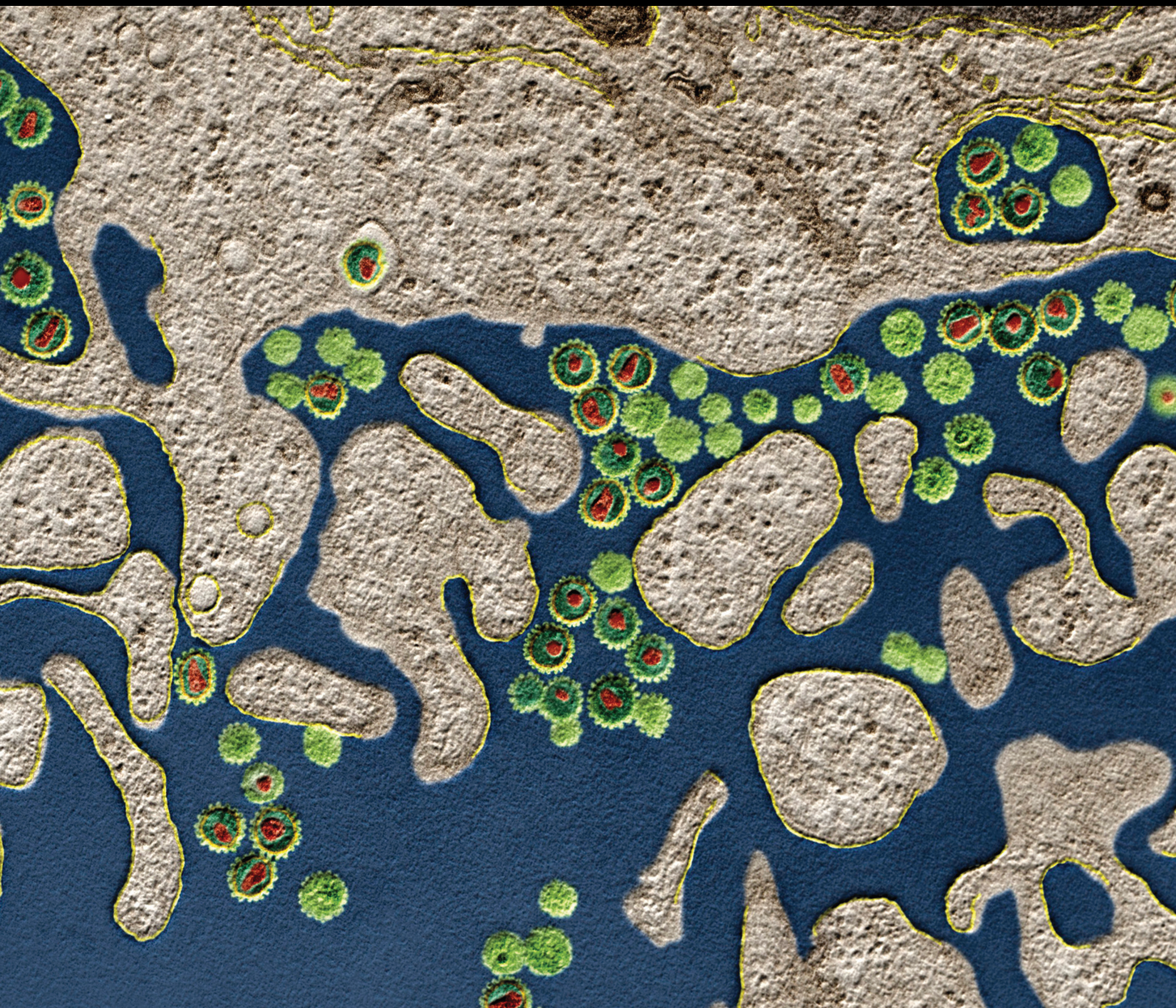


Extracellular Matrix and Immune Niches in Human Disease

Lead Guest Editor: Jian Song

Guest Editors: Christopher J. Pirozzi, Zenghui Teng, and Weidong Cao





Extracellular Matrix and Immune Niches in Human Disease

Journal of Immunology Research

**Extracellular Matrix and Immune
Niches in Human Disease**

Lead Guest Editor: Jian Song





Guest Editors: Christopher J. Pirozzi, Zenghui Teng,
and Weidong Cao



Copyright © 2021 Hindawi Limited. All rights reserved.

This is a special issue published in "Journal of Immunology Research." All articles are open access articles distributed under the Creative Commons Attribution License, which permits unrestricted use, distribution, and reproduction in any medium, provided the original work is properly cited.

Associate Editors

Douglas C. Hooper , USA
Senthamil R. Selvan , USA
Jacek Tabarkiewicz , Poland
Baohui Xu , USA

Academic Editors




Nitin Amdare , USA
Lalit Batra , USA
Kurt Blaser, Switzerland
Dimitrios P. Bogdanos , Greece
Srinivasa Reddy Bonam, USA
Carlo Cavaliere , Italy
Cinzia Ciccacci , Italy
Robert B. Clark, USA
Marco De Vincentiis , Italy
M. Victoria Delpino , Argentina
Roberta Antonia Diotti , Italy
Lihua Duan , China
Nejat K. Egilmez, USA
Theodoros Eleftheriadis , Greece
Eyad Elkord , United Kingdom
Weirong Fang, China
Elizabeth Soares Fernandes , Brazil
Steven E. Finkelstein, USA
JING GUO , USA
Luca Gattinoni , USA
Alvaro González , Spain
Manish Goyal , USA
Qingdong Guan , Canada
Theresa Hautz , Austria
Weicheng Hu , China
Giannicola Iannella , Italy
Juraj Ivanyi , United Kingdom
Ravirajsinh Jadeja , USA
Peirong Jiao , China
Youmin Kang , China
Sung Hwan Ki , Republic of Korea
Bogdan Kolarz , Poland
Vijay Kumar, USA
Esther Maria Lafuente , Spain
Natalie Lister, Australia

Daniele Maria-Ferreira, Saint Vincent and the Grenadines

Eiji Matsuura, Japan
Juliana Melgaço , Brazil
Cinzia Milito , Italy
Prasenjit Mitra , India
Chikao Morimoto, Japan
Paulina Niedźwiedzka-Rystwej , Poland
Enrique Ortega , Mexico
Felipe Passero, Brazil
Anup Singh Pathania , USA
Keshav Raj Paudel, Australia
Patrice Xavier Petit , France
Luis Alberto Ponce-Soto , Peru
Massimo Ralli , Italy
Pedro A. Reche , Spain
Eirini Rigopoulou , Greece
Ilaria Roato , Italy
Suyasha Roy , India
Francesca Santilli, Italy
Takami Sato , USA
Rahul Shivahare , USA
Arif Siddiqui , Saudi Arabia
Amar Singh, USA
Benoit Stijlemans , Belgium
Hiroshi Tanaka , Japan
Bufu Tang , China
Samanta Taurone, Italy
Mizue Terai, USA
Ban-Hock Toh, Australia
Shariq M. Usmani , USA
Ran Wang , China
Shengjun Wang , China
Paulina Wlasiuk, Poland
Zhipeng Xu , China
Xiao-Feng Yang , USA
Dunfang Zhang , China
Qiang Zhang, USA
Qianxia Zhang , USA
Bin Zhao , China
Jixin Zhong , USA
Lele Zhu , China

















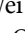



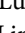

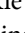








Contents

Role of Matrix Metalloproteinases in Angiogenesis and Its Implications in Asthma

Khuloud Bajbouj , Rakhee K. Ramakrishnan , and Qutayba Hamid 

Review Article (12 pages), Article ID 6645072, Volume 2021 (2021)

Genes Induced by Panax Notoginseng in a Rodent Model of Ischemia-Reperfusion Injury

Lanqing Meng , Qing Huang , Xuebin Li , Ping Liang, Yueyong Li , Xiaohua Huang , Jingjie Zhao , Qiuping Chen , Rong Qiu , Lan Li , Chongdong Jian , Hongfei Yao, Jianmin Huang , Xionglin Tang , Zechen Wang , Zhongheng Wei , Jun Wu , Liuzhi Wei , Qiuju Wei , Qianli Tang , Lu Huang , Jihua Wei , Dinggui Lu , Qunqiang Luo , Kegong Xie , Yang Ouyang , Jian Chen , Genliang Li , Linxue Luo , Linbo He , Chenyi Zhuo , Anding Xu , and Lingzhang Meng 


Research Article (13 pages), Article ID 8873261, Volume 2020 (2020)

Effect of SIS3 on Extracellular Matrix Remodeling and Repair in a Lipopolysaccharide-Induced ARDS Rat Model

Qiong Liang, Qiqing Lin, Yueyong Li, Weigui Luo, Xia Huang, Yujie Jiang, Chunyan Qin, Jin Nong, Xiang Chen, Suren Rao Sooranna, and Liao Pinhu 

Research Article (13 pages), Article ID 6644687, Volume 2020 (2020)

The SIRT3 and SIRT6 Promote Prostate Cancer Progression by Inhibiting Necroptosis-Mediated Innate Immune Response

Weiwei Fu, Hong Li, Haiyang Fu, Shuchao Zhao, Weiping Shi, Mengqi Sun, and Yujun Li 



Research Article (12 pages), Article ID 8820355, Volume 2020 (2020)

Negative Effects of SIGIRR on TRAF6 Ubiquitination in Acute Lung Injury In Vitro

Feng Tian, Qiang Lu, Jie Lei, Yunfeng Ni, Nianlin Xie, Daixing Zhong, Guang Yang, Shaokui Si, and Tao Jiang 



Research Article (9 pages), Article ID 5097920, Volume 2020 (2020)

STK3 Suppresses Ovarian Cancer Progression by Activating NF- κ B Signaling to Recruit CD8⁺ T-Cells

Xiangyu Wang , Fengmian Wang, Zhi-Gang Zhang , Xiao-Mei Yang , and Rong Zhang 


Research Article (17 pages), Article ID 7263602, Volume 2020 (2020)

Effects of miR-373 Inhibition on Glioblastoma Growth by Reducing Limk1 *In Vitro*

Tao Peng, Tiejun Wang, Guohui Liu , and Lixiang Zhou 

Research Article (9 pages), Article ID 7671502, Volume 2020 (2020)

Profiling the Resident and Infiltrating Monocyte/Macrophages during Rejection following Kidney Transplantation

Jie Wang, Peiling Luo, Jingjie Zhao, Junhua Tan, Feifan Huang, Ruiying Ma, Peng Huang, Meiyong Huang, Yuming Huang, Qiuju Wei, Liuzhi Wei, Zechen Wang, and Lingzhang Meng 




Research Article (14 pages), Article ID 5746832, Volume 2020 (2020)

Immune and Inflammation in Acute Coronary Syndrome: Molecular Mechanisms and Therapeutic Implications

Haiming Wang, Zifan Liu, Junjie Shao, Lejian Lin, Min Jiang, Lin Wang, Xuechun Lu, Haomin Zhang, Yundai Chen , and Ran Zhang 




Review Article (11 pages), Article ID 4904217, Volume 2020 (2020)

MPC1 Deficiency Promotes CRC Liver Metastasis via Facilitating Nuclear Translocation of β -Catenin

Guang-Ang Tian, Chun-Jie Xu, Kai-Xia Zhou, Zhi-Gang Zhang , Jian-Ren Gu, Xue-Li Zhang , and Ya-Hui Wang 









Research Article (11 pages), Article ID 8340329, Volume 2020 (2020)

Single-Cell Transcriptome Analysis Profile of Meniscal Tissue Macrophages in Human Osteoarthritis

Jingbin Zhou , Zhihong Zhao , Chen He, Feng Gao, Yu Guo, Feng Qu, and Yujie Liu 

Research Article (16 pages), Article ID 8127281, Volume 2020 (2020)

miR-24-3p/KLF8 Signaling Axis Contributes to LUAD Metastasis by Regulating EMT

Pengyu Jing , Nianlin Xie , Nan Zhao , Ximing Zhu , Pei Li , Guizhou Gao , Haizhou Dang , and Zhongping Gu 

Research Article (8 pages), Article ID 4036047, Volume 2020 (2020)

Assessing the Changes of Mumps Characteristics with Different Vaccination Strategies Using Surveillance Data: Importance to Introduce the 2-Dose Schedule in Quzhou of China

Chunting Zhou, Wei Song , Zhiying Yin , Sheng Li , Xiaoying Gong, Qunjun Fang, and Shuangqing Wang

Research Article (7 pages), Article ID 8130760, Volume 2020 (2020)

Review Article

Role of Matrix Metalloproteinases in Angiogenesis and Its Implications in Asthma

Khuloud Bajbouj ^{1,2} **Rakhee K. Ramakrishnan** ² and **Qutayba Hamid** ^{1,2,3}

¹College of Medicine, University of Sharjah, Sharjah, UAE

²Sharjah Institute for Medical Research, University of Sharjah, Sharjah, UAE

³Meakins-Christie Laboratories, McGill University, Montreal, QC, Canada

Correspondence should be addressed to Khuloud Bajbouj; kbajbouj@sharjah.ac.ae and Qutayba Hamid; qalheialy@sharjah.ac.ae

Received 11 October 2020; Revised 21 January 2021; Accepted 25 January 2021; Published 13 February 2021

Academic Editor: Christopher J. Pirozzi

Copyright © 2021 Khuloud Bajbouj et al. This is an open access article distributed under the Creative Commons Attribution License, which permits unrestricted use, distribution, and reproduction in any medium, provided the original work is properly cited.

Asthma is a chronic airway disorder associated with aberrant inflammatory and remodeling responses. Angiogenesis and associated vascular remodeling are one of the pathological hallmarks of asthma. The mechanisms underlying angiogenesis in asthmatic airways and its clinical relevance represent a relatively nascent field in asthma when compared to other airway remodeling features. Matrix metalloproteinases (MMPs) are proteases that play an important role in both physiological and pathological conditions. In addition to facilitating extracellular matrix turnover, these proteolytic enzymes cleave bioactive molecules, thereby regulating cell signaling. MMPs have been implicated in the pathogenesis of asthma by interacting with both the airway inflammatory cells and the resident structural cells. MMPs also cover a broad range of angiogenic functions, from the degradation of the vascular basement membrane and extracellular matrix remodeling to the release of a variety of angiogenic mediators and growth factors. This review focuses on the contribution of MMPs and the regulatory role exerted by them in angiogenesis and vascular remodeling in asthma as well as addresses their potential as therapeutic targets in ameliorating angiogenesis in asthma.

1. Introduction

Asthma is a highly heterogeneous chronic respiratory disease characterized by inflammation, hyperresponsiveness, and remodeling of the airways. Frequent asthma exacerbations triggered mainly by allergen exposure or viral or bacterial infections are primarily caused by chronic inflammatory processes that progress to a series of structural changes to the bronchial wall, including the resident airway epithelium, basal membrane, fibroblasts, smooth muscles, and blood vessels.

Angiogenesis is characterized by the emergence of new blood vessels from preexisting endothelial lined vessels. It is a normal physiological process that plays an important role in development and wound healing. At the same time, it is also a fundamental process in the pathogenesis of various diseases, such as cancer, obesity, rheumatoid arthritis, psoriasis, cardiovascular diseases, and asthma. Proteolysis being a

key regulator of angiogenesis, proteases such as matrix metalloproteinases (MMPs), the closely related family of a disintegrin and metalloprotease (ADAM) domain proteins, which includes ADAM and ADAMTS (a disintegrin and metalloprotease domain with thrombospondin motifs), as well as cysteine and serine proteases, have been implicated in regulating the angiogenic process.

The various proteolytic enzymes within the MMP family share a similarity in their structures and collectively are capable of breaking down the various known extracellular matrix (ECM) proteins. The growing family of MMPs comprise of members including collagenases, gelatinases, stromelysins, membrane-type MMPs (MT-MMPs), matrilysins, and various other MMPs. Depending on the presence of a transmembrane domain, the MMPs are broadly classified into two—MT-MMPs and secreted MMPs. As part of the homeostatic mechanism, the activated MMPs are deterred by a group of endogenous inhibitors called tissue inhibitors of

metalloproteases (TIMPs). Four members of this family, namely, TIMP-1, TIMP-2, TIMP-3, and TIMP-4, have been identified till date.

This review discusses the current understanding of MMPs and their role in the development of angiogenesis in asthma. Furthermore, we summarize the therapeutic modalities currently under investigation to target MMPs and their implications in improving angiogenesis and vascular remodeling in asthma.

2. Tissue Remodeling in Asthma

Tissue remodeling refers to modifications associated with the normal composition and structural organization of tissues. This can occur in a wide range of tissues and organs, including the airways, lung [1], blood vessels [2], heart [3], and gastrointestinal tract [4, 5]. Airway remodeling is a characteristic feature in patients with pulmonary disorders, such as asthma, chronic obstructive pulmonary disease (COPD), and cystic fibrosis. This event is mainly driven by inflammatory mediators that bring about cellular and structural changes resulting in thickening of the airway wall, thereby leading to airway narrowing and airflow limitation. Airway remodeling in asthmatic patients involves a wide array of pathophysiologic features, including epithelial changes, subepithelial fibrosis, increased smooth muscle mass, and vascular changes, primarily around the large airways. These structural modifications thus affect all cellular layers of the bronchial wall, from airway epithelium, basement membrane, subepithelial fibroblasts, smooth muscles, and cartilage to blood vessels lining the airway wall. Whereas remodeling in patients with COPD involves structural changes mainly to the small airways, remodeling in patients with cystic fibrosis is characterized by fibrotic, glandular, muscular, and vascular changes throughout the lung.

Structural changes in the airway walls are predominantly detected in the more severe forms of asthma, where they are characterized by ECM remodeling, epithelial desquamation, goblet cell hyperplasia, prominent smooth muscle area, vascular remodeling, collagen deposition below the basement membrane, loss of cartilage integrity, and elastolysis [1]. The clinical consequences of remodeling are severe thickening of the airway walls leading to bronchial obstruction during an asthma attack [6]. Some of the earliest structural remodeling changes are observed in the basement membrane, where excessive ECM deposition leads to its thickening and reduction in elasticity. Airway smooth muscle (ASM) cell hyperplasia and hypertrophy are also demonstrated within the smooth muscle layer. Additionally, the mucosal glands are enlarged and associated with excessive mucus production. The continuing inflammation is further linked with the persistence of exacerbations and nonspecific airway hyperresponsiveness (AHR). Besides, the degradation of elastin and cartilage may result in decreased airway wall stiffness and increased airway narrowing. In asthma, remodeling is usually detected in biopsy specimens but is not always clinically demonstrated [7]. Nevertheless, structural remodeling of the bronchial tree paves way for increased AHR and progressively more severity in the course of the disease.

3. Angiogenesis in Asthma

The airways are supplied with blood vessels localized in the bronchial smooth muscle layer, as well as through the capillary network in lamina propria [8]. The bronchial blood vessels are known to undergo alterations in their density, dilation, and permeability under both physiological and pathological conditions. As early as 1960, increased vascularity has been reported in the bronchial mucosa in association with the pathology of asthma [9]. Since the mechanisms underlying angiogenesis in asthmatic airways and its clinical relevance represent a relatively nascent field in asthma when compared to other airway remodeling features, there is a growing interest among scientists in the fields of angiogenesis and neovascularization in asthmatic patients.

Angiogenesis is a process of new blood vessel formation, and it involves several stages that are highly regulated. The early stage of angiogenesis occurs in a preexisting blood vessel localized in close proximity to the inflammatory process. This stage involves increased blood vessel permeability, endothelial cell activation by growth factors, and increased endothelial mitosis. The ensuing second stage involves the degradation of the endothelial basement membrane by matrix metalloproteinases. This is followed by the migration of endothelial cells towards the different angiogenic factors and the establishment of branch points and capillary lumen. The final stage comprises of modeling and stabilization of the new capillary vessel. In the last leg, the endothelial cell junctions are tightened, the basement membrane is established, and the pericytes are recruited.

Several studies have suggested an abnormal increase in the number and size of microvessels within bronchial tissue in remodeled asthmatic airways [10–12]. These vascular changes were observed below the basal lamina in the space between the muscle layer and the surrounding parenchyma. The vascular bed in bronchial lamina propria of asthmatic subjects was significantly enriched with blood vessels than in nonasthmatic subjects [13]. The vasculature also showed marked structural alterations in terms of edematous walls and subendothelial basement membrane thickening. Besides intense eosinophil recruitment and intravascular activation, the intra-arteriolar muscular formations in asthmatics exhibited hypotrophic or atrophic myocytes and fibrosis. Bronchial mucosa microvascularization, in addition to being increased in asthmatic patients in comparison to control, was also found to correlate with the clinical stage of the disease and forced expiratory volume in one second (FEV1) values [13, 14]. Notably, severe asthmatic patients demonstrated a 46% increase in capillary vasculature in the bronchial submucosa when compared to controls [14].

Furthermore, the infiltrating eosinophils, basophils, and mast cells as well as the resident epithelial, endothelial, and ASM cells secrete various angiogenic factors, including hypoxia inducible factor (HIF), vascular endothelial growth factor (VEGF), and angiopoietins, which direct the development of angiogenesis in the submucosa. Airway obstruction and chronic inflammatory processes in asthmatic airways are known to cause the induction of a locally restricted hypoxic environment which further triggers the

initiation of angiogenesis [15]. Elevated HIF levels have been reported across both endobronchial biopsies and in the bronchoalveolar lavage (BAL) fluid of asthmatics [16, 17]. The increased HIF subunits (HIF-1 α and HIF-1 β) in lung tissues also further correlated with VEGF levels [17]. VEGF is known to inhibit the apoptosis of vascular endothelial cells. Elevated VEGF and cysteinyl leukotrienes (Cyst-LTs) levels were detected in asthmatic sputum supernatant when compared to normal subjects [18]. In this study, the authors suggest that Cyst-LTs modulate vascular permeability by stimulating VEGF expression. VEGF causes vessel dilation and edema by increasing the permeability of these abnormal blood vessels [19] resulting in airway thickening and subsequent narrowing. Thus, these vessels, in addition to providing nutrition to the airways, are the source of inflammatory cells and plasma-derived mediators and cytokines [10]. The imbalance in the levels of VEGF and angiopoietin-1 contributes to these vascular abnormalities in asthmatic airways [20]. Angiopoietins play a particularly important role in the final stage of angiogenesis where they stimulate the migration of pericytes and help stabilize the newly formed capillary tubes.

4. Matrix Metalloproteinases in Asthma

In the airways, the basement membrane supporting the surface epithelium is composed of several layers: the basal lamina and the lamina reticularis. In asthma, the basal lamina is of normal thickness, whereas the reticular layer is thickened leading to subepithelial fibrosis of the airways. Clinically, the thickening of the lamina reticularis is a characteristic early feature of the asthmatic bronchus. These features represent one of the most common remodeling patterns of asthma. The ECM produced by connective tissue cells forms a complex network filling the extracellular space of the submucosa. In addition to their role in supporting and maintaining the tissue structure, ECM influences many cellular functions such as development, migration, and proliferation [21]. Abnormal deposition of ECM elements has been described in the submucosal and adventitial areas of the large and small airways of asthmatic patients [22–25]. Although deposition of collagen IV and elastin appears to be decreased in the airway walls of asthmatic patients, collagens I, III, and V, fibronectin, tenascin, hyaluronan, versican, and laminin are increased compared with those seen in healthy subjects [26–30].

MMPs belong to a family of zinc-dependent endopeptidases that play key roles in both physiological processes, such as wound healing [31, 32], as well as in pathological conditions, including inflammation [33] and fibrosis [34]. MMPs are well known to degrade ECM and to regulate cell signaling through the cleavage and processing of bioactive molecules, including growth factors and cytokines. Multiple cell types secrete MMPs including both inflammatory cells, such as macrophages [35] and leukocytes [36, 37], and airway structural cells, such as airway epithelial cells [38, 39], fibroblasts [40, 41], and smooth muscle cells [42]. Several subclasses of MMPs have been identified, including collagenases, gelatinases, stromelysins, and membrane-type MMPs that can

degrade many ECM proteins including collagens, fibronectin, laminin, proteoglycans, entactins, and elastin. Normally, MMPs are secreted as inactive proenzymes, which are activated by the loss of the propeptide under physiologic conditions [21]. MMP expression and activity are tightly regulated by the action of endogenous inhibitors of MMPs, referred to as tissue inhibitors of metalloproteinases (TIMPs). Excessive ECM breakdown resulting from an MMP-TIMP imbalance occurs in various pathologic processes, including inflammation, chronic degenerative diseases, and tumor invasion.

The restoration of functional connective tissue is a major goal of the wound healing process. This regenerative event requires the deposition and accumulation of collagenous and noncollagenous ECM molecules as well as the remodeling of ECM by MMPs. The inhibitors, TIMP-1 and TIMP-2, obstruct the activities of all known MMPs and as such play a key role in maintaining the balance between ECM deposition and degradation in different physiologic processes. Loss of balance in the expression of proteinases and inhibitors may result in tissue degradation in inflammatory diseases [43].

MMP-9 was among the first to be implicated in asthma pathogenesis, where abundant *MMP-9* mRNA expression was noted in submucosal regions of asthmatic bronchial biopsies when compared to normal subjects, especially within the eosinophils in asthmatic tissues [44]. Interestingly, the protein expression was not abundantly seen in the inflammatory cells, but immunoreactivity was rather detected in the ECM. Additionally, neutrophils are another important source of MMP-9 in allergic asthmatic patients [36]. In a 5-year follow-up study, increased MMP-9 and MMP-9/TIMP-1 ratio in the fast FEV1 decline group in asthmatic bronchial biopsy specimens and alveolar macrophages imply their contribution to a greater decline in lung function of patients with chronic asthma [45].

5. Immunomodulatory Role of MMPs in Asthma

MMPs play a key role in immune cell development, effector function, migration, and ligand-receptor interactions. They carry out ectodomain shedding of cytokines and their cognate receptors. MMPs influence immune responses by regulating signal transduction pathways downstream of tumor necrosis factor receptor, interleukin- (IL-) 6 receptor, epidermal growth factor receptor, and Notch signaling, which are all pertinent for inflammatory responses [43].

Inflammation, a key hallmark feature of asthma, is also regulated by MMPs, which exhibit both proinflammatory and anti-inflammatory properties. MMPs facilitate both the recruitment and clearance of inflammatory cells through the cleavage of inflammatory mediators such as chemokine substrates [46]. For instance, MMP-7 (matrilysin)-mediated shedding of syndecan-1, a heparan sulfate proteoglycan, is required for establishing a chemokine gradient for the trans-epithelial migration of leukocytes into the alveolar air spaces [47].

IL-13, a T helper type 2 cytokine, demonstrated the ability to regulate most of pathological processes in allergic

asthma. For example, mice with inducible lung-targeted overexpression of IL-13 showed the pathogenic effects of IL-13 on inflammation and airway remodeling [48, 49]. IL-13 overexpression was found to be sufficient enough to induce most of the features of allergic asthma seen in human patients in other murine models of allergen challenge. These IL-13 transgenic mice harbored significantly high levels of *MMP-2*, *MMP-9*, *MMP-12*, *MMP-13*, *MMP-14*, and *TIMP-1* mRNA expression and *MMP-2*, *MMP-9*, and *MMP-12* activity in the lung tissue as compared to nontransgenic animals [49]. This highlights the pathological and immunomodulatory role of MMPs in allergic asthma.

MMP-deficient mouse models have revealed important information regarding their role in airway inflammation in asthma. MMPs, in particular *MMP-9*, are secreted by inflammatory cells following allergen provocation and in response to T helper type 2 cytokine signaling [50]. These factors facilitate inflammatory cell egress from the tissues to the airway lumen. Additionally, inflammatory cell- and structural cell-derived MMPs also contribute to AHR and remodeling by altering ECM turnover, which affects smooth muscle contraction, airway fibroblast invasion, and submucosal accumulation of collagen. Furthermore, MMP-induced regulation of cell signaling through proteolytic shedding and activation of key growth factors, such as TGF- β 1, stimulates airway cell proliferation and modulates matrix production, contributing to airway fibrosis [50]. *MMP-9* and *MMP-2* have been implicated in the infiltration of eosinophils through the basement membrane into the asthmatic airway walls and the subsequent induction of AHR [51, 52]. This immunomodulatory role of MMPs in asthma provides the attractive possibility of MMP inhibition as a therapeutic option in bronchial asthma.

6. Role of MMPs in Angiogenesis and Asthma

Angiogenesis involves the destruction of the vascular basement membrane and remodeling of the ECM, which paves way for the migration and proliferation of endothelial cells as well as the synthesis of new matrix components. MMPs play an important role in this disruption and neovascularization process, thus constituting a key element in the pathophysiological mechanisms underlying vascular remodeling in asthma. Airway inflammation entails the migration of activated inflammatory cells from the circulation into the airway wall towards the site of injury, and the airway structural cells closely interact with the ECM components in promoting angiogenesis in asthmatic airways. MMPs have largely been studied in aiding this extravasation across the vascular and airway membranes. Table 1 enlists the various MMPs (in their order of relevance) implicated in promoting angiogenesis in asthma.

The major role of MMPs is the breakdown of the vascular basement membrane and ECM paving the way to tissue remodeling and angiogenesis. MMPs cover a broad range of angiogenic functions, from the degradation of the preexisting basement membrane and ECM to the release of a variety of angiogenic and growth factors as well as stimulation of endogenous angiogenic inhibitors.

MMPs thus contribute to vascular remodeling through multiple mechanisms involving proteolysis of type I collagen, regulation of perivascular or smooth muscle cells, modification of platelet-derived growth factor (PDGF) signaling, and processing and mobilization of VEGF [53]. As discussed earlier, among the numerous MMPs, *MMP-9* is the most commonly implicated in asthmatic airways. *MMP-9* is well known to trigger the angiogenic switch in carcinogenesis [54]. The elevated levels of *MMP-9* in asthmatic airways make *MMP-9* a likely pathological angiogenic player in asthma as well. The airway infiltrating cells, including mast cells and basophils, are sources of VEGF in the airways [55, 56]. In a study by Lee et al., VEGF signaling was found to regulate *MMP-9* expression in a murine model of asthma with the inhibition of VEGF receptor contributing to the downregulation of *MMP-9* [57]. Furthermore, VEGF receptor inhibition also led to a reduction in plasma extravasation as well as the number of inflammatory cells (eosinophils, lymphocytes, and neutrophils) in BAL fluids, suggesting a role for *MMP-9* in promoting the migration of inflammatory cells across the endothelial basement membrane. *Mmp-9*, *Mmp-2*, and *Mmp-14* mutant mice show defects in angiogenesis despite normality in their VEGF and VEGFR2 levels [58–60]. The reduction in bronchial vascular extracellular remodeling brought about by inducible NO synthase (iNOS) inhibition was found to be associated with *MMP-9*/*TIMP-1* vascular expression [61], reinforcing the regulatory potential of MMP expression on vascular remodeling.

Extracellular vesicles (EVs) containing MMPs are novel mediators of ECM remodeling [62]. Several cells of the respiratory system, including bronchial epithelial cells, vascular endothelial cells, alveolar macrophages, eosinophils, neutrophils, and fibroblasts, secrete EVs that are crucial for intercellular communications [63, 64]. Exposure to tobacco smoke reportedly induced the release of proteolytic EVs from human macrophages [65]. The gelatinolytic and collagenolytic activities exhibited by these EVs can be predominantly attributed to *MT1-MMP*/*MMP-14*. MMP-containing EVs have been largely studied in cancer models, where they were shown to promote angiogenic activities *in vitro* as well as *in vivo* [66, 67]. Platelet-derived microvesicles stimulated the expression of angiogenic factors, *MMP-9*, VEGF, and IL-8, which promoted angiogenesis in a human syngeneic mouse model of lung cancer [68]. Since asthma patients demonstrate increased levels of EVs [69, 70], it is highly likely that MMP-containing EVs contribute to angiogenesis in asthma.

7. MMP-Targeted Therapeutic Advances in Asthma

Considering the pathological role of angiogenesis in asthma and the limited effectiveness of standard asthma therapy in ameliorating airway remodeling in asthma underlines the importance of identifying potential targets to control the development of angiogenesis and associated vascular remodeling in asthma. The identification of MMPs as crucial regulators of the angiogenic process had led to the development of

TABLE 1: MMPs implicated in promoting angiogenesis in asthma.

Name	Substrates	Cellular sources	Functions	References
MMP-9 (gelatinase-B)	Collagens IV, V, VII, X, and XIV, gelatin, pro-MMP-9, pro-MMP-13, elastin, aggrecan, laminin	Bronchial epithelial cells, endothelial cells, fibroblasts, neutrophils, alveolar macrophages, mast cells, eosinophils, dendritic cells, T cells	(i) Triggers angiogenic switch (ii) Cryptic epitope exposure within collagen IV (iii) Cleavage of latent TGF- β (iv) Proteolytic activation of IL-8 and inactivation of platelet factor-4 (v) VEGF mobilization from ECM (vi) iNOS activation (vii) Endothelial basement membrane disruption (viii) EC growth & migration (ix) Eosinophil infiltration (x) Pericyte recruitment (xi) Hydrolyze plasminogen to angiostatin	[51, 52, 54, 61, 71–74]
MMP-2 (gelatinase-A)	Collagens I, II, III, IV, V, VII, X, XI, and XIV, gelatin, elastin, fibronectin, aggrecan, CCL7, CXCL12	Fibroblasts, bronchial epithelial cells, smooth muscle cells, endothelial cells, neutrophils, macrophages, T cells	(i) Triggers angiogenic switch (ii) Cryptic epitope exposure within collagen IV (iii) Binding to integrin $\alpha v \beta 3$ (iv) VEGF mobilization from ECM (v) Cleavage of latent TGF- β (vi) Smooth muscle proliferation (vii) Endothelial basement membrane disruption (viii) Eosinophil infiltration (ix) Hydrolyze plasminogen to angiostatin	[51, 52, 71, 75, 76]
MMP-7 (matrilysin-2)	Collagens II, III, IV, IX, X, and XI, elastin, pro-MMP-1, pro-MMP-7, pro-MMP-8, pro-MMP-9, pro-MMP-13, gelatin, aggrecan, fibronectin, laminin, syndecan-1, E-cadherin	Smooth muscle cells, epithelial cells, macrophages	(i) EC proliferation (ii) Upregulation of endothelial expression of MMP-1 and MMP-2 (iii) CTGF cleavage to release active VEGF ¹⁶⁵ (iv) Endostatin fragment release from ECM (v) Hydrolyze	[47, 72, 77–79]

TABLE 1: Continued.

Name	Substrates	Cellular sources	Functions	References
			plasminogen to angiostatin	
MMP-1 (collagenase-1)	Collagens I, II, III, VII, VIII, and X, aggrecan, gelatin, pro-MMP-2, pro-MMP-9	Fibroblasts, smooth muscle cells, alveolar epithelial cells, endothelial cells, alveolar macrophages	(i) Degradation of interstitial collagen types I-III (ii) Degradation of perlecan in endothelial basement membrane to release bFGF (iii) CTGF cleavage to release active VEGF (iv) Promotes VEGFR2 expression (v) Endothelial invasion capacity (vi) Smooth muscle hyperplasia	[79–81]
MMP-8 (collagenase-2)	Collagens I, II, III, VII, VIII, and X, aggrecan, gelatin	Neutrophils, fibroblasts, endothelial cells	(i) EC proliferation and migration (ii) PECAM-1 expression (iii) Neutrophil clearance	[82]
MMP-14 (MT1-MMP)	Pro-MMP-2, pro-MMP-13, collagens I, II, and III, gelatin, aggrecan, fibronectin, laminin, proteoglycan, CD44, E-cadherin, syndecan-1	Bronchial epithelial cells, endothelial cells, fibroblasts, alveolar epithelial cells, macrophages	(i) Stimulate invasion into collagen (ii) Pericellular collagenolysis (iii) Proteolytic degradation of antiangiogenic factors (such as decorin) (iv) Stimulate VEGF production (v) Induce EC migration	[83–85]
MMP-12 (metalloelastase)	Elastin, collagen IV, laminin	Epithelial cells, alveolar macrophages	(i) Angiostatin production (ii) Hydrolyze plasminogen to angiostatin (iii) Endostatin release	[86, 87]

Abbreviations: TGF: transforming growth factor; iNOS: inducible nitric oxide synthase; EC: endothelial cell; CTGF: connective tissue growth factor; bFGF: basic fibroblast growth factor; PECAM: platelet endothelial cell adhesion molecule; VEGFR: vascular endothelial growth factor receptor.

therapeutic strategies targeting MMPs. Some of the therapeutic strategies targeting MMPs that are currently under investigation include the use of small molecular MMP inhibitors, TIMPs, antisense technologies, and blocking antibodies, as have been extensively reviewed in [88–90].

Although the airways are equipped with physiological or endogenous inhibitors such as TIMPs, diseased airways cripple the MMP/TIMP ratio favoring pathogenesis and airway remodeling. TIMP-1 antagonizes MMP-9 activity, and a lower MMP-9/TIMP-1 ratio in sputum from untreated stable asthmatics suggests an overproduction of TIMP-1 over MMP-9 in patients with stable asthma [91]. Since TIMP-1

shows anti-angiogenic activity by blocking the endothelial cell response to angiogenic factors and cell migration [92–96], this natural endogenous activity of TIMP-1 may be harnessed to impede angiogenic activity in asthma. However, altering the delicate protease/anti-protease balance needs to be considered with caution as this strategy may backfire leading to worsening outcomes in asthma. The different binding rates and binding affinity of TIMPs constitute another challenge in using it to target the different MMPs.

There are also several exogenous MMP inhibitors available such as hydroxamate derivatives including batimastat, marimastat, and ilomastat. Although these agents have

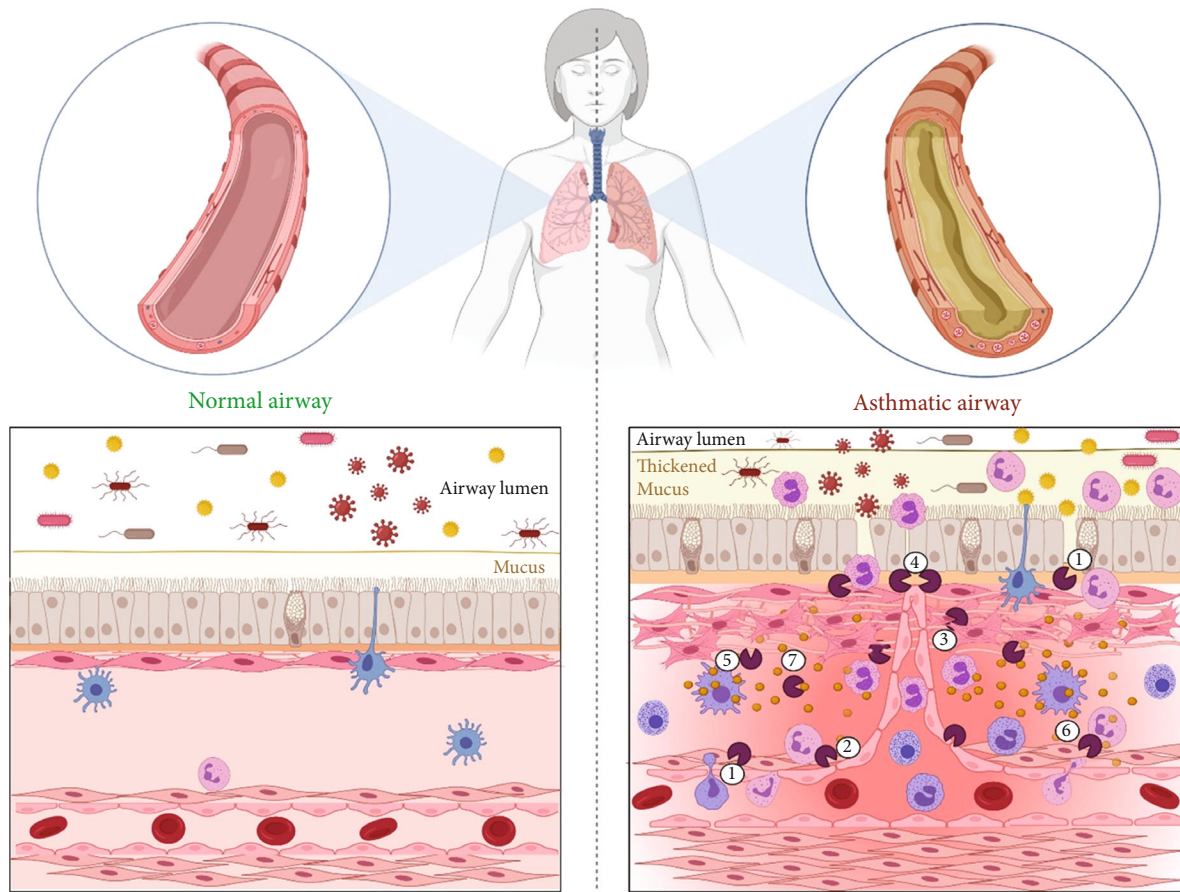


Figure Legend:

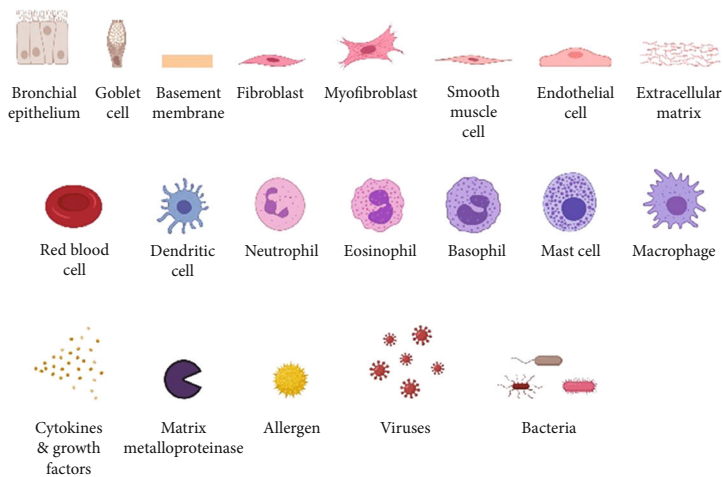


FIGURE 1: Schematic illustration of the involvement of MMPs in facilitating angiogenesis in asthma. In an asthmatic airway microenvironment, MMPs are involved in (1) the extravasation of inflammatory cells into the airways as well as their egress into the airway lumen across the vascular and airway membranes, (2) the degradation of vascular basement membrane, (3) degradation of ECM components (collagen, proteoglycans, elastin, gelatin, fibrin, fibronectin, aggrecan, and laminin), (4) aiding the endothelial sprouting tip to invade into the surrounding stroma, (5) release of proangiogenic cytokines and growth factors (HIF, VEGF, bFGF, PDGF, and TGF- β) from ECM, activated airway structural cells (epithelial, endothelial, fibroblast, and smooth muscle cells), and infiltrating inflammatory cells (eosinophils, neutrophils, basophils, mast cells, and macrophages), (6) regulation of perivascular or smooth muscle cells, and (7) ectodomain shedding of cytokines and their cognate receptors. This complex interplay between the activated cells, MMPs, cytokines, and growth factors directs the development of a vascular network within asthmatic airways. Created with <http://BioRender.com/>.

shown effectiveness in reducing AHR and airway inflammation in murine asthma models, their low specificity renders their activity against various other zinc-containing metalloproteins, including numerous non-MMP enzymes and transcription factors, and hence severe side effects leading to their withdrawal from clinical practice. Their low clinical effectiveness could also be due to the compensatory induction of other MMPs despite downregulation of the specific targeted MMP.

In addition, various other clinically used drugs are also known to modulate MMP activity either directly or indirectly. Corticosteroids, statins, angiotensin-converting enzyme (ACE) inhibitors, and tetracyclines belong to this category. Dexamethasone, a commonly used corticosteroid, selectively and potently inhibits a variety of MMPs, including collagenases and stromelysins, in addition to TIMPs in human alveolar macrophages [97]. The inhaled corticosteroid (ICS), beclomethasone dipropionate (BDP), attenuated the expression of submucosal MMP-9 and increased that of submucosal TIMP-1, suggesting corticosteroid treatment of asthma to ameliorate angiogenesis [98]. In a murine asthma model, inhaled administration of budesonide significantly reduced the vascularity and the expression levels of HIF-1 α and VEGF, supporting an anti-angiogenic role for budesonide in the treatment of human asthma [99]. A placebo-controlled intervention study exploring angiogenic modulation upon ICS treatment in patients with asthma revealed a reduction in microvascular angiogenic remodeling in asthmatic airways in terms of a decrease in vessel numbers, VEGF staining, and number of sprouted vessels in airway biopsy specimens [100].

The subject of targeting angiogenesis in asthma is one of considerable debate considering its role in normal physiological functions. During airway and lung growth, they progressively require good blood supply, which is paralleled by the expression of VEGF and its receptors [101]. Therefore, with therapeutic strategies targeting VEGF using anti-VEGF antibody (Avastin) and anti-VEGFR-1 and anti-VEGFR-2 antibodies, such as in cancer therapeutics, arises the possibility of excessive vascular regression that could compromise drug delivery to the target site and set off unwanted side effects [102].

8. Future Perspectives

Initially thought of as an immunological disorder, asthma is now increasingly appreciated as a disorder affecting the airway wall with aberrant inflammatory and remodeling responses. Asthma is a complex heterogenous disorder with multiple hallmark features, one among which is angiogenesis and vascular remodeling. Angiogenesis appears to facilitate the development of airway edema in the initial stages and further on progress to contribute towards bronchial wall thickening with concomitant reduction in distensibility. MMPs through their actions on ECM degradation and regulation of cell signaling play a role across multiple pathological processes of asthma, including angiogenesis. Figure 1 illustrates the various pathological roles of MMPs in facilitating angiogenesis in asthma.

Although there are improved research and insights into various aspects of angiogenesis and vascular remodeling in asthma, there are several unanswered questions, answers to which could provide a well-rounded understanding of the implications of MMPs in the pathology of angiogenesis in asthma. In comparison to their healthy counterparts, the various cellular players in asthma secrete increased levels of cytokines, chemokines, growth factors, and angiogenic mediators. Despite the well-known anti-inflammatory activity of corticosteroids, their ability to reverse or reduce airway remodeling continues to remain a subject of controversy. Although high doses of ICS affect certain components of remodeling, increased vascularity, for example [100, 103, 104], they do not uniformly target the various remodeling features. The ability of MMPs in regulating both the inflammatory and remodeling aspects of asthma pathology opens the possibility of completely unexplored avenues of asthma therapy. A detailed understanding of the various members of the MMP family and their contribution towards angiogenesis across the various asthma endotypes and phenotypes is lacking. Depending on the disease endotype, targeting specific MMPs and averting their pathological signaling can be beneficial in that subset of patients. Future studies could also potentially help identify novel angiogenic signaling pathways in asthma, and their regulation by MMPs provides opportunities to categorize the various roles played by MMPs in asthma which could be harnessed for therapeutic intervention. Since miRNAs are increasingly being implicated in angiogenesis and endothelial cell function, the ability of MMPs to modulate specific miRNAs is another interesting avenue for research. The search for a non-invasive therapy capable of reducing or even completely abrogating vascular and other remodeling features is another meaningful approach.

In conclusion, asthma being a multifaceted disease calls for the development of new therapeutic strategies that can target the various remodeling features observed in asthmatic airways. The studies discussed above provide insights into the role of MMPs as a potential target to ameliorate angiogenesis among various other remodeling features. The ability of MMPs to target both inflammatory and remodeling processes makes it an attractive option for therapy. Furthermore, MMP levels and vascularity are also correlated with asthma severity indicating their role in asthma pathogenesis and progression. Several animal studies have further reinforced this data supporting the notion that reducing or reversing vascular remodeling may prove beneficial in treating asthma. Although corticosteroids have potential MMP-mediated anti-angiogenic activities, there is a need for novel strategies targeting MMPs. Targeting MMPs is a novel therapeutic strategy for treating the microvascular changes observed in asthma considering their ability to reduce angiogenesis, inflammatory response, and thereby asthma symptoms. Nevertheless, it is crucial to identify the subset of asthma patients that respond and benefit the most from such an approach.

Data Availability

No data were used to support this study.

Conflicts of Interest

The authors declare no conflict of interest.

Authors' Contributions

Conceptualization, investigation, and writing (review and editing) were handled by QH, KB, and RKR; data curation and writing (original draft) were taken care of by KB and RKR; and supervision was managed by KB and QH. All authors have read and agreed to the published version of the manuscript. Khuloud Bajbouj and Rakhee K. Ramakrishnan contributed equally to this work.

Acknowledgments

This work was funded by the University of Sharjah Competitive Grant, Ref. number: 1901090263.

References

- [1] S. Al-Muhsen, J. R. Johnson, and Q. Hamid, "Remodeling in asthma," *The Journal of Allergy and Clinical Immunology*, vol. 128, no. 3, pp. 451–462, 2011.
- [2] D. Rizzoni, M. L. Muiesan, E. Porteri et al., "Vascular remodeling, macro- and microvessels: therapeutic implications," *Blood Pressure*, vol. 18, no. 5, pp. 242–246, 2009.
- [3] M. F. Minicucci, P. S. Azevedo, S. A. Paiva, and L. A. Zornoff, "Cardiovascular remodeling induced by passive smoking," *Inflammation & Allergy Drug Targets*, vol. 8, no. 5, pp. 334–339, 2009.
- [4] I. C. Lawrance, L. Maxwell, and W. Doe, "Altered response of intestinal mucosal fibroblasts to profibrogenic cytokines in inflammatory bowel disease," *Inflammatory Bowel Diseases*, vol. 7, no. 3, pp. 226–236, 2001.
- [5] Q. Gao, M. J. Meijer, F. J. Kubben et al., "Expression of matrix metalloproteinases-2 and -9 in intestinal tissue of patients with inflammatory bowel diseases," *Digestive and liver disease*, vol. 37, no. 8, pp. 584–592, 2005.
- [6] R. Halwani, S. Al-Muhsen, and Q. Hamid, "Airway remodeling in asthma," *Current Opinion in Pharmacology*, vol. 10, no. 3, pp. 236–245, 2010.
- [7] A. M. Vignola, J. Kips, and J. Bousquet, "Tissue remodeling as a feature of persistent asthma," *The Journal of Allergy and Clinical Immunology*, vol. 105, no. 6, pp. 1041–1053, 2000.
- [8] K. Pağan and Z. Bartuzi, "Angiogenesis in bronchial asthma," *International Journal of Immunopathology and Pharmacology*, vol. 28, no. 3, pp. 415–420, 2015.
- [9] M. S. Dunnill, "The pathology of asthma, with special reference to changes in the bronchial mucosa," *Journal of Clinical Pathology*, vol. 13, no. 1, pp. 27–33, 1960.
- [10] D. M. McDonald, "Angiogenesis and remodeling of airway vasculature in chronic inflammation," *American Journal of Respiratory and Critical Care Medicine*, vol. 164, supplement_2, pp. S39–S45, 2001.
- [11] K. Kuwano, C. H. Bosken, P. D. Paré, T. R. Bai, B. R. Wiggs, and J. C. Hogg, "Small airways dimensions in asthma and in chronic obstructive pulmonary disease," *The American Review of Respiratory Disease*, vol. 148, no. 5, pp. 1220–1225, 1993.
- [12] X. Li and J. W. Wilson, "Increased vascularity of the bronchial mucosa in mild asthma," *American Journal of Respiratory and Critical Care Medicine*, vol. 156, no. 1, pp. 229–233, 1997.
- [13] G. Salvato, "Quantitative and morphological analysis of the vascular bed in bronchial biopsy specimens from asthmatic and non-asthmatic subjects," *Thorax*, vol. 56, no. 12, pp. 902–906, 2001.
- [14] A. Grigoraş, I. D. Căruntu, C. C. Grigoraş, T. Mihăescu, and C. Amălinei, "Relationship between immunohistochemical assessment of bronchial mucosa microvascularization and clinical stage in asthma," *Romanian journal of morphology and embryology*, vol. 53, pp. 485–490, 2012.
- [15] R. M. Tuder, J. H. Yun, A. Bhunia, and I. Fijalkowska, "Hypoxia and chronic lung disease," *Journal of molecular medicine*, vol. 85, pp. 1317–1324, 2007.
- [16] S. Huerta-Yepez, G. J. Baay-Guzman, I. G. Bebenek et al., "Hypoxia inducible factor promotes murine allergic airway inflammation and is increased in asthma and rhinitis," *Allergy*, vol. 66, no. 7, pp. 909–918, 2011.
- [17] S. Y. Lee, S. Kwon, K. H. Kim et al., "Expression of vascular endothelial growth factor and hypoxiainducible factor in the airway of asthmatic patients," *Annals of allergy, asthma & immunology*, vol. 97, no. 6, pp. 794–799, 2006.
- [18] G. Papadaki, P. Bakakos, K. Kostikas et al., "Vascular endothelial growth factor and cysteinyl leukotrienes in sputum supernatant of patients with asthma," *Respiratory Medicine*, vol. 107, no. 9, pp. 1339–1345, 2013.
- [19] B. K. Lal, S. Varma, P. J. Pappas, R. W. Hobson 2nd, and W. N. Duran, "VEGF increases permeability of the endothelial cell monolayer by activation of PKB/akt, endothelial nitric-oxide synthase, and MAP kinase pathways," *Microvascular Research*, vol. 62, no. 3, pp. 252–262, 2001.
- [20] T. Makinde, R. F. Murphy, and D. K. Agrawal, "Immunomodulatory role of vascular endothelial growth factor and angiotensin-1 in airway remodeling," *Current Molecular Medicine*, vol. 6, no. 8, pp. 831–841, 2006.
- [21] S. D. Shapiro and R. M. Senior, "Matrix metalloproteinases. Matrix degradation and more," *American Journal of Respiratory Cell and Molecular Biology*, vol. 20, no. 6, pp. 1100–1102, 1999.
- [22] T. Mauad, A. C. Xavier, P. H. Saldiva, and M. Dolhnikoff, "Elastosis and fragmentation of fibers of the elastic system in fatal asthma," *American Journal of Respiratory and Critical Care Medicine*, vol. 160, no. 3, pp. 968–975, 1999.
- [23] T. Mauad, L. F. Silva, M. A. Santos et al., "Abnormal alveolar attachments with decreased elastic fiber content in distal lung in fatal asthma," *American Journal of Respiratory and Critical Care Medicine*, vol. 170, no. 8, pp. 857–862, 2004.
- [24] J. Chakir, J. Shannon, S. Molet et al., "Airway remodeling-associated mediators in moderate to severe asthma: effect of steroids on TGF- β , IL-11, IL-17, and type I and type III collagen expression," *The Journal of Allergy and Clinical Immunology*, vol. 111, no. 6, pp. 1293–1298, 2003.
- [25] M. de Medeiros Matsushita, L. F. da Silva, M. A. dos Santos et al., "Airway proteoglycans are differentially altered in fatal asthma," *The Journal of Pathology*, vol. 207, no. 1, pp. 102–110, 2005.
- [26] W. R. Roche, R. Beasley, J. H. Williams, and S. T. Holgate, "Subepithelial fibrosis in the bronchi of asthmatics," *Lancet*, vol. 1, pp. 520–524, 1989.

- [27] A. Laitinen, A. Altraja, M. Kampe, M. Linden, I. Virtanen, and L. A. Laitinen, "Tenascin is increased in airway basement membrane of asthmatics and decreased by an inhaled steroid," *American Journal of Respiratory and Critical Care Medicine*, vol. 156, no. 3, pp. 951–958, 1997.
- [28] L. A. Laitinen and A. Laitinen, "Inhaled corticosteroid treatment and extracellular matrix in the airways in asthma," *International Archives of Allergy and Immunology*, vol. 107, pp. 215–216, 2004.
- [29] A. Altraja, A. Laitinen, I. Virtanen et al., "Expression of laminins in the airways in various types of asthmatic patients: a morphometric study," *American Journal of Respiratory Cell and Molecular Biology*, vol. 15, no. 4, pp. 482–488, 1996.
- [30] W. R. Roche, "Fibroblasts and asthma," *Clinical and experimental allergy*, vol. 21, no. 5, pp. 545–548, 1991.
- [31] S. E. Gill and W. C. Parks, "Metalloproteinases and their inhibitors: regulators of wound healing," *The International Journal of Biochemistry & Cell Biology*, vol. 40, no. 6–7, pp. 1334–1347, 2008.
- [32] M. G. Rohani and W. C. Parks, "Matrix remodeling by MMPs during wound repair," *Matrix biology*, vol. 44–46, pp. 113–121, 2015.
- [33] L. Nissinen and V. M. Kahari, "Matrix metalloproteinases in inflammation," *Biochimica et Biophysica Acta*, vol. 2014, pp. 2571–2580, 2014.
- [34] M. Giannandrea and W. C. Parks, "Diverse functions of matrix metalloproteinases during fibrosis," *Disease Models & Mechanisms*, vol. 7, no. 2, pp. 193–203, 2014.
- [35] S. Sergejeva, S. Ivanov, J. Lotvall, and A. Linden, "Interleukin-17 as a recruitment and survival factor for airway macrophages in allergic airway inflammation," *American Journal of Respiratory Cell and Molecular Biology*, vol. 33, no. 3, pp. 248–253, 2005.
- [36] I. Ventura, A. Vega, P. Chacon et al., "Neutrophils from allergic asthmatic patients produce and release metalloproteinase-9 upon direct exposure to allergens," *Allergy*, vol. 69, no. 7, pp. 898–905, 2014.
- [37] E. A. Kelly, W. W. Busse, and N. N. Jarjour, "Increased matrix metalloproteinase-9 in the airway after allergen challenge," *American Journal of Respiratory and Critical Care Medicine*, vol. 162, no. 3, pp. 1157–1161, 2000.
- [38] Y. Chiba, Y. Yu, H. Sakai, and M. Misawa, "Increase in the expression of matrix metalloproteinase-12 in the airways of rats with allergic bronchial asthma," *Biological & Pharmaceutical Bulletin*, vol. 30, no. 2, pp. 318–323, 2007.
- [39] S. Goswami, P. Angkasekwinai, M. Shan et al., "Divergent functions for airway epithelial matrix metalloproteinase 7 and retinoic acid in experimental asthma," *Nature Immunology*, vol. 10, no. 5, pp. 496–503, 2009.
- [40] J. L. Ingram, M. J. Huggins, T. D. Church et al., "Airway fibroblasts in asthma manifest an invasive phenotype," *American Journal of Respiratory and Critical Care Medicine*, vol. 2011, p. 183, 2011.
- [41] R. Firszt, D. Francisco, T. D. Church, J. M. Thomas, J. L. Ingram, and M. Kraft, "Interleukin-13 induces collagen type-1 expression through matrix metalloproteinase-2 and transforming growth factor-1 in airway fibroblasts in asthma," *The European Respiratory Journal*, vol. 43, no. 2, pp. 464–473, 2014.
- [42] Y. Ohta, M. Hayashi, T. Kanemaru, K. Abe, Y. Ito, and M. Oike, "Dual modulation of airway smooth muscle contraction by Th2 cytokines via matrix metalloproteinase-1 production," *Journal of Immunology*, vol. 180, no. 6, pp. 4191–4199, 2008.
- [43] R. Khokha, A. Murthy, and A. Weiss, "Metalloproteinases and their natural inhibitors in inflammation and immunity," *Nature Reviews. Immunology*, vol. 13, no. 9, pp. 649–665, 2013.
- [44] I. Ohno, H. Ohtani, Y. Nitta et al., "Eosinophils as a source of matrix metalloproteinase-9 in asthmatic airway inflammation," *American Journal of Respiratory Cell and Molecular Biology*, vol. 16, no. 3, pp. 212–219, 1997.
- [45] F. T. Chung, H. Y. Huang, C. Y. Lo et al., "Increased ratio of matrix metalloproteinase-9 (MMP-9)/tissue inhibitor metalloproteinase-1 from alveolar macrophages in chronic asthma with a fast decline in FEV1 at 5-year follow-up," *Journal of Clinical Medicine*, vol. 8, no. 9, p. 1451, 2019.
- [46] C. M. Overall, G. A. McQuibban, and I. Clark-Lewis, "Discovery of chemokine substrates for matrix metalloproteinases by exosite scanning: a new tool for degradomics," *Biological Chemistry*, vol. 383, no. 7–8, pp. 1059–1066, 2002.
- [47] Q. Li, P. W. Park, C. L. Wilson, and W. C. Parks, "Matrilysin shedding of syndecan-1 regulates chemokine mobilization and transepithelial efflux of neutrophils in acute lung injury," *Cell*, vol. 111, no. 5, pp. 635–646, 2002.
- [48] T. Zheng, Z. Zhu, Z. Wang et al., "Inducible targeting of IL-13 to the adult lung causes matrix metalloproteinase- and cathepsin-dependent emphysema," *The Journal of Clinical Investigation*, vol. 106, no. 9, pp. 1081–1093, 2000.
- [49] S. Lanone, T. Zheng, Z. Zhu et al., "Overlapping and enzyme-specific contributions of matrix metalloproteinases-9 and -12 in IL-13-induced inflammation and remodeling," *The Journal of Clinical Investigation*, vol. 110, no. 4, pp. 463–474, 2002.
- [50] J. L. Ingram and M. Kraft, "Metalloproteinases as modulators of allergic asthma: therapeutic perspectives," *Metalloproteinases In Medicine*, vol. 2, pp. 61–74, 2015.
- [51] K. Kumagai, I. Ohno, S. Okada et al., "Inhibition of matrix metalloproteinases prevents allergen-induced airway inflammation in a murine model of asthma," *Journal of Immunology*, vol. 162, pp. 4212–4219, 1999.
- [52] K. Kumagai, I. Ohno, K. Imai et al., "The involvement of matrix metalloproteinases in basement membrane injury in a murine model of acute allergic airway inflammation," *Clinical and experimental allergy: journal of the British Society for Allergy and Clinical Immunology*, vol. 32, no. 10, pp. 1527–1534, 2002.
- [53] A. Page-McCaw, A. J. Ewald, and Z. Werb, "Matrix metalloproteinases and the regulation of tissue remodelling," *Molecular cell biology*, vol. 8, no. 3, pp. 221–233, 2007.
- [54] G. Bergers, R. Brekken, G. McMahon et al., "Matrix metalloproteinase-9 triggers the angiogenic switch during carcinogenesis," *Nature Cell Biology*, vol. 2, no. 10, pp. 737–744, 2000.
- [55] B. Textor, A. H. Licht, J. P. Tuckermann et al., "JunB is required for IgE-mediated degranulation and cytokine release of mast cells," *Journal of Immunology*, vol. 179, no. 10, pp. 6873–6880, 2007.
- [56] A. de Paulis, N. Prevete, I. Fiorentino et al., "Expression and functions of the vascular endothelial growth factors and their receptors in human basophils," *Journal of Immunology*, vol. 177, no. 10, pp. 7322–7331, 2006.

- [57] K. S. Lee, K. H. Min, S. R. Kim et al., "Vascular endothelial growth factor modulates matrix metalloproteinase-9 expression in asthma," *American journal of respiratory and critical care medicine*, vol. 174, pp. 161–170, 2006.
- [58] T. H. Vu, J. M. Shipley, G. Bergers et al., "MMP-9/gelatinase B is a key regulator of growth plate angiogenesis and apoptosis of hypertrophic chondrocytes," *Cell*, vol. 93, no. 3, pp. 411–422, 1998.
- [59] T. Kato, T. Kure, J. H. Chang et al., "Diminished corneal angiogenesis in gelatinase A-deficient mice," *FEBS Letters*, vol. 508, no. 2, pp. 187–190, 2001.
- [60] Z. Zhou, S. S. Apte, R. Soininen et al., "Impaired endochondral ossification and angiogenesis in mice deficient in membrane-type matrix metalloproteinase I," *Proceedings of the National Academy of Sciences of the United States of America*, vol. 97, no. 8, pp. 4052–4057, 2000.
- [61] C. M. Prado, L. Yano, G. Rocha et al., "Effects of inducible nitric oxide synthase inhibition in bronchial vascular remodeling-induced by chronic allergic pulmonary inflammation," *Experimental Lung Research*, vol. 37, no. 5, pp. 259–268, 2011.
- [62] M. Nawaz, N. Shah, B. R. Zanetti et al., "Extracellular vesicles and matrix remodeling enzymes: the emerging roles in extracellular matrix remodeling, progression of diseases and tissue repair," *Cell*, vol. 7, no. 10, p. 167, 2018.
- [63] T. Nagano, M. Katsurada, R. Dokuni et al., "Crucial role of extracellular vesicles in bronchial asthma," *International Journal of Molecular Sciences*, vol. 20, no. 10, p. 2589, 2019.
- [64] A. Kulshreshtha, T. Ahmad, A. Agrawal, and B. Ghosh, "Pro-inflammatory role of epithelial cell-derived exosomes in allergic airway inflammation," *The Journal of allergy and clinical immunology*, vol. 131, pp. 1194–1203, 2013.
- [65] C. J. Li, Y. Liu, Y. Chen, D. Yu, K. J. Williams, and M. L. Liu, "Novel proteolytic microvesicles released from human macrophages after exposure to tobacco smoke," *The American Journal of Pathology*, vol. 182, no. 5, pp. 1552–1562, 2013.
- [66] C. Grange, M. Tapparo, F. Collino et al., "Microvesicles released from human renal cancer stem cells stimulate angiogenesis and formation of lung premetastatic niche," *Cancer Research*, vol. 71, no. 15, pp. 5346–5356, 2011.
- [67] V. Dolo, S. D'Ascenzo, I. Giusti, D. Millimaggi, G. Taraboletti, and A. Pavan, "Shedding of membrane vesicles by tumor and endothelial cells," *Italian journal of anatomy and embryology*, vol. 110, pp. 127–133, 2005.
- [68] A. Janowska-Wieczorek, M. Wysoczynski, J. Kijowski et al., "Microvesicles derived from activated platelets induce metastasis and angiogenesis in lung cancer," *International Journal of Cancer*, vol. 113, no. 5, pp. 752–760, 2005.
- [69] C. Mazzeo, J. A. Cañas, M. P. Zafra et al., "Exosome secretion by eosinophils: a possible role in asthma pathogenesis," *The Journal of Allergy and Clinical Immunology*, vol. 2015, p. 135, 2015.
- [70] K. P. Hough, L. S. Wilson, J. L. Trevor et al., "Unique lipid signatures of extracellular vesicles from the airways of asthmatics," *Scientific Reports*, vol. 8, no. 1, p. 10340, 2018.
- [71] Q. Yu and I. Stamenkovic, "Cell surface-localized matrix metalloproteinase-9 proteolytically activates TGF-beta and promotes tumor invasion and angiogenesis," *Genes & Development*, vol. 14, no. 2, pp. 163–176, 2000.
- [72] B. C. Patterson and Q. A. Sang, "Angiostatin-converting enzyme activities of human matrilysin (MMP-7) and gelatinase B/type IV collagenase (MMP-9)," *The Journal of Biological Chemistry*, vol. 272, no. 46, pp. 28823–28825, 1997.
- [73] A. Pozzi, W. F. LeVine, and H. A. Gardner, "Low plasma levels of matrix metalloproteinase 9 permit increased tumor angiogenesis," *Oncogene*, vol. 21, no. 2, pp. 272–281, 2002.
- [74] C. F. Chantrain, H. Shimada, S. Jodele et al., "Stromal matrix metalloproteinase-9 regulates the vascular architecture in neuroblastoma by promoting pericyte recruitment," *Cancer Research*, vol. 2004, p. 64, 2004.
- [75] S. Silletti, T. Kessler, J. Goldberg, D. L. Boger, and D. A. Cheresh, "Disruption of matrix metalloproteinase 2 binding to integrin alpha vbeta 3 by an organic molecule inhibits angiogenesis and tumor growth in vivo," *Proceedings of the National Academy of Sciences of the United States of America*, vol. 98, pp. 119–124, 2000.
- [76] M. S. O'Reilly, D. Wiederschain, W. G. Stetler-Stevenson, J. Folkman, and M. A. Moses, "Regulation of angiostatin production by matrix metalloproteinase-2 in a model of concomitant resistance," *The Journal of Biological Chemistry*, vol. 274, no. 41, pp. 29568–29571, 1999.
- [77] N. Huo, Y. Ichikawa, M. Kamiyama et al., "MMP-7 (matrilysin) accelerated growth of human umbilical vein endothelial cells," *Cancer Letters*, vol. 177, no. 1, pp. 95–100, 2002.
- [78] I. Nishizuka, Y. Ichikawa, T. Ishikawa et al., "Matrilysin stimulates DNA synthesis of cultured vascular endothelial cells and induces angiogenesis in vivo," *Cancer Letters*, vol. 173, no. 2, pp. 175–182, 2001.
- [79] G. Hashimoto, I. Inoki, Y. Fujii, T. Aoki, E. Ikeda, and Y. Okada, "Matrix metalloproteinases cleave connective tissue growth factor and reactivate angiogenic activity of vascular endothelial growth factor 165," *The Journal of Biological Chemistry*, vol. 277, no. 39, pp. 36288–36295, 2002.
- [80] J. M. Whitelock, A. D. Murdoch, R. V. Iozzo, and P. A. Underwood, "The degradation of human endothelial cell-derived perlecan and release of bound basic fibroblast growth factor by stromelysin, collagenase, plasmin, and heparinases," *The Journal of Biological Chemistry*, vol. 271, no. 17, pp. 10079–10086, 1996.
- [81] G. Taraboletti, L. Sonzogni, V. Vergani et al., "Posttranscriptional stimulation of endothelial cell matrix metalloproteinases 2 and 1 by endothelioma cells," *Experimental Cell Research*, vol. 258, no. 2, pp. 384–394, 2000.
- [82] C. Fang, G. Wen, L. Zhang et al., "An important role of matrix metalloproteinase-8 in angiogenesis in vitro and in vivo," *Cardiovascular Research*, vol. 99, no. 1, pp. 146–155, 2013.
- [83] A. M. Abu El-Asrar, G. Mohammad, E. Allegaert et al., "Matrix metalloproteinase-14 is a biomarker of angiogenic activity in proliferative diabetic retinopathy," *Molecular Vision*, vol. 24, pp. 394–406, 2018.
- [84] E. I. Deryugina, B. Ratnikov, E. Monosov et al., "MT1-MMP initiates activation of pro-MMP-2 and integrin $\alpha\beta 3$ promotes maturation of MMP-2 in breast carcinoma cells," *Experimental Cell Research*, vol. 263, no. 2, pp. 209–223, 2001.
- [85] V. Knäuper, L. Bailey, J. R. Worley, P. Soloway, M. L. Patterson, and G. Murphy, "Cellular activation of proMMP-13 by MT1-MMP depends on the C-terminal domain of MMP-13," *FEBS Letters*, vol. 532, no. 1-2, pp. 127–130, 2002.
- [86] Z. Dong, R. Kumar, X. Yang, and I. J. Fidler, "Macrophage-derived metalloelastase is responsible for the generation of

- angiostatin in Lewis lung carcinoma," *Cell*, vol. 88, no. 6, pp. 801–810, 1997.
- [87] M. Ferreras, U. Felbor, T. Lenhard, B. R. Olsen, and J. Delaissé, "Generation and degradation of human endostatin proteins by various proteinases," *FEBS Letters*, vol. 486, no. 3, pp. 247–251, 2000.
- [88] B. Fingleton, "MMPs as therapeutic targets—still a viable option?," *Seminars in Cell & Developmental Biology*, vol. 19, no. 1, pp. 61–68, 2008.
- [89] J. A. Jacobsen, J. L. Major Jourden, M. T. Miller, and S. M. Cohen, "To bind zinc or not to bind zinc: an examination of innovative approaches to improved metalloproteinase inhibition," *Biochimica et Biophysica Acta*, vol. 2010, pp. 72–94, 2010.
- [90] A. Agrawal, D. Romero-Perez, J. A. Jacobsen, F. J. Villarreal, and S. M. Cohen, "Zinc-binding groups modulate selective inhibition of MMPs," *ChemMedChem*, vol. 3, no. 5, pp. 812–820, 2008.
- [91] A. M. Vignola, L. Riccobono, A. Mirabella et al., "Sputum metalloproteinase-9/tissue inhibitor of metalloproteinase-1 ratio correlates with airflow obstruction in asthma and chronic bronchitis," *American Journal of Respiratory and Critical Care Medicine*, vol. 198, p. 158, 1998.
- [92] Y. Ikenaka, H. Yoshiji, S. Kuriyama et al., "Tissue inhibitor of metalloproteinases-1 (TIMP-1) inhibits tumor growth and angiogenesis in the TIMP-1 transgenic mouse model," *International Journal of Cancer*, vol. 105, no. 3, pp. 340–346, 2003.
- [93] M. J. Reed, T. Koike, E. Sadoun, E. H. Sage, and P. Puolakkainen, "Inhibition of TIMP1 enhances angiogenesis in vivo and cell migration in vitro," *Microvascular Research*, vol. 65, no. 1, pp. 9–17, 2003.
- [94] M. D. Johnson, H. R. Kim, L. Chesler, G. Tsao-Wu, N. Bouck, and P. J. Polverini, "Inhibition of angiogenesis by tissue inhibitor of metalloproteinase," *Journal of Cellular Physiology*, vol. 160, no. 1, pp. 194–202, 1994.
- [95] U. P. Thorgeirsson, H. Yoshiji, C. C. Sinha, and D. E. Gomez, "Breast cancer; tumor neovasculature and the effect of tissue inhibitor of metalloproteinases-1 (TIMP-1) on angiogenesis," *In vivo*, vol. 10, pp. 137–144, 1996.
- [96] W. G. Stetler-Stevenson, "The tumor microenvironment: regulation by MMP-independent effects of tissue inhibitor of metalloproteinases-2," *Cancer Metastasis Reviews*, vol. 27, no. 1, pp. 57–66, 2008.
- [97] S. D. Shapiro, E. J. Campbell, D. K. Kobayashi, and H. G. Welgus, "Dexamethasone selectively modulates basal and lipopolysaccharide-induced metalloproteinase and tissue inhibitor of metalloproteinase production by human alveolar macrophages," *Journal of Immunology*, vol. 146, pp. 2724–2729, 1991.
- [98] M. Hoshino, M. Takahashi, Y. Takai, and J. Sim, "Inhaled corticosteroids decrease subepithelial collagen deposition by modulation of the balance between matrix metalloproteinase-9 and tissue inhibitor of metalloproteinase-1 expression in asthma," *The Journal of Allergy and Clinical Immunology*, vol. 104, no. 2, pp. 356–363, 1999.
- [99] Y. Sun, J. Wang, H. Li, L. Sun, Y. Wang, and X. Han, "The effects of budesonide on angiogenesis in a murine asthma model," *Archives of medical science : AMS*, vol. 2, no. 2, pp. 361–367, 2013.
- [100] B. N. Feltis, D. Wignarajah, D. W. Reid, C. Ward, R. Harding, and E. H. Walters, "Effects of inhaled fluticasone on angiogenesis and vascular endothelial growth factor in asthma," *Thorax*, vol. 62, no. 4, pp. 314–319, 2007.
- [101] D. Ribatti, I. Puxeddu, E. Crivellato, B. Nico, A. Vacca, and F. Levi-Schaffer, "Angiogenesis in asthma," *Clinical and experimental allergy*, vol. 2009, p. 39, 2009.
- [102] M. Jakkula, T. D. Le Cras, S. Gebb et al., "Inhibition of angiogenesis decreases alveolarization in the developing rat lung," *Lung cellular and molecular physiology*, vol. 279, no. 3, pp. L600–L607, 2000.
- [103] A. Chetta, E. Marangio, and D. Olivieri, "Inhaled steroids and airway remodelling in asthma," *Acta bio-medica: Atenei Parmensis*, vol. 74, no. 3, pp. 121–125, 2003.
- [104] K. Wang, C. T. Liu, Y. H. Wu, Y. L. Feng, and H. L. Bai, "Budesonide/formoterol decreases expression of vascular endothelial growth factor (VEGF) and VEGF receptor 1 within airway remodelling in asthma," *Advances in Therapy*, vol. 25, no. 4, pp. 342–354, 2008.

Research Article

Genes Induced by Panax Notoginseng in a Rodent Model of Ischemia-Reperfusion Injury

Lanqing Meng ^{1,2}, Qing Huang ^{2,3}, Xuebin Li ², Ping Liang ⁴, Yueyong Li ⁵, Xiaohua Huang ^{1,2}, Jingjie Zhao ⁶, Qiuping Chen ⁷, Rong Qiu ^{3,8,9}, Lan Li ^{3,8}, Chongdong Jian ², Hongfei Yao ³, Jianmin Huang ², Xionglin Tang ², Zechen Wang ^{3,8}, Zhongheng Wei ^{5,8}, Jun Wu ⁹, Liuzhi Wei ^{8,10}, Qiuju Wei ^{8,10}, Qianli Tang ⁸, Lu Huang ^{3,8,9}, Jihua Wei ¹¹, Dinggui Lu ¹¹, Qunqiang Luo ¹¹, Kegong Xie ¹¹, Yang Ouyang ², Jian Chen ^{3,11}, Genliang Li ¹², Linxue Luo ¹³, Linbo He ¹⁴, Chenyi Zhuo ¹⁵, Anding Xu ¹ and Lingzhang Meng ⁸

¹Jinan University, Guangzhou City, Guangdong Province, China

²Department of Neurology, Affiliated Hospital of Youjiang Medical University for Nationalities, Baise City, Guangxi Province, China

³Graduate School of Youjiang Medical University for Nationalities, Baise City, Guangxi Province, China

⁴Department of Neurology, The First People's Hospital of Yulin, Yulin City, Guangxi Province, China

⁵Department of Interventional Medicine, Affiliated Hospital of Youjiang Medical University for Nationalities, Baise City, Guangxi Province, China

⁶Life Science and Clinical Research Center, Affiliated Hospital of Youjiang Medical University for Nationalities, Baise City, Guangxi Province, China

⁷Department of Rehabilitation Medicine, Affiliated Hospital of Youjiang Medical University for Nationalities, Baise City, Guangxi Province, China

⁸Center for Systemic Inflammation Research (CSIR), School of Preclinical Medicine, Youjiang Medical University for Nationalities, Baise City, Guangxi Province, China

⁹Urinary Surgery Department, Affiliated Hospital of Youjiang Medical University for Nationalities, Baise City, Guangxi Province, China

¹⁰College of Pharmacy, Youjiang Medical University for Nationalities, Baise City, Guangxi Province, China

¹¹Trauma Center, Affiliated Hospital of Youjiang Medical University for Nationalities, Baise City, Guangxi Province, China

¹²Department of Biochemistry and Molecular Biology, Youjiang Medical University for Nationalities, Baise City, Guangxi Province, China

¹³Department of Gynaecology and Obstetrics, Affiliated Hospital of Youjiang Medical University for Nationalities, Baise City, Guangxi Province, China

¹⁴Shangsi People's Hospital, Fangchenggang City, Guangxi Province, China

¹⁵Department of Hepatological Surgery, Affiliated Hospital of Youjiang Medical University for Nationalities, Baise City, Guangxi Province, China

Correspondence should be addressed to Anding Xu; tlil@jnu.edu.cn and Lingzhang Meng; lingzhang.meng@ymcn.edu.cn

Received 13 September 2020; Revised 15 October 2020; Accepted 19 October 2020; Published 26 November 2020

Academic Editor: Jian Song

Copyright © 2020 Lanqing Meng et al. This is an open access article distributed under the Creative Commons Attribution License, which permits unrestricted use, distribution, and reproduction in any medium, provided the original work is properly cited.

Stroke is a cerebrovascular disease that results in decreased blood flow. Although Panax notoginseng (PN), a Chinese herbal medicine, has been proven to promote stroke recovery, its molecular mechanism remains unclear. In this study, middle cerebral artery occlusion (MCAO) was induced in rats with thrombi generated by thread and subsequently treated with PN. After that, staining with 2,3,5-triphenyltetrazolium chloride was employed to evaluate the infarcted area, and electron microscopy was used to assess ultrastructural changes of the neurovascular unit. RNA-Seq was performed to determine the differential expressed

genes (DEGs) which were then verified by qPCR. In total, 817 DEGs were identified to be related to the therapeutic effect of PN on stroke recovery. Further analysis by Gene Ontology analysis and Kyoto Encyclopedia of Genes and Genomes revealed that most of these genes were involved in the biological function of nerves and blood vessels through the regulation of neuroactive live receptor interactions of PI3K-Akt, Rap1, cAMP, and cGMP-PKG signaling, which included in the 18 pathways identified in our research, of which, 9 were reported firstly that related to PN's neuroprotective effect. This research sheds light on the potential molecular mechanisms underlying the effects of PN on stroke recovery.

1. Introduction

Stroke is a major cause of death in the world, and it can also lead to long-term disability [1]. Ischemic stroke is due to cerebral artery occlusion, which interrupts the blood supply of the brain, resulting in hypoxia and a lack of nutrients, proceeded by a series of complex pathological changes. A common feature of ischemic stroke is cerebral ischemia and reperfusion injury (CIRI) which results in serious damage (Eltzschig and Eckle, 2011), including pathological processes such as excitatory glutamate toxicity, energy failure, free radical formation, oxidative stress, inflammatory response, Ca^{2+} overload, and apoptosis [2]. The concept of neurovascular unit (NVU) was first recognized in 2001, and alterations in the composition of the NVU have been shown to increase vulnerability to the damaging effects of ischemic stroke [3]. While the NVU has become an integral component in the study of biomarkers of ischemic stroke [4], effective neuroprotective drug targets in CIRI are yet to be determined.

Panax notoginseng is a precious Chinese herbal medicine, which is grown mainly in Wenshan Prefecture, Yunnan Province, China. It has been reported that at least twenty saponins were contained in this material, including notoginsenoside R1, ginsenoside Rb1, and ginsenoside Rg1 [5, 6]. It is anti-inflammatory and antioxidative, and it is able to regulate the balance of neurotransmitters and promoting the regeneration of nerves and blood vessels [7–9]. Our previous studies have shown that *Panax notoginseng* saponins (PNS), an extract of PN, have both anti-inflammatory and neuroprotective effects [10]. Previously, it has been reported that PN exerted neuroprotective effect in stroke through antioxidative and anti-inflammatory properties [11]; in combination with *Angelica sinensis*, it could also inhibit NF- κ B signaling and DNA binding activity, downregulate NO, NLRP3 inflammasome formation, and influence microglial pyroptosis [12, 13]. PN may also influence the expression of Nogo-A, NgR, and p75, regulate NgR1/RhoA/Rock2 pathway, thus contribute to the recovery of nerve function in stroke [14, 15]. However, further studies need to be conducted to explore underlying mechanism(s) of PN's protective effects on NVU, especially in stroke.

In this study, we first evaluated the effect of PN on the ultrastructure of the NVU, and then used the RNA-sequencing methods to study the gene expression changes caused by PN on the brain ischemia-reperfusion injury rats. The differentially expressed genes (DEGs) and their signal pathways were also examined in an attempt to gain a better understanding of all the biochemical mechanisms involved in this process.

2. Materials and Methods

2.1. Animal and Experimental Design. Sprague-Dawley (SD) female rats (250 ± 30 g) were purchased from Changsha Tianqin Biotechnology Co., Ltd, (Hunan, China). Before the experiments, all rats were maintained under standard laboratory conditions (a 12:12 hours of day and night cycle, a relative humidity of $60 \pm 5\%$ at room temperature of $22 \pm 2^\circ\text{C}$ and free access to food and water). This research was approved by the Animal Experimental Ethics Committee of Youjiang Medical University for Nationalities.

The middle cerebral artery occlusion (MCAO) model has been described in detail [16]. Briefly, we exposed the right internal and external carotid arteries; then, we cut external carotid artery about 3 mm above the common carotid artery bifurcation. After a silk suture was tied around the external carotid stump, a nylon filament (diameter: 0.265 mm, rounded tip, dipped in heparin) was then inserted into the external carotid artery and gently advanced into the internal carotid artery, 17–19 mm from the carotid bifurcation until a detection of slight resistance. A nylon thread was then tied into the vascular lumen. After sterilization, suture incision and following 2 h of ischemia, the thrombus was pulled out for about 1 cm to complete reperfusion injury. Rats in the sham group underwent the same surgical procedures except for the nylon thread procedure. The ambient temperature was kept constant by maintaining the rectal temperature in the rats at $37 \pm 1^\circ\text{C}$.

After being allowed to adapt to the environment for 7 days, at least 10 animals were randomly distributed in each group. The intervention group was administrated with PN (Sigma-Aldrich, #1291719) intragastrically at a dose of 100 mg/kg-1 every 12 hours. The dose in this study was chosen based on previous study [13] and our preliminary experiments. Basically, 3 groups were designed in our study: the Sham group, the MCAO group which treated with saline for 7 days, and the MCAO group which treated with PN for 7 days. Both saline and PN administration started 2 hours after surgery. All rats were fasted but allowed free access to water.

2.2. Evaluation of Neurological Defects. Neurobehavioral impairment of rats was assessed in a double-blind manner by two independent observers according to Longa's [16]. Detailed information of this evaluation method was summarized in the supplementary table (available here).

The rats with 1–3 points were considered as successful modeling for I/R injury and were scored again for validation 7 days after surgery.

After 7 days, 6 rats were selected from each group and anesthetized. The rats in this study were anesthetized by IP injection of Ketamine (80 mg/kg) and Xylazine (8 mg/kg);

supplemental heat was provided to avoid hypothermia during anesthesia, according to IACUC guidelines [17, 18]. Brain tissue was separated rapidly, and the area of cerebral infarction was measured using 2,3,5-triphenyltetrazolium chloride (TTC) staining in order to show the impaired area of cerebral ischemia.

2.3. Ultrastructural Changes of NVU [19, 20]. 7 days after the procedure, the cortex around the ischemic focus (1 mm × 1 mm × 1 mm) was immersed in 2.5% glutaraldehyde for 2-4 hours and washed 3 times with 0.1 M phosphate buffer (pH 7.4) for 15 minutes. The samples were fixed in osmic acid for 2 hours at room temperature, washed 3 times with 0.1 M phosphate buffer (pH 7.4) for 15 minutes, and fixed and stored at 4°C. Subsequently, samples were dehydrated in an alcohol gradient (50%-70%-80%-90%-95%-100%-100% ethanol-100% acetone-100% acetone) and embedded in EPON 812 epoxy resin. Ultrathin sections of 50 nm were stained with 3% saturated solution of uranyl acetate and 6% lead citrate staining solution. The ultrastructure of neurons, astrocytes, and endothelial cells was observed using a JEOL-1011 transmission electron microscope (JEOL, Japan) at 80 kV.

2.4. RNA Extraction, Library Construction, and Sequencing. According to the manufacturer's protocol, total RNA was extracted with Trizol kit (Invitrogen, USA). RNA quality was evaluated on the Agilent 2100 Bioanalyzer (Agilent Technologies, USA) and verified by RNase-free agarose gel electrophoresis. After extraction, oligo (dT) beads were used to enrich eukaryotic mRNA; then, Ribo-Zero™ magnetic kit (Epicentre, USA) was used to remove rRNA.

The mRNA acquired above was treated with fragmentation buffer, then reverse transcribed into cDNA. Second-strand cDNA was synthesized with DNA polymerase I, RNase H, and dNTP, and then purified with a QiaQuick PCR extraction kit (Qiagen, Netherlands); end-repaired, poly(A) tails were added and ligated to Illumina sequencing adapters. The ligation products were separated and selected based on size with agarose gel electrophoresis, and PCR amplification and sequencing were performed with Illumina HiSeq2500.

2.5. Assembling and Processing Sequencing Raw Data. Clean readings were obtained by removing reads which contain adapters, those with more than 10% of unknown nucleotides (N) and low-quality reads containing more than 50% of low quality (Q value ≤ 20) bases. Using StringTie v1.3.1 [21, 22], transcripts were assembled from sequenced raw data processed by the HISAT2. 2.4 [23] method. For each transcription region, a fragment per kilobase of transcript per million mapped reads (FPKM) [24] value was calculated to quantify its expression abundance and variation, using the StringTie software.

2.6. Differentially Expressed Genes. RNAs differential expression analysis was performed by using DESeq2 [25] software between two different groups (and by edge R [26] between two samples). The genes with a false discovery rate (FDR) below 0.05 and an absolute fold-change ≥ 2 were considered

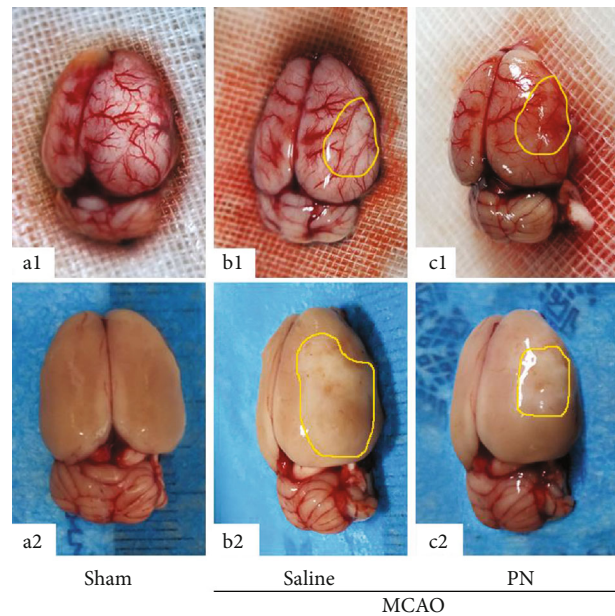


FIGURE 1: Brain tissue samples of rats from each group. (a) Sham group, (a1) cerebral vessels are abundant and clearly visible, (a2) brain tissue is full and symmetrical. (b) MCAO group treated with saline, (b1) blood vessels around the infarction show exudation, blocked blood vessels are seen to be collapsed and atrophied, and (b2) brain tissue is swollen and white. (c) MCAO group treated with PN, (c1) blood vessels around the infarction are mostly new, with less exudation than MCAO group and (c2) brain tissue is not swollen obviously. The yellow lines indicate the infarct area. Similar experiments were performed at least 5 times.

to be DEGs. qPCR was performed in order to verify the expression of these screened DEGs between the different groups.

2.7. Validation of the RNA-Sequencing Results by qPCR. To verify the reliability of sequencing results, qPCR was used to verify gene expression in the same batches of MCAO and PN samples ($n = 6$), and β -actin was used as an internal reference. The 20 μ L reaction system contained 5 μ L of cDNA, 0.5 μ L of each primer, 0.5 μ L 2 x SYBR Green qPCR SuperMix (Invitrogen), and 4 μ L dH₂O, and the reaction conditions were as follows: 50°C for 2 min, 95°C for 2 min, 95°C for 15 s, and 60°C for 32 s plate read for 40 cycles followed by melting curve analysis (60°C to 95°C). The $2^{-\Delta\Delta Ct}$ method was used to determine the relative amount of mRNA, and 3 measurements were made for each sample. Primers used for Ctn amplification are 5'-ATGTGGAAA GCTTCAGCAGGCC-3' (forward) and 5'-TCACGGCA CT CCGGACCCAA-3' (reversed); primers used for Cxcl1 amplification are 5'-AAATGGTGAAGGTCGGTGTGAA-3' (forward) and 5'-CAACAATCTC CACTTTGCCACTG-3' (reversed); primers used for Snap25 amplification are 5'-AGGACTTTGGTTATGTTGGAT-3' (forward) and 5'-GATTTAAGCTTGTT ACAGG-3' (reversed); primers used for Nox1 amplification are 5'-CTTTAGCATCCATA TCCGCATT-3' (forward) and 5'-GACTGGTGGCATG

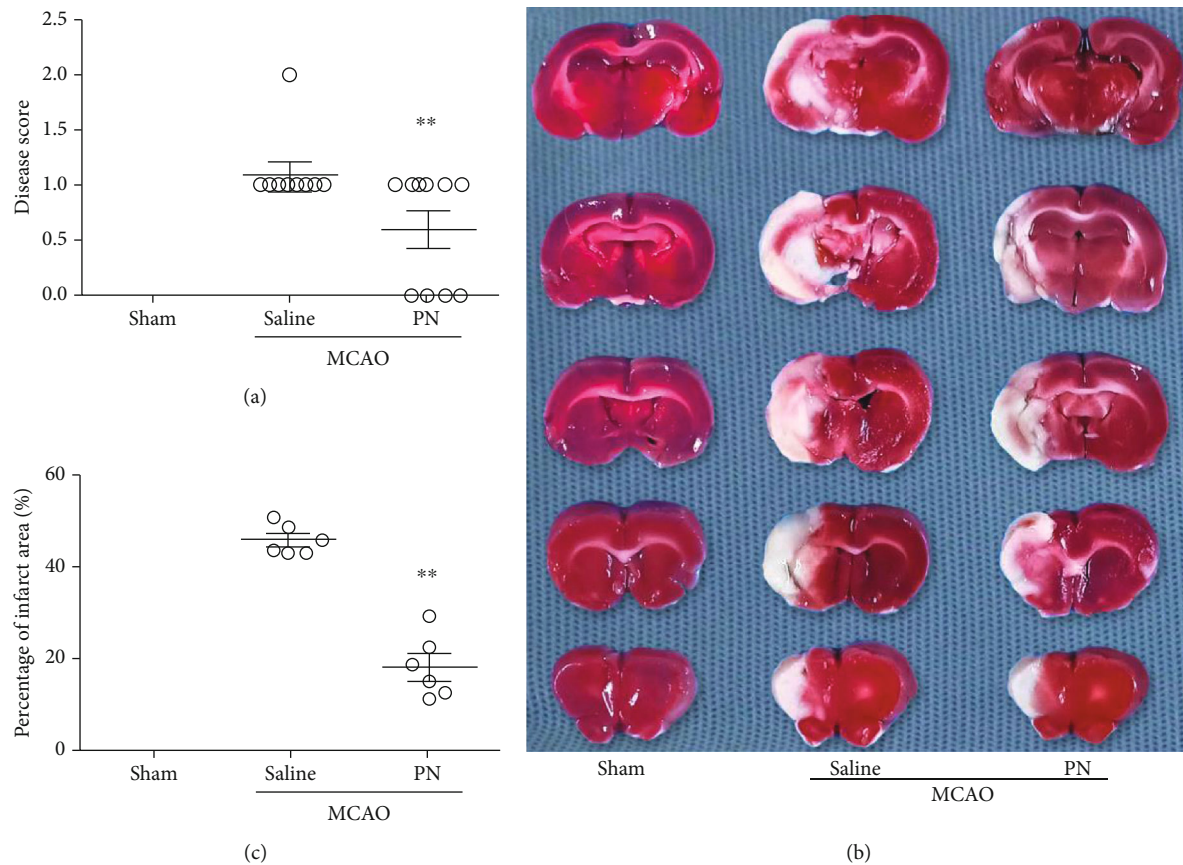


FIGURE 2: The effects of PN on MCAO in rat infarction volume. (a) Compared with the MCAO group treated with saline, scores of neural function were decreased in the PN group ($n = 10$ in each group). (b) TTC staining, normal tissues are red and infarcted tissues are white. PN can effectively reduce the range of cerebral infarction in rats. (c) Compared with MCAO group, the infarct area and percentage in the PN group decreased significantly ($n = 6$ in each group). In (a) and (c), data shown indicated as mean \pm SEM values. Similar experiments were performed at least 3 times. * $P < 0.05$; ** $P < 0.01$; *** $P < 0.001$.

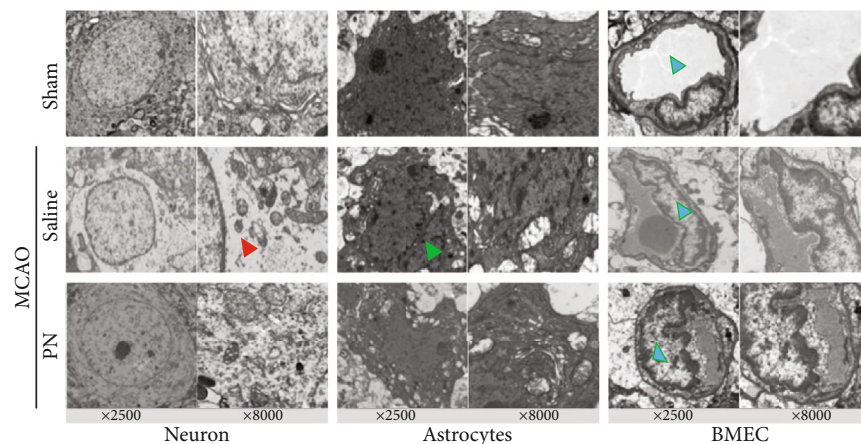


FIGURE 3: The effect of PN on ultrastructural changes of NVU. Similar experiments were performed at least 4 times. BMEC represents brain microvascular endothelial cell. The red triangle indicates a severe swollen/inflammation around neuron, the green triangle indicates an irregular nucleus. The blue triangle indicates the lumen side of brain microvascular.

TC ACAATA-3' (reversed); primers used for Bcl2 amplification are 5'-ACGAGTGG GATACTGGAGATG-3' (forward) and 5'-TAGCGACGAGAGAAGTCATCC-3' (reversed);

primers used for Kdr amplification are 5'-TCACGGTTGGG CTACTGC-3' (forward) and 5'-AGACCTTCTGCCATCA CG-3' (reversed); primers used for Foxo3 amplification are

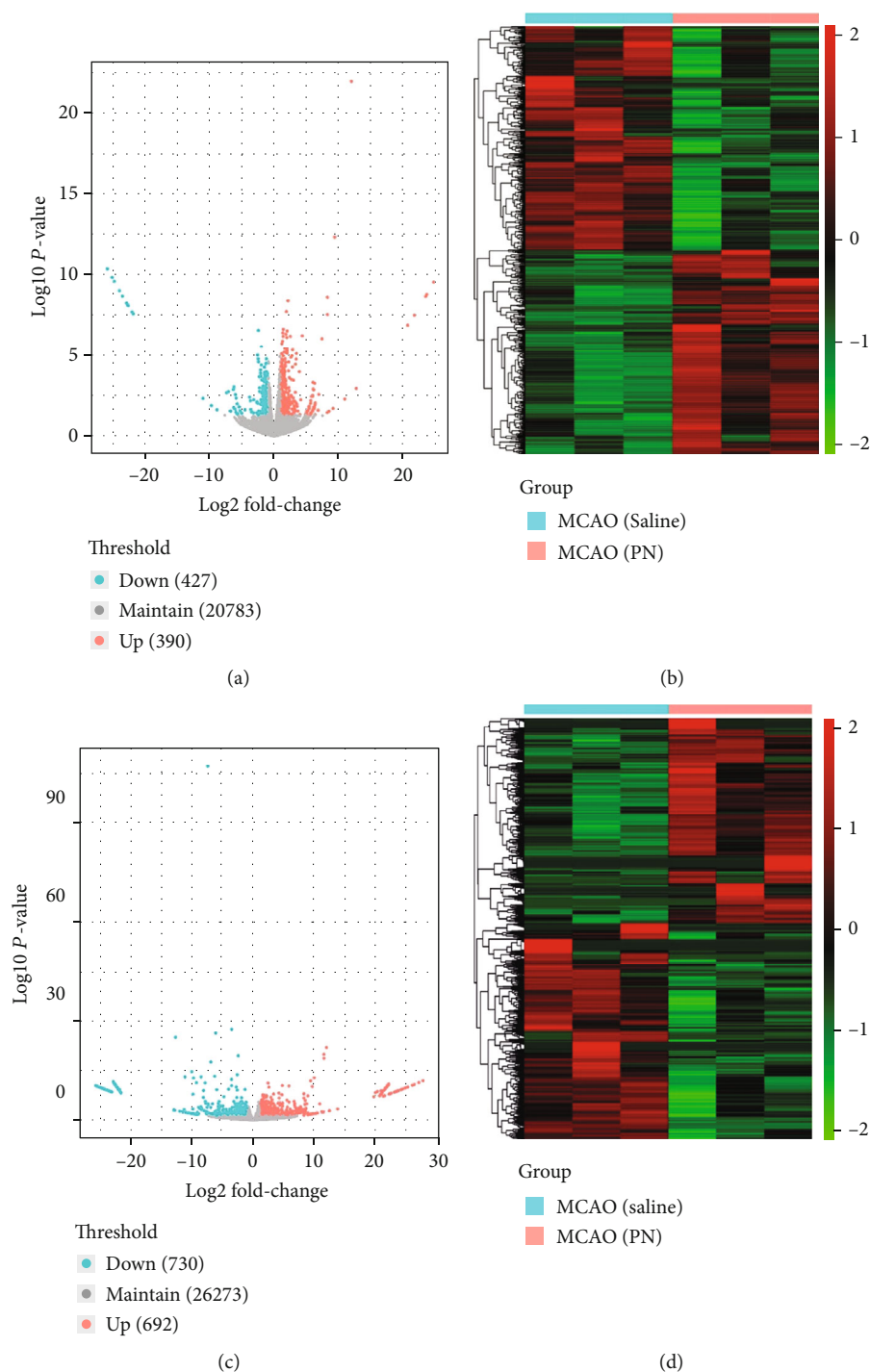


FIGURE 4: Volcano plots and hierarchical clustering heat map of DEGs and DETs. (a) Volcano map for DEGs where red represents upregulated genes and green represents downregulated genes. (b) Heat map for hierarchical clustering of DEGs. (c) Volcano map for DETs, red represents upregulated transcripts, and green represents downregulated transcripts. (d) Heat map for hierarchical clustering of DETs). $n = 3$ in each group.

5'-TGGATGACCTGCTAGATAACAT-3' (forward) and 5'-AACACGGTACTGTTAAAGGAGC-3' (reversed); primers used for Notch3 amplification are 5'-GCTGGCGTCTCTTCACAACA-3' (forward) and 5'-TGGTCGCGCAGTACTCTTAT-3' (reversed); primers used for β -actin (reference gene used in this study) amplification are 5'-AGGAAATCG

TGCGTGACAT-3' (forward) and 5'-GAACCGCTCATTGCGATAG-3' (reversed).

2.8. Enrichment Analysis of DEGs. In order to understand the biological functions and pathways of DEGs in rat cerebral ischemia after PN intervention, we used an annotation and

TABLE 1: The partially DEGs from RNA-Seq [MCAO(Saline)/MCAO(PN)].

Ensembl gene ID	Gene symbol	Log2-fold change	P value	P adj	Style
ENSRNOG00000050994	Ctnn	12.67967226	0.001172369	0.104286972	Up
ENSRNOG00000002802	Cxcl1	2.948761024	0.007257485	0.253659663	Up
ENSRNOG00000006037	Snap25	1.675988534	0.0003127	0.046747614	Up
ENSRNOG00000048706	Nox1	1.96651	0.011922266	0.31373928	Up
ENSRNOG00000002791	Bcl2	-1.777692036	0.003557504	0.176645472	Down
ENSRNOG00000046829	Kdr	-1.524693848	0.000278591	0.044899468	Down
ENSRNOG00000000299	Foxo3	-1.159297737	0.035026006	0.476124441	Down
ENSRNOG00000004346	Notch3	-1.450412508	0.014108102	0.337843688	Down

TABLE 2: The partially DETs from RNA-Seq [MCAO(Saline)/MCAO(PN)].

Transcript ID	Gene ID	Gene symbol	Log2-fold change	P value	P adj	Style
ENSRNOT00000000508	ENSRNOG00000000439	Ager	3.050138008	0.022180829	0.401239754	Up
ENSRNOT00000000553	ENSRNOG00000000473	Pfdn6	2.208199784	0.002663896	0.121543007	Up
ENSRNOT00000000657	ENSRNOG00000000546	Nt5dc1	1.080452666	0.036038318	0.50948505	Up
ENSRNOT00000000817	ENSRNOG00000000657	Nek7	3.035450677	0.001253867	0.070869068	Up
ENSRNOT00000002487	ENSRNOG00000001816	Rfc4	1.358324579	0.00530658	0.182793209	Up
ENSRNOT00000000205	ENSRNOG000000024631	Chadl	-1.127386831	0.006102632	0.202410056	Down
ENSRNOT00000000824	ENSRNOG00000000661	Hps4	-2.446591496	0.004995283	0.177592248	Down
ENSRNOT00000001185	ENSRNOG00000000886	Caln1	-1.460830778	0.015749777	0.338238335	Down
ENSRNOT00000001248	ENSRNOG00000000940	Flt1	-1.41782469	0.001002321	0.059826058	Down
ENSRNOT00000001479	ENSRNOG00000001117	Fbx18	-1.477639058	0.020547561	0.386592868	Down

visualization integrated OmicShare cloud platform to analyze and visualize the biological functions and pathways of differential genes.

2.9. Statistical Analysis. All data are expressed as mean \pm SEM, and statistical analysis was performed using the SPSS 22.0 statistical software (IBM, Chicago, Illinois). The experimental data were analyzed by one-way analysis of variance. Student's paired *t*-test was used to compare qPCR results, and *P* values < 0.05 were considered statistically significant. GO Analysis was based on the GO database. Fisher's exact test and multiple comparison test were used to calculate the significance level (*P* value) and false positive rate (FDR) of each function. *P* value < 0.05 was the criterion for significance screening. Pathway analysis was based on the KEGG database, and Fisher's exact test and chi-square test were used for the DEGs. A pathway in which the target gene participated in was analyzed for significance and selected according to *P* value < 0.05 .

3. Results

3.1. The Effects of PN on MCAO in Rats Infarction Volume. In order to evaluate the protective effect of PN on cerebral ischemia, on the seventh day of the experiment, the neurological functions were assessed blindly using the Longa Neurological Severity Score; the brain was removed after anesthesia (Figure 1) and subjected to TTC staining in order to evaluate the scope of infarction (Figure 2). Comparing with the MCAO group treated with saline, PN-treated animals

showed decreased disease score (Figure 2(a)) and significantly less infarct area (Figures 2(b) and 2(c)).

3.2. Ultrastructural Regulation of the NVU after PN Treatment. Ultrastructural changes in the NVU were observed after 7 days of cerebral ischemia. Figure 3 shows in the Sham group the neurons, and astrocytes are clearly visible and have large and rounded nuclei. The microvascular endothelial cells are clear structures without edema around them, and the lumen is normal. At high magnification, the binuclear membrane appears clear and complete with a clear field of view of the integrity of the cell structure. Organelles, such as lysosomes, are distributed throughout the cytoplasm. The surface of vascular endothelial cells is smooth and flat; and the endothelium, basement membrane, and foot processes are in close contact.

In the MCAO group, the neurons and astrocytes are irregular and show an accumulation of chromatin. Cytoplasm lysis and vacuole formation were observed. There appears to be estrogen receptor expansion, mitochondrial bending, disorder, shrinkage, and vacuolation in the cytoplasm. Mitochondrial and other organ-related injuries were more severe than those in the treatment group. Edema around blood vessels is obvious, showing vacuoles or blank areas (Figure 3).

In the PN group, the nuclei of neurons appear more normal with the nuclear membrane being intact, and the nucleoli are visible. The astrocyte structure is more complete than in the MCAO group with the nuclear morphology being more complete and clear, the microvascular endothelial cells are

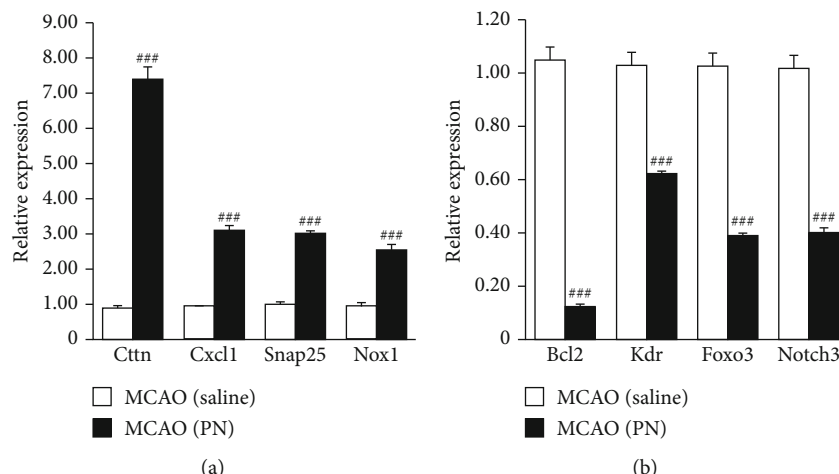


FIGURE 5: Verification of DEGs obtained from RNA-Seq by qPCR. Significance level according to nonparametric test (Cruskal-Wallis test, $n = 6$ in each group). Data shown indicated as mean \pm SEM values. Similar results were obtained from at least 3 independent experiments. * $P < 0.05$; ** $P < 0.01$; *** $P < 0.001$.

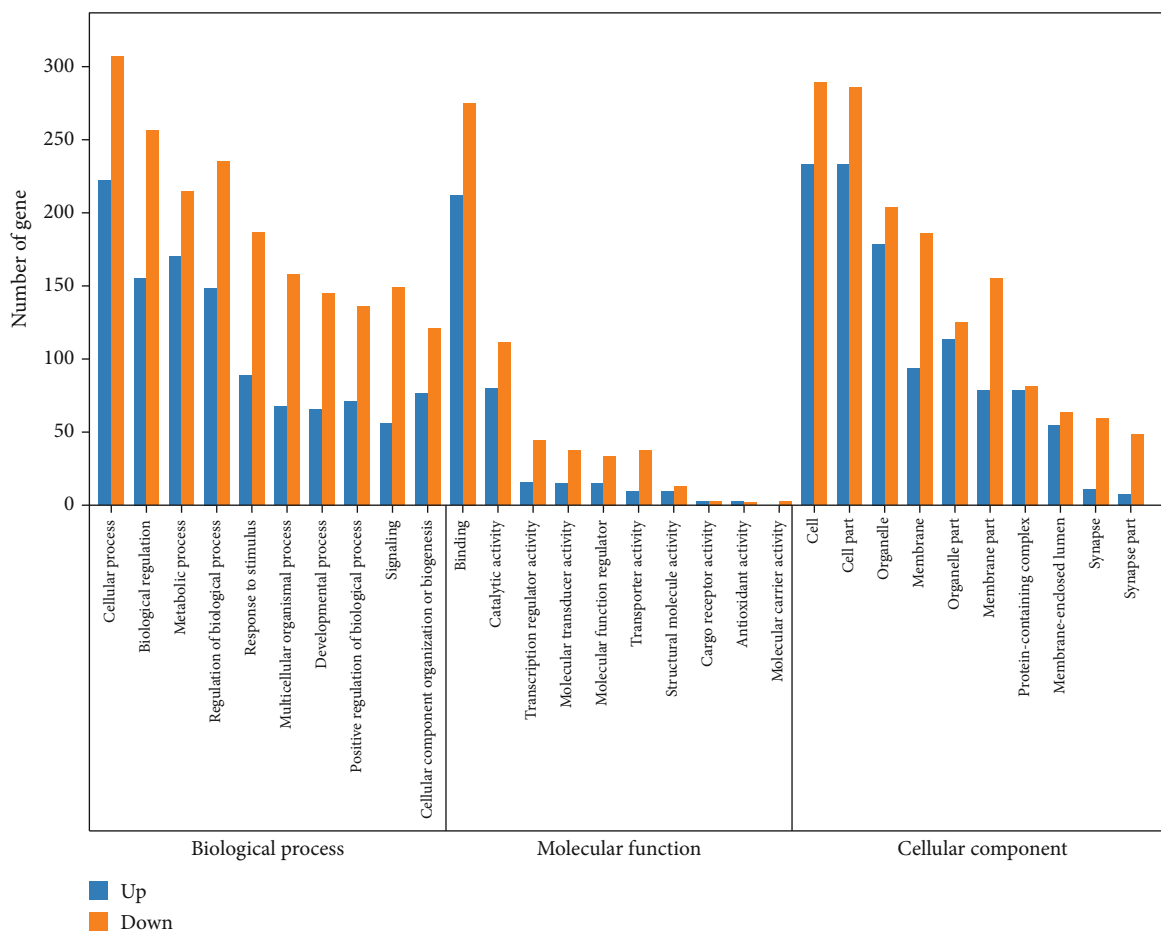


FIGURE 6: Gene ontology enrichment analysis of DEGs. The ordinate is the number of genes, the abscissa is the GO name. Blue refers to the upregulated genes; orange refers to the downregulated genes.

not deformed significantly, and the lumen is basically unobstructed. The peripheral edema is reduced compared with the MCAO group (Figure 3).

3.3. *Gene Expression and Transcript Data Analysis.* To investigate the molecular mechanism of the protective effect of PN on MCAO in rats, brain tissue gene expression profiles of the

TABLE 3: GO classification of DEGs in MCAO(Saline)/MCAO(PN) (Top30).

Term	Description	Type	Count	P value
GO:0031323	Regulation of cellular metabolic process	BP	218	2.85E-06
GO:0001568	Blood vessel development	BP	40	2.99E-06
GO:0001944	Vasculature development	BP	41	3.22E-06
GO:0006836	Neurotransmitter transport	BP	23	3.64E-06
GO:0080090	Regulation of primary metabolic process	BP	213	3.85E-06
GO:0019222	Regulation of metabolic process	BP	230	3.92E-06
GO:0065008	Regulation of biological quality	BP	153	4.21E-06
GO:0072358	Cardiovascular system development	BP	41	4.92E-06
GO:0050905	Neuromuscular process	BP	14	5.87E-06
GO:0007626	Locomotory behavior	BP	20	6.12E-06
GO:0003676	Nucleic acid binding	MF	163	1.31E-06
GO:0097159	Organic cyclic compound binding	MF	233	1.29E-05
GO:1901363	Heterocyclic compound binding	MF	230	1.40E-05
GO:0046872	Metal ion binding	MF	138	1.89E-05
GO:0043169	Cation binding	MF	141	2.04E-05
GO:0005488	Binding	MF	488	5.61E-05
GO:0016263	Ion binding	MF	200	0.002322647
GO:0043565	Sequence-specific DNA binding	MF	53	0.001285424
GO:0003677	DNA binding	MF	85	0.001632778
GO:0003690	Double-stranded DNA binding	MF	44	0.001941181
GO:0045202	Synapse	CC	70	3.86E-08
GO:0044456	Synapse part	CC	55	2.90E-06
GO:0098794	Postsynapse	CC	40	4.36E-06
GO:0098984	Neuron to neuron synapse	CC	23	0.000185124
GO:0005622	Intracellular	CC	454	0.000264158
GO:0045211	Postsynaptic membrane	CC	20	0.000272495
GO:0097060	Synaptic membrane	CC	25	0.000310002
GO:0098978	Blutamatergic synapse	CC	26	0.000423116
GO:0032279	Asymmetric synapse	CC	21	0.000463989
GO:0034707	Chloride channel complex	CC	6	0.000580336

*BP: biological process; MF: molecular function; CC: cellular component; Count: gene number listed in GO term.

Sham, MCAO, and PN groups were measured by using RNA-Seq. A total of 817 DEGs were observed in MCAO group compared to PN group, of which, 390 genes were upregulated and 427 were downregulated (Figures 4(a) and 4(b), Table 1). In addition, there were 1422 differentially expressed transcripts (DETs) which included 692 upregulated and 730 downregulated transcripts (Figures 4(c) and 4(d), Table 2).

3.4. RNA-Seq Validation by qPCR. To verify the expression of the DEGs obtained from the RNA-Seq results between MCAO and PN groups, we randomly selected 8 genes for validation, including 4 upregulated genes (Ctnn, Cxcl1, Snap25, and Nox1) and 4 downregulated genes (Bcl2, Kdr, Foxo3 and Notch3). The relative expression was determined by the $2^{-\Delta\Delta Ct}$ method, and the results were consistent with the expression trends seen during RNA-Seq analysis (Figure 5). The qPCR results were consistent with the sequencing experiments.

3.5. GO and Pathway Analyses. In order to determine the functions and pathways of DEGs and DETs related to PN treatment, we performed GO and pathway analysis. Using $P < 0.01$ identified 332 GO terms, 202 of which were related to nerves and 55 were related to blood vessels, of which the following GO terms: cellular process (GO:0009987), biological regulation (GO:0065007), metabolic process (GO:0008152), regulation of biological process (GO:0050789), response to stimulus (GO:0050896), binding (GO:0005488), catalytic activity (GO:0003824), transcription regulator activity (GO:0140110), molecular transducer activity (GO:0060089), molecular function regulator (GO:0098772), cell (GO:0005623), cell part (GO:0044464), organelle (GO:0043226), membrane (GO:0016020), and organelle part (GO:0044422) were significantly different between saline and PN-treated groups. This indicates that the above biological processes are potentially related to the therapeutic function of PN.

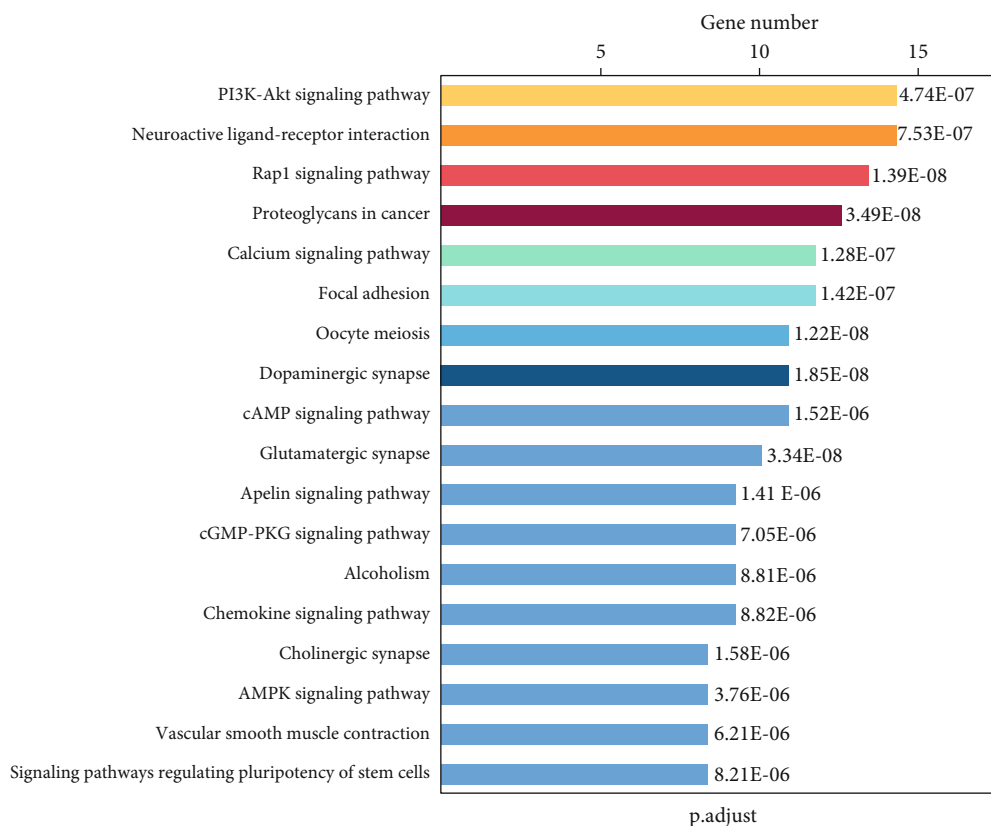


FIGURE 7: The list of top 18 enriched pathway analysis of DEGs.

According to the enrichment degree of functional annotation, the top 10 biological processes, molecular functions, and cellular composition are shown in Figure 6 and Table 3. KEGG pathway analysis leads to a better understanding of the role of PN in the treatment of cerebral ischemia. 39 pathways were screened with *P* values of less than 0.05, of which 18 pathways were enriched with more than 10 genes. These include PI3K-Akt (ko04151), Rap1 (ko04015), neuroactive ligand-receptor interaction (ko04080), calcium (ko04020), focal adhesion (ko04510), oocyte meiosis (ko04114), cAMP (ko04024), glutamatergic synapse (ko04724), dopaminergic synapse (ko04728), apelin (ko04371), cGMP - PKG (ko04022), chemokine (ko04062), cholinergic synapse (ko04725), vascular smooth muscle contraction (ko04270), AMPK (ko04152), and signaling pathways regulating pluripotency of stem cells (ko04550) (Figure 7), and the genes participated in the above pathways were listed in Table 4. These pathways and genes may play an important role in the anti-ischemic effect of PN (Figure 8).

4. Discussion

It has been proven that PN possesses therapeutic properties against stroke, and it has been reported in previous studies about the molecular mechanism(s) explaining PN's clinical outcomes [11–13]. However, most of previous research focused on single a gene/pathway, still no systemic evaluation of PN's molecular mechanism(s) in neuroprotection effect.

In this case, based on a rat stroke model treated with PN, we employed the second generation sequencing technology, which is a high-throughput method, in combination of qPCR and transmission electron microscopy; this study identified 817 DEGs potentially related to PN's neuroprotection effect, and we firstly identified 18 pathways involved in its therapeutic effect.

The development of stroke involves energy metabolism disorder, inflammatory response, free radical formation, calcium overload and apoptosis, and destruction of blood-brain barrier [2]. These adverse factors cause pathological damage to neurons, glial cells, and microvessels in the NVU [27].

In this study, we investigated the protective effect of PN on ischemic stroke in rats. Compared with the MCAO model group, PN treatment can significantly decrease the infarct volume/size in rats with cerebral ischemia and reduce the volume of cerebral infarction as shown by TTC staining. Hence, PN has an anti-ischemic effect. Ultrastructural results show that PN can reduce the pathological changes of the NVU in ischemic stroke.

KEGG pathway analysis showed PN's therapeutic effect involves various pathways such as PI3K-Akt pathway, Neuroactive ligand-receptor interaction, Rap1 signaling pathway, proteoglycans in cancer, calcium signaling pathway, focal adhesion, oocyte meiosis, cAMP signaling pathway, Glutamatergic synapse, Dopaminergic synapse, Apelin signaling pathway, cGMP-PKG signaling pathway, Alcoholism, Chemokine signaling pathway, Cholinergic synapse, Vascular

TABLE 4: A list of the top 18 KEGG pathway DEGs.

Pathway ID	Pathway	Genes
ko04151	PI3K-Akt signaling pathway	Lpar4, Col6a5, Ppp2r3c, Foxo3, Flt1, Bcl2, Gsk3b, Pdpk1, Erbb2, Epha2, Gnb4, Igf1r, Fn1, Kdr, Chrm2, Itga1, Ppp2r2c.
ko04080	Neuroactive ligand-receptor interaction	Rxfp2, Lpar4, Gcgr, Adora2a, Adora1, Apln, Gabrb2, Drd2, Grin2b, Grik3, Aplnr, Adra1a, Oprd1, EdnrB, Cysltr2, Grin2a, Chrm2.
ko04015	Rap1 signaling pathway	Lpar4, Map2k3, Flt1, Adora2a, Rapgef4, Adcy5, Drd2, Grin2b, Epha2, Igf1r, Plce1, Rapgef1, Tln2, Grin2a, Kdr, Adcy1.
ko05205	Proteoglycans in cancer	Rock1, Plaur, Ctnn, Itpr2, Timp3, Pdpk1, Erbb2, Itpr1, Igf1r, Plce1, Fn1, Ank1, Camk2a, Kdr, Fzd3.
ko04020	Calcium signaling pathway	Ppp3r1, Adora2a, Itpr2, Itpkb, Erbb2, Itpr1, Adra1a, EdnrB, Plce1, Cysltr2, Camk2a, Grin2a, Chrm2, A dcy1.
ko04510	Focal adhesion	Col6a5, Rock1, Flt1, Bcl2, Gsk3b, Pdpk1, Erbb2, Igf1r, Fn1, Rapgef1, Shc3, Tln2, Kdr, Itga1.
ko04114	Oocyte meiosis	Rps6ka6, Pttg1, Spdya, Esp11, Fbxo5, Ppp3r1, Itpr2, Adcy5, Itpr1, Igf1r, Camk2a, Cpeb3, Adcy1.
ko04024	cAMP signaling pathway	Rock1, Cfr, Adora2a, Rapgef4, Adcy5, Adora1, Drd2, Grin2b, Plce1, Camk2a, Grin2a, Chrm2, Adcy1.
ko04724	Glutamatergic synapse	Ppp3r1, Arrb1, Itpr2, Adcy5, Itpr1, Grin2b, Grik3, Slc1a3, Shank1, Grin2a, Shank3, Gnb4, Adcy1.
ko04728	Dopaminergic synapse	Ppp2r3c, Itpr2, Adcy5, Gsk3b, Ddc, Itpr1, Drd2, Grin2b, Gnb4, Camk2a, Grin2a, Ppp2r2c.
ko04371	Apelin signaling pathway	Itpr2, Adcy5, Apln, Notch3, Itpr1, Aplnr, Gnb4, Klf2, Hdac4, Acta2, Adcy1.
ko04022	cGMP-PKG signaling pathway	Rock1, Ppp3r1, Itpr2, Adcy5, Adora1, Itpr1, Adra1a, Oprd1, EdnrB, Gucy1a2, Adcy1.
ko05034	Alcoholism	Adora2a, Camkk2, Adcy5, Ddc, Drd2, Grin2b, Gnb4, Shc3, Hdac4, Grin2a, LOC103690190.
ko04062	Chemokine signaling pathway	Cxcl1, Rock1, Foxo3, Adcy5, Gsk3b, Gnb4, Grk5, Cxcl12, Shc3, Arrb1, Adcy1.
ko04725	Cholinergic synapse	Itpr2, Adcy5, Bcl2, Kcnq3, Itpr1, Gnb4, Camk2a, Chrm2, Adcy1, Slc18a3.
ko04270	Vascular smooth muscle contraction	Rock1, Adora2a, Itpr2, Adcy5, Prkch, Itpr1, Adra1a, Gucy1a2, Acta2, Adcy1.
ko04152	AMPK signaling pathway	Ppp2r3c, Cfr, Foxo3, Camkk2, Pdpk1, Adipor2, Adra1a, Scd, Igf1r, Ppp2r2c.
ko04550	Signaling pathways regulating pluripotency of stem cells	Gsk3b, Tbx3, Skil, Lifr, Isl1, Igf1r, Bmpr1, Neurog1, Apc2, Fzd3.

smooth muscle contraction, and AMPK signaling pathway. Nine of which were firstly reported in this research to be related to PN.

It has been reported that PN exerts different molecular mechanisms and pathways related to its neuroprotective effect. Panax notoginseng saponins are the representative bioactive agent of PN extracts, and it is widely used in the treatment of ischemic stroke, probably due to its inhibition of apoptosis *via* upregulation of SIRT1 and antioxidants [28]. PN and its extract are known to have a variety of protective neurovascular mechanisms. For example, PNS protects cerebral microvascular endothelial cells by activating the PI3K/Akt/Nrf2 antioxidant signal pathway [29]. Notoginsenoside R1 plays a neuroprotective role by activating the estrogen receptor-dependent Akt/Nrf2 pathway to inhibit NADPH oxidase activity and mitochondrial dysfunction [30]. Ginsenoside Rb1 can upregulate the expression of GDNF to inhibit neuron apoptosis [31] and promote motor function recovery and axon regeneration in mice after stroke through the cAMP/PKA/CREB signaling pathway [32]. Ginsenoside Rd has been shown to inhibit microglial proteasome activity and inflammatory response [33, 34] through mitochondrial protection, apoptosis inhibition, and energy recov-

ery. Ginsenoside Rg1 can regulate the inhibition of NMDA receptor channels and L-type voltage-dependent calcium channels on Ca^{2+} influx and the decrease of intracellular-free Ca^{2+} caused by it, thus playing a neuroprotective role [2]. Studies have also shown that the cGMP-PKG pathway mediates the proliferation of neural stem cells after cerebral ischemia [35]. Ras-associated protein 1 (Rap1) is known to be involved in integrin and cadherin-mediated adhesion, which can mediate angiogenesis in endothelial cells [36].

In our research, we identified another 9 pathways potentially related to PN's neuroprotective effect, including Neuroactive ligand-receptor interaction, proteoglycans in cancer, focal adhesion, oocyte meiosis, Apelin signaling pathway, Alcoholism, Chemokine signaling pathway, Cholinergic synapse, and Vascular smooth muscle contraction.

Genetically modified animals should be used to confirm the biological/pathological role of these newly identified pathways related to PN's therapeutic effect against stroke.

5. Conclusions

The NVU is the structural and functional unit of the nervous system. Our study shows that PN has a protective effect on

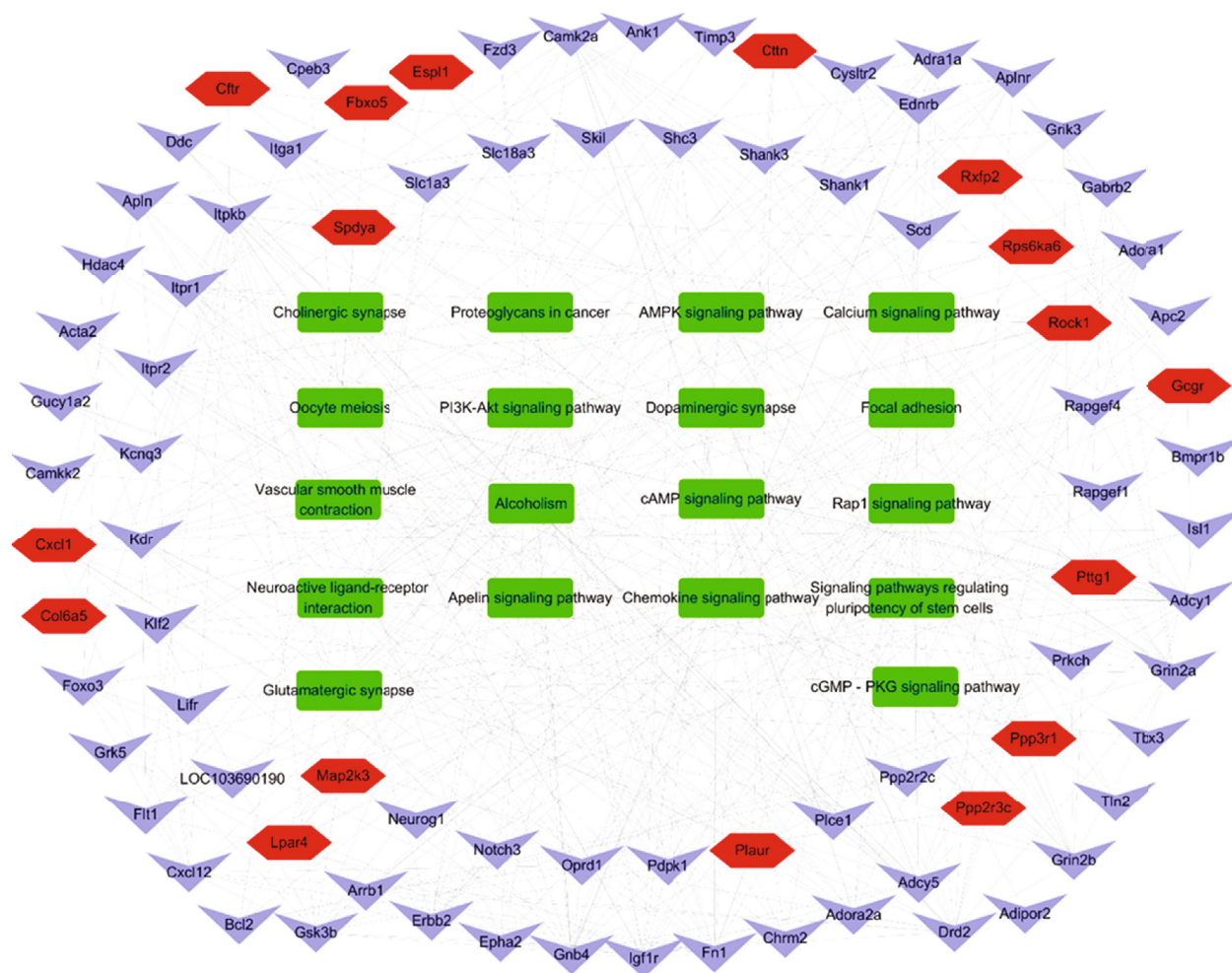


FIGURE 8: The important pathways and gene network map of PN anti-ischemic stroke. Green represents the pathways, purple represents the downregulated genes, and red represents the upregulated genes.

cerebral ischemia by protecting the NVU. The molecular mechanisms involved may include the PI3K-Akt pathway, neuroactive ligand-receptor interactions, Rap1 signaling pathway, cAMP signaling pathway, and cGMP-PKG signaling pathway. The interaction of proteins in these pathways may be potential key targets for our future understanding of the neuroprotective effects of PN in ischemic stroke.

Data Availability

The datasets and code generated or analyzed in this study are available from the corresponding author upon reasonable request.

Ethical Approval

This study was approved by the Ethics Committee of the Affiliated Hospital of Youjiang Medical University for Nationalities (Baise City, Guangxi Province, China), in accordance with the Declaration of Helsinki.

Conflicts of Interest

The authors declare that this research was conducted in the absence of any commercial or financial relationships that could be construed as potential conflicts of interest.

Authors' Contributions

Qing Huang, Lanqing Meng, Xiaohua Huang, Qiuping Chen, and Jingjie Zhao performed the main experiments. Lanqing Meng, Qing Huang, Rong Qiu, Xiaohua Huang, and Jingjie Zhao induced the animal models and collected tissues. Chongdong Jian, Qianli Tang, Jianmin Huang, Linxue Luo, and Xionglin Tang scored the disease. Xuebin Li, Yueyong Li, Jingjie Zhao, LiuZhi Wei, Qiuju Wei, Zechen Wang, and Zhongheng Wei collected data and performed data analysis. Jun Wu, Rong Qiu, Lu Huang, and Lan Li performed the transmission electron microscopy experiments. Liuzhi Wei, Qiuju Wei, Zechen Wang, Linxue Luo, Rong Qiu, Jihua Wei, Genliang Li, and Lu Huang performed RNA abstraction experiments. Yueyong Li, Xuebin Li, and Lingzhang Meng

validated the differential expressed genes by qPCR. Lingzhang Meng and Anding Xu initiated and supervised the project and wrote the manuscript. All the authors approved the final manuscript. Lanqing Meng, Qing Huang, Xuebin Li, Ping Liang, Yueyong Li, Xiaohua Huang, Hongfei Yao, Qiuping Chen, Rong Qiu, Lan Li, Chongdong Jian and Hongfei Yao contributed equally to this study. Ping Liang substantially contributed to the design of the study especially during the initiation of this study, helped greatly establish rat model for this work, and performed part of qPCR experiments for this study. Hongfei Yao search and design most of the primers for qPCR experiments, performed functional assay through KEGG databases, and helped solve some technique problems especially when using the Internet databases.

Acknowledgments

The authors thank all the colleagues for their support and cooperations in this study. The authors would also like to thank Dr Dev Sooranna, Imperial College London, for editing the manuscript. This research was funded by grants from the National Natural Science Foundation of China (Nos. 81660791, 81460614, 81860226, and 81860244), from the Guangxi Natural Science Foundation (Nos. 2019JJA140059, 2019JJA140529, 2019JJA140177, and Z2016419), from the Guangxi Clinic Medicine Research Center of Hepatobiliary Diseases (Nos. AD17129025), from the Special Funding for Guangxi Special Experts (Nos. GRCT[2019]13), and from the Guangxi Zhuang Autonomous Region Health Department Self-financing for Scientific Research Project (Z2012005).

Supplementary Materials

Supplementary Table: Longa's method of evaluation of neurological defects. The severity of neurological defects could be indicated by rat behaviors and was scored from 0 to 4. (*Supplementary Materials*)


References

- [1] E. J. Benjamin, P. Muntner, A. Alonso et al., "Heart disease and stroke Statistics-2019 update: a report from the American Heart Association," *Circulation*, vol. 139, no. 10, pp. e56–e528, 2019.
- [2] W. Xie, P. Zhou, Y. Sun et al., "Protective effects and target network analysis of ginsenoside Rg1 in cerebral ischemia and reperfusion injury: a comprehensive overview of experimental studies," *Cells*, vol. 7, no. 12, p. 270, 2018.
- [3] W. Cai, K. Zhang, P. Li et al., "Dysfunction of the neurovascular unit in ischemic stroke and neurodegenerative diseases: an aging effect," *Ageing Research Reviews*, vol. 34, pp. 77–87, 2017.
- [4] A. Steliga, P. Kowiański, E. Czuba, M. Waśkow, J. Moryś, and G. Lietzau, "Neurovascular Unit as a Source of Ischemic Stroke Biomarkers-Limitations of Experimental Studies and Perspectives for Clinical Application," *Translational stroke research*, vol. 11, 2019.
- [5] Y. C. Loh, C. S. Tan, Y. S. Ch'ng, C. H. Ng, Z. Q. Yeap, and M. F. Yam, "Mechanisms of action of Panax notoginseng ethanolic extract for its vasodilatory effects and partial characterization of vasoactive compounds," *Hypertension Research*, vol. 42, no. 2, pp. 182–194, 2019.
- [6] X. Yang, X. Xiong, H. Wang, and J. Wang, "Protective effects of panax notoginseng saponins on cardiovascular diseases: a comprehensive overview of experimental studies," *Evidence-Based Complementary and Alternative Medicine*, vol. 2014, 13 pages, 2014.
- [7] H. Zhao, Z. Han, G. Li, S. Zhang, and Y. Luo, "Therapeutic Potential and Cellular Mechanisms of Panax Notoginseng on Prevention of Aging and Cell Senescence-Associated Diseases," *Aging and disease*, vol. 8, no. 6, pp. 721–739, 2017.
- [8] Z. Hui, D.-J. Sha, S.-L. Wang et al., "Panaxatriol saponins promotes angiogenesis and enhances cerebral perfusion after ischemic stroke in rats," *BMC Complementary and Alternative Medicine*, vol. 17, no. 1, p. 70, 2017.
- [9] X. Shi, W. Yu, L. Liu et al., "Panax notoginseng saponins administration modulates pro- /anti-inflammatory factor expression and improves neurologic outcome following permanent MCAO in rats," *Metabolic Brain Disease*, vol. 32, no. 1, pp. 221–233, 2017.
- [10] L. Meng, J. Lin, Q. Huang et al., "Panax notoginseng saponins attenuate oxygen–glucose deprivation/ reoxygenation-induced injury in human sh-sy5y cells by regulating the expression of inflammatory factors through miR-155," *Biological & Pharmaceutical Bulletin*, vol. 42, no. 3, pp. 462–467, 2019.
- [11] L. Liu, G. A. Anderson, T. G. Fernandez, and S. Doré, "Efficacy and mechanism of Panax ginseng in experimental stroke," *Frontiers in Neuroscience*, vol. 13, p. 294, 2019.
- [12] J. Hu, C. Zeng, J. Wei et al., "The combination of Panax ginseng and Angelica sinensis alleviates ischemia brain injury by suppressing NLRP3 inflammasome activation and microglial pyroptosis," *Phytomedicine*, vol. 76, p. 153251, 2020.
- [13] V. Rastogi, J. Santiago-Moreno, and S. Doré, "Ginseng: a promising neuroprotective strategy in stroke," *Frontiers in Cellular Neuroscience*, vol. 8, p. 457, 2014.
- [14] L. Liu, L. Zhu, Y. Zou et al., "Panax notoginseng saponins promotes stroke recovery by influencing expression of Nogo-A, NgR and p75NGF, in vitro and in vivo," *Biological & Pharmaceutical Bulletin*, vol. 37, no. 4, pp. 560–568, 2014.
- [15] X. Shi, W. Yu, T. Yang et al., "Panax notoginseng saponins provide neuroprotection by regulating NgR1/RhoA/ROCK2 pathway expression, in vitro and in vivo," *Journal of Ethnopharmacology*, vol. 190, pp. 301–312, 2016.
- [16] E. Z. Longa, P. R. Weinstein, S. Carlson, and R. Cummins, "Reversible middle cerebral artery occlusion without craniectomy in rats," *Stroke*, vol. 20, no. 1, pp. 84–91, 1989.
- [17] S. Mohan and P. L. Foley, "Everything you need to know about satisfying IACUC protocol requirements," *ILAR Journal*, vol. 60, no. 1, pp. 50–57, 2019.
- [18] A. Tsukamoto, N. Niino, M. Sakamoto, R. Ohtani, and T. Inomata, "The validity of anesthetic protocols for the surgical procedure of castration in rats," *Experimental Animals*, vol. 67, no. 3, pp. 329–336, 2018.
- [19] I. Kwon, E. H. Kim, G. J. del Zoppo, and J. H. Heo, "Ultrastructural and temporal changes of the microvascular basement membrane and astrocyte interface following focal cerebral ischemia," *Journal of Neuroscience Research*, vol. 87, no. 3, pp. 668–676, 2009.
- [20] H.-Q. Shi, Y. Zhang, M.-H. Cheng et al., "Sodium sulfide, a hydrogen sulfide-releasing molecule, attenuates acute cerebral ischemia in rats," *CNS Neuroscience & Therapeutics*, vol. 22, no. 7, pp. 625–632, 2016.

- [21] M. Pertea, D. Kim, G. M. Pertea, J. T. Leek, and S. L. Salzberg, "Transcript-level expression analysis of RNA-seq experiments with HISAT, StringTie and Ballgown," *Nature Protocols*, vol. 11, no. 9, pp. 1650–1667, 2016.
- [22] M. Pertea, G. M. Pertea, C. M. Antonescu, T. C. Chang, J. T. Mendell, and S. L. Salzberg, "StringTie enables improved reconstruction of a transcriptome from RNA-seq reads," *Nature Biotechnology*, vol. 33, no. 3, pp. 290–295, 2015.
- [23] D. Kim, B. Langmead, and S. L. Salzberg, "HISAT: a fast spliced aligner with low memory requirements," *Nature Methods*, vol. 12, no. 4, pp. 357–360, 2015.
- [24] A. Mortazavi, B. A. Williams, K. McCue, L. Schaeffer, and B. Wold, "Mapping and quantifying mammalian transcriptomes by RNA-Seq," *Nature Methods*, vol. 5, no. 7, pp. 621–628, 2008.
- [25] M. I. Love, W. Huber, and S. Anders, "Moderated estimation of fold change and dispersion for RNA-seq data with DESeq2," *Genome Biology*, vol. 15, no. 12, 2014.
- [26] M. D. Robinson, D. J. McCarthy, and G. K. Smyth, "edgeR: a Bioconductor package for differential expression analysis of digital gene expression data," *Bioinformatics*, vol. 26, no. 1, pp. 139–140, 2009.
- [27] G. J. del Zoppo, "The neurovascular unit in the setting of stroke," *Journal of Internal Medicine*, vol. 267, no. 2, pp. 156–171, 2010.
- [28] Y. Bo, Z. Jian, S. Zhi-Jun et al., "Panax notoginseng saponins alleviates advanced glycation end product-induced apoptosis by upregulating SIRT1 and antioxidant expression levels in HUVECs," *Experimental and Therapeutic Medicine*, vol. 20, no. 5, 2020.
- [29] S. Hu, Y. Wu, B. Zhao et al., "Panax notoginseng saponins protect cerebral microvascular endothelial cells against oxygen-glucose deprivation/reperfusion-induced barrier dysfunction via activation of PI3K/Akt/Nrf2 antioxidant signaling pathway," *Molecules*, vol. 23, no. 11, p. 2781, 2018.
- [30] W. Xie, T. Zhu, X. Dong et al., "HMGB1-triggered inflammation inhibition of notoginseng leaf triterpenes against cerebral ischemia and reperfusion injury via MAPK and NF- κ B signaling pathways," *Biomolecules*, vol. 9, no. 10, p. 512, 2019.
- [31] Q. L. Yuan, C. X. Yang, P. Xu et al., "Neuroprotective effects of ginsenoside Rb1 on transient cerebral ischemia in rats," *Brain Research*, vol. 1167, no. 1, pp. 1–12, 2007.
- [32] X. Gao, X. Zhang, L. Cui et al., "Ginsenoside Rb1 promotes motor functional recovery and axonal regeneration in post-stroke mice through cAMP/PKA/CREB signaling pathway," *Brain Research Bulletin*, vol. 154, pp. 51–60, 2020.
- [33] D. H. D. W. Kim, D. H. D. W. Kim, B. H. Jung et al., "Ginsenoside Rb2 suppresses the glutamate-mediated oxidative stress and neuronal cell death in HT22 cells," *Journal of Ginseng Research*, vol. 43, no. 2, pp. 326–334, 2019.
- [34] G. Zhang, F. Xia, Y. Zhang et al., "Ginsenoside Rd is efficacious against acute ischemic stroke by suppressing microglial proteasome-mediated inflammation," *Molecular Neurobiology*, vol. 53, no. 4, pp. 2529–2540, 2016.
- [35] X. Huan, C. Oumei, Q. Hongmei, Y. Junxia, M. Xiaojiao, and J. Qingsong, "PDE9 inhibition promotes proliferation of neural stem cells via cGMP-PKG pathway following oxygen-glucose deprivation/reoxygenation injury in vitro," *Neurochemistry International*, vol. 133, p. 104630, 2020.
- [36] G. Carmona, S. Göttig, A. Orlandi et al., "Role of the small GTPase Rap1 for integrin activity regulation in endothelial cells and angiogenesis," *Blood*, vol. 113, no. 2, pp. 488–497, 2009.

Research Article

Effect of SIS3 on Extracellular Matrix Remodeling and Repair in a Lipopolysaccharide-Induced ARDS Rat Model

Qiong Liang,^{1,2} Qiqing Lin,^{1,3} Yueyong Li,^{1,4} Weigui Luo,² Xia Huang,² Yujie Jiang,² Chunyan Qin,² Jin Nong,⁵ Xiang Chen,⁶ Suren Rao Sooranna,⁷ and Liao Pinhu⁵ 

¹The First Clinical Medical College of Jinan University, Guangzhou City, Guangdong Province, China

²Department of Respiratory Medicine, Affiliated Hospital of Youjiang Medical University for Nationalities, Baise City, Guangxi Province, China

³Emergency Department, Affiliated Hospital of Youjiang Medical University for Nationalities, Baise City, Guangxi Province, China

⁴Department of Intervention Medicine, Affiliated Hospital of Youjiang Medical University for Nationalities, Baise City, Guangxi Province, China

⁵Intensive Care Unit, Affiliated Hospital of Youjiang Medical University for Nationalities, Baise City, Guangxi Province, China

⁶Intensive Care Unit, People's Hospital of Guangxi Zhuang Autonomous Region, Nanning City, Guangxi Province, China

⁷Department of Metabolism, Digestion and Reproduction, Imperial College London, Chelsea & Westminster Hospital, 369 Fulham Road London, SW10 9NH, UK

Correspondence should be addressed to Liao Pinhu; liaopinhu@163.com

Received 11 October 2020; Revised 4 November 2020; Accepted 5 November 2020; Published 26 November 2020

Academic Editor: Jian Song

Copyright © 2020 Qiong Liang et al. This is an open access article distributed under the Creative Commons Attribution License, which permits unrestricted use, distribution, and reproduction in any medium, provided the original work is properly cited.

The remodeling of the extracellular matrix (ECM) in the parenchyma plays an important role in the development of acute respiratory distress syndrome (ARDS), a disease characterized by lung injury. Although it is clear that TGF- β 1 can modulate the expression of the extracellular matrix (ECM) through intracellular signaling molecules such as Smad3, its role as a therapeutic target against ARDS remains unknown. In this study, a rat model was established to mimic ARDS via intratracheal instillation of lipopolysaccharide (LPS). A selective inhibitor of Smad3 (SIS3) was intraperitoneally injected into the disease model, while phosphate-buffered saline (PBS) was used in the control group. Animal tissues were then evaluated using histological analysis, immunohistochemistry, RT-qPCR, ELISA, and western blotting. LPS was found to stimulate the expression of RAGE, TGF- β 1, MMP2, and MMP9 in the rat model. Moreover, treatment with SIS3 was observed to reverse the expression of these molecules. In addition, pretreatment with SIS3 was shown to partially inhibit the phosphorylation of Smad3 and alleviate symptoms including lung injury and pulmonary edema. These findings indicate that SIS3, or the blocking of TGF- β /Smad3 pathways, could influence remodeling of the ECM and this may serve as a therapeutic strategy against ARDS.

1. Introduction

Acute respiratory distress syndrome (ARDS) is a diffuse pulmonary parenchymal injury characterized by injury of the pulmonary epithelium and vascular endothelial cells as well as inflammatory infiltration, hyaline membrane formation, matrix repair, and pulmonary interstitial fibrosis. Lipopolysaccharide (LPS) is a major component of the cell walls of gram-negative bacteria that possesses powerful inflammatory effects and plays a significant role in the occurrence and pro-

gression of ARDS [1]. The pathogenesis of ARDS is complex and is a hotspot in the study of pulmonary diseases [2, 3].

Extracellular matrix (ECM) metabolism serves in the regulation of lung function and morphology. ECM remodeling encompasses changes in fibrin collagen, the basement membrane, and elastin. Matrix cells synthesize and secrete extracellular polysaccharides and macromolecules, such as proteins and proteoglycans, which are distributed on the cell surface or between cells, forming a network structure between cells. During the course of ARDS, activated

polymorphonuclear leukocytes (PMNs) and macrophages release various inflammatory cytokines and proteolytic enzymes that degrade the ECM, affecting and changing the functions of the cell and matrix and triggering ECM remodeling. At the same time, proteolytic enzymes released by the PMNs and macrophages can digest alloproteins and damage host proteins, including the ECM.

Proteolytic enzymes also support and establish connections as well as affecting various pathophysiological processes, such as cell shape, metabolism, function, adhesion, proliferation, and differentiation through the cell signaling transduction system [3]. The temporary pulmonary matrix formed following ARDS injury can activate an inflammatory reaction and induce the transformation of epithelial cells into fibroblasts, leading to local connective tissue and continuous matrix remodeling during the repair of lung injury. Intra-alveolar fibrosis (remodeling) can cause alveolar occlusions and eventually a loss of alveolar function [4].

Persistent inflammatory and fibrotic alveolitis and increased inflammation in the early stages of ARDS are the primary mechanisms which lead to alveolar membrane and fibrosis injuries. The resulting persistent inflammatory response can destroy the ECM, leading to changes in a lung structure. Some studies have shown that changes in the fibroplasia in ARDS may be related to persistent inflammation following lung injury, the generation and degradation of the temporary matrix after lung injury, and the change in the lining components of the epithelial cells [5]. According to the extent of ECM remodeling, the injured lung may be completely repaired. However, ECM remodeling disorders can lead to pulmonary fibrosis (PF); therefore, the prognosis for ARDS can be very poor [6].

Receptor for advanced glycation end-products (RAGE), matrix metalloproteinases (MMPs), and tissue inhibitors of metalloproteinases (TIMPs) participate in remodeling of the ECM in ARDS [4]. RAGE is also one of the biomarkers of pulmonary epithelial injury [7, 8] and is a transmembrane and multiligand receptor belonging to the immunoglobulin superfamily. The receptor structure includes three parts: extramembrane, transmembrane, and intracellular membrane domains. RAGE is primarily distributed in type I alveolar epithelial cells, alveolar macrophages, and bronchiole epithelial cells, and it is highly expressed in the lung but low in other organs of the body. RAGE also plays a protective role in the lung, where its activation modulates cell signaling and propagation of the inflammatory response [9]. Overexpression of RAGE can increase alveolar cell apoptosis and inhibit cell proliferation [10]. Moreover, the absence of RAGE in pulmonary epithelial cells can lead to their fibrosis which can, in turn, lead to the occurrence and development of PF [11]. Calfee et al. [12] reported an increase in RAGE plasma levels in patients with severe ARDS, and a relationship between mortality in ARDS patients with high tidal volume ventilation was further established.

MMPs usually play important roles in various pathological conditions, such as wound repair and inflammatory leukocyte infiltration. In destructive lung diseases, it has been reported that MMP1, MMP2, MMP3, MMP7, MMP8, MMP9, MMP10, and MMP12 contribute to tissue injury

[13]. However, in acute lung injury, especially in LPS-induced ARDS, the activation of MMP2 and MMP9 exacerbates pulmonary inflammation [14]. MMP2 can degrade a variety of collagen substrates, and it stimulates the release of vascular endothelial growth factor, thus driving endothelial genesis, and contributes to tissue repair and/or damage, while MMP9 degrades the ECM components such as gelatin, fibronectin, and fibrillin. Uncontrolled synthesis and degradation of the ECM play an important role in various pathological conditions. The pathogenesis of ARDS can lead to expression of MMPs in cells including alveolar epithelial cells, macrophages, neutrophils, and fibroblasts [3, 5, 15]. MMPs are zinc-dependent endopeptidases that are upregulated in most pulmonary inflammatory diseases, which lead to the degradation of the pulmonary ECM [16]. MMPs primarily affect the biological activities of these mediators by degrading the ECM and participating in the lysis of inflammatory cytokines and chemokines secreted into the ECM, thus influencing cell behavior or aggravating lung injury [17, 18]. MMPs, in turn, regulate inflammation by interacting with cytokines and chemokines [19].

The prognosis is affected by cell proliferation and fibrosis-induced PF after ARDS. Many studies have shown that transforming growth factor- β (TGF- β) is related to the repair of posttraumatic fibrosis. TGF- β is produced by monocytes, lymphocytes, epithelial cells, and fibroblasts, and these regulate the proliferation, differentiation, migration, adhesion, and metabolism of the ECM through autocrine or paracrine mechanisms while participating in embryonic development, injury, and repair [20]. TGF- β is highly expressed in injured cells and tissues and is involved in the repair of fibrosis and proliferation of various injuries including ARDS [21, 22]. The longer the duration of highly expressed TGF- β , the more difficult it is to alleviate the clinical manifestations of ARDS. Clinical studies have shown that high levels of TGF- β were associated with more serious cases of ARDS and those with worse prognosis [23].

The most important role of TGF- β 1 in the pathology of PF is the expression of the ECM gene mediated by the molecules referred to as small mothers against decapentaplegic 3 (Smad3). In canonical TGF- β /Smad signaling, the active TGF- β ligand binds to the receptor, T β RII, which then recruits T β RI. TGF- β subsequently triggers a cell response by activating the TGF- β receptor, which triggers the phosphorylation of Smad2 and Smad3 proteins. Phosphorylated Smad2 or 3 can bind with common-mediator Smad (co-Smad) and is translocated into the nucleus to exert its transcriptional activity in order to regulate downstream gene expression [24]. Smad3, unlike Smad2, has been shown to play a profibrotic role in kidney fibrosis [25]. Smad3 directly regulates the expression of various fibrogenic genes, such as those associated with the ECM and TIMPs [26]. Furthermore, Smad3 can also stimulate TGF- β 1 expression to enhance TGF- β /Smad signaling through positive feedback. The prognosis is thereby influenced by cell proliferation following ARDS. Selective inhibitors of Smad3 (SIS3) are synthetic chemicals which strongly inhibit the phosphorylation of Smad3 induced by TGF- β 1 [27]. Recent studies have shown that SIS3 has antifibrotic and anti-inflammatory

effects in bleomycin- (BLM-) induced PF in mice [28]. Evidently, SIS3 attenuates the regulatory mechanism of TGF- β by selectively inhibiting Smad3 [28].

These data illustrate the antifibrotic and anti-inflammatory effects of SIS3 *in vivo*. However, its role in the pathogenesis of ARDS requires further elucidation. It is anticipated that studies into matrix remodeling and repair in ARDS may provide potential intervention indicators for improving the prognosis of ARDS [2, 3].

2. Materials and Methods

2.1. LPS-Induced ARDS Rat Model and Experimental Program. All procedures in this study were conducted in accordance with the guidelines of the National Institute of Health and approved by the Animal Protection and Utilization Committee of the Youjiang Medical University for Nationalities. Six- to eight-week-old male Sprague-Dawley (SD) rats were obtained from the Laboratory Animal Center of the Youjiang Medical University for Nationalities (Baise, Guangxi Province, China) and raised in a pathogen-free environment. A total of 40 adult male SD rats were randomly divided into four groups: a control group (CTL, $n = 10$, no treatment); a ARDS group (ARDS, $n = 10$, intratracheal instillation of 5 mg/kg of LPS, Sigma-Aldrich, St. Louis, MO, USA); and a ARDS and SIS3 group (ARDS + SIS3, $n = 10$, intraperitoneal injection of 2.5 mg/kg of SIS3 [29] for 2 h following 5 mg/kg of LPS intratracheal instillation). The ARDS and phosphate-buffered saline (PBS) group (ARDS + PBS, $n = 10$), the same as in the ARDS + SIS3 group but where an equal amount of PBS replaced the SIS3.

The rats used in this study were anesthetized 24 h after LPS intratracheal instillation, with ketamine at a dose of 80 mg/kg, together with xylazine at a dose of 8 mg/kg, by intraperitoneal injection, as recommended by the IACUC guidelines. 5–8 mL blood biopsies were collected by cardiac puncture under deep terminal anaesthesia with 25 G needled syringes inserted into the left ventricle. Blood biopsies were withdrawn slowly to avoid the heart from collapsing. After taking blood biopsies, the rats were killed by cervical dislocation, and then, the lung tissues were collected.

Following 30 min of coagulation, tubes were centrifuged at 2000 \times g for 20 min and stored at -80°C for subsequent analysis. The bronchoalveolar lavage fluid (BALF) of the left lung was obtained using endotracheal intubation 24 h after LPS intratracheal instillation, and the lung was then washed with PBS (4°C , 15 mL/kg) five times. The flushing fluid was centrifuged at 4°C for 10 min at 1500 \times g, and the supernatant was collected for protein concentration measurements. The sediment was resuspended using 50 μL of PBS, and the number of cells was counted. The right upper lobe was examined via histopathology and immunohistochemistry, and the right part of the middle lobe was weighed to obtain the wet-to-dry (W/D) weight ratio. The rest of the lower lobe of the right lung was preserved at -80°C , and the total RNA and/or protein was isolated. For histopathology and immunohistochemical staining, tissues were fixed in 10% neutral formaldehyde and paraffin embedded, and 4 μm thickness sections were cut. These were either stained with hematoxy-

lin and eosin (HE) or subjected to immunohistochemical staining.

2.2. Masson's Trichrome Staining. A commercial Masson's trichrome staining kit (Solarbio, #G135) was used to perform Masson's staining, considering collagen is the main part of ECM [30]. Briefly, lung biopsies were embedded in paraffin after fixation with 4% buffered paraformaldehyde, and sectioned into 4 μm . After dipping in to Bouin's solution for 2 h at 37°C , the slides were stained with Celestine blue dye for 2 min and Mayer's solution for 3 min. Following an acid ethanol differentiation step for 10 sec, sections were dipped in Lichun red magenta solution for 10 min, phosphomolybdic acid solution for 10 min, aniline blue solution for 5 min, and a weak acid for 2 min. The slides were carefully washed with PBS after each staining procedure. Then, the slides were dipped twice in ethanol for 10 sec each. After two dips of 2 min in xylene, the slides were mounted with Balsam.

2.3. RT-qPCR. Gene expressions for RAGE, TGF- β 1, MMP2, and MMP9 mRNAs from rat lung tissue were evaluated using the FastStart Universal SYBR Green Master (ROX) (Roche, Germany) and real-time PCR. The RNA of the frozen lung tissue was isolated using a total RNA rapid separation kit (Tiangen, China), and the DNA strand was synthesized by using the first-strand cDNA synthesis kit (Thermo Scientific k1622, USA) according to the manufacturer's instructions. All primers used were synthesized by Shenggong (Shanghai, China; Table 1). Following 5 min of initial activation at 95°C , PCR was carried out for 40 cycles at 95°C for 10 s and 60°C for 30 s. Glyceraldehyde-3-phosphate dehydrogenase (GAPDH) was measured simultaneously and used as the housekeeping gene. The threshold cycle (Ct) values were measured as previously described, and the comparative gene expression was calculated using the $2^{-\Delta\Delta\text{Ct}}$ method.

2.4. ELISA. RAGE, TGF- β 1, MMP2, and MMP9 concentrations in the rat sera and BALF were determined using a rat RAGE ELISA kit (EK0971 from Boster Biological Technology, China), a rat TGF- β 1 ELISA kit (MB100B, R&D Systems), a rat MMP2 ELISA kit (MMP200, R&D Systems), and a rat MMP9 ELISA kit (CSB-E08008r Cusabio, Wuhan, China), respectively, following the manufacturer's protocols.

2.5. Lung W/D Ratio Analysis. The ARDS rats were euthanized after 24 h, and the right middle lobe was dissected and weighed. Subsequently, the tissues were dried in an oven at 60°C for 72 h and reweighed. The corresponding W/D weight ratios were then calculated.

2.6. Neutrophil Number. The total cell number and neutrophils in the BALF were counted using a hemocytometer and light microscopy, and the ratio of neutrophils to total cells was calculated.

2.7. Western Blot Analysis. The protein concentration of lung homogenate was measured using bovine serum albumin (BSA) as the standard. Equivalent amounts of total protein (50 μg) were separated on 10–12% SDS-PAGE gels subjected

TABLE 1: The rat primer sequences used in this study.

Gene	GenBank number	Sense primer (5'-3')	Antisense primer (5'-3')
RAGE	G170807E03	ACCTTCAGGCTCAACCAAC	GGGACTCTTCACGCTTCG
TGF- β 1	59086	ACCAAGGAGACGGAATACAGG	AGGTGTTGAGCCCTTCCAG
MMP2	G170807E05	ACCACGGATCTGAGCAAT	TACTGGACCCACGCCTAC
MMP9	G170807E09	TTGGCTTCCTCCGTGATT	CCCTACTGCTGGTCCTTC
β -Actin	G170807E01	GAGAGGGAAATCGTGCGT	GGAGGAAGAGGATGCGC

to electrophoresis and were electrophoretically transferred onto nitrocellulose membranes. These were blocked with 5% milk for 30–60 min and incubated with primary antibodies against RAGE (1 : 500 dilution, Sc365154, Santa Cruz Biotechnology), TGF- β 1 (1 : 1000 dilution, 3711, Cell Signaling Technology), MMP2 (1 : 1000 dilution, GTX104577, Gene Tex), MMP9 (1 : 1000 dilution, 13667, Cell Signaling Technology), Smad3 (1 : 1000 dilution, 9523, Cell Signaling Technology), phospho-Smad3 (1 : 1000 dilution, 9520, Cell Signaling Technology), and GAPDH (1 : 20000 dilution, 10494-1-AP, Proteintech Group) at 4°C overnight. Following primary antibody incubation, membranes were incubated with goat anti-rabbit/rat IgG (1 : 5000 dilution, 9936, Cell Signaling Technology) linked to horseradish peroxidase at room temperature for 60 min. The proteins recognized by the antibody complexes were then visualized using enhanced chemiluminescence (Solarbio, Beijing, China). The optical density of each marker band was analyzed using ImageJ version 1.48 software.

2.8. Immunohistochemistry. 4 μ m thickness paraffin sections were pasted onto slides for conventional dewaxing treatment. The sections were microwaved in a citrate buffer for 15 min (pH 6.0), and endogenous peroxidase was blocked by hydrogen peroxide and goat serum. The slices were then incubated with polyclonal RAGE (1 : 200, Sc365154, Santa Cruz Biotechnology, United Kingdom), TGF- β 1 (1 : 100, BS6152, Bioword Technology, Inc., China), MMP2 (1 : 200, GTX104577, GeneTex, North, America), and MMP9 (1 : 50, BM4089, Boster Biological Technology, China) antibodies overnight at 4°C. The equivalent concentrations of polyclonal nonimmune IgG were used as controls. Then, sections were incubated with secondary HRP-En Vision IgG antibody at room temperature for 20 min and followed by incubation with a streptavidin solution. Color development was carried out using 3,3'-diaminobenzidine tetrahydrochloride.

2.9. HE Staining and Lung Injury Score. The lung tissues were immersed in 4% paraformaldehyde for 24 h and transferred to ethanol, dehydrated through a serial alcohol gradient, and embedded in paraffin wax blocks. 4 μ m thickness lung tissue sections were dewaxed in xylene, which then underwent HE staining. Lung injury was scored according to the following five categories, which were assessed using a rating of 0–2 for each of the following standards: (a) neutrophils in the alveolar space, (b) neutrophils in the interstitial space, (c) hyaline membranes, (d) protein fragments filled with air spaces, and (e) thickening of the alveolar septum. The total

damage score was calculated by the following equation: score = $(20 \times a + 14 \times b + 7 \times c + 7 \times d + 2 \times e) / (\text{number of fields} \times 100)$ [31].

2.10. Statistical Analysis. The data are expressed as the means \pm standard deviations (SD). The statistical analysis was conducted using SPSS 19.0 software and GraphPad Prism 5.0 (San Diego, California, USA). The comparisons between two groups were analyzed using Student's *t*-test. The differences among multiple groups were analyzed using ANOVA. In all cases, $P < 0.05$ was considered to be statistically significant.

3. Results

3.1. LPS-Induced RAGE, TGF- β 1, MMP2, and MMP9 Genes Were Suppressed by SIS3 in the ARDS Rat Model. The expression of RAGE, TGF- β 1, MMP2, and MMP9 mRNA in lung tissues was analyzed using RT-qPCR in the ARDS rat model. Accordingly, RAGE, TGF- β 1, MMP2, and MMP9 mRNA expression was found to be increased in lung homogenates after LPS induction. Meanwhile, the expression of RAGE, TGF- β 1, MMP2, and MMP9 mRNA in lung homogenates was observed to be suppressed by SIS3 ($P < 0.05$ in all cases; Figures 1(a)–1(d)).

3.2. SIS3 Inhibited LPS-Induced RAGE, TGF- β 1, MMP2, and MMP9 Protein Expression in ARDS Rats. Immunohistochemical staining of lung tissue sections showed that RAGE, TGF- β 1, MMP2, and MMP9 were primarily expressed in the cytoplasm of alveolar epithelial cells in normal lung tissues of rats. RAGE, TGF- β 1, MMP2, and MMP9 expression in the ARDS group was observed to be significantly higher than those in the control group. Notably, treatment with SIS3 decreased RAGE, TGF- β 1, MMP2, and MMP9 expression. However, PBS did not affect RAGE, TGF- β 1, MMP2, and MMP9 expression in the ARDS + PBS group of rats (Figure 2).

3.3. SIS3 Relieved Acute Lung Inflammation and Injury in the ARDS Rat Model. HE staining of pathological rat lung tissues demonstrated the presence of clear lung structures, with little or no alveolar and alveolar interstitial inflammatory cell infiltration, no edema, and no erythrocytes or other exudates in the control group. In the ARDS group, lesions were identified to be extensive and primarily manifested as lung edema, hemorrhage, infiltration of neutrophils, alveolar damage, pulmonary interstitial thickening, narrowing of the alveolar

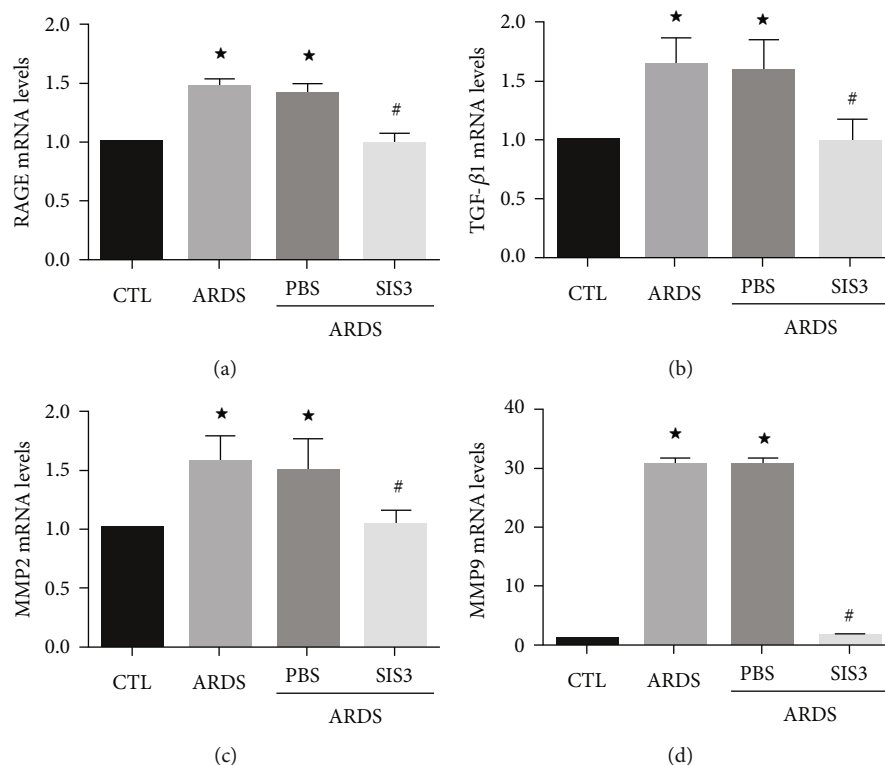


FIGURE 1: SIS3 inhibits mRNA expression of RAGE, TGF- β 1, MMP2, and MMP9 in lung homogenates of ARDS rats. The mRNA levels of RAGE, TGF- β 1, MMP2, and MMP9 were determined using real-time PCR and were standardized to β -actin. The results suggested that SIS3 inhibited the increase of (a) RAGE, (b) TGF- β 1, (c) MMP2, and (d) MMP9 in LPS-induced lung homogenates of ARDS rats, while no effect was seen upon pretreatment with PBS. The data are presented as the means \pm SD ($n = 10$). * $P < 0.05$ vs. CTL; # $P < 0.05$ vs. ARDS.

cavity, and an increasing lung injury score. The pathological changes in the ARDS + SIS3 group were evident by slight edema with a small amount of spotting and sheet hemorrhaging. Lung injury and inflammation (usually characterized by leukocyte infiltration) in the rats were alleviated by the inhibitor of SIS3 (Figure 3(a)). Moreover, the lung injury scores decreased from 0.77 ± 0.01 to 0.54 ± 0.01 (Figure 3(b)), whereas pretreatment with PBS had no effect in ARDS rats.

Rats administered with LPS exhibited an altered alveolar capillary barrier with increased lung W/D weight ratios (Figure 4(a)), upregulated inflammatory responses with an increased number of cells (Figure 4(b)), increased number of neutrophils (Figure 4(c)), and increased neutrophil ratios (Figure 4(d)) in the BALF. As illustrated in Figure 4(a), the W/D ratio of the ARDS group was observed to be $33.7 \pm 4.7\%$ which was higher than that of the control group, indicating the presence of pulmonary edema ($P < 0.05$, $n = 10$). However, the W/D ratio in the ARDS + SIS3 group was $18.3 \pm 2.15\%$, which was lower than that in the ARDS group, indicating that SIS3 attenuated the degree of pulmonary edema induced by LPS ($P < 0.05$ in all cases).

The total number of cells in the BALF was markedly higher in the ARDS group than the control group (control group: $3.31 \pm 0.2 \times 10^5/\text{mL}$, ARDS group: $16.54 \pm 0.33 \times 10^5/\text{mL}$; $P < 0.05$ in all cases). Additionally, the total number of cells in the BALF decreased by $31.2 \pm 1.7\%$ in the ARDS

+SIS3 group when compared to the ARDS group. The number of neutrophils was observed to be higher in the ARDS group than in the control group (control group: $0.93 \pm 0.07 \times 10^5/\text{mL}$, ARDS group: $13.55 \pm 0.29 \times 10^5/\text{mL}$; $P < 0.05$). The number of neutrophils also decreased by $50.7 \pm 2.35\%$ in the ARDS + SIS3 group when compared to the ARDS group ($P < 0.05$ in all cases). The changes in the neutrophil ratios were found to be consistent with changes in the total number of cells as well as the number of neutrophils.

3.4. The Effect of SIS3 on the ECM Expression due to LPS-Induced ARDS Rats. SIS3 pretreatment reduced inflammation in the ARDS rat model. Western blot analysis of homogenized rat lung tissue showed that, compared to those of the control group, the protein levels of RAGE (Figure 5(a)), TGF- β 1 (Figure 5(b)), MMP2 (Figure 5(c)), and MMP9 (Figure 5(d)) in the lung tissues of the ARDS group increased by 1.54 ± 0.05 , 2.87 ± 0.07 , 2.44 ± 0.12 , and 6.38 ± 1.27 times, respectively, while those of the ARDS + SIS3 group decreased by 19.34 ± 1.74 , 63.10 ± 1.89 , 57.90 ± 4.97 , and $81.78 \pm 2.09\%$ compared to that of the ARDS group, respectively ($P < 0.05$ in all cases). The levels of RAGE, TGF- β 1, MMP2, and MMP9 in the ARDS+SIS3 group were 19.34 ± 1.74 , 63.10 ± 1.89 , 57.90 ± 4.97 , and $81.78 \pm 4.97\%$ lower than those in the ARDS group, respectively.

Immunohistochemistry measurements of the lung sections showed markedly increased leukocyte infiltration in

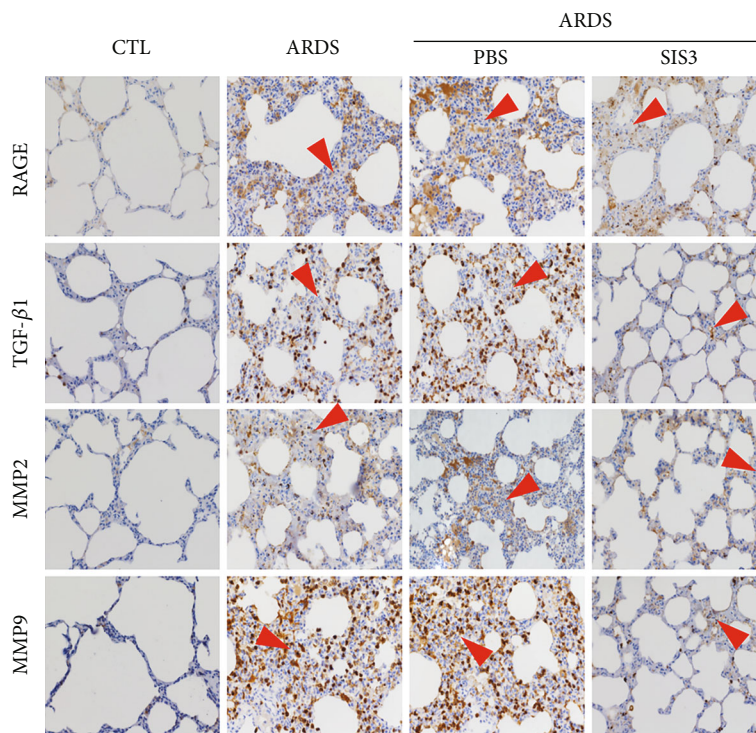


FIGURE 2: SIS3 pretreatment decreases the protein expression and localization of RAGE, TGF- β 1, MMP2, and MMP9 in ARDS rats. Immunohistochemical staining of lung tissue sections showed that RAGE, TGF- β 1, MMP2, and MMP9 were expressed in the bronchial smooth muscle, airways, and alveolar epithelial cells of rats. The expression levels of RAGE, TGF- β 1, MMP2, and MMP9 in the ECM of ARDS rats induced by LPS were significantly higher than those of the control group. RAGE, TGF- β 1, MMP2, and MMP9 were reduced by pretreatment with SIS3, and no effect was found upon pretreatment with PBS. The micrographs were magnified at 400x. The red triangles indicate infiltrated leukocytes.

the ARDS group, and considering that ARDS is an acute inflammatory disease, most of these should be neutrophils [32] (Figures 2 and 3). Neutrophils play an important role in host defense against infection through the secretion of various factors such as proteinases and neutrophil extracellular traps. However, these factors can also be toxic which will therefore result in tissue damage [33]. After treatment with SIS3, the infiltrated leukocytes were markedly decreased (Figures 2 and 3).

In addition, ELISA demonstrated that the serum and BALF levels of RAGE, TGF- β 1, MMP2, and MMP9 in the ARDS group were 8.02 ± 1.7 , 4.16 ± 0.49 , 2.87 ± 0.29 , and 2.13 ± 0.12 times (for sera) and 10.70 ± 1.36 , 5.38 ± 0.87 , 2.93 ± 0.24 , and 2.76 ± 0.24 times (for BALF) higher than those in the control group ($P < 0.05$ in all cases). The levels of RAGE, TGF- β 1, MMP2, and MMP9 in the ARDS + SIS3 group were 68 ± 4.98 , 55.20 ± 4.71 , 49.20 ± 3.90 , and $28.40 \pm 4.48\%$ (for sera) and 64.30 ± 4.37 , 58.80 ± 3.04 , 42.70 ± 3.49 , and $47.40 \pm 6.38\%$ (for BALF), which were lower than those in the ARDS group ($P < 0.05$ in all cases, Figures 6(a)–6(d)). The protein levels of RAGE, TGF- β 1, MMP2, and MMP9 in rats pretreated with PBS were not significantly different from those seen in the ARDS group. In summary, SIS3 inhibited the RAGE, TGF- β 1, MMP2, and MMP9 protein expression levels in both the serum and BALF of ARDS rats.

3.5. SIS3 Inhibited the Activation of Phospho-Smad3 in the ARDS Rat Model. Western blot analysis showed that LPS activated Smad3 signaling by increasing Smad3 phosphorylation, while SIS3 pretreatment blocked LPS-induced phospho-Smad3 ($P < 0.05$ in all case; Figure 7).

3.6. SIS3 Alleviated Abnormal Collagen Expression and Distribution. With Masson's trichrome staining, the fibrosis in different groups was compared and analyzed (Figure 3(a)). It was seen that pathological fibrosis was usually driven by the ECM. In this experiment, collagen fibers were shown in blue. In the ARDS group, markedly, more blue stain was seen in the lung interstitium which means there was an upregulated expression of collagen when compared with the CTL group. After treatment with SIS3, the abnormal collagen distribution was significantly alleviated, but this was not seen in the ARDS group treated with PBS.

4. Discussion

Acute lung injury (ALI) and ARDS are two types of pulmonary complications that are caused by various conditions, such as sepsis, trauma, and pulmonary inflammation. A key step in its development is an uncontrolled inflammatory response. In this regard, LPS has been shown to trigger the inflammatory response in a dose-dependent and cell-

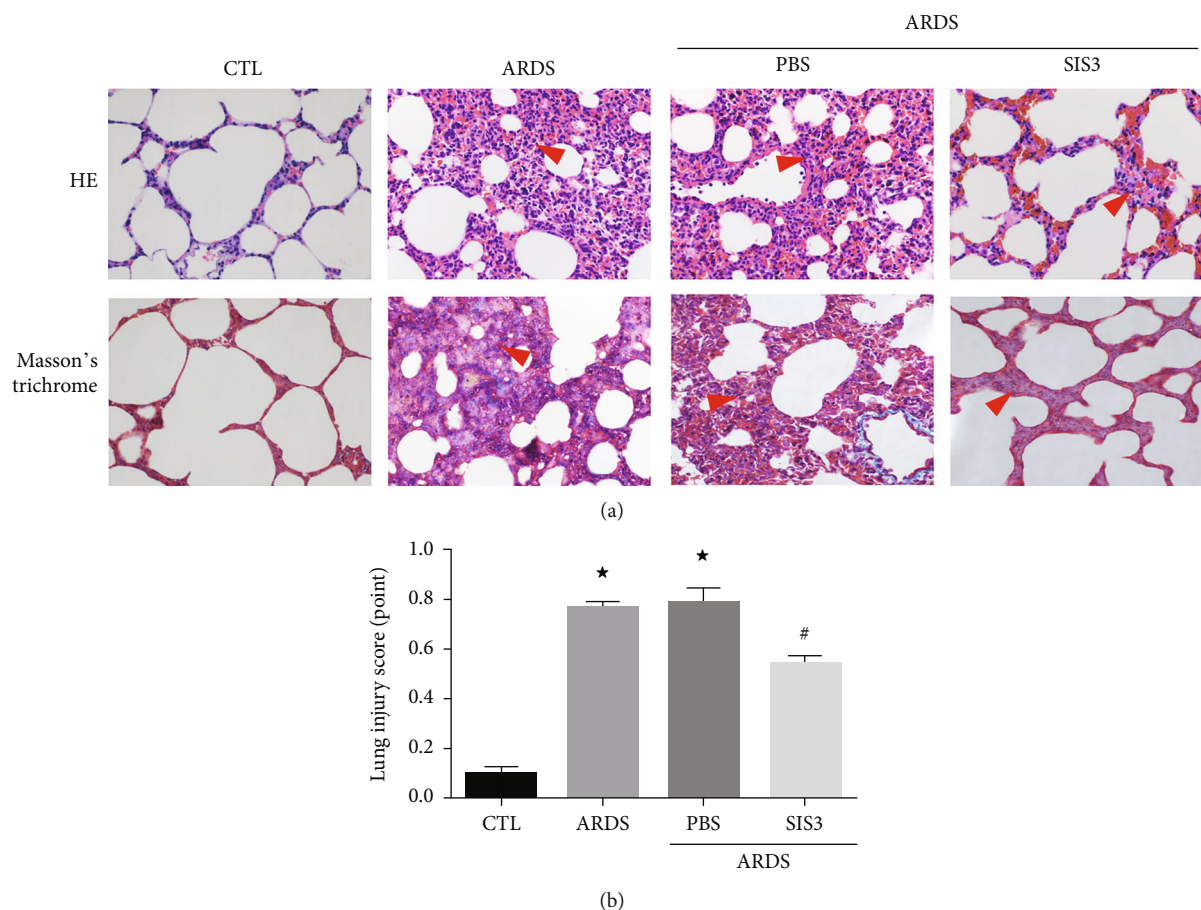


FIGURE 3: The inflammatory response was reduced by SIS3 pretreatment in LPS-induced acute lung injury. (a) Histological staining was performed to compare lung injury among the different groups. Both HE staining (upper panel) and Masson's trichrome staining (lower panel) show drastic leukocyte infiltration in the lung interstitium in the ARDS group, and the leukocyte infiltration was markedly alleviated after treatment of SIS3. Masson's trichrome staining reveals abnormal fibrosis and collagen distribution which was stained as blue, in the ARDS group, and significantly less blue stain is seen in the ARDS group treated with SIS3. The red triangles indicate the infiltrated sites. The photomicrographs were magnified to 400x. (b) HE staining was used to score lung injury. In the ARDS group, the lung injury was 0.77 ± 0.01 , and after treatment with SIS3, the score decreased to 0.54 ± 0.01 (* $P < 0.05$ vs. CTL; # $P < 0.05$ vs. ARDS). Data are presented as the means \pm SD ($n = 10$).

specific manner. Sepsis is the most important cause of ARDS [34]. LPS is a major component of gram-negative bacteria and has been used to induce ALI/ARDS and other inflammatory diseases in several *in vivo* experiments. Moreover, LPS has been successfully used in establishing an ARDS rat model [35]. Therefore, in this study, an LPS-induced ARDS rat model was established in our laboratory, and the remodeling role of the ECM gene, SIS3, in LPS-induced ARDS rats was analyzed. Accordingly, SIS3 treatment was found to regulate the secretion of cytokines as well as the degradation of collagen synthesis in remodeling and repairing the ECM, which reversed LPS-induced lung injury, improved pulmonary edema, improved histopathological features, reversed the protein and RNA expression of several ECM genes, downregulated the phosphorylation of Smad3, and repressed LPS-induced acute lung inflammation.

The ECM plays an important role in lung growth, development, lung tissue damage, and repair as well as being involved in the development of some lung diseases, significantly affecting the prognosis of ARDS. Li et al. [36] suggested

that the inhibition of RAGE or NF- κ B could alleviate LPS-induced lung injury in neonatal rats. Additionally, accumulating data have suggested a crucial role of RAGE in the pathogenesis of ALI and ARDS, indicating that this receptor is potentially an important therapeutic participant in ALI/ARDS [10]. In an environment of advanced glycated end-products, the ECM is regulated by the RAGE-dependent pathway, which increases the expression of RAGE as well as MMP2 and MMP9 [37]. Both of these gelatinases degrade type IV collagen and are primary constituents of basement membranes and play an important role in lung pathology [38]. The action of gelatinase is essential for basement membrane remodeling, which is observed in various pulmonary inflammatory diseases such as ARDS. MMP primarily affects the biological activities of these mediators by degrading the ECM and participating in the lysis of inflammatory cytokines and chemokines secreted into the ECM, which ultimately influence cell behavior and aggravate lung injury [17, 18].

Torii et al. demonstrated a significantly higher concentration of MMP2 and MMP9 in the BALF of ARDS patients

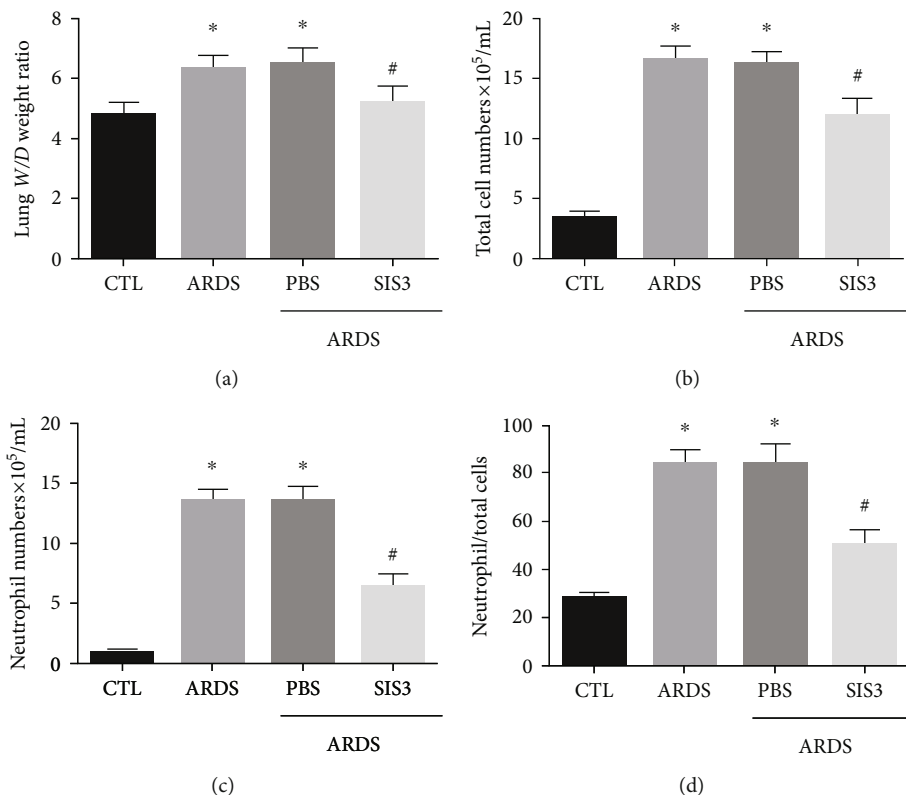


FIGURE 4: SIS3 pretreatment alleviates lung injury and focal inflammation in LPS-induced ARDS. (a) BALF was collected 24 h after intratracheal instillation of LPS. The alteration of the alveolar capillary barrier was weakened by SIS3 pretreatment in ARDS rats, which was seen in an increase of the lung *W/D* ratio. (b–d) The total cells, neutrophils, and neutrophil ratio in the BALF were higher in the ARDS group than in the control group. The values were also lower in the ARDS + SIS3 group when compared to the ARDS group, respectively. The data are presented as the means \pm SD ($n = 10$). * $P < 0.05$ vs. CTL; # $P < 0.05$ vs. ARDS.

compared to healthy subjects [39]. The levels of these MMPs were found to be elevated in BALF of ALI patients [40]. LPS stimulation was shown to immediately activate MMP2 and MMP9 production in BALF among ALI rats [41]. In this study, LPS was found to increase RAGE, TGF- β 1, MMP2, and MMP9 mRNA and protein expression in LPS-induced ARDS rats. These results were in accord with those of previous studies, which primarily implicated MMPs in the pathogenesis of ARDS in promoting lung inflammation and/or injury to the alveolar capillary barrier in animal models of ALI [42]. The present data suggest that RAGE, TGF- β 1, MMP2, and MMP9 may all participate in airway remodeling associated with inflammatory processes of the lung. During onset of ALI and ARDS, lung edema appears as a consequence of microvascular leakage associated with endothelial injury [43, 44].

Smad3 is considered the final integration factor of various fibrogenic signals and can regulate the expression of ECM-involved genes directly. Moreover, SIS3 is a small molecule which is a specific inhibitor of Smad3 and acts by inhibiting its phosphorylation. In this study, the lungs of the LPS-induced ARDS rats showed markedly increased levels of phosphorylated Smad3 when compared to the control group, and the signaling ligand, TGF- β 1, also exhibited increased levels of expression. However, levels of phosphorylated Smad3 and TGF- β 1 were both found to be suppressed in the SIS3-treated lungs of LPS-induced ARDS rats. These

findings suggest that blocking Smad3 phosphorylation by SIS3 may have a therapeutic potential for ARDS, although further studies are required to confirm these findings.

TGF- β signaling is necessary in many fibrogenic events, including fibroblast activation and eventual ECM deposition [45–47]. SIS3 is a useful tool to evaluate TGF- β -regulated cellular mechanisms via selective inhibition of Smad3 [27]. The corresponding results suggest that SIS3 significantly inhibited LPS-induced ALI and significantly improved the lung histopathological features of LPS-induced ARDS in rats as well as reducing the expression levels of RAGE, TGF- β , MMP2, and MMP9. Recent studies have indicated that SIS3 treatment delays the early development of diabetic nephropathy in type I diabetic mouse models by inhibiting epithelial-mesenchymal transition and fibrosis [48].

SIS3 has also been shown to attenuate BLM-induced PF in mice [28]. SIS3 has been shown to protect unilateral ureteral obstruction of the kidneys against fibrosis, apoptosis, and inflammation injury through the inhibition of TGF- β /Smad3 signaling [49]. Through Smad-dependent signal transduction [50], TGF upregulates MMP2 and changes the matrix components to promote epithelial repair [51]. Another study carried out an immunohistochemical analysis and demonstrated that MMP2 and MMP9 expression was evident in alveolar macrophages and interstitial neutrophils [52]. The present study demonstrated through *in vivo*

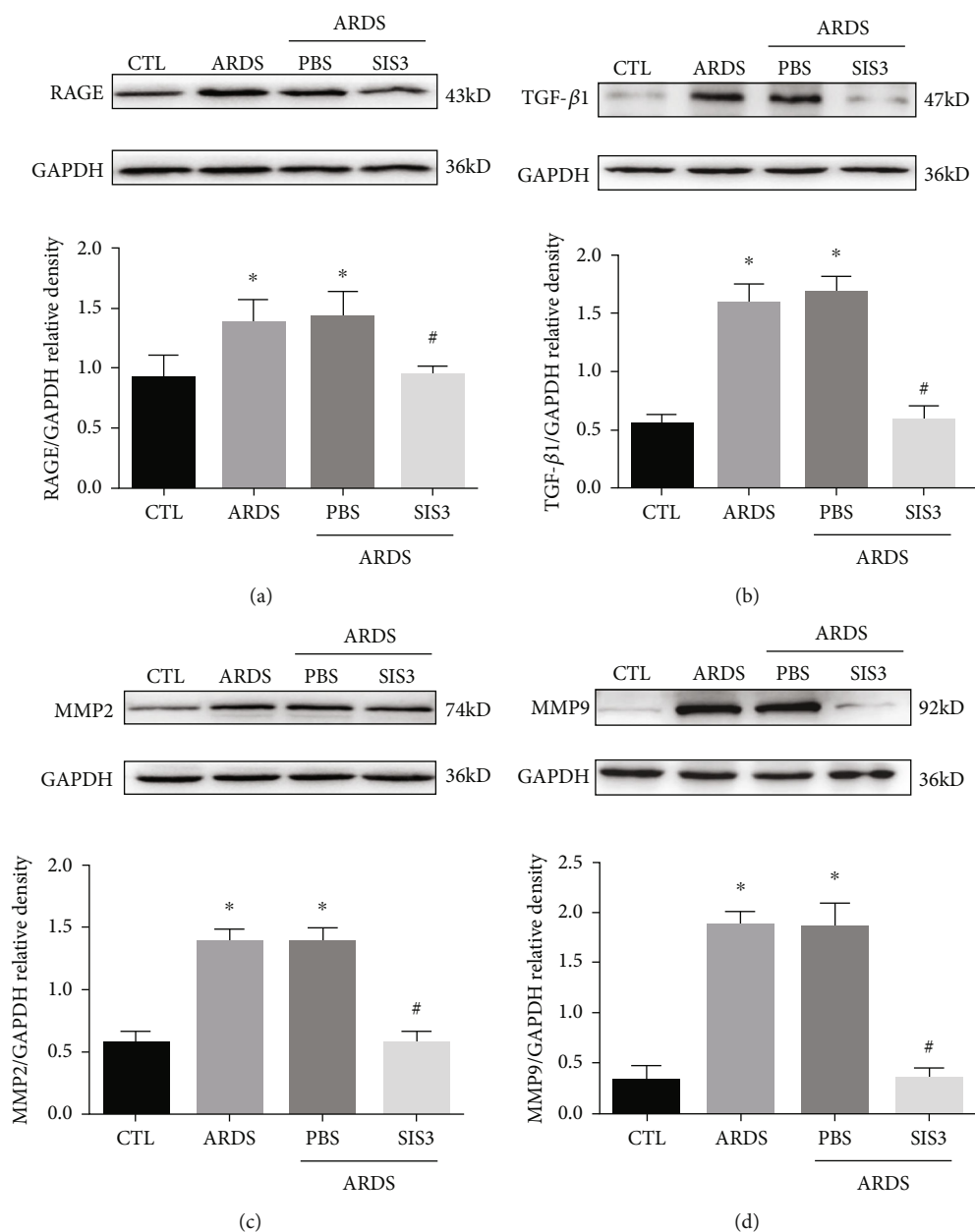


FIGURE 5: SIS3 inhibited the protein expression of RAGE, TGF- β 1, MMP2, and MMP9 proteins in lung homogenates acquired from ARDS rats. The expression levels of RAGE, TGF- β 1, MMP2, and MMP9 proteins in lung tissue homogenates, sera, and BALF of ARDS rats and were determined using western blotting analysis at 24 h after LPS intervention. The results of western blotting showed that SIS3 inhibited LPS-induced (a) RAGE, (b) TGF- β 1, (c) MMP2, and (d) and MMP9 protein expression in the lung homogenates. The data are presented as the means \pm SD ($n = 10$). * $P < 0.05$ vs. CTL; # $P < 0.05$ vs. ARDS.

experiments that LPS increased RAGE, TGF- β 1, MMP2, and MMP9 expression in the ECM and caused rat lung injury. Furthermore, this study illustrated that SIS3 inhibited these effects and reduced lung injury in ARDS rats. Immunohistochemical staining indicated that pretreatment of ARDS rats with SIS3 reduced lung injury caused by LPS, which was consistent with a previous study showing that SIS3 attenuated BLM-induced PF in mice [28]. Moreover, pharmacological inhibition of Smad3 or phospho-Smad3 has been shown to reduce BLM-induced PF in rats [53, 54]. The findings of this study indicated that blocking of Smad3 by the chemical inhibitor, SIS3, had a tendency to repair the ECM.

Intratracheal instillation of LPS induces acute lung inflammation with infiltration of inflammatory cells, which synthesize and secrete a wide variety of cytokines, chemokines, reactive oxygen species, and proteases, leading to aberrant fibroproliferation and matrix synthesis in mice. In this study, the intratracheal injection of LPS resulted in lung injury characterized by a significant increase in the lung W/D ratio and BALF total protein concentration, an upregulated inflammatory response with an increased number of total cells, an increased number of neutrophils, and an increased neutrophil ratio in the BALF. In addition, pretreatment with SIS3 significantly decreased the lung W/D ratio as an index of

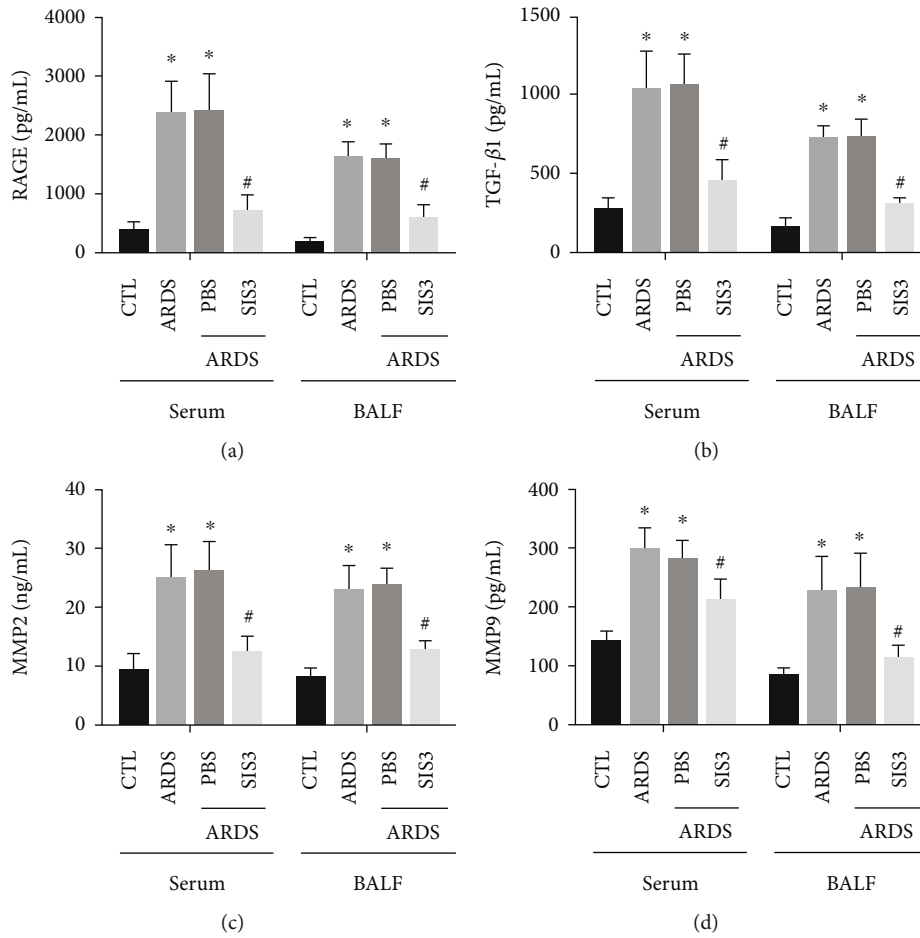


FIGURE 6: SIS3 pretreatment prevented the reduction of the expression of RAGE, TGF-β1, MMP2, and MMP9 in LPS-induced ARDS. The effects of SIS3 on the protein expression levels of (a) RAGE, (b) TGF-β1, (c) MMP2, and (d) MMP9 in the BALF and sera of the ARDS rats were determined using ELISA. The results demonstrated that the levels of RAGE, TGF-β1, MMP2, and MMP9 proteins were significantly higher in the ARDS group than in the control group, while the levels of RAGE, TGF-β1, MMP2, and MMP9 in the SIS3 group were lower than those in the ARDS group. The protein levels of RAGE, TGF-β1, MMP2, and MMP9 in LPS-administered pretreatment with PBS were not different from those of the ARDS group. The data are presented as the means ± SD of three independent experiments in triplicate (n = 10). *P < 0.05 vs. CTL; #P < 0.05 vs. ARDS.

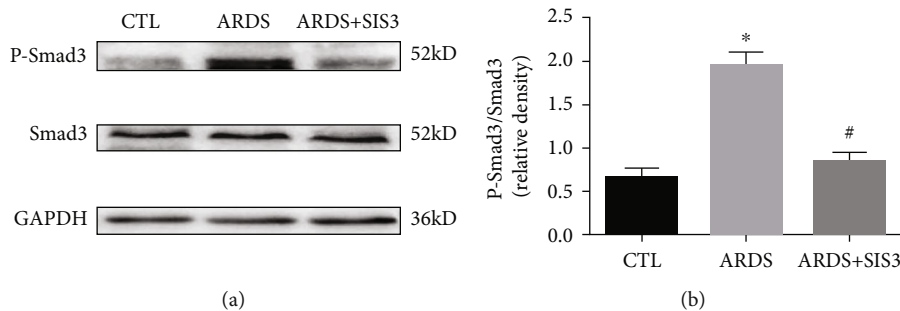


FIGURE 7: Phosphorylation of smad3 was inhibited by SIS3 in the lung tissue of ARDS rats. The activation of Smad3 was evaluated using western blotting analysis, and the amount of phospho-Smad3 formed was analyzed 24 h after treatment with either LPS or PBS. GAPDH was used as the loading control. The data are presented as the means ± SD (n = 10). *P < 0.05 vs. CTL; #P < 0.05 vs. ARDS.

interstitial edema, number of total cells, neutrophils, and the neutrophil ratio in the BALF in LPS-induced rats. These findings were consistent with a previous study that demonstrated that the number of lymphocytes, macrophages, and neutro-

phils in the BALF was significantly decreased after administration of SIS3 to BLM-treated mice [28]. Overall, the present study showed that the inhibitory effect of SIS3 on LPS-induced ARDS in the rat model may be due to its

inhibition of acute pulmonary inflammatory cell infiltration, regulation of cytokines, and reduction of related collagen synthesis.

5. Conclusions

The inhibitory effect of SIS3 on LPS-induced ALI in ARDS rats may be related to the inhibition of inflammatory cell infiltration, regulation of cytokine secretion, and degradation of collagen synthesis, thereby remodeling and repairing the ECM by TGF- β /Smad3. This may be a potential area for exploring a novel therapeutic strategy to combat ARDS.

Data Availability

The datasets and codes generated or analyzed in this study are available from the corresponding author upon reasonable request.

Conflicts of Interest

The authors declare that this research was conducted in the absence of any commercial or financial relationships that could be construed as a potential conflict of interest.

Authors' Contributions

Q Liang and Q Lin contributed equally to this study. LP initiated and designed this study. Q Liang, Q Lin and Y Li established the animal model and performed most of the experiments for this study including HE staining, RT-qPCR and WB. WL, XH, YJ and JN performed tissue isolation and sectioning. CQ and XC prepared sera and performed the ELISA. All the members performing laboratory experiments helped each other with all the techniques. SRS provided professional consultant services and techniques helped to edit the manuscript. LP, Q Liang, Q Lin and YL performed the statistical analyses. All the authors read and approved the final manuscript. Qiong Liang and Qiqing Lin contributed equally to this study.

Acknowledgments

The authors would like to thank Dr Lingzhang Meng from the Center for Systemic Inflammation Research (CSIR) of Youjiang Medical University for Nationalities for his support with biochemical and molecular biology techniques. This study was supported by Grant Nos. 81560321, 81760350, and 82060022 from the National Natural Science Foundation of China.

References

- [1] N. Adachi, T. Numakawa, M. Richards, S. Nakajima, and H. Kunugi, "New insight in expression, transport, and secretion of brain-derived neurotrophic factor: implications in brain-related diseases," *World Journal of Biological Chemistry*, vol. 5, no. 4, pp. 409–428, 2014.
- [2] E. Azoulay, G. Citerio, J. Bakker et al., "Year in review in Intensive Care Medicine 2013: II. Sedation, invasive and noninvasive ventilation, airways, ARDS, ECMO, family satisfaction, end-of-life care, organ donation, informed consent, safety, hematological issues in critically ill patients," *Intensive Care Medicine*, vol. 40, no. 3, pp. 305–319, 2014.
- [3] Y. Aschner, R. L. Zemans, C. M. Yamashita, and G. P. Downey, "Matrix metalloproteinases and protein tyrosine kinases," *Chest*, vol. 146, no. 4, pp. 1081–1091, 2014.
- [4] A. H. Hergueter, K. Nguyen, and C. A. Owen, "Matrix metalloproteinases: all the RAGE in the acute respiratory distress syndrome," *American Journal of Physiology. Lung Cellular and Molecular Physiology*, vol. 300, no. 4, pp. L512–L515, 2011.
- [5] C. Sharp, A. B. Millar, and A. R. L. Medford, "Advances in understanding of the pathogenesis of acute respiratory distress syndrome," *Respiration*, vol. 89, no. 5, pp. 420–434, 2015.
- [6] P. R. Rocco, S. C. Dos, and P. Pelosi, "Lung parenchyma remodeling in acute respiratory distress syndrome," *Minerva Anestesiologica*, vol. 75, no. 12, pp. 730–740, 2009.
- [7] L. B. Ware, T. Koyama, Z. Zhao et al., "Biomarkers of lung epithelial injury and inflammation distinguish severe sepsis patients with acute respiratory distress syndrome," *Critical Care*, vol. 17, no. 5, article R253, 2013.
- [8] M. I. García-Laorden, J. A. Lorente, C. Flores, A. S. Slutsky, and J. Villar, "Biomarkers for the acute respiratory distress syndrome: how to make the diagnosis more precise," *Annals of Translational Medicine*, vol. 5, no. 14, p. 283, 2017.
- [9] R. Blondonnet, J. M. Constantin, V. Sapin, and M. Jabaudon, "A pathophysiologic approach to biomarkers in acute respiratory distress syndrome," *Disease Markers*, vol. 2016, Article ID 3501373, 20 pages, 2016.
- [10] W. A. Guo, P. R. Knight, and K. Raghavendran, "The receptor for advanced glycation end products and acute lung injury/acute respiratory distress syndrome," *Intensive Care Medicine*, vol. 38, no. 10, pp. 1588–1598, 2012.
- [11] M. A. Queisser, F. M. Kouri, M. Königshoff et al., "Loss of RAGE in pulmonary Fibrosis," *American Journal of Respiratory Cell and Molecular Biology*, vol. 39, no. 3, pp. 337–345, 2008.
- [12] C. S. Calfee, L. B. Ware, M. D. Eisner et al., "Plasma receptor for advanced glycation end products and clinical outcomes in acute lung injury," *Thorax*, vol. 63, no. 12, pp. 1083–1089, 2008.
- [13] A. M. Houghton, "Matrix metalloproteinases in destructive lung disease," *Matrix Biology*, vol. 44–46, pp. 167–174, 2015.
- [14] Y. Liang, N. Yang, G. Pan, B. Jin, S. Wang, and W. Ji, "Elevated IL-33 promotes expression of MMP2 and MMP9 via activating STAT3 in alveolar macrophages during LPS-induced acute lung injury," *Cellular & Molecular Biology Letters*, vol. 23, no. 1, p. 52, 2018.
- [15] A. Davey, D. F. McAuley, and C. M. O'Kane, "Matrix metalloproteinases in acute lung injury: mediators of injury and drivers of repair," *European Respiratory Journal*, vol. 38, no. 4, pp. 959–970, 2011.
- [16] R. E. Vandenbroucke and C. Libert, "Is there new hope for therapeutic matrix metalloproteinase inhibition?," *Nature Reviews Drug Discovery*, vol. 13, no. 12, pp. 904–927, 2014.
- [17] M. D. Sternlicht and Z. Werb, "How matrix metalloproteinases regulate cell behavior," *Annual Review of Cell and Developmental Biology*, vol. 17, no. 1, pp. 463–516, 2001.
- [18] R. Khokha, A. Murthy, and A. Weiss, "Metalloproteinases and their natural inhibitors in inflammation and immunity," *Nature Reviews Immunology*, vol. 13, no. 9, pp. 649–665, 2013.
- [19] A. Dufour and C. M. Overall, "Missing the target: matrix metalloproteinase antitargets in inflammation and cancer,"

- Trends in Pharmacological Sciences*, vol. 34, no. 4, pp. 233–242, 2013.
- [20] M. S. Wilson and T. A. Wynn, “Pulmonary fibrosis: pathogenesis, etiology and regulation,” *Mucosal Immunology*, vol. 2, no. 2, pp. 103–121, 2009.
- [21] S. Avasara, F. Zhang, G. Liu, R. Wang, S. D. London, and L. London, “Curcumin modulates the inflammatory response and inhibits subsequent fibrosis in a mouse model of viral-induced acute respiratory distress syndrome,” *PLoS One*, vol. 8, no. 2, article e57285, 2013.
- [22] N. Fujino, H. Kubo, T. Suzuki et al., “Administration of a specific inhibitor of neutrophil elastase attenuates pulmonary fibrosis after acute lung injury in mice,” *Experimental Lung Research*, vol. 38, no. 1, pp. 28–36, 2012.
- [23] R. de Pablo, J. Monserrat, E. Reyes et al., “Sepsis-induced acute respiratory distress syndrome with fatal outcome is associated to increased serum transforming growth factor beta-1 levels,” *European Journal of Internal Medicine*, vol. 23, no. 4, pp. 358–362, 2012.
- [24] X. M. Meng, P. M. K. Tang, J. Li, and H. Y. Lan, “TGF- β ²/Smad signaling in renal fibrosis,” *Frontiers in Physiology*, vol. 6, p. 82, 2015.
- [25] X. M. Meng, X. R. Huang, A. C. K. Chung et al., “Smad2 protects against TGF- β /Smad3-mediated renal fibrosis,” *Journal of the American Society of Nephrology*, vol. 21, no. 9, pp. 1477–1487, 2010.
- [26] F. Verrecchia, M. L. Chu, and A. Mauviel, “Identification of novel TGF- β /Smad gene targets in dermal fibroblasts using a combined cDNA microarray/promoter transactivation approach,” *Journal of Biological Chemistry*, vol. 276, no. 20, pp. 17058–17062, 2001.
- [27] M. Jinnin, H. Ihn, and K. Tamaki, “Characterization of SIS3, a novel specific inhibitor of Smad3, and its effect on transforming growth factor- β 1-induced extracellular matrix expression,” *Molecular Pharmacology*, vol. 69, no. 2, pp. 597–607, 2006.
- [28] J. Shou, J. Cao, S. Zhang et al., “SIS3, a specific inhibitor of smad3, attenuates bleomycin-induced pulmonary fibrosis in mice,” *Biochemical and Biophysical Research Communications*, vol. 503, no. 2, pp. 757–762, 2018.
- [29] L. Liu, Y. Zhu, M. Noe, Q. Li, and P. J. Pasricha, “Neuronal transforming growth factor beta signaling via SMAD3 contributes to pain in animal models of chronic pancreatitis,” *Gastroenterology*, vol. 154, no. 8, pp. 2252–2265.e2, 2018.
- [30] L. Sorokin, “The impact of the extracellular matrix on inflammation,” *Nature Reviews Immunology*, vol. 10, no. 10, pp. 712–723, 2010.
- [31] G. Matute-Bello, G. Downey, B. B. Moore et al., “An official American Thoracic Society workshop report: features and measurements of experimental acute lung injury in animals,” *American Journal of Respiratory Cell and Molecular Biology*, vol. 44, no. 5, pp. 725–738, 2011.
- [32] A. E. Williams, R. J. José, P. F. Mercer et al., “Evidence for chemokine synergy during neutrophil migration in ARDS,” *Thorax*, vol. 72, no. 1, pp. 66–73, 2016.
- [33] A. E. Williams and R. C. Chambers, “The mercurial nature of neutrophils: still an enigma in ARDS?,” *American Journal of Physiology. Lung Cellular and Molecular Physiology*, vol. 306, no. 3, pp. L217–L230, 2014.
- [34] E. Cario, I. M. Rosenberg, S. L. Brandwein, P. L. Beck, H. C. Reinecker, and D. K. Podolsky, “Lipopolysaccharide activates distinct signaling pathways in intestinal epithelial cell lines expressing Toll-like receptors,” *Journal of Immunology*, vol. 164, no. 2, pp. 966–972, 2000.
- [35] R. J. McCallip, H. Ban, and O. N. Uchakina, “Treatment with the hyaluronic acid synthesis inhibitor 4-methylumbelliferone suppresses LPS-induced lung inflammation,” *Inflammation*, vol. 38, no. 3, pp. 1250–1259, 2015.
- [36] Y. Li, R. Wu, Y. Tian et al., “RAGE/NF- κ B signaling mediates lipopolysaccharide induced acute lung injury in neonate rat model,” *International Journal of Clinical and Experimental Medicine*, vol. 8, no. 8, pp. 13371–13376, 2015.
- [37] A. I. Serban, L. Stanca, O. I. Geicu, M. C. Munteanu, M. Costache, and A. Dinischiotu, “Extracellular matrix is modulated in advanced glycation end products milieu via a RAGE receptor dependent pathway boosted by transforming growth factor- β 1 RAGE,” *Journal of Diabetes*, vol. 7, no. 1, pp. 114–124, 2015.
- [38] J. Lanchou, M. Corbel, M. Tanguy et al., “Imbalance between matrix metalloproteinases (MMP-9 and MMP-2) and tissue inhibitors of metalloproteinases (TIMP-1 and TIMP-2) in acute respiratory distress syndrome patients,” *Critical Care Medicine*, vol. 31, no. 2, pp. 536–542, 2003.
- [39] K. Torii, K. Iida, Y. Miyazaki et al., “Higher concentrations of matrix metalloproteinases in bronchoalveolar lavage fluid of patients with adult respiratory distress syndrome,” *American Journal of Respiratory and Critical Care Medicine*, vol. 155, no. 1, pp. 43–46, 1997.
- [40] C. M. O’Kane, S. W. McKeown, G. D. Perkins et al., “Salbutamol up-regulates matrix metalloproteinase-9 in the alveolar space in the acute respiratory distress syndrome,” *Critical Care Medicine*, vol. 37, no. 7, pp. 2242–2249, 2009.
- [41] C. Y. Wang, M. Shang, C. L. Zhou, L. Z. Feng, Q. S. Zhou, and K. Hu, “Mechanism of cxc chemokine ligand 5 (CXCL5)/cxc chemokine receptor 2 (CXCR2) bio-axis in mice with acute respiratory distress syndrome,” *Medical Science Monitor*, vol. 25, pp. 5299–5305, 2019.
- [42] N. Yamakawa, T. Uchida, M. A. Matthay, and K. Makita, “Proteolytic release of the receptor for advanced glycation end products from in vitro and in situ alveolar epithelial cells,” *American Journal of Physiology. Lung Cellular and Molecular Physiology*, vol. 300, no. 4, pp. L516–L525, 2011.
- [43] G. Feng, B. Sun, and T. Z. Li, “Daidzein attenuates lipopolysaccharide-induced acute lung injury via toll-like receptor 4/NF- κ B pathway,” *International Immunopharmacology*, vol. 26, no. 2, pp. 392–400, 2015.
- [44] S. Han and R. K. Mallampalli, “Correction: the acute respiratory distress syndrome: from mechanism to translation,” *Journal of Immunology*, vol. 194, no. 11, p. 5569, 2015.
- [45] J. Yang, M. Velikoff, E. Canalis, J. C. Horowitz, and K. K. Kim, “Activated alveolar epithelial cells initiate fibrosis through autocrine and paracrine secretion of connective tissue growth factor,” *American Journal of Physiology. Lung Cellular and Molecular Physiology*, vol. 306, no. 8, pp. L786–L796, 2014.
- [46] P. Zerr, K. Palumbo-Zerr, J. Huang et al., “Sirt1 regulates canonical TGF- β signalling to control fibroblast activation and tissue fibrosis,” *Annals of the Rheumatic Diseases*, vol. 75, no. 1, pp. 226–233, 2015.
- [47] N. Okumura, R. Minamiyama, L. T. Ho et al., “Involvement of ZEB1 and Snail1 in excessive production of extracellular matrix in Fuchs endothelial corneal dystrophy,” *Laboratory Investigation*, vol. 95, no. 11, pp. 1291–1304, 2015.

- [48] J. Li, X. Qu, J. Yao et al., "Blockade of endothelial-mesenchymal transition by a Smad3 inhibitor delays the early development of streptozotocin-induced diabetic nephropathy," *Diabetes*, vol. 59, no. 10, pp. 2612–2624, 2010.
- [49] X. Ji, H. Wang, Z. Wu et al., "Specific inhibitor of Smad3 (SIS3) attenuates fibrosis, apoptosis, and inflammation in unilateral ureteral obstruction kidneys by inhibition of transforming growth factor β (TGF- β)/Smad3 signaling," *Medical Science Monitor*, vol. 24, pp. 1633–1641, 2018.
- [50] L. Lucarini, M. Durante, C. Lanzi et al., "HYDAMTIQ, a selective PARP-1 inhibitor, improves bleomycin-induced lung fibrosis by dampening the TGF- β /SMAD signalling pathway," *Journal of Cellular and Molecular Medicine*, vol. 21, no. 2, pp. 324–335, 2017.
- [51] E. Lechapt-Zalcman, V. Prulière-Escabasse, D. Advenier et al., "Transforming growth factor- β 1 increases airway wound repair via MMP-2 upregulation: a new pathway for epithelial wound repair?," *American Journal of Physiology. Lung Cellular and Molecular Physiology*, vol. 290, no. 6, pp. L1277–L1282, 2006.
- [52] J. L. Dooley, D. Abdel-Latif, C. D. St. Laurent, L. Puttagunta, D. Befus, and P. Lacy, "Regulation of inflammation by Rac2 in immune complex-mediated acute lung injury," *American Journal of Physiology-Lung Cellular and Molecular Physiology*, vol. 297, no. 6, pp. L1091–L1102, 2009.
- [53] C. Wang, X. Song, Y. Li et al., "Low-dose paclitaxel ameliorates pulmonary fibrosis by suppressing TGF- β 1/Smad3 pathway via miR-140 upregulation," *PLoS One*, vol. 8, no. 8, article e70725, 2013.
- [54] Y. Qu, L. Zhang, Z. Kang, W. Jiang, and C. Lv, "Ponatinib ameliorates pulmonary fibrosis by suppressing TGF- β 1/Smad3 pathway," *Pulmonary Pharmacology & Therapeutics*, vol. 34, pp. 1–7, 2015.

Research Article

The SIRT3 and SIRT6 Promote Prostate Cancer Progression by Inhibiting Necroptosis-Mediated Innate Immune Response

Weiwei Fu, Hong Li, Haiyang Fu, Shuchao Zhao, Weiping Shi, Mengqi Sun, and Yujun Li 

Department of Pathology, The Affiliated Hospital of Qingdao University, Qingdao, Shandong 266003, China

Correspondence should be addressed to Yujun Li; liyujun.66@163.com

Received 13 August 2020; Revised 17 September 2020; Accepted 23 October 2020; Published 17 November 2020

Academic Editor: Jian Song

Copyright © 2020 Weiwei Fu et al. This is an open access article distributed under the Creative Commons Attribution License, which permits unrestricted use, distribution, and reproduction in any medium, provided the original work is properly cited.

The sirtuins (SIRT), including seven family members, belong to class III histone deacetylase (HDAC) enzymes, which have been intensively investigated in cancers. Although the function of SIRT in the cancer immunology is explored, SIRT-specific mechanisms regulating necroptosis-related innate immune response are not clear. In our present study, we found that both the mRNA and protein expression levels of SIRT3 and SIRT6 are significantly increased in the PCa tissues (HR, CI $P = 3.30E - 03$; HR, CI $P = 2.35E - 08$; and HR, CI $P = 9.20E - 08$) and were associated with patients' Gleason score and nodal metastasis. Furthermore, multivariate analysis showed that the PCa patients with higher expression levels of SIRT3 and SIRT6 had shorter overall survival (OS). Mechanistically, we found that SIRT3 and SIRT6 promote prostate cancer progress by inhibiting RIPK3-mediated necroptosis and innate immune response. Knockdown of both SIRT3 and SIRT6 not only activates TNF-induced necroptosis but also refreshes the corresponding recruitment of macrophages and neutrophils. Overall, our study identified that SIRT3 and SIRT6 are key regulators of necroptosis during prostate cancer progression.

1. Introduction

Prostate cancer (PCa) is the fifth leading cause of cancer-associated death worldwide. In 2018, over 1.3 million new cases and 359,000 deaths were reported [1], suggesting that it is urgent to identify novel diagnostic and prognostic biomarkers for PCa's better treatment. As a heterogeneous tumor, PCa undergoes epigenetic alterations, such as histone acetylation, to provide driving forces for its reprogramming [2, 3]. Histone acetyltransferases (HAT) and deacetylases (HDACs) are central enzymes to alter protein acetylation [4].

The sirtuin (SIRT) family, consisting of seven members (SIRT1-7), is highly conserved NAD⁺-dependent class III histone deacetylases (HDACs) [5, 6]. Although the SIRT family shares a conserved catalytic core domain, they are functionally distinct due to their divergent enzymatic activity and cellular localization. Studies have found that the SIRT family members act as critical modulators in cellular metabolism [7], DNA repair [8], gene expression [9], mitochondrial biology in cancer [10], metabolic diseases [11], neurodegeneration [12], aging [13], etc. In addition, evidence suggests that the SIRT have dual function in the cancer

development [12]. Until now, the SIRT modulators such as nicotinamide, suramin, EX-527, sirtinol, and salermide have emerged as innovative anticancer strategies [14, 15]. These SIRT modulators have shown promising therapeutic effectiveness in lymphoma [16], glioma [17], melanoma [18], gastric cancer [19], and chronic myeloid leukemia [20]. Therefore, it is needed to further understand the clinical values of SIRT in PCa. In fact, the clinical significance of SIRT in PCa was found several years ago. A study has demonstrated that *SIRT6* was overexpressed in the PCa tissues compared with normal tissues, and its inhibition led to apoptosis and enhanced sensitivity of chemotherapeutic drugs [21]. In addition, *SIRT7* was increased and could serve as a predictive biomarker for PCa aggressiveness and chemoresistance [22].

Necroptosis is an inflammatory cell death, which is mediated by receptor-interacting serine/threonine-protein kinase 1 (RIPK1), RIPK3, and downstream initiator pseudokinase mixed lineage kinase domain-like protein (MLKL). Upon stimulation by TNF α , RIPK1 was recruited to the cytoplasmic membrane and formed a complex with several death-domain containing proteins, such as TRADD, TRAF2/5, and RIPK3.

RIPK1 subsequently activates RIPK3, which is required for their substrate MLKL phosphorylation [23]. The phosphorylated MLKL then traffics to the membrane and enables membrane rupture and the release of cellular contents including damage-associated molecular patterns (DAMPs), thus leading to the induction of inflammation [24]. Within the whole process, the kinase activities of RIPK1 and RIPK3 are critical for activating necroptosis. Plenty of studies suggest that necroptosis is closely linked with autoimmune, inflammatory, neurodegenerative disease [25]. Several inhibitors of RIPK1 have been applied in clinical trials. One recent study identified a RIP1-HAT1-SIRT complex and demonstrated that targeting them is a promising strategy in the treatment and prevention of cancer [26].

However, it is still unclear how SIRT3 and SIRT6 regulate RIPK1/RIPK3-mediated necroptosis and in turn maintain prostate cancer progress. In the present study, we analyzed the expression levels and genetic alterations of SIRTs in the PCa patients and tried to reveal the clinical significance of SIRTs in PCa progression using online databases. Our data showed that the expressions of both SIRT3 and SIRT6 are dramatically increased, which is closely linked with the overall survival of prostate cancer patients. With regard to the biology function of SIRT3/6, we found that SIRT3 and SIRT6 strongly control the necroptosis signaling pathway and in turn suppress the recruitment of innate immune cell macrophages and neutrophils.

2. Results

2.1. The Expression Level of SIRT3 and SIRT6 Is Upregulated in the PCa Patients. To explore the clinical significance of the SIRT family, we analyzed the mRNA and protein levels in the UALCAN (<http://ualcan.path.uab.edu>) and Human Protein Atlas websites (<https://www.proteinatlas.org>). As shown in Figure 1(a), higher mRNA levels of *SIRT3*, *SIRT6*, and *SIRT7* were observed in the PCa samples compared with those of the normal tissues (HR, CI $P = 3.30E - 03$; HR, CI $P = 2.35E - 08$; and HR, CI $P = 9.20E - 08$). However, other SIRT members indiscriminately expressed between normal and PCa tissues. The protein expressions of individual SIRT members were also examined. As indicated in Supplementary Figure 1A and 1C, the protein levels of SIRT6 and SIRT7 were obviously higher in the PCa tissues, whereas, in the normal prostate tissues, the SIRT6 and SIRT7 were rarely expressed.

Next, we analyzed the relationship between the mRNA expression levels of SIRT members and the clinicopathological parameters of the PCa patients in UALCAN (including patients' Gleason score and nodal metastasis status). Compared with the normal prostate tissues, the mRNA expression levels of SIRT3, SIRT6, and SIRT7 were significantly associated with the Gleason score, that is, patients with higher Gleason scores tended to have higher expression of *SIRT3*, *SIRT6*, and *SIRT7*. However, other SIRT family members did not show a consistent trend (Figure 1(b)). Importantly, patients with the nodal metastasis also tended to have higher expression levels of *SIRT3*, *SIRT6*, and *SIRT7* (Figure 2(a)),

suggesting that these they may be involved in the regulation of PCa metastasis.

2.2. The Higher Expression of SIRT3 and SIRT6 in PCa Patients Is Linked to Unfavorable Outcome. The patients from the TCGA dataset (PCa multiforme, $n = 499$) in SurvExpress (<http://bioinformatica.mty.itesm.mx:8080/Biomatec/SurvivaX.jsp>) were divided into low-risk and high-risk groups using the median expression level of individual SIRT as a cutoff (Figure 2(b)). Our results showed that the high-risk PCa patients with high expression levels had poorer OS compared with the low-risk group (Figure 2(b), HR = 7.58, 95% CI: 82.17, and $P = 0.026$).

Then, we downloaded the clinical data (Supplementary Table 1) and mRNA expression levels of SIRTs from the FireBrowse website (<http://firebrowse.org/api-docs/>) for Cox survival regression analysis. In the univariate analysis, we found that age (HR = 1.039, 95% CI: 1.006-1.074, and $P = 0.020$), Gleason score (HR = 1.629, 95% CI: 1.329-1.997, and $P < 0.001$), stage (HR = 1.693, 95% CI: 1.051-2.726, and $P = 0.030$), SIRT3 (HR = 0.999, 95% CI: 0.998-1.000, and $P = 0.014$), and SIRT6 (HR = 0.999, 95% CI: 0.997-1.000, and $P = 0.037$) were all independent risk factors for OS of PCa patients (Supplementary Table 2). The multivariate analysis exhibited that PCa patients with higher mRNA levels of SIRT3 (HR = 0.998, 95% CI: 0.997-0.999, and $P = 0.003$) and SIRT6 (HR = 0.998, 95% CI: 0.997-0.999 $P = 0.007$) tended to have poorer OS (Supplementary Tables 3-9).

In addition, the results also confirmed that the SIRT6 and SIRT7 protein levels were associated with the OS of PCa patients ($P = 0.044$ and $P = 0.017$, respectively, Supplementary Figure 1B and 1D). However, other SIRT members showed no correlation with the survival (data not shown).

Genetic mutation in the SIRT gene may serve as a prognostic biomarker for PCa patients. We analyzed the genetic alterations and their associations with OS in cBioPortal (<http://www.cbioportal.org>). Data displayed that the predominant alteration in SIRT genes was gene amplification. And in the 3801 sequenced PCa patients, genetic alterations were observed in 183 PCa patients, and the mutation rate was 11% (Figure 2(c)). Of note, the frequency of each alteration in the SIRT gene from 16 PCa studies is shown in Figure 2(d). Furthermore, results from the Kaplan-Meier plot and log-rank test revealed that the PCa patients with genetic alterations in SIRTs tended to have shorter OS (Figure 2(d), $P < 0.001$), indicating that SIRT gene mutations indeed could affect the PCa progression.

2.3. Both SIRT3 and SIRT6 Control RIPK3-Induced Necroptosis. Necroptosis is a kind of programmed inflammatory cell death. The dysregulated necroptosis signaling pathway is linked to various cancer progressions. A recent study showed that pan-SIRT inhibitor, MC2494, can efficiently prevent the early steps of carcinogenesis via promoting RIPK1 acetylation [26]. In order to determine whether SIRT3 and SIRT6 regulate TNF-induced necroptosis, we stably knock down either SIRT3 or SIRT6 genes that fused with a GFP cDNA controlled by an inducible promoter in

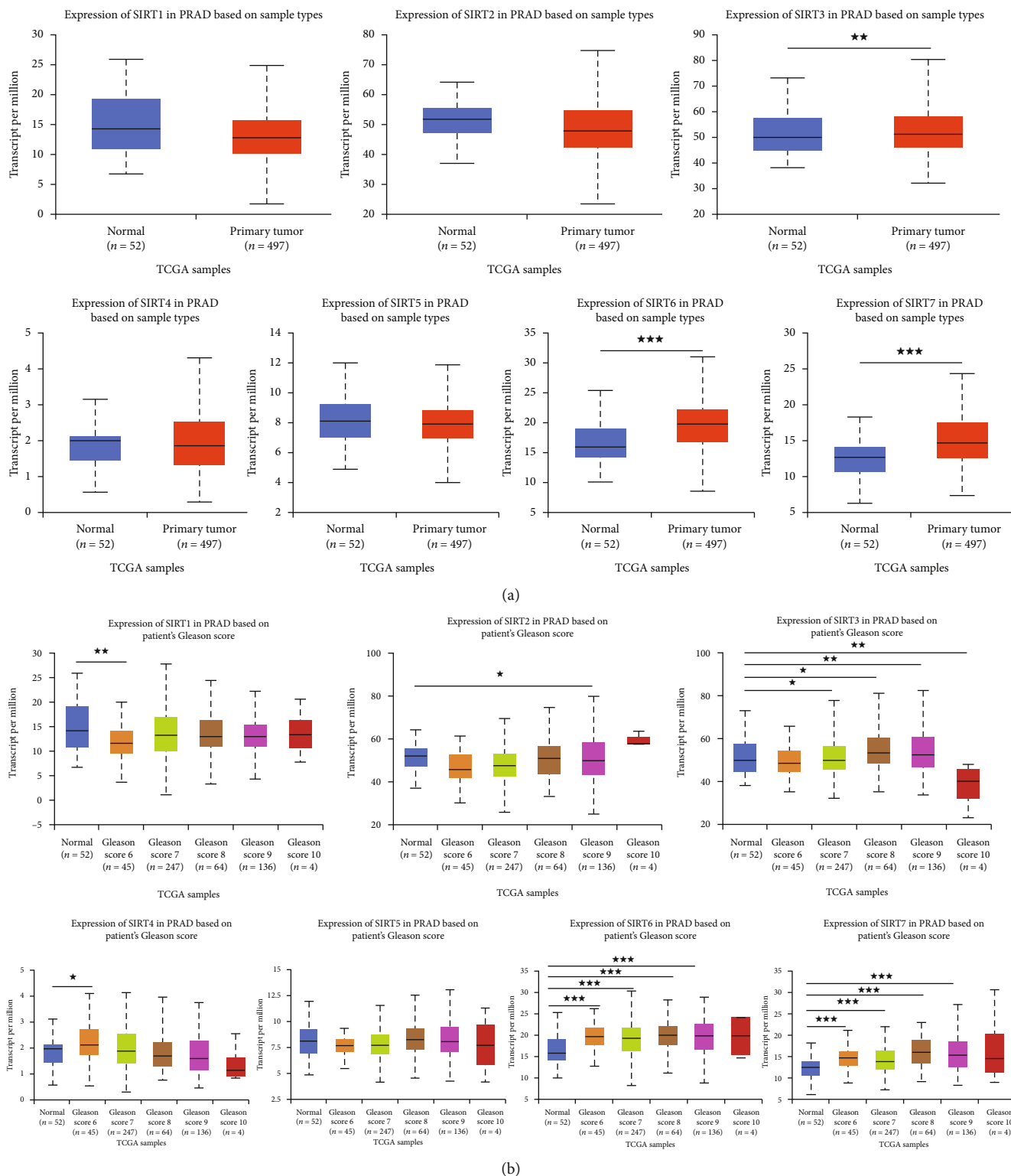
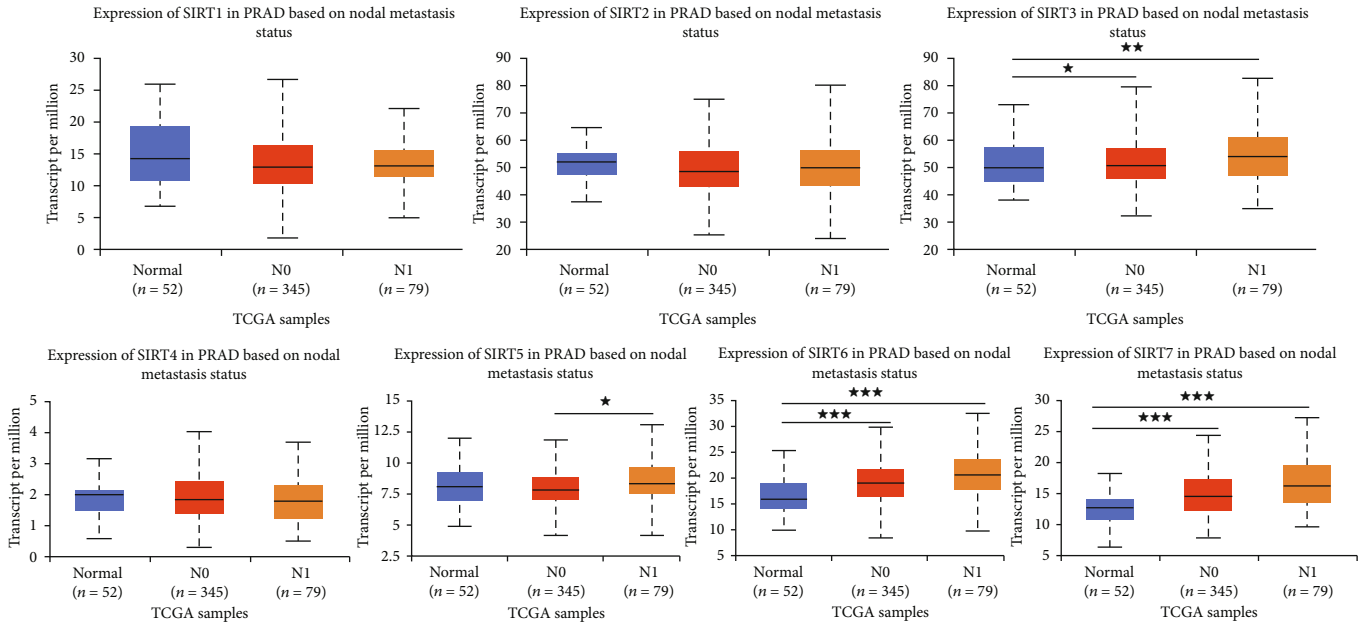


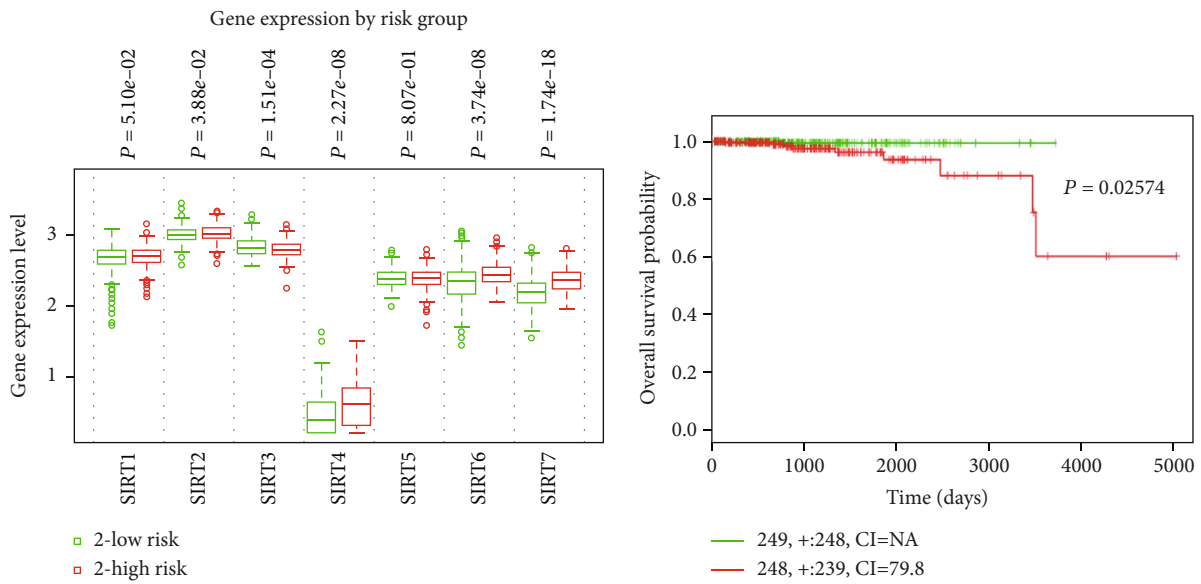
FIGURE 1: The higher expression of SIRT3 and SIRT6 in the PCa patients. (a) mRNA expression levels of SIRT3/6/7 were found to be overexpressed in primary PCa tissues compared to normal prostate samples. ** $P < 0.01$ and *** $P < 0.001$. (b) Compared to the normal prostate tissues, the mRNA expression levels of SIRT3/6/7 in PCa samples were significantly correlated with the Gleason score; SIRT1/2/4/5 did not show consistent trend. * $P < 0.01$, ** $P < 0.01$, and *** $P < 0.001$.

prostate cell lines, LNCaP, PC3, and DU145. The cell death was analyzed by tracking a cytotoxic red signal using a live image system. As shown in Figures 3(a) and 3(b) and S2A-

C, in comparing with shRNA control, loss of SIRT3 and SIRT6 dramatically increases TNF-induced cell death, which is manifested by an enhanced red signal. To validate



(a)



(b)

FIGURE 2: Continued.

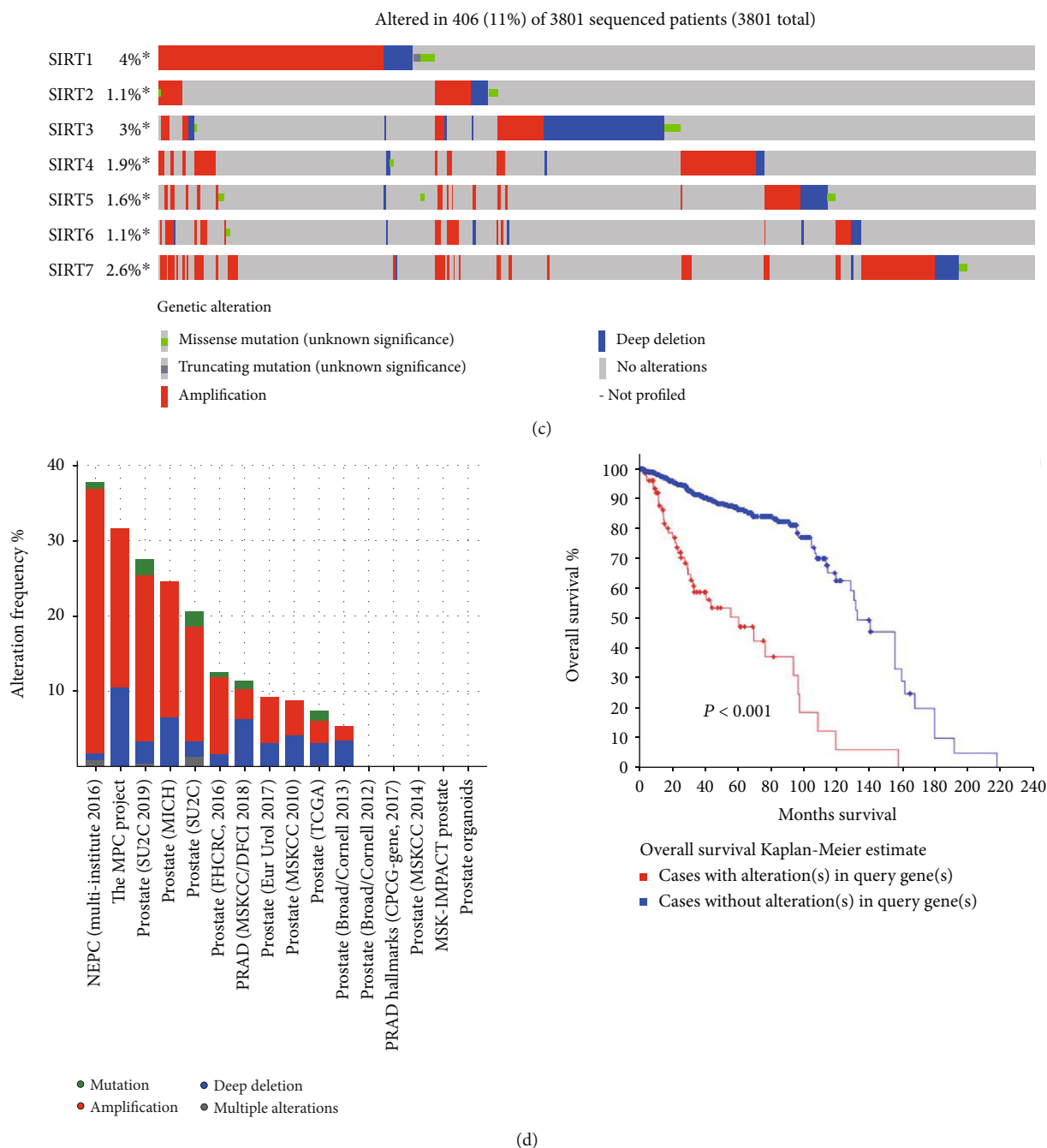


FIGURE 2: The higher expression of SIRT3 and SIRT6 in PCa patients is linked to unfavorable outcome. (a) The mRNA expression levels of SIRT3/5/6/7 were correlated with the nodal metastasis of PCa. N0: no regional lymph node metastasis; N1: metastases in 1 to 3 axillary lymph nodes. * $P < 0.01$, ** $P < 0.01$, and *** $P < 0.001$. (b) The box plots of expression of SIRT genes in low (green) and high (red) risk groups of TCGA-PRAD patients. *x*-axis: gene expression value of each gene; *P* values are above the box plot. Kaplan-Meier survival plots showed that the high expression of the SIRTs was associated with poor survival in TCGA-PRAD patients. Red: high-risk group; green: low-risk group; top right corner inset: numbers of high- and low-risk samples, numbers of censored samples marked with and CI of each risk group; *x*-axis: time (days); *y*-axis: overall survival probability. (c) Gene alterations in SIRT genes queried from 3801 patients in 16 studies. (d) The frequency of alterations in SIRT genes in 16 individual prostate cancer studies. Genetic alterations in SIRTs were associated with shorter OS of PRAD patients.

whether shSIRT3 and shSIRT6 induce RIPK3-mediated necroptosis, we treated cells with RIPK3 inhibitor GSK' 872. As shown in Figure 3(d), RIPK3 inhibition via GSK' 872 completely rescues shSIRT3- and shSIRT6-induced cell

death. Correspondingly, loss of SIRT3 and SIRT6 dramatically activates RIPK3 phosphorylation and their downstream effector MLKL phosphorylation (Figure 3(c)). However, there is no alteration in the expression of RIPK1

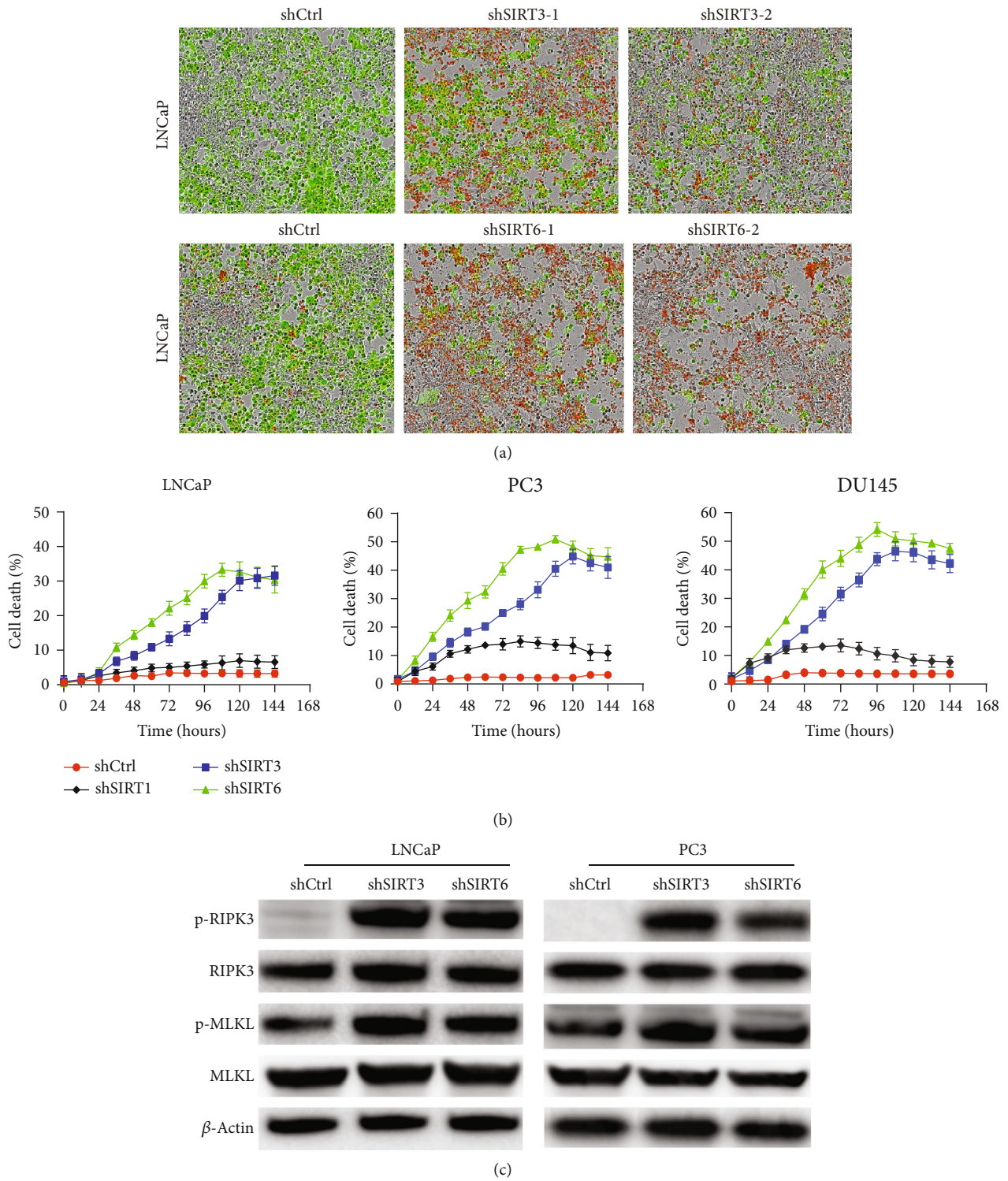


FIGURE 3: Continued.

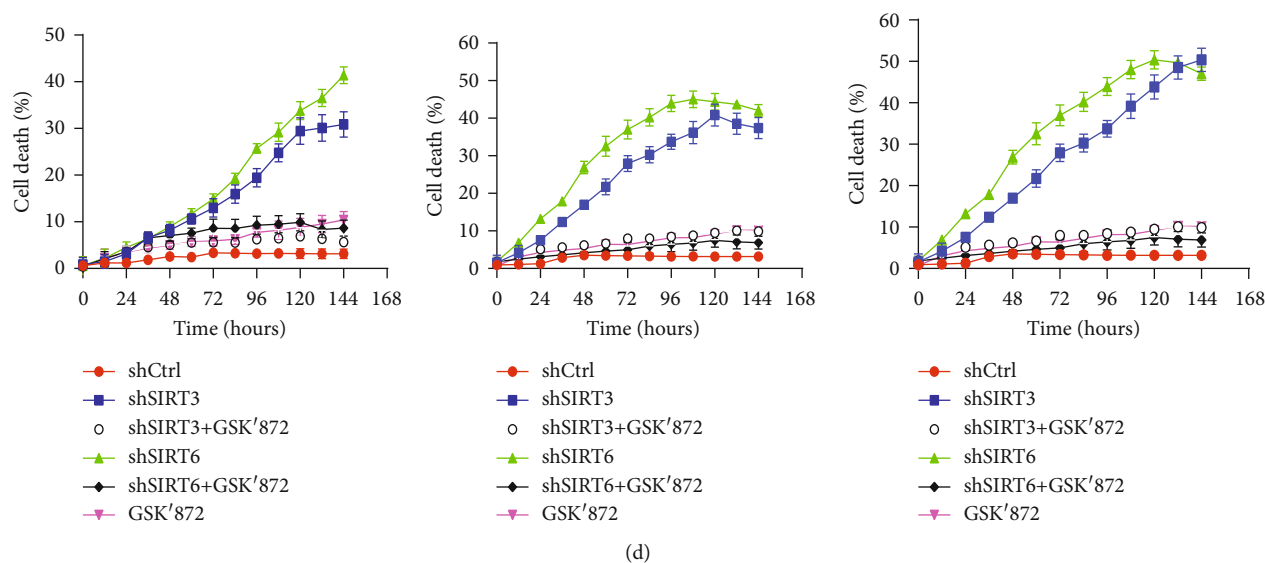


FIGURE 3: RIPK3-induced necroptosis is mediated by SIRT3 and SIRT6. (a) LNCaP cells stabilized expressed shSIRT3 and shSIRT6 with recombinant GFP and were treated with TNF (20 ng/ml). Cell death was tracked by staining with cytotoxic red and monitored by Incucyte. (b) Cell death curve of LNCaP, PC3, and DU145 cells after induction of control, SIRT1, SIRT3, or SIRT6 shRNA expression with doxycycline. (c) Western blot analysis of p-RIPK3 and p-MLKL protein levels in LNCaP and PC3 cells treated with 20 ng/ml TNF. (d) Cell death curve of LNCaP cells treated by RIPK3 inhibitor GSK'872 after induction of control, SIRT3, or SIRT6 shRNA expression with doxycycline.

phosphorylation and cleaved caspase 8 (Figure S2B). Overall, these data suggest both SIRT3 and SIRT6 are required to control RIPK1/RIPK3-induced necroptosis.

2.4. Both SIRT3 and SIRT6 Promote Prostate Cancer Progress via Suppressing Necroptosis-Mediated Innate Immune Response. To determine whether SIRT3 and SIRT6 are required for the growth of prostate cancer in vivo, we generated the LNCaP cell line with shRNA of SIRT3 and SIRT6 after doxycycline induction using a lentivirus transduction system. These cells were subsequently injected in mice. When tumors grew to 30-60 mm³, shRNA expression was induced. As shown in Figure 4(a), the expression of SIRT3 and SIRT6 shRNAs dramatically inhibited tumor growth in comparison with controls. There is no alteration in the mouse body weight. Necroptosis is widely regarded as an inflammatory lytic cell death. Therefore, shSIRT3- and shSIRT6-mediated necroptosis activation would be expected to promote innate inflammation. We next assessed the recruitment of immune cells including CD4+ T cells, macrophages, and neutrophils. As shown in Figures 4(b) and 4(c), deletion of SIRT3 and SIRT6 dramatically increased the infiltration of CD4+ T cells and macrophages as well as neutrophils. Accordingly, CCL8 and CXCL2 were significantly upregulated in shSIRT3- and shSIRT6-implanted mice but showed impaired induction in shCtrl mice (Figure 4(d)). In summary, these results suggest that SIRT3 and SIRT6 promote prostate cancer progress by suppressing necroptosis-mediated immune response.

3. Materials and Methods

3.1. Ethics Statement. Our study protocol was approved by the Ethics Committee of the Affiliated Hospital of Qingdao

University. As all the data were retrieved from the online databases, it could be confirmed that all informed consent had been obtained.

We utilized the UALCAN (<http://ualcan.path.uab.edu>) [27] which is from the TCGA database to analyze the mRNA expressions of seven SIRT members in the PCa tissues and their association with clinicopathologic parameters. Direct comparison of protein expression between human normal and cancer tissues was performed by immunohistochemistry in the Human Protein Atlas (<https://www.proteinatlas.org>) [28].

3.2. The Cancer Genome Atlas (TCGA) Database. We downloaded the PCa mRNA profile and corresponding clinical data from the TCGA database (<http://gdac.broadinstitute.org/>) [29]. We investigated the associations of SIRT expression with clinicopathological parameters and outcomes. The correlations between SIRT expression and clinicopathological parameters were analyzed by the chi-square (χ^2) or Fisher's exact test. Statistical analyses were conducted with the software GraphPad Prism 6 and SPSS 19.0.

3.3. Construction and Validation of the Prognostic Gene Signature. The association of mRNA expression with survival was further analyzed with multivariate Cox regression using SurvExpress [30]. A prognosis risk score was calculated on the basis of a linear combination of seven gene expressions multiplied by a regression coefficient (β) derived from the multivariate Cox proportional hazard regression model of each gene with the following formula: risk score = expression of gene1 \times β_1 gene1 + expression of gene2 \times β_2 gene2 + ...expression of gene n \times β_7 gene7. We selected the data from a total of 499 patients in the PCa cohorts available

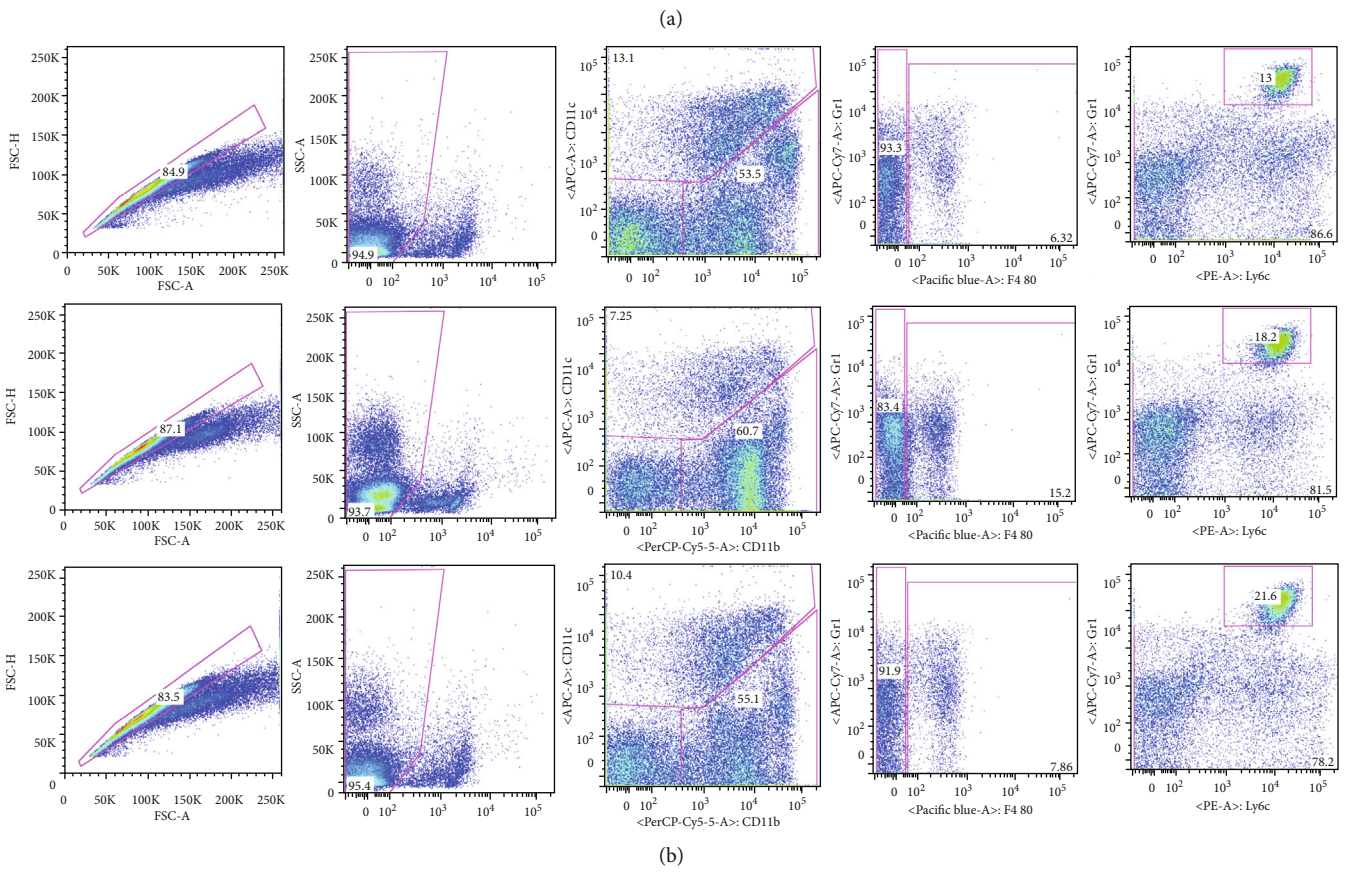
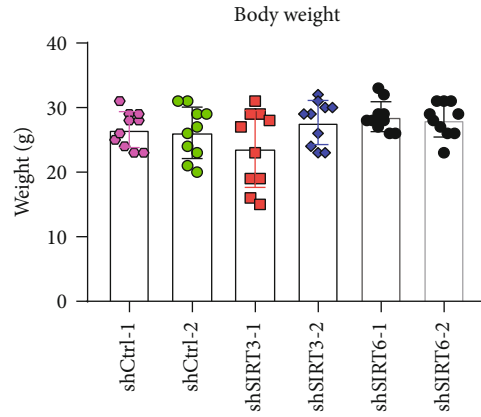
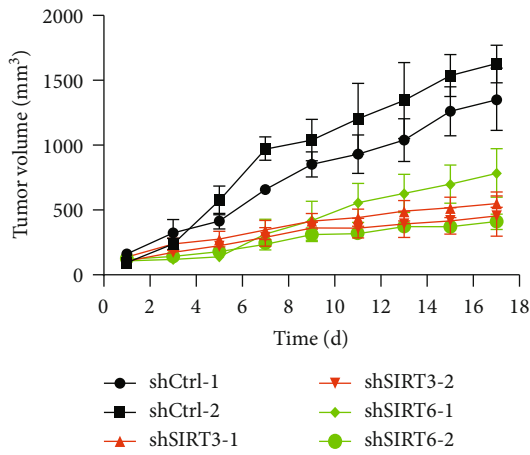


FIGURE 4: Continued.

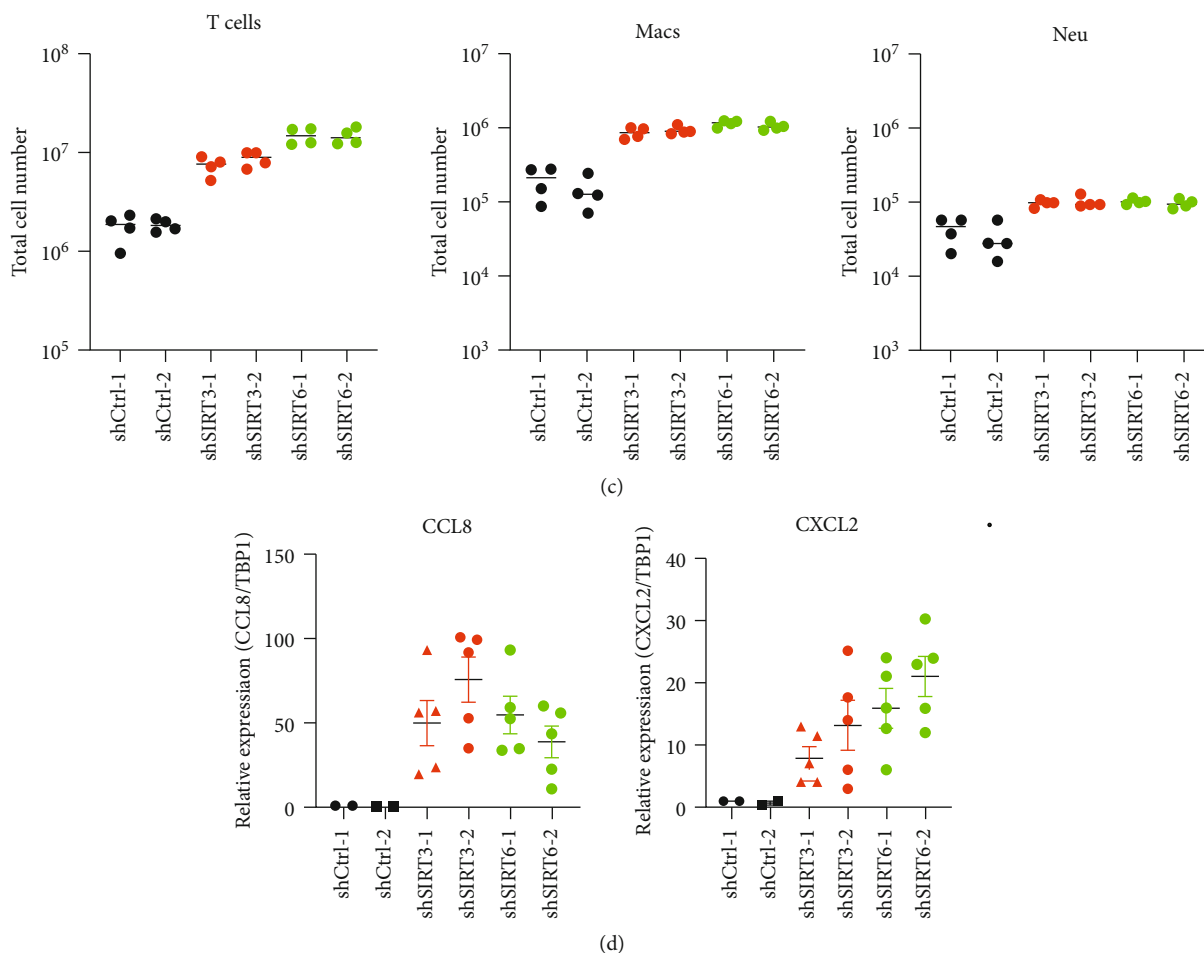


FIGURE 4: Necroptosis-induced innate immune cell recruitment controlled by both SIRT3 and SIRT6 is required to suppress prostate cancer progress. (a) Growth curves of xenografted tumors (LNCaP) after induction of control, SIRT3, or SIRT6 shRNA expression with doxycycline in vivo. Relative tumor volumes were calculated by normalizing against the tumor volume at day 1 following doxycycline administration. Body weight was tested daily. (b) Representative experiment of flow cytometric analysis of T cells, macrophages, and neutrophils in doxycycline-induced xenografted tumors (LNCaP). (c) The total number of T cells, macrophages, and neutrophils was shown in the histograms. Results represent mean \pm SD of three independent experiments. * $P < 0.05$. (d) The relative expression of CCL8 and CXCL2 is shown in the histograms. GAPDH was used as the internal control. Results represent mean \pm SD of three independent experiments. * $P < 0.05$ and ** $P < 0.01$.

in the SurvExpress database: the TCGA-PCa cohort for individual survival analysis.

3.4. cBioPortal. The cBioPortal is an open access resource (<http://www.cbioportal.org/>) for interactive exploration of multidimensional cancer genomic data [31]. To investigate various aspects of SIRT3 and SIRT6, genomic profiles including amplification, deep deletion, missense mutations, and copy number variance (CNV) data have been extracted from GISTIC and mRNA Expression z-Scores (RNASeq V2 RSEM). OS was also measured based on online instruction of cBioPortal.

3.5. Generation of Lentiviruses. To generate recombinant SIRT3 and SIRT6 shRNA with green fluorescent protein (GFP), we used pLKO.1 lentiviral expression vector containing the puromycin resistance gene. The lentiviruses were generated by coexpressing VSV-G and delta-8.9 in HEK-293T cells and then concentrated using PEG-it (System Biosciences).

For inducible expression of SIRT3 and SIRT6 shRNAs in tumor xenograft studies, we used pLVUTH-KRAB-KM vector with tet-inducible promoter. Cells were transduced with a lentivirus containing SIRT3 and SIRT6 shRNA for at least three days before adding puromycin for selection.

3.6. Western Blotting. For immunoblot analysis of necroptosis-related proteins, cell pellets were collected by trypsin digestion followed by lysis in RIPA buffer. Total protein concentration was measured with a BCA protein assay kit. Proteins were separated by electrophoresis through 4%–12% polyacrylamide gels, following electrophoretic transfer of proteins onto NC membranes with a Trans-Blot® Turbo™ Transfer System (Bio-Rad). Nonspecific binding was blocked by incubation with 5% nonfat milk, and then membranes were incubated with primary antibodies against p-RIPK3 (57220, Cell Signaling Technology [CST]), RIPK3 (95702, CST), p-MLKL (74921, CST), and MLKL (37705, CST). Membranes were then washed and incubated with the

appropriate HRP-conjugated secondary antibodies (7076, anti-mouse IgG; 7074, anti-rabbit IgG). The proteins of interest were visualized by enhanced chemiluminescence (Millipore, Billerica, MA, USA).

3.7. RT-PCR Analysis. RNA was extracted using an RNeasy Mini Kit (74104, QIAGEN) according to the manufacturer's instructions. The isolated RNA was reverse-transcribed into cDNA using a First-Strand cDNA Synthesis Kit (4368814, Applied Biosystems). Real-time quantitative PCR was performed on an ABI 7500 RT-PCR instrument using 2x SYBR Green (4368706, Applied Biosystems) and the appropriate primers.

3.8. Cytotoxic Assay. LNCaP, PC3, and DU145 were cultured as described in ATCC. For cell death assay, cells were seeded in 96-well plates at 70% confluence for 1 day. On the next day, cells were stimulated with 20 ng/ml TNF (T6674, Millipore Sigma) and 1 μ M GSK'872 (S8465, Selleckchem) and stained with Cytotoxic Red (4632, Essen Bioscience Inc.) following the manufacturers' protocols. The plate was scanned, and fluorescence and phase-contrast images (4 image fields/well) were acquired in real time every 2 hours after stimulation. Resulting images were analyzed using the software package supplied with the Incucyte imager (Essen Bioscience).

3.9. Flow Cytometry. Tumors were first dissected and then washed with ice-cold PBS. Washed tumors were cut into small pieces, which were incubated in PBS containing 10 mM HEPES, 5 mM EDTA, and 1 mM DTT at 37°C for 30 minutes with gentle shaking. The tumor segments were further digested in RPMI medium containing 0.5 mg/ml collagenase D at 37°C for 1.5 hours. The supernatant from the digested tumors was passed through a 70 μ m cell strainer and enriched using 37.5% Percoll to isolate immune cells. The following monoclonal antibodies were used for flow cytometry: Gr1 (RB6-8C5; 108426), F4/80 (BM8; 123116), and CD4 (GK1.5; 100408) from BioLegend; CD11b (M1/70; 48-0112-82) from Invitrogen; and CD11c (HL3; 557401) from BD Pharmingen. Cells were gated on live single-cell populations and hematopoietic cells using the CD45.2 gate followed by separation of each of the specific cell populations using the following cell surface markers: macrophages (CD11b+, F4/80+), dendritic cells (CD11c+ Gr1-), neutrophils (CD11b+, Gr1hi), and CD4 T cells (CD3+, CD4+).

4. Discussion

The SIRT family comprises a family of NAD⁺-dependent protein-modifying enzymes with activities in lysine deacetylation, adenosinediphospho- (ADP-) ribosylation, and/or diacylation [32]. In the present study, we intended to explore their expression levels and genetic alterations with the clinicopathological characteristics of PCa from the online public databases and assess their association with necroptosis-mediated innate immune response. Our results showed that the expression levels of SIRT3/6/7 were significantly associated with patients' Gleason score and nodal

metastasis. The PCa patients with higher expression of SIRT3/6 had poorer OS, and the SIRTs' genetic alterations were served as predictive biomarkers for poor OS. Mechanistically, the higher expression of both SIRT3 and SIRT6 inhibits RIPK3 and MLKL activation, which subsequently blocks necroptosis-mediated innate immune response. Blockade of both SIRT3 and SIRT6 ameliorated necroptosis suppression. The xenograft mouse model further showed that the SIRT3 and SIRT6 blockade enhances macrophage and neutrophil recruitment and thereby suppresses prostate cancer progress. Together, all these data suggested that the SIRT expression levels and genetic mutations have essential clinical values for PCa.

SIRT1 was widely studied in the PCa. Fu et al. [33] has found that SIRT1 interacted with androgen receptor (AR) and deacetylated its Lys⁶³⁰, leading to PCa cell growth suppression. Dai et al. [34] also found that SIRT1 acted as the AR's corepressor, and downregulation of *SIRT1* would enhance the transcriptional regulation of AR. However, Kojima et al. has reported that the upregulation of *SIRT1* could promote the PCa cell growth and induce chemoresistance in AR-negative PC3 and DU145 cells. These results suggested the dual function of *SIRT1* in PCa progression, which are dependent on the AR status. In the present study, our integrated network by cBioPortal also showed that AR was tightly related with *SIRT1*.

Until now, little was known about the roles of *SIRT2*, *SIRT3*, *SIRT4*, and *SIRT5* in the PCa. *SIRT2* was discovered as a regulator of aging in the budding yeast *Saccharomyces cerevisiae* [35]. Moreover, Damodaran et al. has reported that *SIRT2* deletion portended worse clinicopathological outcomes [36]. *SIRT3*, *SIRT4*, and *SIRT5* were primarily mitochondrial proteins, which have emerged as critical regulators of diverse biological events, such as cancer progression [10]. In the present study, we found that a higher expression level of *SIRT3* was associated with poorer PCa patients' OS, suggesting that it plays a critical role in the PCa development. Besides, a previous study demonstrated that *SIRT3* could suppress the PCa metastasis through promoting FOXO3A and inhibiting the Wnt/ β -catenin pathway [37]. Inconsistent with it, our results showed that *SIRT3* was highly expressed in the PCa samples compared with the normal tissues, and its level was associated with Gleason's score and nodal metastasis. The reason is due to the androgen hormone condition, just as Lee et al. [38] showed that the expression level of *SIRT3* was overexpressed in hormone-sensitive cells (LAPC4 and LNCaP), however, reduced in castrate-resistant cells (PC3, DU145, 22RV1, and C4-2).

It is reported that the *SIRT6* was overexpressed in PCa tissues. Knockdown of *SIRT6* could lead to cell cycle arrest, apoptosis, and DNA damage through decreasing *BCL2* gene expression [21]. For *SIRT7*, Haider et al. [22] showed that its expression level was increased as PCa progressed into the high grade stage. In the present study, the upregulation of *SIRT6/SIRT7* in PCa samples and their strong association with Gleason score and nodal metastasis could confirm their oncogenic roles.

Moreover, in search of SIRT gene mutations and their 50 frequently altered neighbor genes, we found that the SIRT

mutations may regulate a large number of proteins which are involved in the tumor growth. *AR*, *RBI*, and *P53*, which were implicated in the PCa onset and progression [39, 40], were highly associated with SIRT mutations. Interestingly, pathway analysis in GO and KEGG also indicated that cellular pathways, including NAD⁺-dependent histone deacetylase activity and the apoptotic signaling pathway in response to DNA damage by the p53 class mediator and regulation of cellular response to heat, were highly related to SIRT gene alterations. These findings unveiled several excellent candidates for future study.

Necroptosis has already been intensively studied in the last few decades. It was widely accepted that necroptosis is a lytic inflammatory cell death that functions as an executioner in the antitumor immunity of cancer therapy. However, the specific function of necroptosis in cancer is mysterious. One recent study demonstrated that sirtuins are able to control RIPK1-caspase 8-induced apoptosis in cancer. This occurs via a precise regulation of RIPK1 acetylation [26]. Our data corroborate the close link between SIRT3 and SIRT6 with necroptosis key adaptor RIPK3 activation. In conclusion, our study revealed the comprehensive clinical significance of SIRTs in PCa and provided clear further insights.

Data Availability

The data used to support the findings of this study are available from the corresponding author upon request.

Conflicts of Interest

All authors declare there are no competing interests related to this manuscript.

Acknowledgments

This work was supported by the Youth Fund of Affiliated Hospital of Qingdao University (2018-50).

Supplementary Materials

Supplementary Figure 1: representative immunohistochemistry images and prognostic values of SIRT6/7 in PCa derived from the Human Protein Atlas. (a, c) A little protein level of SIRT6 was found in normal prostate tissues, while its level was strongly detected in PCa samples. SIRT7 was expressed in PCa but not in normal prostate tissues. (b, d) Higher expression levels of SIRT6 and SIRT7 were associated with poorer OS of PCa patients. Supplementary Figure 2: RIPK3-induced necroptosis is mediated by SIRT3 and SIRT6. (a) Western blot analysis of SIRT3 and SIRT6 protein levels in LNCaP cells after induction of control, SIRT3, or SIRT6 shRNA expression with doxycycline. (b) Western blot analysis of p-RIPK1 and cleaved caspase 8 in LNCaP and PC3 cells treated with 20 ng/ml TNF. (c) PC3 cells stabilized expressed shSIRT3 and shSIRT6 with recombinant GFP and were treated with TNF (20 ng/ml). Cell death was tracked by staining with cytotoxic red and monitored by Incucyte. Supplementary Table 1-8: basic characteristics of prostate cancer

patients and univariate/multivariate analysis of overall survival in prostate cancer patients. Clinical data of prostate cancer patients showed that SIRT3 and SIRT6 are all independent risk factors for OS of PCa patients, which are independent on age, Gleason score, tumor stage, and pathology stage. All of these data are from the FireBrowse website (<http://firebrowse.org/api-docs/>). Supplementary Table 1: basic characteristics of prostate cancer patients. Supplementary Table 2: univariate analysis of overall survival in prostate cancer patients. Supplementary Table 3: multivariate analysis of overall survival in prostate cancer patients. SIRT1. Supplementary Table 4: multivariate analysis of overall survival in prostate cancer patients. SIRT2. Supplementary Table 5: multivariate analysis of overall survival in prostate cancer patients. SIRT3. Supplementary Table 6: multivariate analysis of overall survival in prostate cancer patients. SIRT4. Supplementary Table 7: multivariate analysis of overall survival in prostate cancer patients. SIRT5. Supplementary Table 8: multivariate analysis of overall survival in prostate cancer patients. SIRT6. Supplementary Table 9: multivariate analysis of overall survival in prostate cancer patients. SIRT7. (*Supplementary Materials*)


References

- [1] F. Bray, J. Ferlay, I. Soerjomataram, R. L. Siegel, L. A. Torre, and A. Jemal, "Global cancer statistics 2018: GLOBOCAN estimates of incidence and mortality worldwide for 36 cancers in 185 countries," *CA: a Cancer Journal for Clinicians*, vol. 68, no. 6, pp. 394–424, 2018.
- [2] A. Cimadamore, S. Gasparrini, M. Scarpelli et al., "Epigenetic modifications and modulators in prostate cancer," *Critical Reviews in Oncogenesis*, vol. 22, no. 5-6, pp. 439–450, 2017.
- [3] K. Ruggero, S. Farran-Matas, A. Martinez-Tebar, and A. Aytes, "Epigenetic regulation in prostate cancer progression," *Current Molecular Biology Reports*, vol. 4, no. 2, pp. 101–115, 2018.
- [4] T. Eckschlager, J. Plch, M. Stiborova, and J. Hrabeta, "Histone deacetylase inhibitors as anticancer drugs," *International Journal of Molecular Sciences*, vol. 18, no. 7, p. 1414, 2017.
- [5] R. Marmorstein, "Structure and chemistry of the Sir2 family of NAD⁺-dependent histone/protein deacetylases," *Biochemical Society Transactions*, vol. 32, pp. 904–909, 2004.
- [6] S. Michan and D. Sinclair, "Sirtuins in mammals: insights into their biological function," *The Biochemical Journal*, vol. 404, no. 1, pp. 1–13, 2007.
- [7] Z. Frydzinska, A. Owczarek, and K. Winiarska, "Sirtuins and their role in metabolism regulation," *Postepy Biochemii*, vol. 65, no. 1, pp. 31–40, 2019.
- [8] J. E. Choi and R. Mostoslavsky, "Sirtuins, metabolism, and DNA repair," *Current Opinion in Genetics & Development*, vol. 26, pp. 24–32, 2014.
- [9] M. Roth and W. Y. Chen, "Sorting out functions of sirtuins in cancer," *Oncogene*, vol. 33, no. 13, pp. 1609–1620, 2014.
- [10] J. George and N. Ahmad, "Mitochondrial sirtuins in cancer: emerging roles and therapeutic potential," *Cancer Research*, vol. 76, no. 9, pp. 2500–2506, 2016.
- [11] R. H. Houtkooper, E. Pirinen, and J. Auwerx, "Sirtuins as regulators of metabolism and healthspan," *Nature Reviews Molecular Cell Biology*, vol. 13, no. 4, pp. 225–238, 2012.
- [12] D. J. Bonda, H. G. Lee, A. Camins et al., "The sirtuin pathway in aging and Alzheimer disease: mechanistic and therapeutic

- considerations," *Lancet Neurology*, vol. 10, no. 3, pp. 275–279, 2011.
- [13] J. A. Hall, J. E. Dominy, Y. Lee, and P. Puigserver, "The sirtuin family's role in aging and age-associated pathologies," *The Journal of Clinical Investigation*, vol. 123, no. 3, pp. 973–979, 2013.
- [14] G. Botta, L. P. De Santis, and R. Saladino, "Current advances in the synthesis and antitumoral activity of SIRT1-2 inhibitors by modulation of p53 and pro-apoptotic proteins," *Current Medicinal Chemistry*, vol. 19, no. 34, pp. 5871–5884, 2012.
- [15] P. Pengsaa, S. Pothinam, B. Udomthavornsuk, and V. Titapan, "Risk factors for survival in patients performed radical hysterectomy for cervical carcinoma," *Journal of the Medical Association of Thailand*, vol. 72, no. 8, pp. 427–432, 1989.
- [16] G. Perez-Chacon, C. de Los Rios, and J. M. Zapata, "Indole-3-carbinol induces cMYC and IAP-family downmodulation and promotes apoptosis of Epstein-Barr virus (EBV)-positive but not of EBV-negative Burkitt's lymphoma cell lines," *Pharmacological Research*, vol. 89, pp. 46–56, 2014.
- [17] X. He, H. Nie, Y. Hong, C. Sheng, W. Xia, and W. Ying, "SIRT2 activity is required for the survival of C6 glioma cells," *Biochemical and Biophysical Research Communications*, vol. 417, no. 1, pp. 468–472, 2012.
- [18] W. Dai, J. Zhou, B. Jin, and J. Pan, "Class III-specific HDAC inhibitor tenovin-6 induces apoptosis, suppresses migration and eliminates cancer stem cells in uveal melanoma," *Scientific Reports*, vol. 6, no. 1, article 22622, 2016.
- [19] S. Hirai, S. Endo, R. Saito et al., "Antitumor effects of a sirtuin inhibitor, tenovin-6, against gastric cancer cells via death receptor 5 up-regulation," *PLoS One*, vol. 9, no. 7, article e102831, 2014.
- [20] H. Yuan, Z. Wang, L. Li et al., "Activation of stress response gene SIRT1 by BCR-ABL promotes leukemogenesis," *Blood*, vol. 119, no. 8, pp. 1904–1914, 2012.
- [21] Y. Liu, Q. R. Xie, B. Wang et al., "Inhibition of SIRT6 in prostate cancer reduces cell viability and increases sensitivity to chemotherapeutics," *Protein & Cell*, vol. 4, no. 9, pp. 702–710, 2013.
- [22] R. Haider, F. Massa, L. Kaminski et al., "Sirtuin 7: a new marker of aggressiveness in prostate cancer," *Oncotarget*, vol. 8, no. 44, pp. 77309–77316, 2017.
- [23] T. Molnár, A. Mázló, V. Tslaf, A. G. Szöllösi, G. Emri, and G. Koncz, "Current translational potential and underlying molecular mechanisms of necroptosis," *Cell Death & Disease*, vol. 10, no. 11, article 860, 2019.
- [24] L. Duprez, N. Takahashi, F. van Hauwermeiren et al., "RIP kinase-dependent necrosis drives lethal systemic inflammatory response syndrome," *Immunity*, vol. 35, no. 6, pp. 908–918, 2011.
- [25] Z. Liu and F. K. Chan, "Regulatory mechanisms of RIPK1 in cell death and inflammation," *Seminars in Cell & Developmental Biology*, vol. S1084-9521, no. 19, pp. 30243–30245, 2020.
- [26] V. Carafa, A. Nebbioso, F. Cuomo et al., "RIP1-HAT1-SIRT complex identification and targeting in treatment and prevention of cancer," *Clinical Cancer Research*, vol. 24, no. 12, pp. 2886–2900, 2018.
- [27] D. S. Chandrashekar, B. Bashel, S. A. H. Balasubramanya et al., "UALCAN: a portal for facilitating tumor subgroup gene expression and survival analyses," *Neoplasia*, vol. 19, no. 8, pp. 649–658, 2017.
- [28] A. Asplund, P. H. D. Edqvist, J. M. Schwenk, and F. Pontén, "Antibodies for profiling the human proteome—the Human Protein Atlas as a resource for cancer research," *Proteomics*, vol. 12, no. 13, pp. 2067–2077, 2012.
- [29] K. Tomczak, P. Czerwinska, and M. Wiznerowicz, "The Cancer Genome Atlas (TCGA): an immeasurable source of knowledge," *Contemporary Oncology (Poznan, Poland)*, vol. 19, no. 1A, pp. A68–A77, 2015.
- [30] R. Aguirre-Gamboa, H. Gomez-Rueda, E. Martínez-Ledesma et al., "SurvExpress: an online biomarker validation tool and database for cancer gene expression data using survival analysis," *PLoS One*, vol. 8, no. 9, article e74250, 2013.
- [31] J. Gao, B. A. Aksoy, U. Dogrusoz et al., "Integrative analysis of complex cancer genomics and clinical profiles using the cBioPortal," *Science Signaling*, vol. 6, no. 269, article pl1, 2013.
- [32] J. Du, H. Jiang, and H. Lin, "Investigating the ADP-ribosyltransferase activity of sirtuins with NAD analogues and 32P-NAD," *Biochemistry*, vol. 48, no. 13, pp. 2878–2890, 2009.
- [33] M. Fu, M. Liu, A. A. Sauve et al., "Hormonal control of androgen receptor function through SIRT1," *Molecular and Cellular Biology*, vol. 26, no. 21, pp. 8122–8135, 2006.
- [34] Y. Dai, D. Ngo, L. W. Forman, D. C. Qin, J. Jacob, and D. V. Faller, "Sirtuin 1 is required for antagonist-induced transcriptional repression of androgen-responsive genes by the androgen receptor," *Molecular Endocrinology*, vol. 21, no. 8, pp. 1807–1821, 2007.
- [35] M. Kaerberlein, M. McVey, and L. Guarente, "The SIR2/3/4 complex and SIR2 alone promote longevity in *Saccharomyces cerevisiae* by two different mechanisms," *Genes & Development*, vol. 13, no. 19, pp. 2570–2580, 1999.
- [36] S. Damodaran, N. Damaschke, J. Gawdzik et al., "Dysregulation of sirtuin 2 (SIRT2) and histone H3K18 acetylation pathways associates with adverse prostate cancer outcomes," *BMC Cancer*, vol. 17, no. 1, article 874, 2017.
- [37] R. Li, Y. Quan, and W. Xia, "SIRT3 inhibits prostate cancer metastasis through regulation of FOXO3A by suppressing Wnt/ β -catenin pathway," *Experimental Cell Research*, vol. 364, no. 2, pp. 143–151, 2018.
- [38] J. H. Lee, B. Yang, A. J. Lindahl et al., "Identifying dysregulated epigenetic enzyme activity in castrate-resistant prostate cancer development," *ACS Chemical Biology*, vol. 12, no. 11, pp. 2804–2814, 2017.
- [39] A. A. Hamid, K. P. Gray, G. Shaw et al., "Compound genomic alterations of TP53, PTEN, and RB1 tumor suppressors in localized and metastatic prostate cancer," *European Urology*, vol. 76, no. 1, pp. 89–97, 2019.
- [40] B. S. Taylor, N. Schultz, H. Hieronymus et al., "Integrative genomic profiling of human prostate cancer," *Cancer Cell*, vol. 18, no. 1, pp. 11–22, 2010.

Research Article

Negative Effects of SIGIRR on TRAF6 Ubiquitination in Acute Lung Injury In Vitro

Feng Tian,¹ Qiang Lu,¹ Jie Lei,¹ Yunfeng Ni,¹ Nianlin Xie,¹ Daixing Zhong,¹ Guang Yang,¹ Shaokui Si,² and Tao Jiang¹ 

¹Department of Thoracic Surgery, Tangdu Hospital, Fourth Military Medical University, Xi'an, China

²Department of Respiration, Third Hospital of Baoji, Baoji, China

Correspondence should be addressed to Tao Jiang; jiangtaochest@163.com

Received 24 June 2020; Revised 2 September 2020; Accepted 5 October 2020; Published 15 October 2020

Academic Editor: Zenghui Teng

Copyright © 2020 Feng Tian et al. This is an open access article distributed under the Creative Commons Attribution License, which permits unrestricted use, distribution, and reproduction in any medium, provided the original work is properly cited.

In this study, the effects of single immunoglobulin IL-1 receptor-related protein (SIGIRR) on tumor necrosis factor- (TNF-) receptor-associated factor 6 (TRAF6) ubiquitination in acute lung injury (ALI) were evaluated in both alveolar epithelial cells and alveolar macrophage cells in vitro. Our results found that SIGIRR negatively regulated TRAF6 ubiquitination and such SIGIRR inhibition could enhance the TRAF6 expression in both alveolar epithelial cells (AECs) and alveolar macrophage cells (AMCs). SIGIRR knockdown may increase NF- κ B activity via TRAF6 regulation by the classical but not the nonclassical NF- κ B signaling pathway. Such modulation between TRAF6 and SIGIRR could affect cytokine secretion and exacerbate the immune response; the IL-8, NFKB1, and NFKBIA mRNA levels were reduced after SIGIRR overexpression. The current study reveals the molecular mechanisms of the negative regulatory roles of SIGIRR on the innate immune response related to the LPS/TLR-4 signaling pathway and provides evidence for strategies to clinically treat inflammatory diseases.

1. Introduction

Acute lung injury (ALI) is an acute hypoxic respiratory dysfunction resulting from multiple factors [1–3]. The continuous progressive phase of ALI develops into acute respiratory distress syndrome (ARDS) [4, 5]. The pathological feature of the above process was the injury of alveolar capillary endothelial cells and alveolar epithelial cells (AECs) combined with extensive pulmonary edema and minimal atelectasis. ALI has a poor prognosis and can rapidly progress to multiple organ failures with a 30%–70% mortality rate [6–8]. Therefore, it is very important to study the pathogenesis and prevention measures of ALI. It has been proven that the lipopolysaccharide- (LPS-) Toll-like receptor-4 (TLR-4) signaling pathway plays a key role in the pathologic process of ALI [9–11]. Suppression of the LPS/TLR-4-mediated innate immune response is highly effective for the control of ALI.

In the development of ALI, TLRs play an important role in the above pathology process and regulate the innate

immune response by inducing the release of various inflammatory factors [12, 13]. LPS/TLR-4 could modulate the above process by NF- κ B activation, leading to the release of a large number of cytokines and chemokines from AECs and alveolar macrophage cells (AMCs) [14, 15].

Single immunoglobulin IL-1 receptor-related protein (SIGIRR), also named Toll-like receptor/interleukin-1 receptor 8 (TIR8), is a member of the TLR superfamily [16, 17]. It has been demonstrated that SIGIRR is highly expressed in epithelial tissues, including the kidney, colon, spleen, and liver, but is weakly expressed in the brain and muscle [18, 19]. In our previous study [20], it was first discovered that SIGIRR is highly expressed in human normal AECs obtained from 20 lung cancer patients with surgically resected adjacent lung normal tissues. Our data also provide evidence that SIGIRR overexpression could effectively inhibit LPS-induced ALI and inflammatory responses. The inflammatory response induced by LPS, IL-1, or other proinflammatory factors was more serious in SIGIRR knockout mice than in wild-type mice [21, 22]. In addition, some reports have

shown that IL-1R/TLR-4 can directly interact with the intracellular TIR domain of SIGIRR [23, 24]. It has been shown that TLRs play a key role in the pathological process of ALI, and other studies have also proven that there are negative effects of SIGIRR on the TLR signaling pathway [25, 26], but the relationship between SIGIRR and lung injury and the detailed molecular mechanism are still unknown; in addition, there are few studies about the above process. Thus, exploring the downstream target molecule of SIGIRR and elucidating the mechanism of the above process will help us find new therapeutic methods for the clinical treatment of ALI.

It has been demonstrated that the downregulation of the LPS-TLR-4 pathway could significantly inhibit the severity of LPS-induced inflammation [27]. SIGIRR is one of the molecules that inhibits TLR-4. In previous reports, high expression of SIGIRR was observed in normal human AECs, and SIGIRR overexpression inhibited LPS-induced ALI [28, 29]. Tumor necrosis factor- (TNF-) receptor-associated factor 6 (TRAF6) can activate kinase 1 (TAK1) and TAK1-binding protein 2 (TAB2), which are related to NF- κ B activation and cytokine secretion [30, 31]. In addition, TRAF6 was the downstream target for IL-1R-associated kinase (IRAK) that could be recruited by MyD88. It has been reported that NF- κ B activation resulted from the TRAF6-TRIF-binding process, which could affect the immune response combined with TLR-4 [32–34].

However, it was still unclear if there is a relationship between SIGIRR and TRAF6 and if this interaction of the above two molecules would affect the downstream targets of the inflammatory response. Thus, in our current study, the interaction between SIGIRR and TRAF6 was explored by evaluating TRAF6 autoubiquitination regulated by SIGIRR expression. However, it is known that the activation of NF- κ B is related to the ubiquitination of TRAF6.

We hypothesized that such modulation between the above two molecules would change NF- κ B activation and cytokine secretion and affect the further immune response related to the effects of the LPS/TLR-4 signaling pathway. The implementation of the study will be helpful to reveal the molecular mechanisms of the negative regulatory roles of SIGIRR on the innate immune response and will provide experimental evidence for the clinical treatment of inflammatory diseases, especially for ALI.

2. Materials and Methods

2.1. Cell Culture. AECs and AMCs were obtained from the American Type Culture Collection (Manassas, VA). Cells were cultured with Dulbecco's modified Eagle's medium (DMEM, Gibco, Carlsbad, CA) supplemented with 10% fetal calf serum (FCS) and 1% penicillin/streptomycin at 37°C in a humidified incubator with 95% air and 5% CO₂. Cells were passaged every 3 days to maintain growth. HEK293 cells were used and transfected with the indicated vectors in the glutathione S-transferase (GST) pull-down and coimmunoprecipitation experiments as previously described [35, 36]. In brief, the SIGIRR with HA and TRAF6 with Flag were prepared as previously described [20]. By immunoblotting

analysis, SDS-PAGE methods were used to elute proteins. Anti-SIGIRR and anti-TRAF6 antibodies were used in the above protocol.

2.2. Western Blotting. First, lysing buffer including 150 mM NaCl, 0.01 M EDTA, 0.01 M EGTA, 0.01 M Tris-HCl (pH 7.5), 1% Triton X-100, 0.01 M β -glycerophosphate, 0.01 M Na₃VO₄, and 1 μ g/ml leupeptin was used to obtain the protein from AECs and AMCs. A BCA test was performed to determine the protein concentrations of the cell lysates. Then, the normal procedure of western blotting was performed as previously described [20]. Antibodies against TRAF6 (1 : 1000) and SIGIRR (1 : 1000) were purchased from Cell Signaling Technology (Beverly, MA, USA).

2.3. Quantitative PCR. Quantitative PCR, which was performed as previously described [20, 37], was used to observe the mRNA expression levels of TRAF6, SIGIRR, and the above cytokines.

2.4. NF- κ B Reporter Assay. After cell transfection, an NF- κ B firefly luciferase reporter was used to evaluate NF- κ B activity according to the manufacturer's instructions. First, the above cells were lysed in passive lysis buffer, and then, a dual-luciferase assay was used to quantify the luciferase activity [38, 39].

2.5. Statistics. Statistical analyses were performed using GraphPad Prism. All data are expressed as the mean \pm SEM. $P < 0.05$ was considered statistically significant.

3. Results

3.1. Effect of SIGIRR on TRAF6 Ubiquitination. The interaction between SIGIRR and TRAF6 was observed through GST pull-down and coimmunoprecipitation experiments using anti-SIGIRR and anti-TRAF6 antibodies. GST pull-down assay was performed using purified GST-fusion SIGIRR and His-tagged TRAF6 proteins. His-TRAF6 interacted with GST-SIGIRR, whereas GST alone did not exhibit any pull-down activity with His-TRAF6 protein. Lysed HEK293 cells including proteins were pulled down with purified GST-GFP or GST-SIGIRR (Figures 1(a) and 1(b)).

The results from the GST pull-down and coimmunoprecipitation experiments showed that there is an interaction between SIGIRR and TRAF6. HEK293 cells were cotransfected with SIGIRR, Flag-TRAF6, and HA-ubiquitin, and the results showed that the above cotransfection could reduce the TRAF6 ubiquitination level in HEK293 cells (Figure 1(c)). Ubiquitination modification could also regulate the following gene expression or function changes in the physiological processes. And thus, NF- κ B activation could be regulated by the ubiquitination of TRAF6 [40, 41]. HEK293 cells (Figure 1(d)) were cultured and transfected according to the previous protocol [35, 36]. In addition, colocalization between SIGIRR and TRAF6 in HEK293 cells was also evaluated by immunofluorescence confocal microscopy. The results suggested that SIGIRR and TRAF6 colocalized to the cytoplasm or the cytoplasmic membrane (Figure 1(e)).

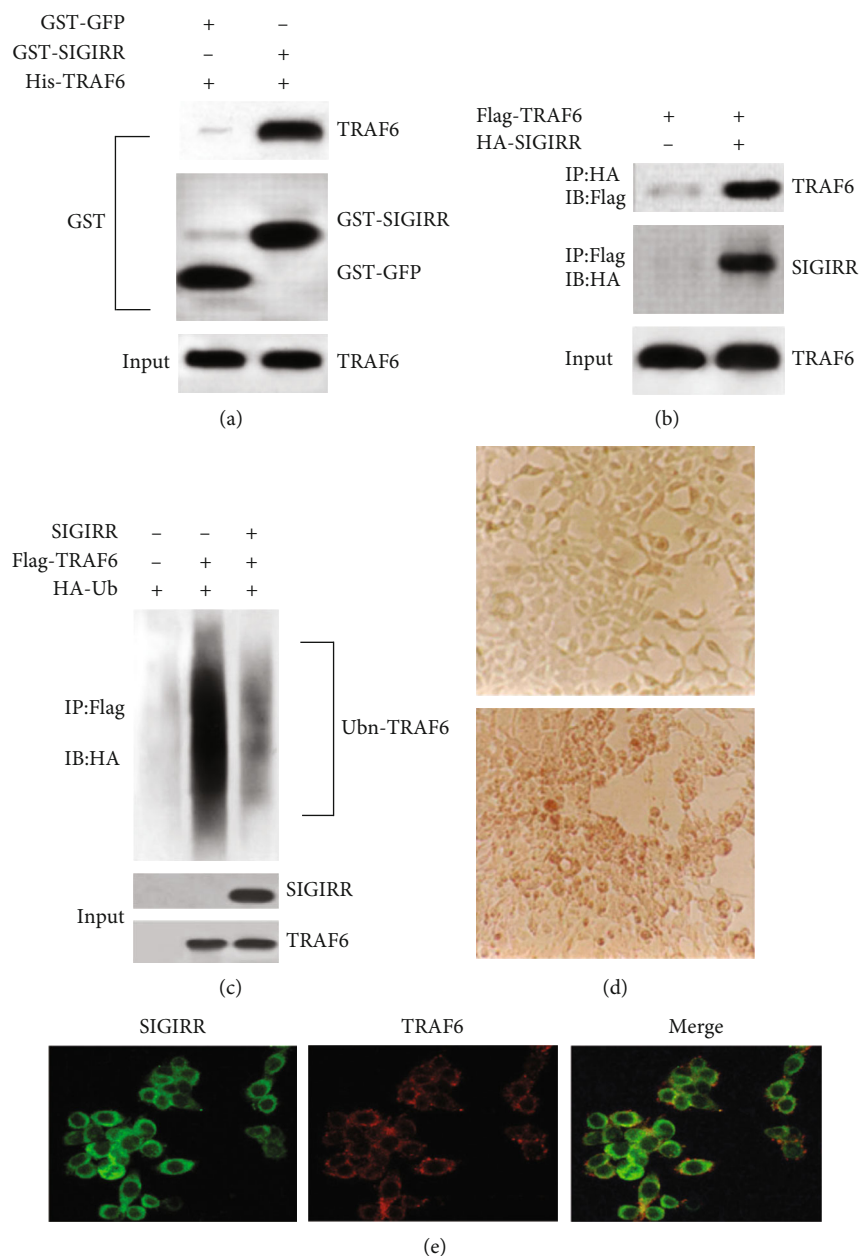


FIGURE 1: Analysis by pull-down and coimmunoprecipitation experiments of the interaction between SIGIRR and TRAF6 and resultant (auto) ubiquitinylation of TRAF6. (a) GST pull-down assay was performed using purified GST-fusion SIGIRR and His-tagged TRAF6 proteins. (b) A lysate from HEK293 cells cotransfected with Flag-TRAF6 or HA-SIGIRR was subjected to immunoprecipitation with anti-HA or anti-Flag antibody, respectively. (c) A lysate from HEK293 cells cotransfected with SIGIRR, Flag-TRAF6, or HA-ubiquitin, respectively, was subjected to immunoprecipitation with anti-Flag antibody. (d) HEK293 cells were cultured and cotransfected with the above reagents. (e) Colocalization between SIGIRR and TRAF6 in HEK293 cells was also evaluated by immunofluorescence confocal microscopy.

3.2. Effect of SIGIRR on TRAF6 Expression Both in AECs and in AMCs. AECs and AMCs were first cultured by a normal protocol. To evaluate the effect of SIGIRR on TRAF6 expression, western blotting analyses and quantitative PCR assay were performed in the following experiments to detect TRAF6 expression and mRNA levels both in AECs and in AMCs, respectively. The results demonstrated that SIGIRR expression and the mRNA levels were reduced significantly both in AECs (Figures 2(a) and 2(c)) and in AMCs

(Figures 2(b) and 2(d)) after transection with SIGIRR_shRNA#1 or SIGIRR_shRNA#2. After that, our results also provided clear evidence that both TRAF6 expressions (Figures 2(e) and 2(f)) and the mRNA levels (Figures 2(g) and 2(h)) increased obviously in cells that were treated with SIGIRR_shRNA compared with those in the untreated cells for both AEC and AMC groups.

Furthermore, SIGIRR_cDNA was transfected to obtain the overexpression of SIGIRR both in AECs and in AMCs.

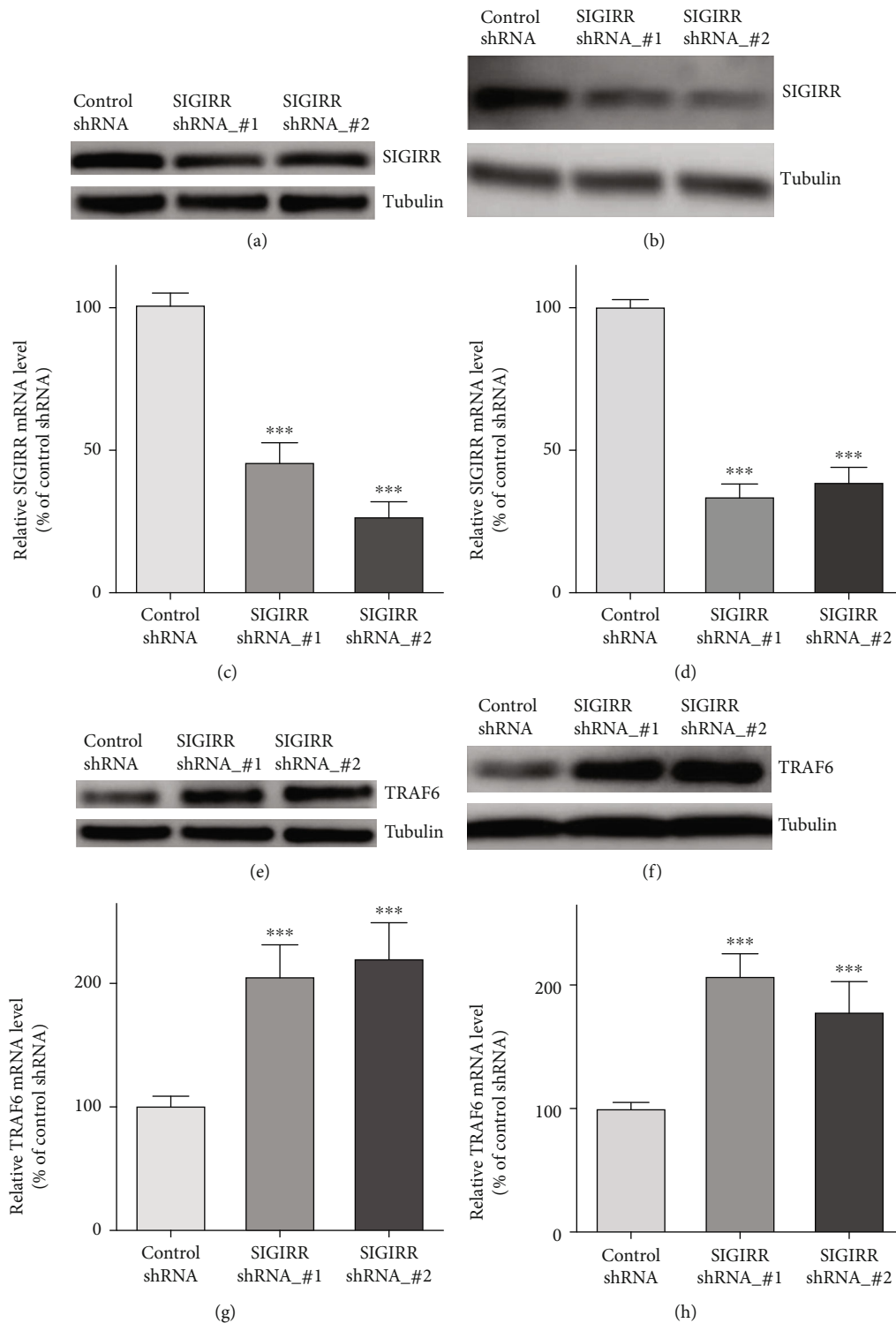


FIGURE 2: Effect of SIGIRR on TRAF6 expression both in AECs and in AMCs. (a, b) The results using western blot demonstrated that SIGIRR expression was reduced significantly both in AECs and in AMCs after transfection with SIGIRR_shRNA#1 or SIGIRR_shRNA#2. (c, d) The results using quantitative PCR demonstrated that SIGIRR mRNA levels were reduced significantly in AECs and AMCs after the above transfection. (e, f) TRAF6 expression by using western blot obviously increased in SIGIRR_shRNA-treated cells compared with those in control cells both in AECs and in AMCs. (g, h) TRAF6 mRNA levels by using quantitative PCR obviously increased in SIGIRR_shRNA-treated cells compared with those in control cells both in AECs and in AMCs. The data represent three independent experiments with four samples for each treatment. ** $P < 0.01$ and *** $P < 0.001$.

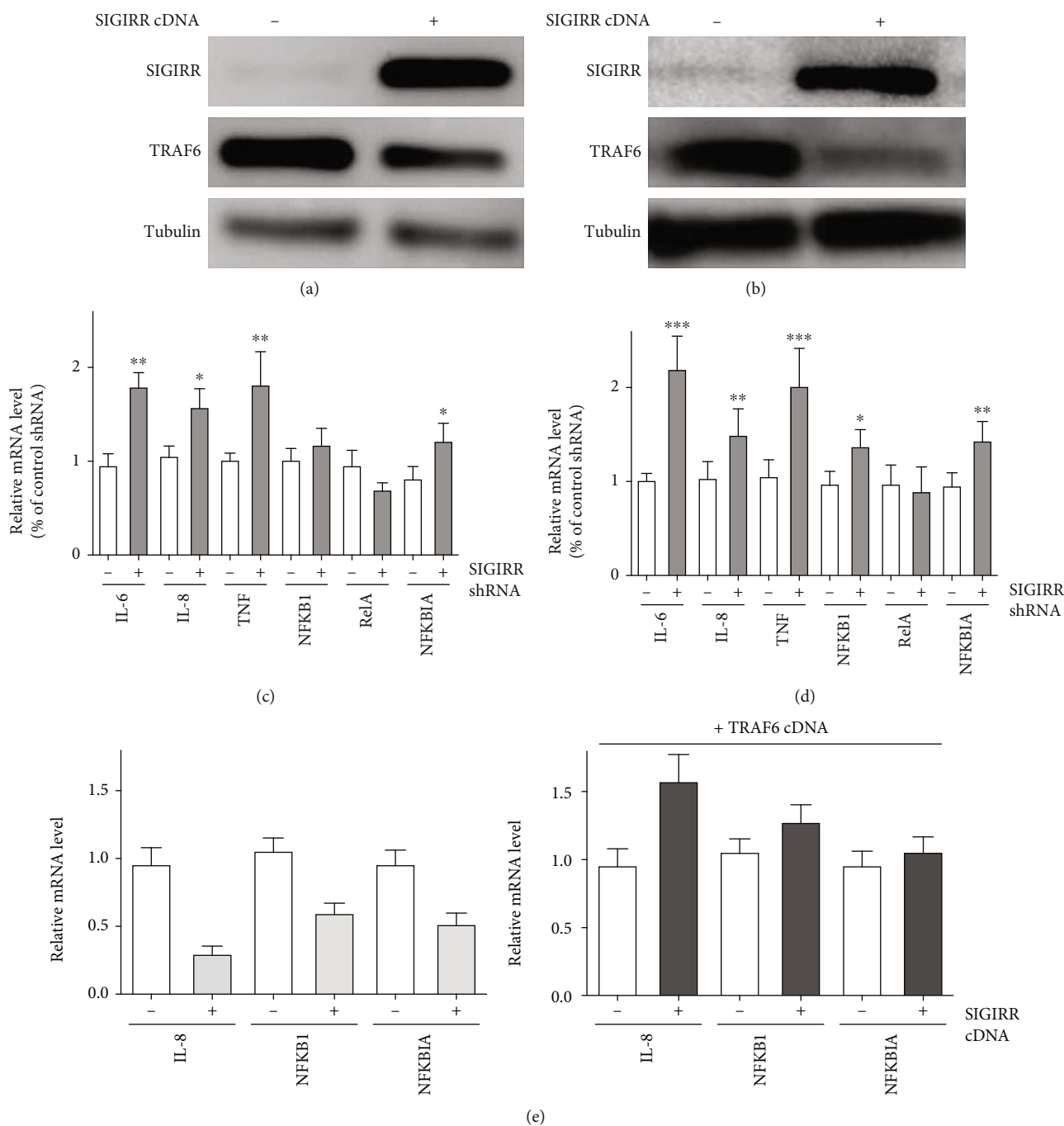


FIGURE 3: Effect of TRAF6 reversal of SIGIRR in AMCs. (a, b) SIGIRR overexpression was performed to detect changes on SIGIRR and TRAF6 in AECs and AMCs. (c, d) The mRNA levels of downstream NF- κ B signaling molecules, including IL-6, IL-8, TNF- α , NFKBIA, NFKB1, and RelA, were observed in the presence or absence of SIGIRR_shRNA in AECs and AMCs. (e) The rescue experiments were performed by cotransfection with TRAF6_cDNA and SIGIRR_shRNA in AMCs. The data represent three independent experiments with four samples for each treatment. ** $P < 0.01$ and *** $P < 0.001$.

Using western blotting analyses, increased SIGIRR expression was observed after SIGIRR_cDNA transfection, and TRAF6 expression was decreased significantly both in AECs (Figure 3(a)) and in AMCs (Figure 3(b)) compared with that in control cells. Thus, the above data suggested that the negative regulation of SIGIRR on TRAF6 was observed and that such inhibition of SIGIRR by a specific shRNA could enhance TRAF6 expression both in AECs and in AMCs.

3.3. Effect of SIGIRR/TRAF6 on the NF- κ B Signaling Pathway Both in AECs and in AMCs. Next, the effect of SIGIRR expression on the NF- κ B target gene network was observed by quantitative PCR assay. After specific inhibition of SIGIRR expression by using SIGIRR_shRNA, the mRNA levels of several downstream NF- κ B signaling molecules, including IL-6, IL-8, TNF- α , and NFKBIA, were significantly increased both in AECs and in AMCs compared with the

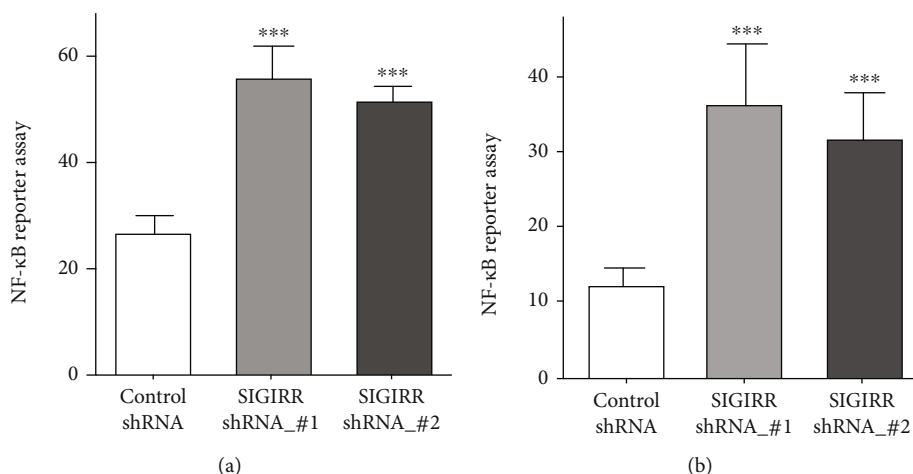


FIGURE 4: Inhibition of SIGIRR can affect the activity of the NF- κ B pathway in AECs and AMCs. (a, b) NF- κ B report experiments were performed to observe the effect of SIGIRR_shRNA on NF- κ B activity in AECs and AMCs. The data represent three independent experiments with four samples for each treatment. ** $P < 0.01$ and *** $P < 0.001$.

levels in the control group. However, for another two molecules, NFKB1 and RelA, the above significant enhancements in the mRNA levels were not obtained, and there were no changes in the presence or absence of SIGIRR_shRNA in AECs and AMCs. The difference was that IL-6, IL-8, TNF- α , and NFKBIA belong to the classical NF- κ B signaling pathway between the two above groups of downstream molecules, but NFKB1 and RelA were the molecules of the nonclassical pathway [31, 32]. The above results provide evidence that SIGIRR knockdown may affect the classical but not the nonclassical NF- κ B signaling pathway both in AECs (Figure 3(c)) and in AMCs (Figure 3(d)), but further details should be focused to clarify the underlying mechanism in the future. In addition, overexpression of SIGIRR was also performed to detect the changes on the above downstream molecules. The results showed that obvious inhibition of the IL-8, NFKB1, and NFKBIA mRNA levels in AMC was obtained after SIGIRR_cDNA transfection (Figure 3(e)).

Furthermore, the rescued experiments were also performed by cotransfection with TRAF6_cDNA in the presence or absence of SIGIRR overexpression in AMC, which reversed the effect of SIGIRR on NF- κ B downstream molecules. The IL-8, NFKB1, and NFKBIA mRNA levels were significantly enhanced after SIGIRR overexpression transfection in the presence of TRAF6_cDNA transfection in AMC (Figure 3(e)). Thus, the above data provide evidence that SIGIRR affects the downstream molecules of the classical NF- κ B signaling pathway by modulating TRAF6.

NF- κ B receptor experiments were performed to observe the effect of SIGIRR on NF- κ B activity. AECs and AMCs were transfected with SIGIRR_shRNA to reduce SIGIRR expression. The results of the NF- κ B activity assay showed that inhibition of SIGIRR expression significantly increased NF- κ B activity both in AECs and in AMCs (Figure 4).

3.4. Effect of SIGIRR on TNFAIP3 Expression Both in AECs and in AMCs. TNFAIP3 expression and the mRNA levels both in AECs and in AMCs were evaluated after SIGIRR_shRNA transfection using western blotting and quantitative

PCR assay, respectively. It has been proven that NF- κ B activity was regulated by TNFAIP3 negatively [42–44]. The results showed that inhibition of SIGIRR expression could significantly reduce TNFAIP3 expression and the mRNA levels in the above cells compared with those in the control cells (Figures 5(a) and 5(b)). In addition, SIGIRR overexpression by SIGIRR_cDNA enhanced TNFAIP3 expression and the mRNA levels both in AECs (Figure 5(c)) and in AMCs (Figure 5(d)).

4. Discussion

ALI is a progressive, acute, hypoxic respiratory dysfunction that results from multiple factors [3, 4]. It has been demonstrated that suppression of LPS/TLR-4 greatly promotes the development of ALI. Inhibition of LPS/TLR-4 plays a key role in the above pathological process and mediates the innate immune response that is induced by different inflammatory factors [11–14].

In this study, we addressed the mechanisms through which the interaction of SIGIRR and TRAF6 affects ALI. The effect of SIGIRR on TRAF6 was observed by different methods. Our current study provided the following evidences: (1) SIGIRR and TRAF6 were colocalized in the cells, and overexpression of SIGIRR could reduce the ubiquitination level of TRAF6; (2) negative regulation of SIGIRR on TRAF6 was observed, and inhibition of SIGIRR could enhance the expression of TRAF6 both in AECs and in AMCs; (3) SIGIRR knockdown by shRNA may increase the NF- κ B activity by the classical NF- κ B signaling pathway but not the nonclassical pathway, and SIGIRR overexpression could reduce the IL-8, NFKB1, and NFKBIA mRNA levels, which could be rescued by TRAF6 overexpression; and (4) SIGIRR could affect TNFAIP3 expression.

SIGIRR, also named Toll-like receptor/interleukin-1 receptor 8 (TIR8), and a member of the TLR-IL-1R receptor superfamily were involved in the pathological process of ALI by regulating the NF- κ B activation to release the cytokines and chemokines, and increased SIGIRR expression could

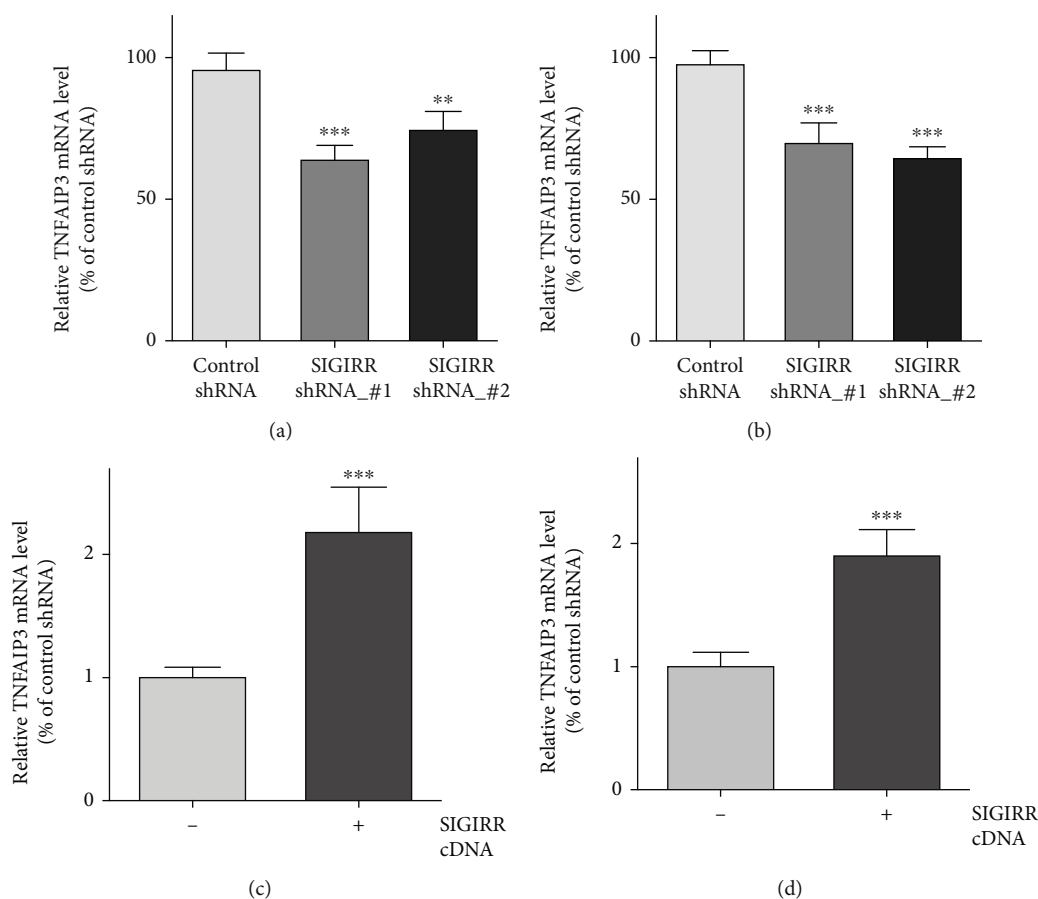


FIGURE 5: Effect of SIGIRR on TNFAIP3 expression both in AECs and in AMCs. (a, b) The TNFAIP3 mRNA levels both in AECs and in AMCs were evaluated after SIGIRR_shRNA transfection using the quantitative PCR assay. (c, d) TNFAIP3 mRNA levels were obviously enhanced both in AECs and in AMCs after SIGIRR overexpression by SIGIRR_cDNA application. The data represent two independent experiments with four mice per group. $**P < 0.01$ and $***P < 0.001$.

inhibit LPS-induced ALI by downregulating the LPS-TLR-4 pathway [17, 18]. MyD88 is involved in the pathway of IL-1R-associated kinase and TRAF6. In addition, SIGIRR could negatively regulate multiple LR-IL-1R receptor-mediated signaling transduction pathways, while the negative regulatory mechanism of SIGIRR has not been fully elucidated [23, 45]. Thus, the effect of the LPS/TLR-4 signaling pathway on the interaction of SIGIRR and TRAF6 was observed. The treatment of ALI by SIGIRR would be a possible route. However, whether the effect is related to its inhibition of TRAF6 further reveals the molecular mechanism by which SIGIRR negatively regulates inflammation. The results showed that SIGIRR and TRAF6 colocalize in cells in ALI. The ubiquitination of TRAF6 was reduced by SIGIRR overexpression, which regulates NF- κ B activation. Inhibition of SIGIRR significantly increased the expression of TRAF6 in alveolar epithelium and macrophages, thereby further affecting the activity of NF- κ B molecules and regulating the levels of the downstream signals IL-6, IL-8, TNF- α , and NFKBIA.

ALI and ARDS are clinically critical diseases. Currently, there are no specific therapies for ALI/ARDS [7]. TLRs are important pathogen pattern recognition receptors in the innate immune system [10]. The immune response com-

bined with TLR-4 could induce the TRAF6-TRIF-binding process and NF- κ B activation [33]. Excessive activation of TLR signaling plays a key role in the uncontrolled inflammatory response regulated by SIGIRR. Taken together, the data presented herein provide a new perspective on the relevance of ALI. Thus, such modulation between TRAF6 and SIGIRR could affect cytokine secretion and induce a further immune response. SIGIRR plays a negative regulatory role in the above process, such as ALI, related to the LPS/TLR-4 signaling pathway. Our previous data provided the evidence that SIGIRR inhibits the transcriptional activity of NF- κ B and reduces the amount of cytokines produced, protecting these cells from acute LPS-induced damage [20]. In addition, TNFAIP3 could regulate NF- κ B activity negatively [43]. Current results also found that the TNFAIP3 level will be regulated by changing SIGIRR expression.

Our above results provided the data that SIGIRR could interact with TRAF6 and reduce its expression due to the ubiquitination that was the critical factor for NF- κ B activation. The current study revealed the molecular mechanisms of the negative regulatory roles of SIGIRR on the innate immune response and will provide experimental evidence for the clinical treatment of inflammatory diseases.

Data Availability

The data used to support the findings of this study are included within the article.

Conflicts of Interest

The authors declare no conflict of interest.

Authors' Contributions

F.T., Q.L., X.L., and T.J. designed the plan. F.T., Q.L., X.L., and Y.N. performed the experiments. J.L., D.Z., and N.X. performed the cell culture. F.T., J.L., G.Y., S.S., and D.Z. analysed the results. F.T. and T.J. wrote the manuscript. All authors reviewed the manuscript. Feng Tian, Qiang Lu, and Jie Lei contributed equally to this work.

Acknowledgments

This work was supported by the grant (No. 81300051; No. 81770068) from the National Natural Science Foundation of China.

References

- [1] C. E. Evans and Y. Y. Zhao, "Impact of thrombosis on pulmonary endothelial injury and repair following sepsis," *American Journal of Physiology. Lung Cellular and Molecular Physiology*, vol. 312, no. 4, pp. L441–L451, 2017.
- [2] M. T. Voelker, A. Bergmann, T. Busch et al., "The effects of hemoglobin glutamer-200 and iNO on pulmonary vascular tone and arterial oxygenation in an experimental acute respiratory distress syndrome," *Pulmonary Pharmacology & Therapeutics*, vol. 49, pp. 130–133, 2018.
- [3] G. Voiriot, K. Razazi, V. Amsellem et al., "Interleukin-6 displays lung anti-inflammatory properties and exerts protective hemodynamic effects in a double-hit murine acute lung injury," *Respiratory Research*, vol. 18, no. 1, p. 64, 2017.
- [4] T. G. Shah, D. Predescu, and S. Predescu, "Mesenchymal stem cells-derived extracellular vesicles in acute respiratory distress syndrome: a review of current literature and potential future treatment options," *Clinical and Translational Medicine*, vol. 8, no. 1, p. 25, 2019.
- [5] M. Briel, M. Meade, A. Mercat et al., "Higher vs lower positive end-expiratory pressure in patients with acute lung injury and acute respiratory distress syndrome," *JAMA*, vol. 303, no. 9, pp. 865–873, 2010.
- [6] M. A. Matthay, L. B. Ware, and G. A. Zimmerman, "The acute respiratory distress syndrome," *The Journal of Clinical Investigation*, vol. 122, no. 8, pp. 2731–2740, 2012.
- [7] A. Dushianthan, M. P. W. Grocott, A. D. Postle, and R. Cusack, "Acute respiratory distress syndrome and acute lung injury," *Postgraduate Medical Journal*, vol. 87, no. 1031, pp. 612–622, 2011.
- [8] H. Flori, M. K. Dahmer, A. Sapru, M. W. Quasney, and Pediatric Acute Lung Injury Consensus Conference Group, "Comorbidities and assessment of severity of pediatric acute respiratory distress syndrome," *Pediatric Critical Care Medicine*, vol. 16, 5 Supplement 1, pp. S41–S50, 2015.
- [9] J. S. Bednash, N. Weathington, J. Londino et al., "Targeting the deubiquitinase STAMBP inhibits NALP7 inflammasome activity," *Nature Communications*, vol. 8, no. 1, p. 15203, 2017.
- [10] A. Sivanantham, D. Pattarayan, R. Bethunaickan et al., "Tannic acid protects against experimental acute lung injury through downregulation of TLR4 and MAPK," *Journal of Cellular Physiology*, vol. 234, no. 5, pp. 6463–6476, 2019.
- [11] K. T. Cheng, S. Xiong, Z. Ye et al., "Caspase-11-mediated endothelial pyroptosis underlies endotoxemia-induced lung injury," *The Journal of Clinical Investigation*, vol. 127, no. 11, pp. 4124–4135, 2017.
- [12] L. Perrin-Cocon, A. Aublin-Gex, S. E. Sestito et al., "TLR4 antagonist FP7 inhibits LPS-induced cytokine production and glycolytic reprogramming in dendritic cells, and protects mice from lethal influenza infection," *Scientific Reports*, vol. 7, no. 1, p. 40791, 2017.
- [13] S. A. Lee, S. H. Lee, J. Y. Kim, and W. S. Lee, "Effects of glycyrrhizin on lipopolysaccharide-induced acute lung injury in a mouse model," *Journal of Thoracic Disease*, vol. 11, no. 4, pp. 1287–1302, 2019.
- [14] M. Mittal, C. Tirupathi, S. Nepal et al., "TNF α -stimulated gene-6 (TSG6) activates macrophage phenotype transition to prevent inflammatory lung injury," *Proceedings of the National Academy of Sciences*, vol. 113, no. 50, pp. E8151–E8158, 2016.
- [15] L. Meng, L. Li, S. Lu et al., "The protective effect of dexmedetomidine on LPS-induced acute lung injury through the HMGB1-mediated TLR4/NF- κ B and PI3K/Akt/mTOR pathways," *Molecular Immunology*, vol. 94, pp. 7–17, 2018.
- [16] M. Molgora, E. Bonavita, A. Ponzetta et al., "IL-1R8 is a checkpoint in NK cells regulating anti-tumour and anti-viral activity," *Nature*, vol. 551, no. 7678, pp. 110–114, 2017.
- [17] M. Molgora, D. Supino, A. Mantovani, and C. Garlanda, "Tuning inflammation and immunity by the negative regulators IL-1R2 and IL-1R8," *Immunological Reviews*, vol. 281, no. 1, pp. 233–247, 2018.
- [18] T. M. Bauman, A. J. Becka, P. D. Sehgal, W. Huang, and W. A. Ricke, "SIGIRR/TIR8, an important regulator of TLR4 and IL-1R-mediated NF- κ B activation, predicts biochemical recurrence after prostatectomy in low-grade prostate carcinomas," *Human Pathology*, vol. 46, no. 11, pp. 1744–1751, 2015.
- [19] K. Ueno-Shuto, K. Kato, Y. Tasaki et al., "Lipopolysaccharide decreases single immunoglobulin interleukin-1 receptor-related molecule (SIGIRR) expression by suppressing specificity protein 1 (Sp1) via the toll-like receptor 4 (TLR4)-p38 pathway in monocytes and neutrophils," *The Journal of Biological Chemistry*, vol. 289, no. 26, pp. 18097–18109, 2014.
- [20] T. Feng, N. Yunfeng, Z. Jinbo et al., "Single immunoglobulin IL-1 receptor-related protein attenuates the lipopolysaccharide-induced inflammatory response in A549 cells," *Chemico-Biological Interactions*, vol. 183, no. 3, pp. 442–449, 2010.
- [21] H. P. Sham, K. H. Walker, R. E. E. Abdunnour et al., "15-epilipoxin A4, resolvin D2, and resolvin D3 induce NF- κ B regulators in bacterial pneumonia," *Journal of Immunology*, vol. 200, no. 8, pp. 2757–2766, 2018.
- [22] M. B. Watson, D. A. Costello, D. G. Carney, K. McQuillan, and M. A. Lynch, "SIGIRR modulates the inflammatory response in the brain," *Brain, Behavior, and Immunity*, vol. 24, no. 6, pp. 985–995, 2010.
- [23] A. Anselmo, F. Riva, S. Gentile et al., "Expression and function of IL-1R8 (TIR8/SIGIRR), a regulatory member of the IL-1

- receptor family in platelets," *Cardiovascular Research*, vol. 111, no. 4, pp. 373–384, 2016.
- [24] E. Guven-Maiorov, O. Keskin, A. Gursoy, and R. Nussinov, "A structural view of negative regulation of the toll-like receptor-mediated inflammatory pathway," *Biophysical Journal*, vol. 109, no. 6, pp. 1214–1226, 2015.
- [25] D. A. Costello, D. G. Carney, and M. A. Lynch, " α -TLR2 antibody attenuates the β -mediated inflammatory response in microglia through enhanced expression of SIGIRR," *Brain, Behavior, and Immunity*, vol. 46, pp. 70–79, 2015.
- [26] C. Kadota, S. Ishihara, M. M. Aziz et al., "Down-regulation of single immunoglobulin interleukin-1R-related molecule (SIGIRR)/TIR8 expression in intestinal epithelial cells during inflammation," *Clinical and Experimental Immunology*, vol. 162, no. 2, pp. 348–361, 2010.
- [27] A. Płóciennikowska, A. Hromada-Judycka, K. Borzęcka, and K. Kwiatkowska, "Co-operation of TLR4 and raft proteins in LPS-induced pro-inflammatory signaling," *Cellular and Molecular Life Sciences*, vol. 72, no. 3, pp. 557–581, 2015.
- [28] X. Chen, X. Wu, Y. Zhao et al., "A novel binding protein of single immunoglobulin IL-1 receptor-related molecule: paralemmin-3," *Biochemical and Biophysical Research Communications*, vol. 404, pp. 1029–1033, 2010.
- [29] J. Neagos, T. J. Standiford, M. W. Newstead, X. Zeng, S. K. Huang, and M. N. Ballinger, "Epigenetic regulation of tolerance to toll-like receptor ligands in alveolar epithelial cells," *American Journal of Respiratory Cell and Molecular Biology*, vol. 53, no. 6, pp. 872–881, 2015.
- [30] G. Moon, J. Kim, Y. Min et al., "Phosphoinositide-dependent kinase-1 inhibits TRAF6 ubiquitination by interrupting the formation of TAK1-TAB2 complex in TLR4 signaling," *Cellular Signalling*, vol. 27, no. 12, pp. 2524–2533, 2015.
- [31] H. Fujikawa, M. Farooq, A. Fujimoto, M. Ito, and Y. Shimomura, "Functional studies for the TRAF6 mutation associated with hypohidrotic ectodermal dysplasia," *The British Journal of Dermatology*, vol. 168, no. 3, pp. 629–633, 2013.
- [32] S. K. Ippagunta, J. A. Pollock, N. Sharma et al., "Identification of toll-like receptor signaling inhibitors based on selective activation of hierarchically acting signaling proteins," *Science Signaling*, vol. 11, no. 543, p. eaaq1077, 2018.
- [33] M. Murphy, Y. Xiong, G. Pattabiraman, F. Qiu, and A. E. Medvedev, "Pellino-1 positively regulates toll-like receptor (TLR) 2 and TLR4 signaling and is suppressed upon induction of endotoxin tolerance," *The Journal of Biological Chemistry*, vol. 290, no. 31, pp. 19218–19232, 2015.
- [34] E. Pauls, S. K. Nanda, H. Smith, R. Toth, J. S. C. Arthur, and P. Cohen, "Two phases of inflammatory mediator production defined by the study of IRAK2 and IRAK1 knock-in mice," *Journal of Immunology*, vol. 191, no. 5, pp. 2717–2730, 2013.
- [35] Y. Kitagawa, M. Yamaguchi, M. Zhou, M. Nishio, M. Itoh, and B. Gotoh, "Human parainfluenza virus type 2 V protein inhibits TRAF6-mediated ubiquitination of IRF7 to prevent TLR7- and TLR9-dependent interferon induction," *Journal of Virology*, vol. 87, no. 14, pp. 7966–7976, 2013.
- [36] J. Zhang, W. Ma, S. Tian et al., "RanBPM interacts with T β RI, TRAF6 and curbs TGF induced nuclear accumulation of T β RI," *Cellular Signalling*, vol. 26, no. 1, pp. 162–172, 2014.
- [37] R. Sundar, S. K. Gudey, C.-H. Heldin, and M. Landström, "TRAF6 promotes TGF β -induced invasion and cell-cycle regulation via Lys63-linked polyubiquitination of Lys178 in TGF β type I receptor," *Cell Cycle*, vol. 14, no. 4, pp. 554–565, 2015.
- [38] Y. Mikami, T. Iwase, Y. Komiyama, N. Matsumoto, H. Oki, and K. Komiyama, "Secretory leukocyte protease inhibitor inhibits expression of polymeric immunoglobulin receptor via the NF- κ B signaling pathway," *Molecular Immunology*, vol. 67, no. 2, pp. 568–574, 2015.
- [39] W. Wang, W. J. Guan, R. Q. Huang et al., "Carbocysteine attenuates TNF- α -induced inflammation in human alveolar epithelial cells in vitro through suppressing NF- κ B and ERK1/2 MAPK signaling pathways," *Acta Pharmacologica Sinica*, vol. 37, no. 5, pp. 629–636, 2016.
- [40] D. Mukhopadhyay and H. Riezman, "Proteasome-independent functions of ubiquitin in endocytosis and signaling," *Science*, vol. 315, pp. 201–205, 2007.
- [41] C. M. Pickart, "Mechanisms underlying ubiquitination," *Annual Review of Biochemistry*, vol. 70, no. 1, pp. 503–533, 2001.
- [42] I. E. Wertz, K. M. O'Rourke, and H. Zhou, "De-ubiquitination and ubiquitin ligase domains of A20 downregulate NF- κ B signalling," *Nature*, vol. 430, no. 7000, pp. 694–699, 2004.
- [43] N. Shembade, A. Ma, and E. W. Harhaj, "Inhibition of NF- κ B signaling by A20 through disruption of ubiquitin enzyme complexes," *Science*, vol. 327, no. 5969, pp. 1135–1139, 2010.
- [44] D. L. Boone, E. E. Turer, and E. G. Lee, "The ubiquitin-modifying enzyme A20 is required for termination of toll-like receptor responses," *Nature Immunology*, vol. 5, no. 10, pp. 1052–1060, 2004.
- [45] K. Yao, S.-Y. Lee, C. Peng et al., "RSK2 is required for TRAF6 phosphorylation-mediated colon inflammation," *Oncogene*, vol. 37, no. 26, pp. 3501–3513, 2018.

Research Article

STK3 Suppresses Ovarian Cancer Progression by Activating NF- κ B Signaling to Recruit CD8⁺ T-Cells

Xiangyu Wang ^{1,2}, Fengmian Wang,^{1,2} Zhi-Gang Zhang ³, Xiao-Mei Yang ³,
and Rong Zhang ^{1,2}

¹The Third School of Clinical Medicine, Southern Medical University, Guangzhou 510500, China

²Department of Obstetrics and Gynecology, Fengxian Central Hospital Affiliated to the Southern Medical University, Shanghai 201499, China

³State Key Laboratory of Oncogenes and Related Genes, Shanghai Cancer Institute, Ren Ji Hospital, School of Medicine, Shanghai Jiao Tong University, Shanghai 201109, China

Correspondence should be addressed to Xiao-Mei Yang; xmyang@shsci.org and Rong Zhang; rongzhang@163.com

Received 6 July 2020; Revised 11 August 2020; Accepted 26 August 2020; Published 29 September 2020

Academic Editor: Jian Song

Copyright © 2020 Xiangyu Wang et al. This is an open access article distributed under the Creative Commons Attribution License, which permits unrestricted use, distribution, and reproduction in any medium, provided the original work is properly cited.

Serine/threonine protein kinase-3 (STK3) is a critical molecule of the Hippo pathway but little is known about its biological functions in the ovarian cancer development. We demonstrated the roles of STK3 in ovarian cancer. Existing databases were used to study the expression profile of STK3. STK3 was significantly downregulated in OC patients, and the low STK3 expression was correlated with a poor prognosis. In vitro cell proliferation, apoptosis, and migration assays, and in vivo subcutaneous xenograft tumor models were used to determine the roles of STK3. The overexpression of STK3 significantly inhibited cell proliferation, apoptosis, and migration of ovarian cancer cells in vitro and tumor growth in vivo. Bisulfite sequencing PCR analysis was performed to validate the methylation of STK3 in ovarian cancer. RNA sequencing and gene set enrichment analysis (GSEA) were used to compare the transcriptome changes in the STK3 overexpression ovarian cancer and control cells. The signaling pathway was analyzed by western blotting. STK3 promoted the migration of CD8⁺ T-cells by activating nuclear transcription factor κ B (NF- κ B) signaling. STK3 is a potential predictor of OC. It plays an important role in suppressing tumor growth of ovarian cancer and in chemotaxis of CD8⁺ T-cells.

1. Introduction

Ovarian cancer (OC) is the most frequent cause of death among gynecologic malignancies [1]. Due to its asymptomatic development, the disease is frequently diagnosed at advanced and incurable stages [2]. Although there is a high response rate to surgery and chemotherapy, the majority of patients subsequently relapse [3]. Therefore, it is important to identify effective molecular targets influencing tumor progression.

STK3 is a key molecule in the Hippo pathway, which controls cell development, proliferation, apoptosis, and various stress responses [4]. STK3 plays a role in inhibiting the progression of gastric cancer, hepatocellular carcinoma, and

breast cancer by activating Hippo signaling [5–7]. STK3 also regulates the immune system in infections [8]. However, it is unclear whether STK3 can exert cancer-suppressing effects by regulating the functions of the immune system.

CD8⁺ T-cells play an important role in inhibiting the development of ovarian cancer [9]. The chemotaxis of CD8⁺ T-cells is regulated by a variety of chemokines, of which CXCL16 and CX3CL1 are the most important on CD8⁺ T-cells [10, 11]. The low expression of CXCL16 in breast cancer, osteosarcoma, renal clear cell carcinoma, and melanoma is associated with a poor prognosis [12–14]. The CX3CL1 expression is increased in the renal clear cell carcinoma tissues of patients receiving bevacizumab, accompanied by infiltration of CD8⁺ T-cells [15]. NF- κ B can affect

the infiltration of CD8⁺ T-cells in pancreatic ductal adenocarcinoma cells by regulating the generation of CXCL16 and CX3CL1 and thereby promoting the apoptosis of pancreatic ductal adenocarcinoma cells [16]. However, it is unclear whether STK3 can activate NF- κ B signaling and suppress ovarian cancer growth.

In this study, we demonstrated that STK3 was downregulated in ovarian cancer via epigenetic methylation of its promoter DNA. STK3 inhibited proliferation and metastasis of ovarian cancer cells. The overexpression of STK3 in ovarian cancer cells induced cell cycle arrest at G2/M and a higher rate of cell apoptosis. We also found that STK3 promoted the recruitment of CD8⁺ T-cells via an increase in chemokine CXCL16 and CX3CL1 production in human ovarian cancer cells. This was possibly mediated by the regulation of the NF- κ B signaling pathway. Our results revealed a new molecular mechanism for serous ovarian cancer malignancy mediated by STK3 through regulating NF- κ B signaling and CD8⁺ T-cell recruitment.

2. Materials and Methods

2.1. Data Mining. The mRNA expression profiles for normal ovarian surface epithelium and ovarian cancer were downloaded from UCSCXena (<https://xena.ucsc.edu>) and GEO (<https://www.ncbi.nlm.nih.gov/geo/>). The survival data of patients were downloaded from TCGA (<https://www.cancer.gov/about-nci/organization/ccg/research/structural-genomics/tcga>) and GSE9899.

2.2. Cell Culture and Clinical Samples. IOSE80, OVCAR3, OVCAR8, CAOV3, ES-2, and HEK293T cell lines were all purchased from Cell Bank of the Chinese Academy of Sciences (Shanghai, China). All of the cells were cultured following the instructions of the American Type Culture Collection (ATCC, Manassas, VA, USA).

2.3. Reagents. The antibodies used in this study were against STK3 (ab52641, Abcam, Cambridge, MA, USA), Phospho-I κ B α (#2859, Cell Signaling Technology), I κ B α (#4812, Cell Signaling Technology), Phospho-NF- κ B p65 (#3033, Cell Signaling Technology), β -actin (GB11001, Servicebio, Wuhan, China), and NF- κ B p65 (#8242, Cell Signaling Technology) for western blotting. Secondary antibodies were purchased from Jackson ImmunoResearch (West Grove, PA, USA). Chemicals and biochemical used were DAC (A3656, Sigma-Aldrich, St. Louis, MO, USA) and TSA (S1045, Selleck, Shanghai, China). CXCL16 and CX3CL1 concentrations were measured in the medium of ovarian cancer cells using enzyme-linked immunosorbent assay (ELISA) kits (R&D Systems, Abingdon, UK) according to manufacturer's instructions.

2.4. Quantitative Real-Time PCR. Total RNA was extracted from cells in each group using Trizol kits, and qualified total RNA samples were subjected to reverse transcription. Total RNA was taken to synthesize complementary deoxyribonucleic acid (cDNA) using the PrimeScriptTMRT reagent Kit (RR047A, TAKARA, Japan). The specific reaction conditions were 37°C for 30 min and 85°C for 30 s. Quantitative analysis

was carried out using the ABI 7500 fluorescence PCR amplification instrument (Applied Biosystems; Thermo Fisher Scientific, Inc.). *RPS18* was used as an endogenous control, and Ct values were processed using the $2^{-\Delta\Delta Ct}$ method. The sequences of primers used in this experiment were shown in Table 1.

2.5. Western Blot Analysis. For western blot analysis, total protein samples were extracted from cells using RIPA lysis buffer with a protease inhibitor (Beyotime, Jiangsu, China). An equal amount of protein (60 μ g/lane) was loaded on 10% or 8% SDS-polyacrylamide gels and then transferred to a pure nitrocellulose blotting membrane (Pall Life Science, AZ, USA). Next, the membrane was blocked in 5% nonfat milk for 1 h and then probed with primary antibodies against STK3, β -actin, Phospho-I κ B α , I κ B α , Phospho p65, and p65 overnight at 4°C. Then, the membranes were incubated with anti-rabbit secondary antibodies. Finally, immunoreactivity was detected using the Odyssey Infrared Imaging System (Gene Company Limited, Hong Kong, China).

2.6. DAC and TSA Treatment. Cells were treated with 5 or 10 μ M of 5-aza-2'-deoxycytidine (DAC, Sigma-Aldrich, St. Louis, MO, USA) or 300 nM trichostatin A (TSA, Selleckchem, TX, USA) for 3 d, and the drug media were replaced every 24 h. Control cells were incubated with the same volume of DMSO. In the combined treatment group, cells were cultured in the presence of 5 μ M of DAC for 2 d and were then treated for an additional 24 h with 300 nM of TSA.

2.7. Plasmid Construction and Transfection. The human STK3 was subcloned into the pcDNATM3.1 vector. STK3 and the mock vector were packaged into the virus, and titers were determined. Target cells were infected with 1×10^8 lentivirus-transducing units and 6 μ g/ml polybrene (TR-1003, Sigma-Aldrich, Germany). After 72 h, the infected cells were screened in the presence of 3 μ g/ml puromycin. The qPCR and western blot also verified the overexpression efficacy of STK3.

2.8. Cell Viability Assays. Cell viability was determined using a cell counting kit-8 (CK04, Dojindo, Japan). Briefly, water-soluble formazan dye was added to the culture medium and incubated for 2 h in 5% CO₂. The developed color was measured at 450 nm using an ELISA plate reader.

2.9. Colony Formation Assay. The 1×10^3 cells/mL single-cell suspension was made in RPMI1640 or DMEM. The colonies were stained with 0.04% crystal violet and 2% ethanol in PBS and then incubated at 37°C for 21 days. The stained colonies were photographed under a light microscope (Olympus).

2.10. Transwell Migration and Invasion. Cells were seeded in the upper chamber of transwell plates (Corning, NY, NY USA) with serum-free medium. 10% FBS medium was added to the lower chamber of the transwell. Next, cells were transfected as described above for 48 h. For the invasion experiments, the upper chamber was covered with culture medium and matrigel (BD Biosciences, San Jose, CA, USA) mixture. Finally, cells on the top of the chamber were

TABLE 1: The oligonucleotide sequence of primers used in this experiment.

Genes	Forward primer (5'-3')	Reverse primer (5'-3')
STK3	GCUGGAAAUAUUCUCCUATT	UAAGGAGAAUAUUUCCAGCTT
CXCL16	CCCGCCATCGGTTTCAGTTC	CCCCGAGTAAGCATGTCCAC
CX3CL1	ACTCTTGCCCACCCTCAGC	TGGAGACGGGAGGCACTC
RPS18	CAGCCAGGTCCTAGCCAATG	CCATCTATGGGCCCGAATCT

removed with cotton swabs, while cells that went through the membrane were stained with 0.5% crystal violet and counted under a microscope at 100x magnification.

2.11. Flow Cytometry Test of Cell Cycle. Ten ml of cell suspension ($1 - 5 \times 10^6$ cells/mL) was spun at 500–1000 rpm for 5 min. The cell pellet was washed with PBS once and fixed in 3.70% ice ethanol at 4°C for 2 h. After washing with PBS twice, the cells were suspended in PBS containing 50 mg/L RNase A and 25 μ g/mL PI and incubated in darkness at 25°C for 15 min. The cells at different phases were measured using flow cytometry with an excitation wave length of 488 nm and an emission wave length greater than 560 nm to detect PI signal.

2.12. Flow Cytometry Test of Apoptosis. Ten ml of cell suspension ($1 - 5 \times 10^6$ cells/mL) was spun at 500–1000 rpm for 5 min. The cell pellet was washed with PBS once and fixed in 70% ice ethanol at 4°C for 2 h. After the fixation solution was removed, the cells were suspended in 3 ml PBS for 5 min. Cells were transfected with lentivirus for 48 h and serum-free starved for 24 h. This was filtered once with a 400 gauge filter and centrifuged at 1000 rpm for 5 min, and then the cell pellet was stained with 50 mg/mL propidium iodide and Annexin V–fluorescein isothiocyanate (BD Pharmingen, Franklin Lakes, NJ, USA) following manufacturer's instructions. Both the living and dead cells were measured using flow cytometry with an exciting wave length of 488 nm and an emission wave length greater than 630 nm.

2.13. Xenograft Transplantation. Female nude (BALB/c) mice (4 weeks old) were purchased from the East China Normal University. Mice were randomly divided into two groups. OS cells stably expressing vector or lenti-STK3 were propagated, and 1×10^7 cells were inoculated subcutaneously into the right side of the posterior flank of the mice. Tumor growth was examined at the indicated time points, and tumor volumes were measured. After 4 weeks, the mice were killed, weighed, excised, fixed, and embedded in paraffin and sectioned for the histological examination of the PCNA and TUNEL expression.

2.14. Statistical Analysis. Data are presented as means \pm SD. Statistical analyses were done using SPSS V.16.0 for Windows (IBM) or GraphPad Prism (GraphPad Software, San Diego, CA, USA). Cumulative survival time was calculated by the Kaplan-Meier method and analyzed by the log-rank test. Correlation of the STK3 expression with clinical parameters in patients with ovarian cancer was evaluated by χ^2 test. Correlation was determined using the Spearman's test.

Student's *t*-test was used for paired comparisons between groups. *P* values <0.05 were considered to be statistically significant.

3. Results

3.1. STK3 Was Downregulated in Ovarian Cancer and Correlated with Prognosis. To investigate the level of STK3 in ovarian cancers, we first compared the expression of STK3 in ovarian cancer and matching normal ovarian surface epithelial tissue samples via GTEX and TCGA. Notably, STK3 was significantly downregulated in ovarian cancer based on the analysis of TCGA and GEO datasets (*P* value <0.05) (Figure 1(a)). We also investigated whether the STK3 expression was correlated with prognosis in ovarian cancer patients. In TCGA cohorts, which included 428 samples of ovarian cancer, the low STK3 expression was associated with poorer overall survival and progression-free survival prognosis (*P* value <0.05) (Figure 1(b)). The poor prognosis in ovarian cancer also correlated with the lower STK3 expression in GSE9899 (*P* value <0.05) (Figure 1(b)). These results suggest that the STK3 expression influences the progression of ovarian cancer.

3.2. The Overexpression of STK3 Inhibited the Proliferation, Migration, and Invasion of Ovarian Cancer Cells. To study the expression pattern of STK3 in ovarian cancer, we compared the level of STK3 in a normal human ovarian surface epithelium cell line (IOSE80) with levels in ovarian cancer cell lines (CAOV3, OVCAR3, OVCAR8, and ES-2). The STK3 expression levels detected by western blot were lower in most tested ovarian cancer cells compared with IOSE80 (Figure 2(a)).

To further explore the role of STK3 in ovarian cancer progression in vitro, we established stable STK3-overexpressing cells by lentivirus-mediated transfection. Quantitative real-time polymerase chain reaction (qPCR) and western blotting confirmed the efficiency of the STK3 overexpression in OVCAR3 and OVCAR8 cells (Figure 2(b)). We determined the effect of STK3 on the proliferation of ovarian cancer cells through CCK-8 and colony formation assays. The results showed that, compared with the control group, the proliferation and clone formation ability of ovarian cancer cells OVCAR3 and OVCAR8 were significantly inhibited by overexpressing STK3 (*P* value <0.05) (Figure 2(c)).

We used flow cytometry to detect the effect of STK3 on the ovarian cancer cell cycle distribution. Cell cycle analysis showed that the proportion of OVCAR3 and OVCAR8 cells in the G2/M phase significantly increased after exposure to overexpressing STK3 (*P* value <0.05) (Figure 2(d)).

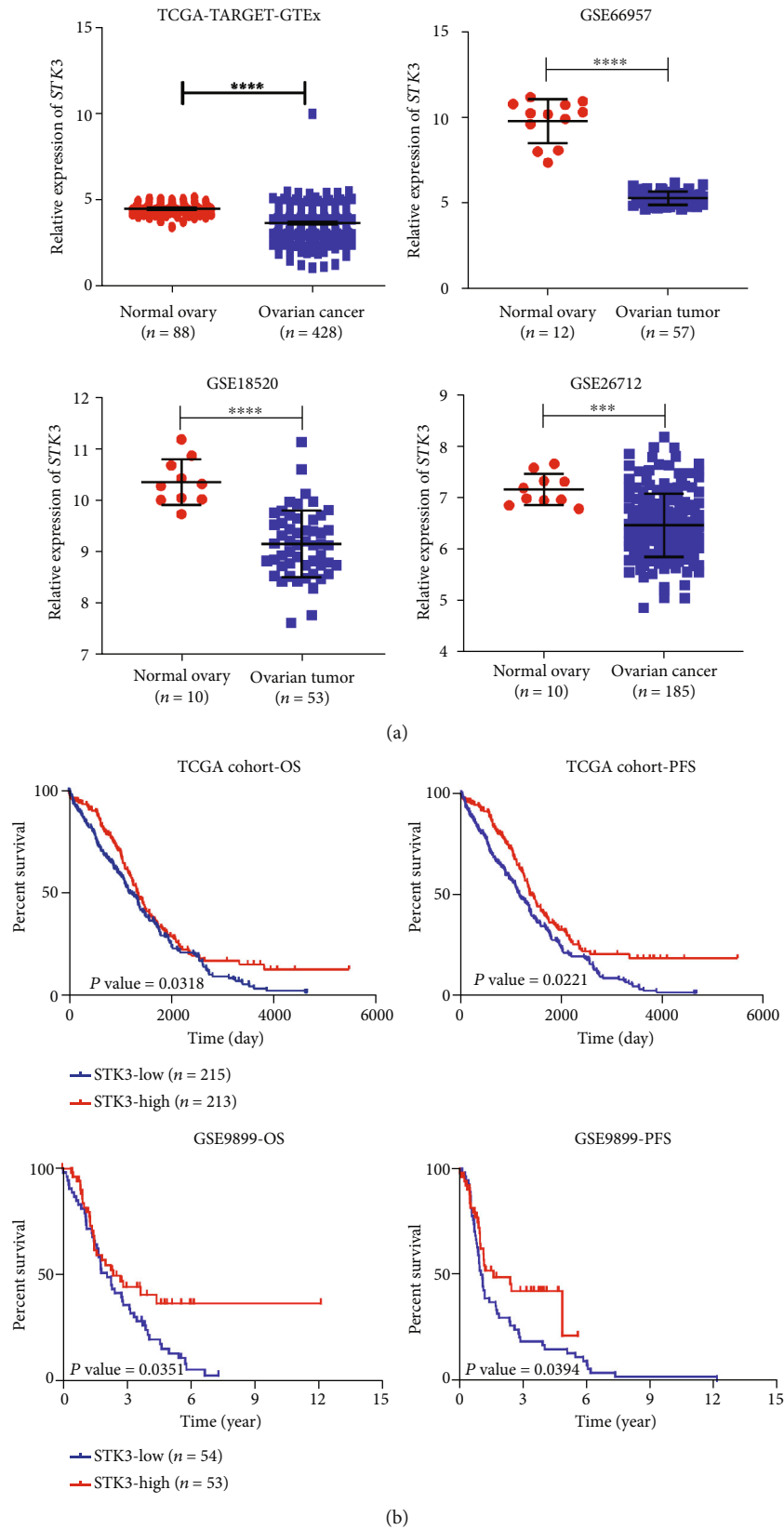


FIGURE 1: Database analysis showed that STK3 was downregulated in ovarian cancer tissues, and the overexpression of STK3 was closely related to better prognosis. (a) Analysis of the mRNA level expression of STK3 in the TCGA database and GEO database (two-tailed Student's *t*-test, $***P < 0.001$; $****P < 0.0001$). (b) Analysis of the overall survival period and progression-free survival period according to the STK3 expression in the TCGA database and GEO database (log-rank test).

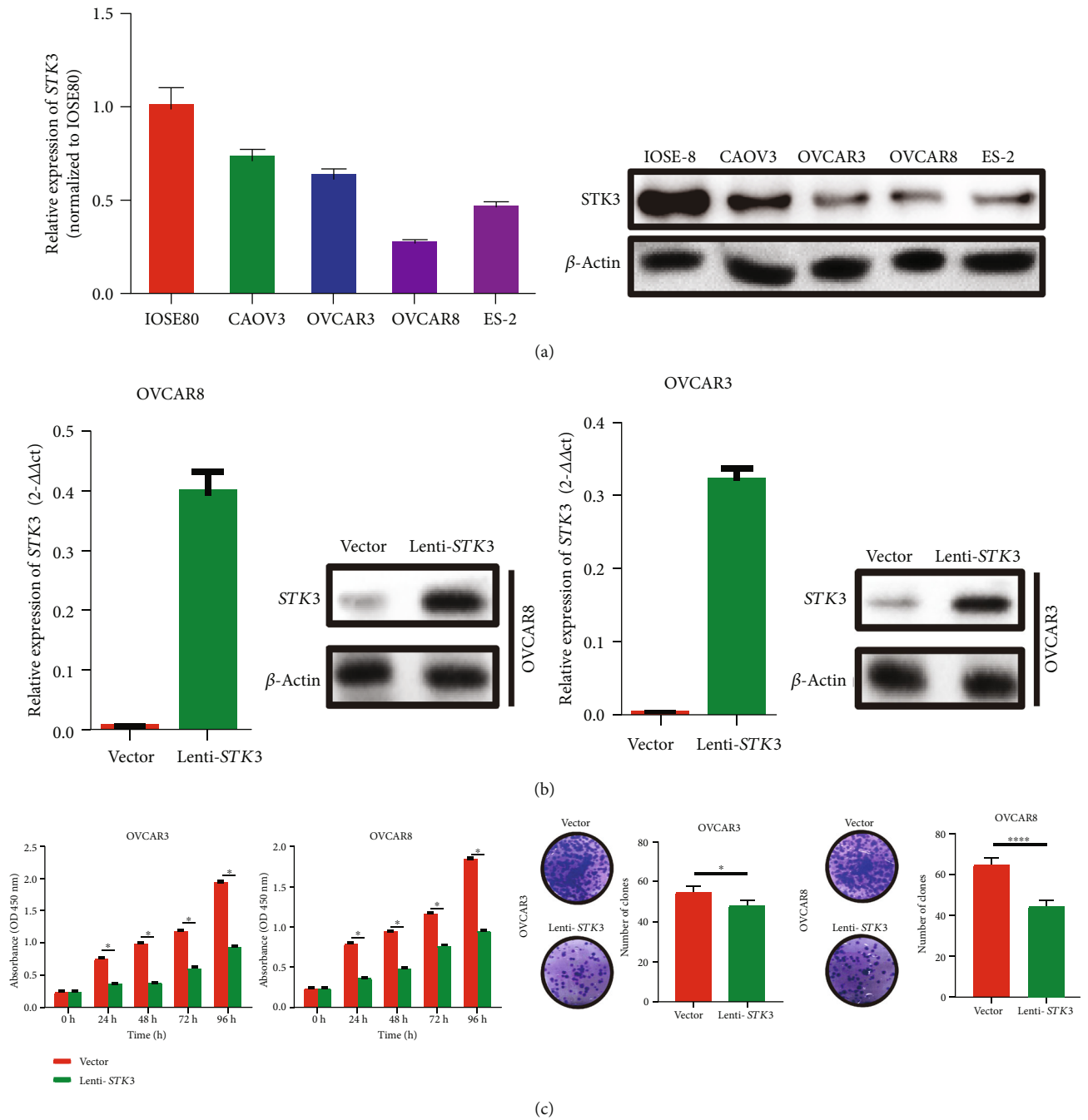
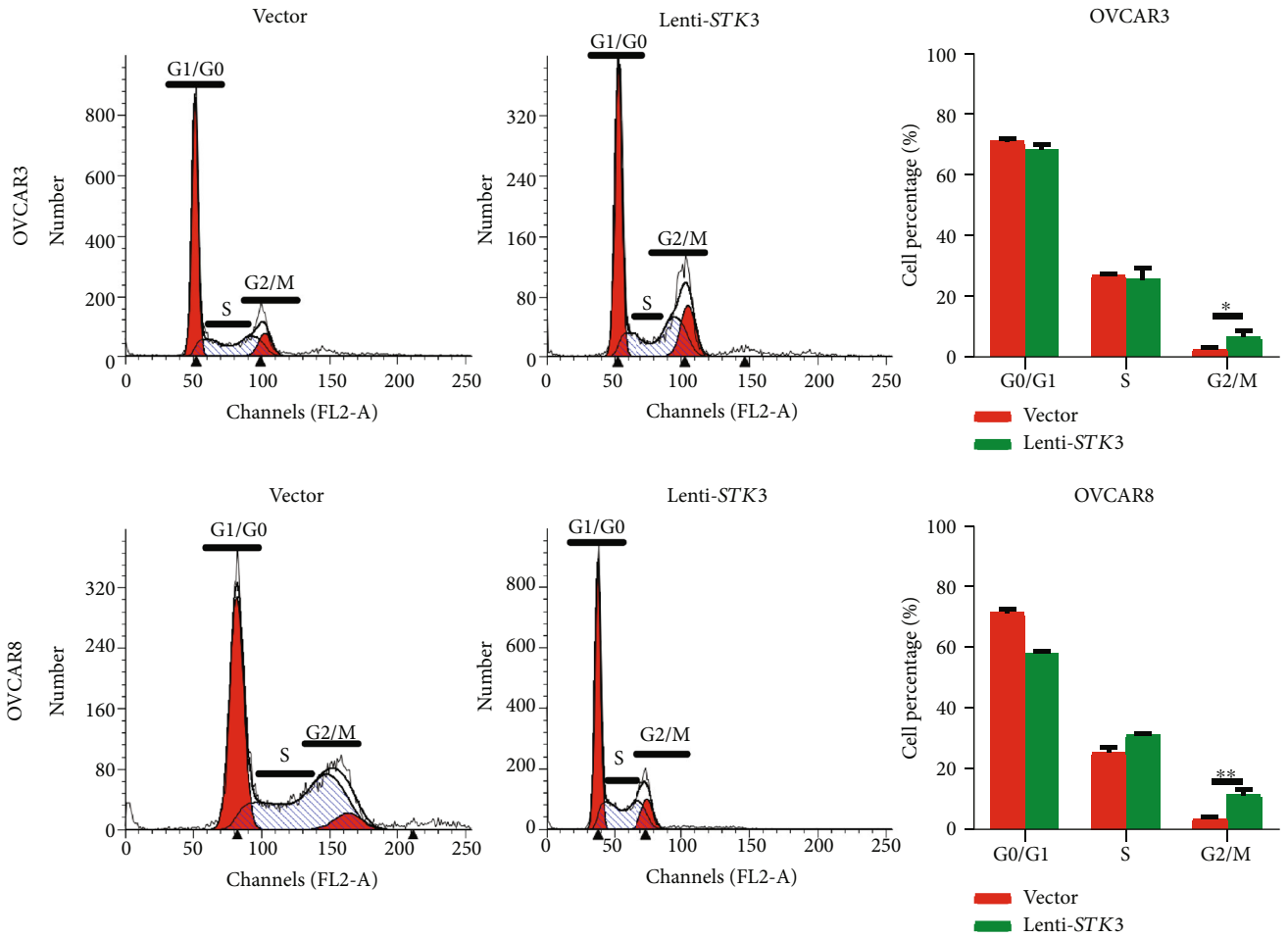
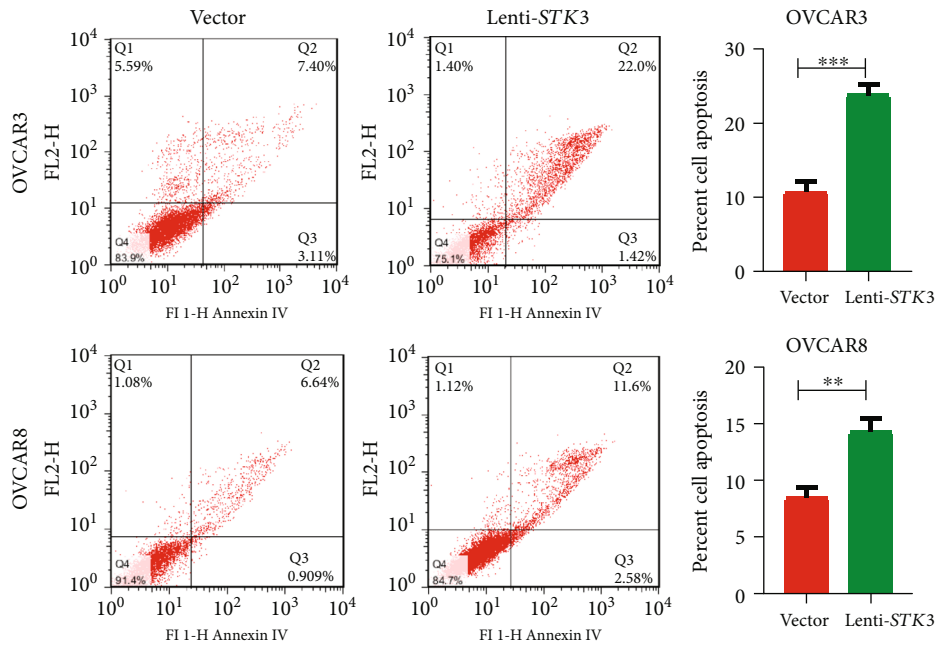


FIGURE 2: Continued.

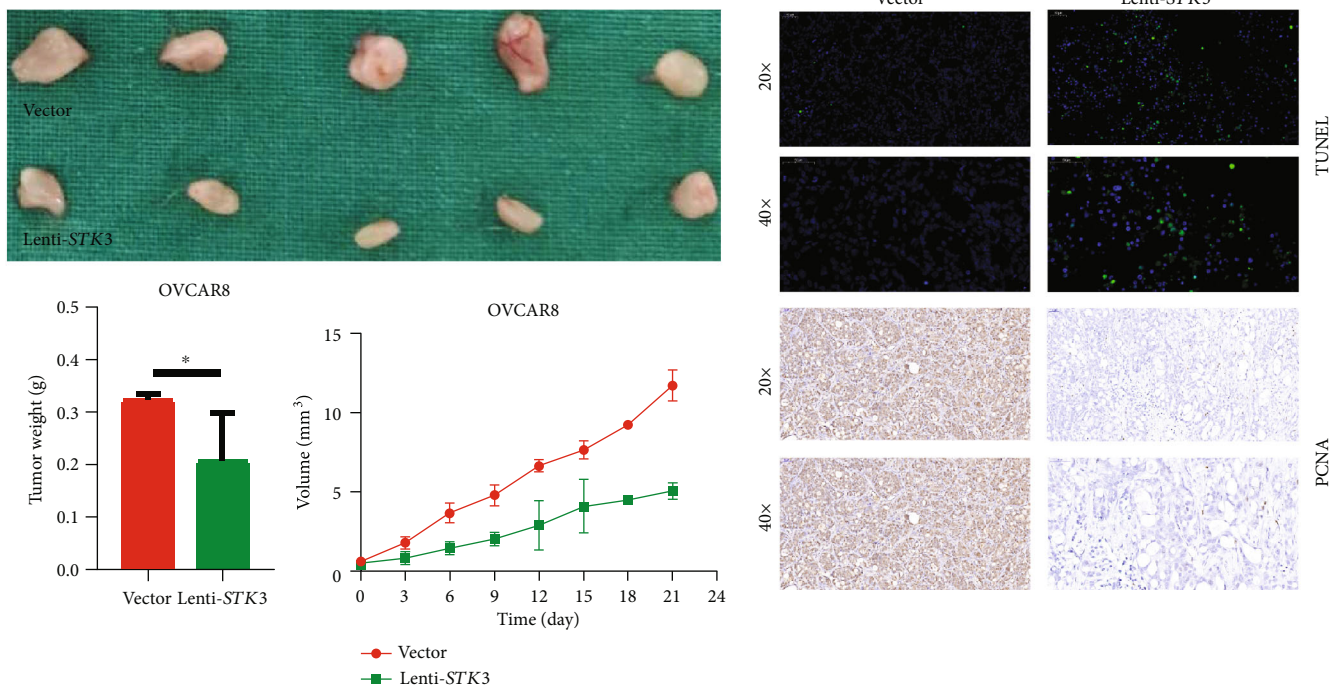


(d)

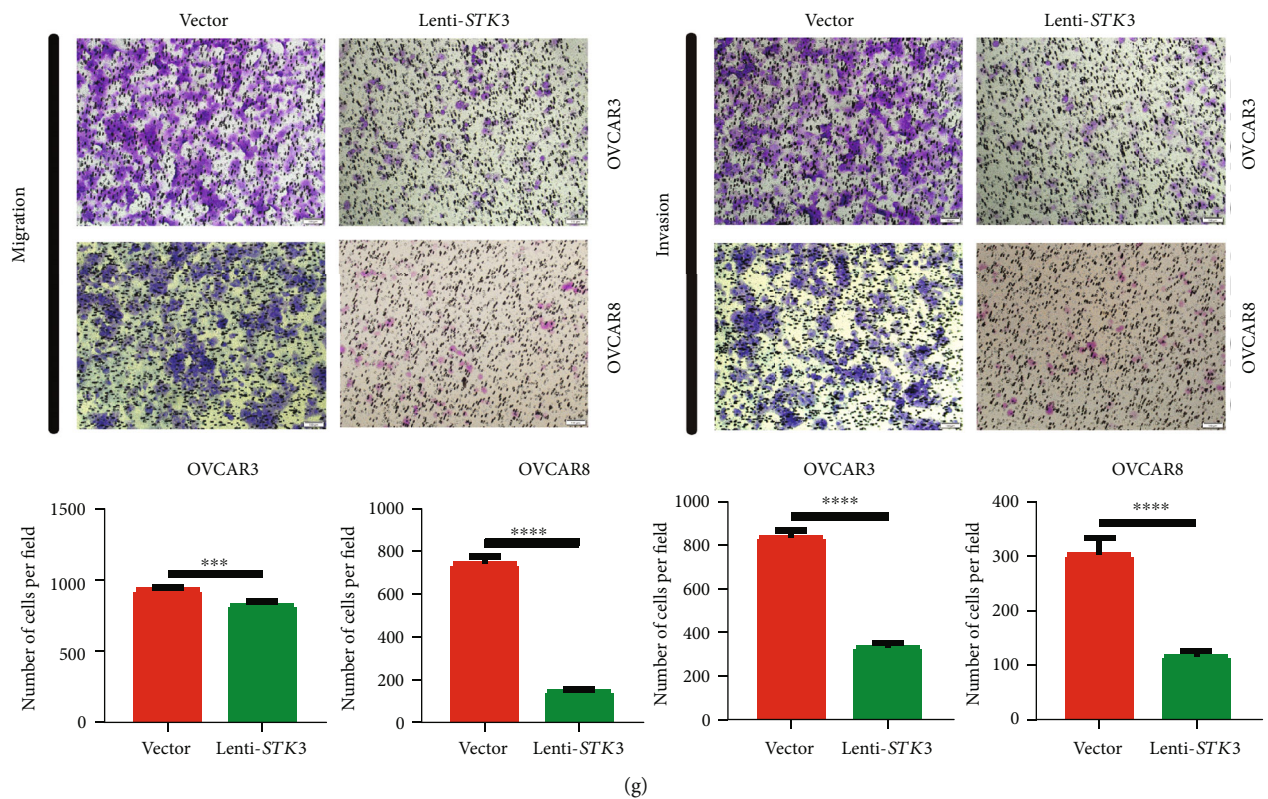


(e)

FIGURE 2: Continued.



(f)



(g)

FIGURE 2: Continued.

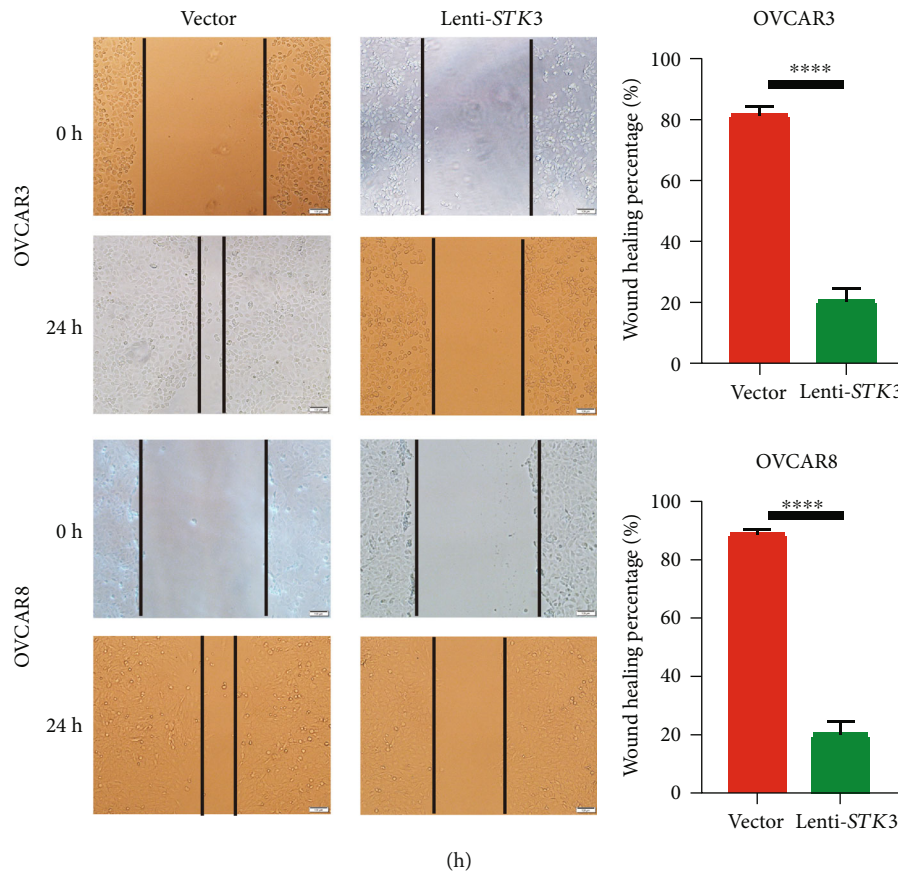


FIGURE 2: Overexpressed STK3 can inhibit the invasion and proliferation of ovarian cancer cells in vitro and in vivo. (a) The STK3 expression in five different cell lines measured by qRT-PCR and Western blotting. (b) The STK3 overexpression was confirmed by Western blotting and qRT-PCR in OVCAR3 and OVCAR8 cell lines. (c) Effect of the STK3 overexpression on the proliferation and colony formation of OVCAR3 and OVCAR8 cells in vitro (two-tailed Student's *t*-test, * $P < 0.05$; *** $P < 0.001$). (d) The overexpression of STK3 arrested ovarian cancer cells at G2/M. The cell cycle distribution of OVCAR3 and OVCAR8 cells detected by flow cytometry (two-tailed Student's *t*-test, * $P < 0.05$). (e) The overexpression of STK3 promotes ovarian cancer cell apoptosis, as detected by cell apoptosis assays (two-tailed Student's *t*-test, ** $P < 0.01$; *** $P < 0.001$). (f) Morphologic characteristics of tumors from mice inoculated with vector and lenti-STK3/OVCAR8 cells. Tumor weights and volumes of the vector and lenti-STK3 groups are shown (two-tailed Student's *t*-test, ** $P < 0.01$). The overexpression of STK3 can inhibit the invasion and migration of ovarian cancer cells. (g) Effect of the STK3 overexpression on invasion and migration of OVCAR3 and OVCAR8 cells by cell migration and invasion assays (two-tailed Student's *t*-test, *** $P < 0.001$; **** $P < 0.0001$). Scale bar: 100 μm . (h) Effect of the STK3 overexpression on the migration of OVCAR3 and OVCAR8 cells detected by wound healing assays (two-tailed Student's *t*-test, *** $P < 0.001$; **** $P < 0.0001$). Scale bar: 100 μm .

We determined the effect of STK3 on ovarian cancer cells apoptosis by annexin V/PI staining and flow cytometry analysis in vitro. The results showed that the apoptosis rate of the lenti-STK3 group in OVCAR3 cell line was significantly higher than that of the control group ($17.72 \pm 0.3358\%$ versus $9.887 \pm 0.1203\%$, P value < 0.05). Similarly, the apoptosis rate of the lenti-STK3 group in OVCAR8 cell line was also significantly higher than that in control group (P value < 0.05) (Figure 2(e)).

Finally, lentivector or lenti-STK3 OVCAR8 cells were subcutaneously injected into nude mice to assess in vivo growth of tumors. The results showed that the tumor volume and tumor weight of the lentivector group were larger than those of the lenti-STK3 group. These results indicate that the overexpression of STK3 significantly inhibited the growth of ovarian cancer (P value < 0.05) (Figure 2(f)).

To determine the effect of STK3 on the migration and invasion in ovarian cancer cells, we first examined the migration of OVCAR3 and OVCAR8 cells via transwell invasion and migration assays after overexpressing STK3. The results showed that, compared with the control group, the invasive and migratory abilities of ovarian cancer cells were significantly decreased after exposure to overexpressed STK3 (P value < 0.05) (Figure 2(g)).

We also used a wound healing assay to determine the effect of STK3 on the migration of serous ovarian cancer cells OVCAR3 and OVCAR8. The results showed that the migration ability of serous ovarian cancer cells was significantly decreased in the STK3 overexpression group compared with the control group (P value < 0.05) (Figure 2(h)). Thus, the overexpression of STK3 inhibited the invasion and migration of ovarian cancer cells.

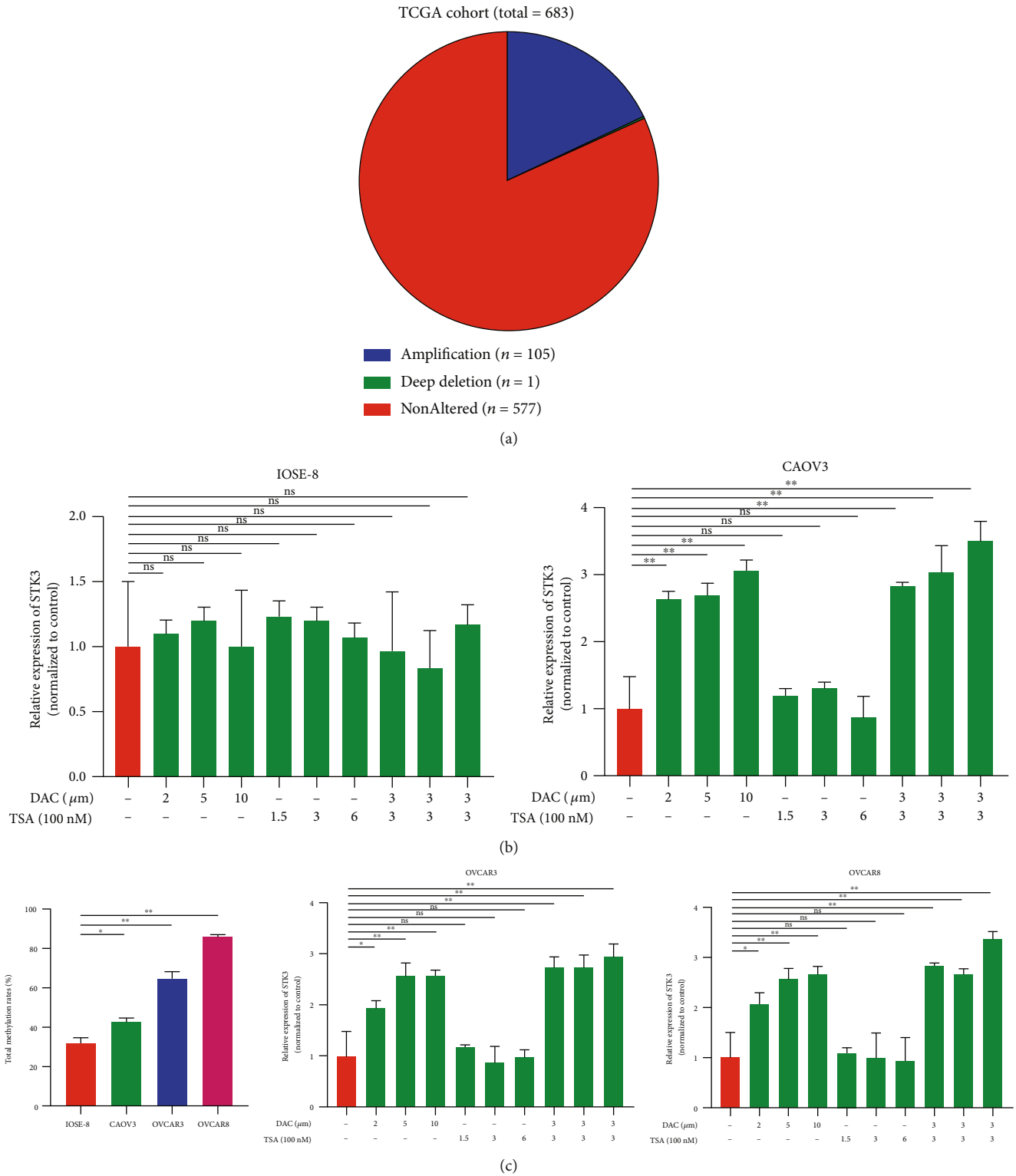
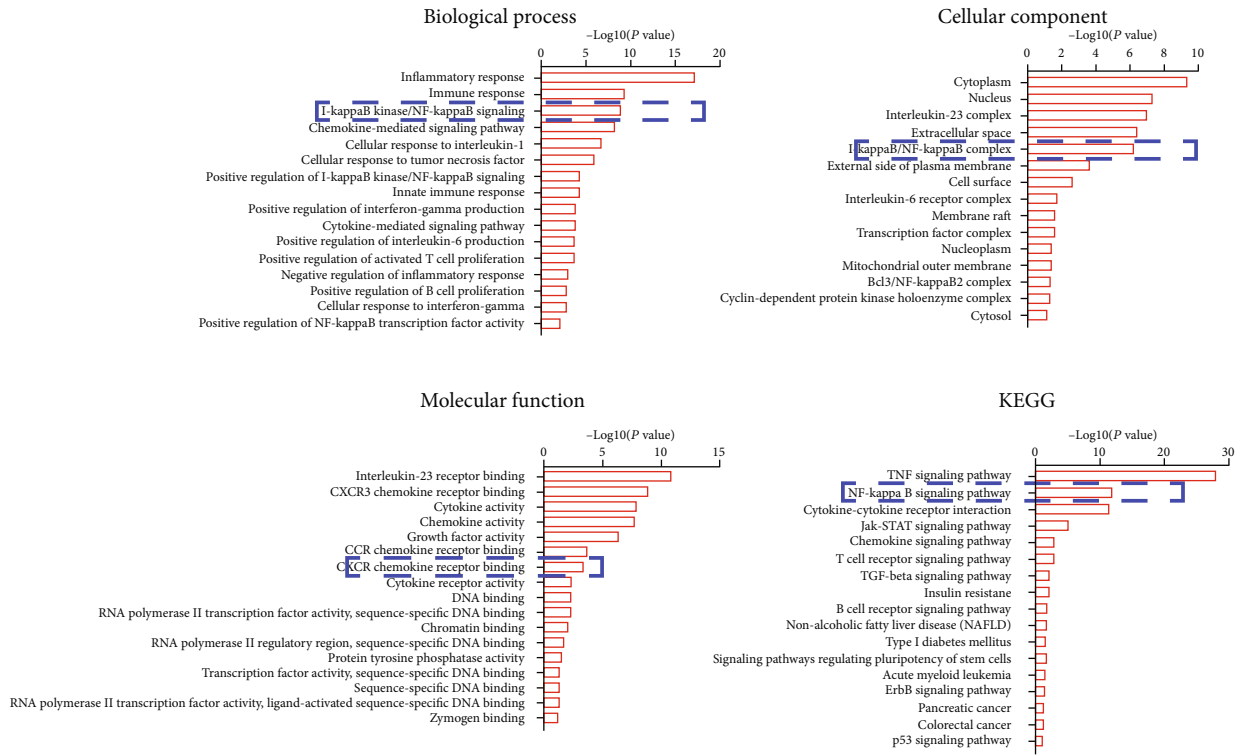
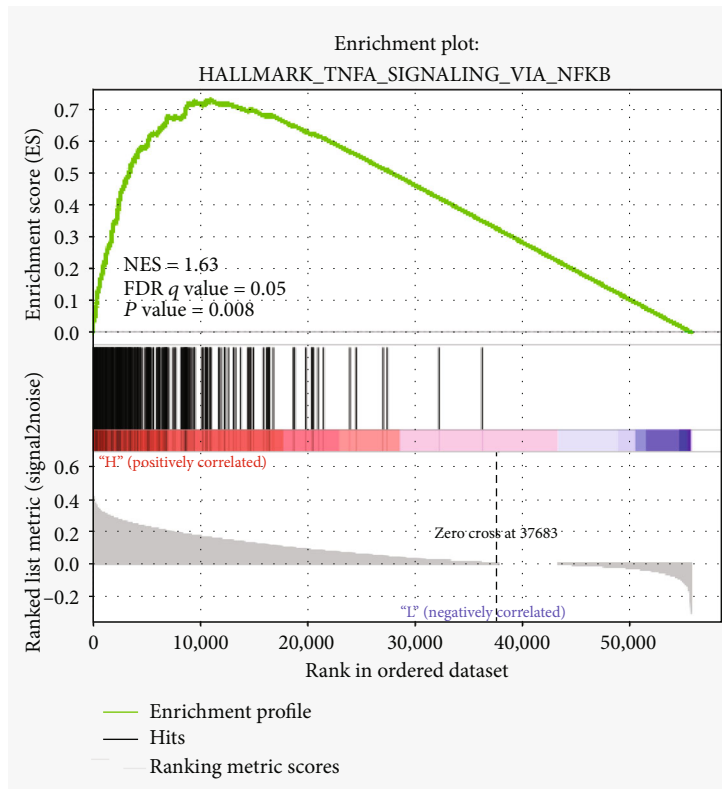


FIGURE 3: The STK3 expression in ovarian cancer cell lines. (a) Statistics of STK3-mutated samples derived from 683 patients in cBioportal. (b) The mRNA expression of STK3 was evaluated by real-time qPCR in cell lines (IOSE80, CAOV3, OVCAR3, and OVCAR8) treated with DMSO, DAC, TSA, or DAC plus TSA (two-tailed Student's *t*-test, ***P* < 0.01). (c) Total methylation rates of STK3 promoter in the human osteoblast cell line IOSE80 and three ovarian cancer cell lines (CAOV3, OVCAR3, and OVCAR8) are shown. (two-tailed Student's *t*-test, **P* < 0.05, ***P* < 0.01).



(a)



(b)

FIGURE 4: Continued.

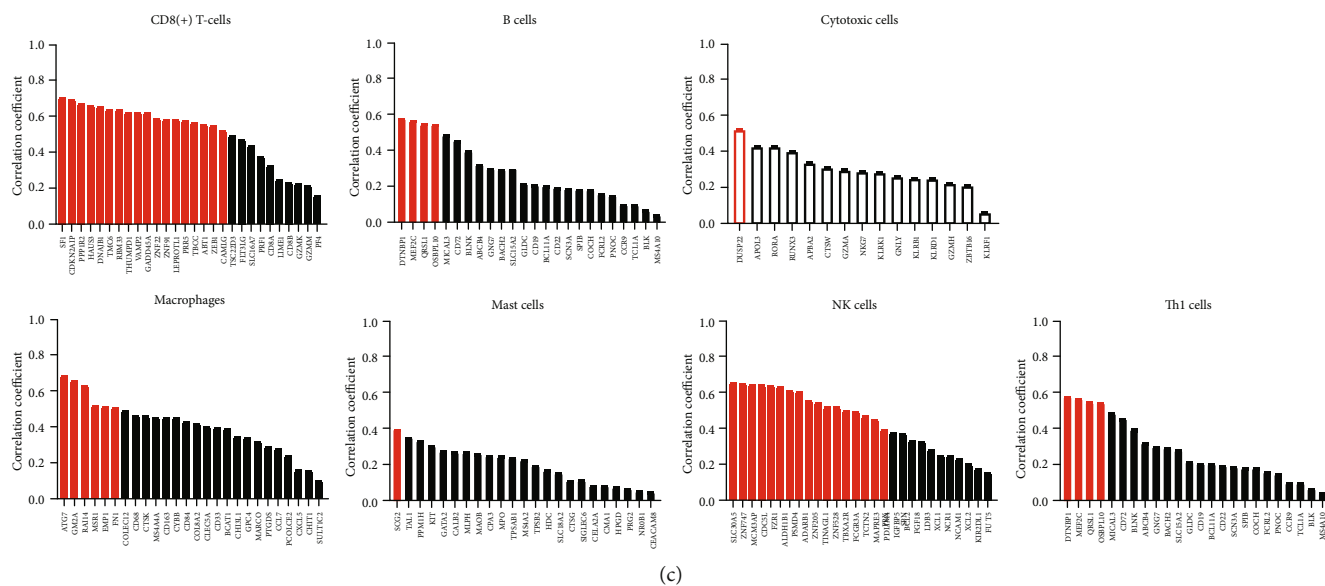


FIGURE 4: STK3 is correlated with CD8+ T cell infiltration and the NF- κ B signaling pathway in ovarian cancer. (a) Representative GO and KEGG categories affected by the STK3 expression in OVCAR8 cells. (b) Gene set enrichment analysis (GSEA) using reactome gene sets compared the TCGA ovarian database. NES: normalized enrichment score. (c) The correlation between STK3 and specific gene signatures of different immune cells.

3.3. STK3 Is Downregulated in Ovarian Cancer via Epigenetic Promoter DNA Methylation. Genetic or epigenetic mechanisms (or both) might cause dysregulation of the STK3 expression in ovarian cancer. STK3 is located on chromosome 8q22.2, and there is no deletion in this region in ovarian cancer (Figure 3(a)). We explored the epigenetic regulation of the STK3 expression in ovarian cancer. Using 5-aza-20-deoxycytidine (DAC), a specific methyltransferase inhibitor, and Trichostatin A (TSA), a histone deacetylase inhibitor, we found that the mRNA expression level of STK3 in ovarian cancer cells was significantly increased after DAC treatment (P value < 0.05), but not by TSA treatment. The expression of STK3 increased only slightly in IOSE80 treated with DAC (P value < 0.05) (Figure 3(b)). To validate the methylation-mediated downregulation of STK3 in ovarian cancer, we performed bisulfite sequencing PCR of DNA from IOSE80, CAO3, OVCAR3, and OVCAR8 cells. The STK3 promoter in ovarian cancer cells showed significantly higher levels of methylation compared with that in IOSE80 (CAO3: 43%; OVCAR3: 64%; and OVCAR8: 87%) (Figure 3(c) P value < 0.05). These data indicated that epigenetic methylation suppresses the expression level of STK3 in ovarian cancer.

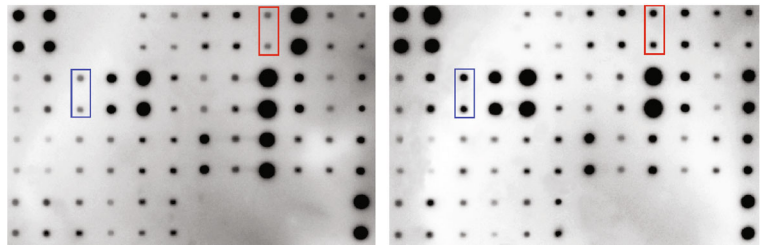
3.4. STK3 Correlates with CD8⁺ T-Cell in Ovarian Cancer. To study the possible mechanism of STK3 in ovarian cancer, we compared the transcriptome of STK3 overexpressed ovarian cancer OVCAR8 cells with that of control cells by high-throughput transcriptome sequencing (RNA-seq, supplementary Table 1). The differentially expressed genes were analyzed by GO analysis and KEGG enrichment analysis. The results showed that overexpressing STK3 significantly affected multiple inflammatory responses, including I-kappaB

kinase/NF-kappa B signaling, I-kappa B kinase/NF-kappa B signaling complex, CXCR chemokine receptor binding, and NF-kappa B signaling pathway, indicating a regulatory role of STK3 in ovarian cancer immune microenvironment (Figure 4(a)).

We used GSEA to analyze the differentiated genes in the high and low STK3 expression groups in the TCGA ovarian cancer database. The results indicated that the STK3 expression was related to the NF- κ B signaling pathway, which was TNFA_SIGNALING_VIA_NFKB. STK3 may regulate immune microenvironment of ovarian cancer cells by affecting NF- κ B signaling (Figure 4(b)).

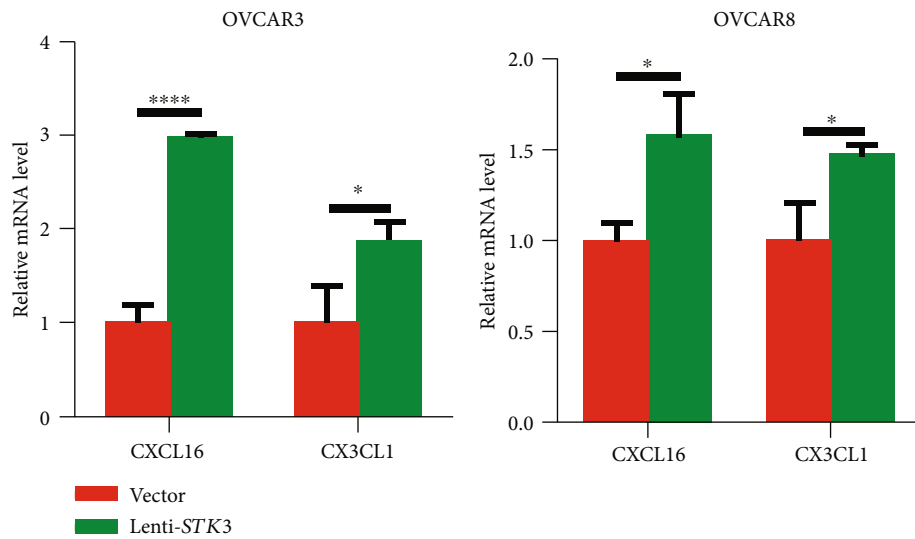
To characterize the potential immune components in the tumor microenvironment affected by STK3, an immunome compendium was built by publicly available data from purified immune cell subsets. According to the previous studies, we investigated both innate immune cells (mast cells, macrophages, and natural killer cells) and adaptive immune cells (B cell, Th1, and CD8+ T cell) as well as cytotoxic cells [17]. We observed that STK3 was specifically correlated with the gene signatures of CD8+ T-cells. In contrast, no obvious correlation was found in the expression of STK3 and other immune component-related genes. STK3 might exhibit a regulatory role on CD8+ T cell infiltration in ovarian cancer (Figure 4(c)).

3.5. The Overexpression of STK3 Promoted the Release of CXCL16 and CX3CL1 and Migration of CD8+ T-Cells by Activating NF- κ B Signaling. To study the chemokines regulated by STK3 that promote CD8+ T-cell infiltration, the chemokine profiles of conditional medium from vector and lenti-STK3 OVCAR8 cells were analyzed using the RayBio Human Cytokine Antibody Array. Consistent with the

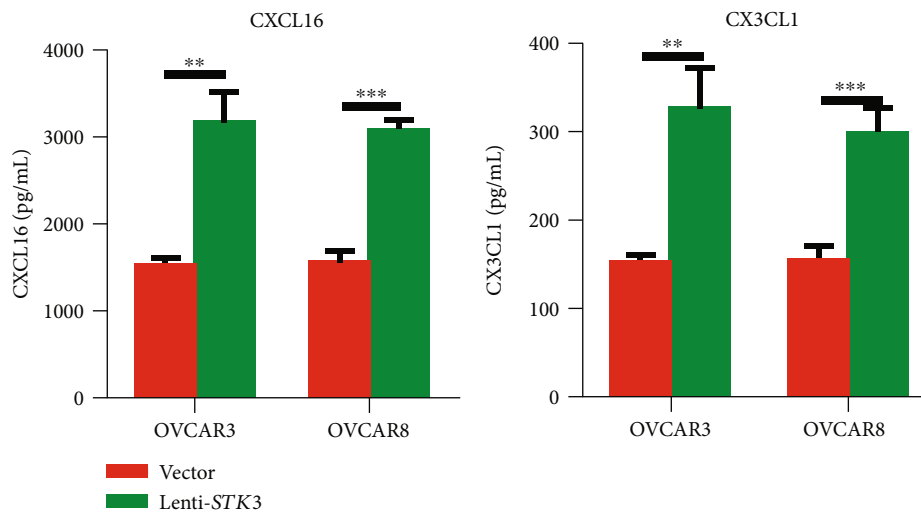


Chemokines	Log2(fold change)	Regulation
CXCL16	0.85	Up
CX3CL1	0.18	Up

(a)

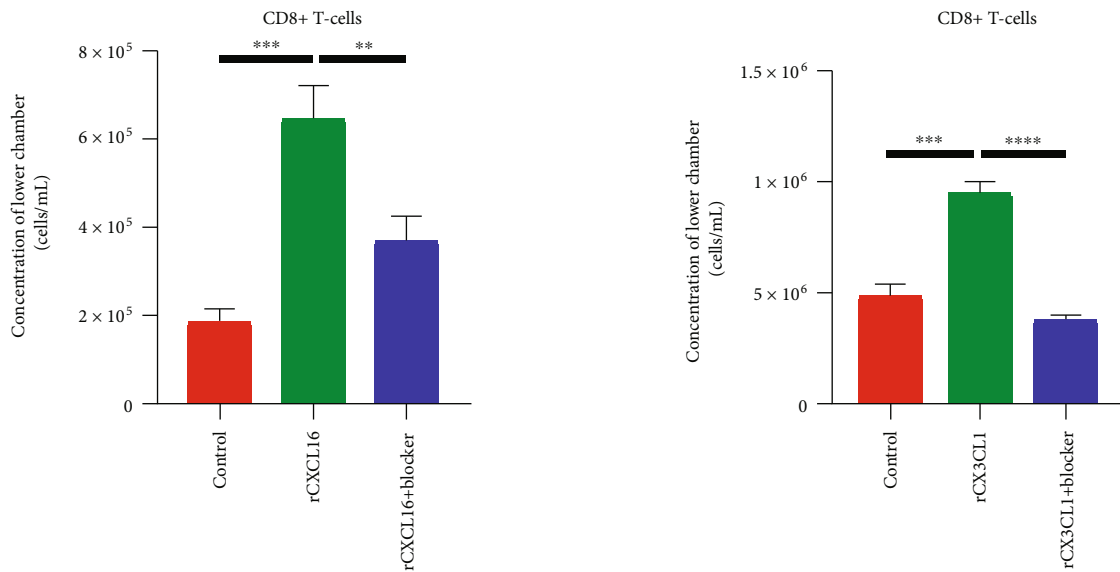
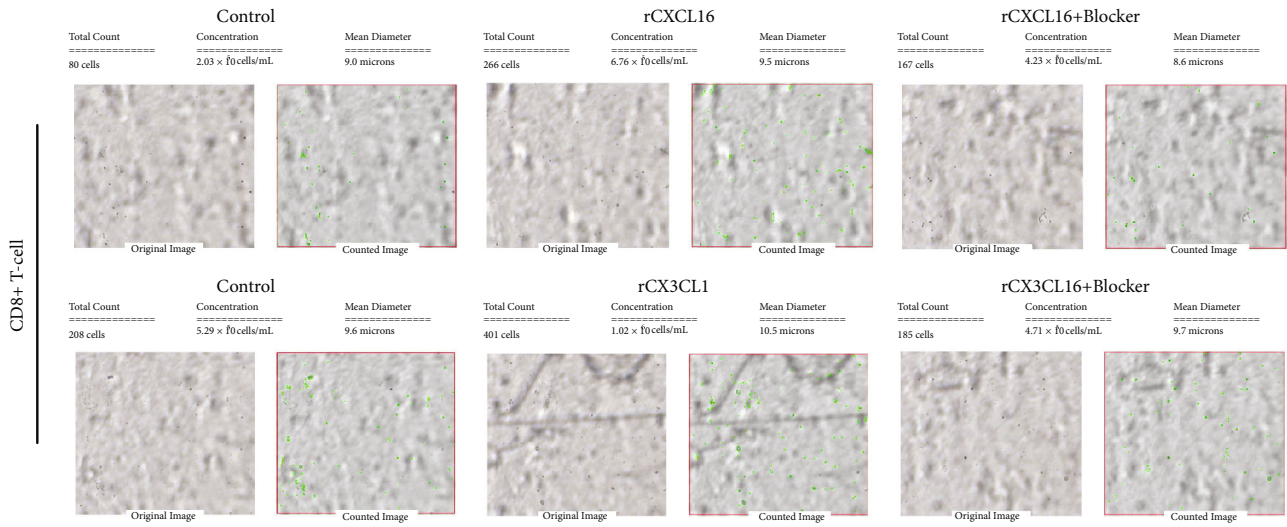


(b)



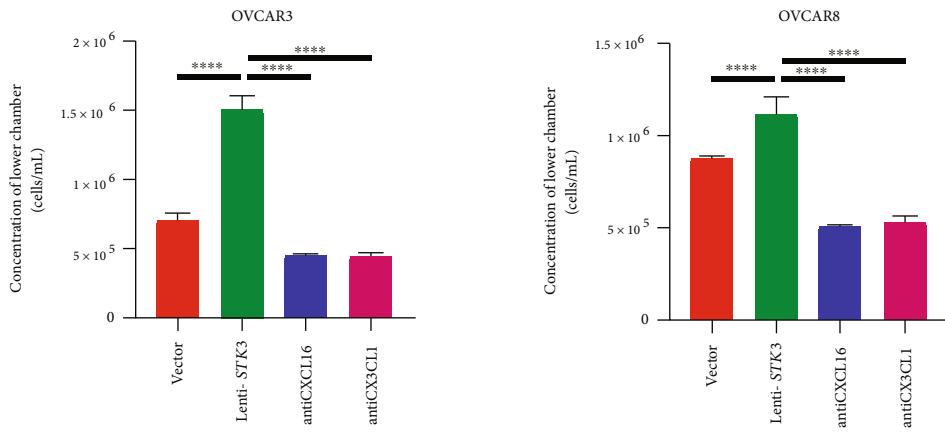
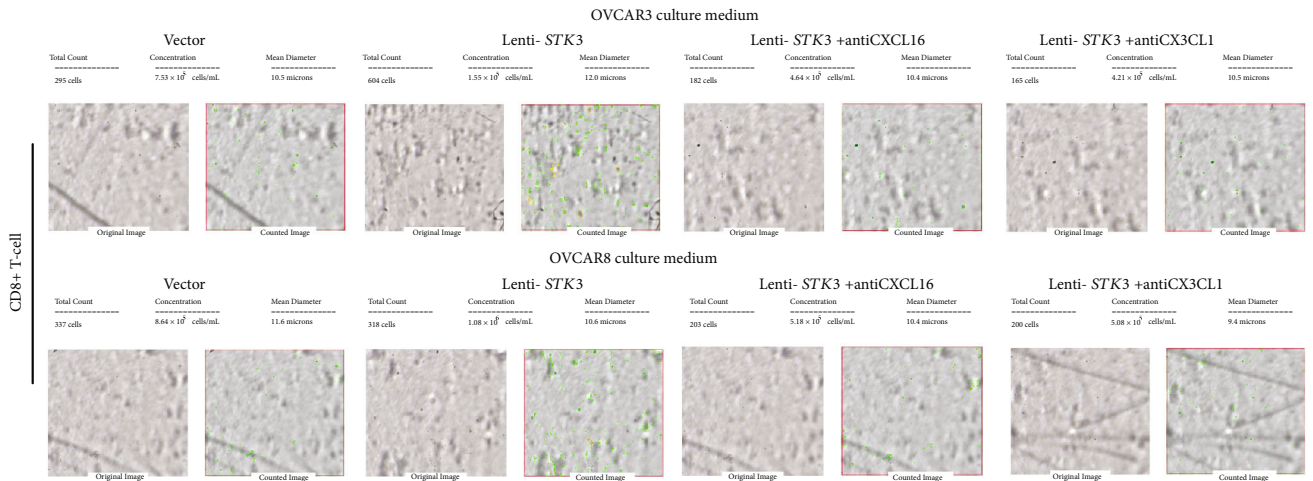
(c)

FIGURE 5: Continued.

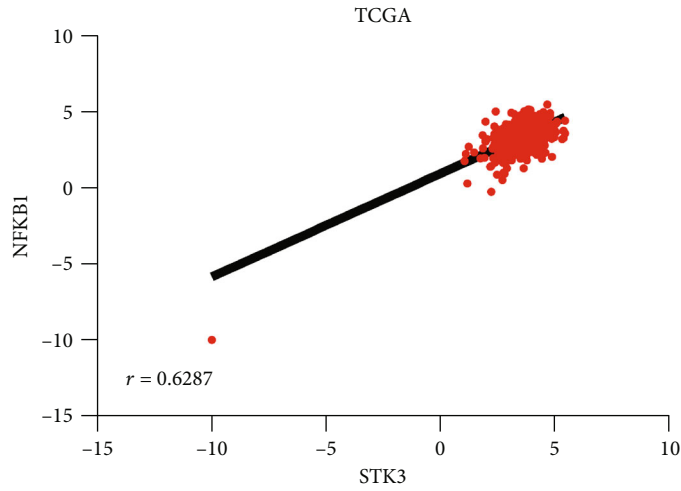


(d)

FIGURE 5: Continued.



(e)



(f)

FIGURE 5: Continued.

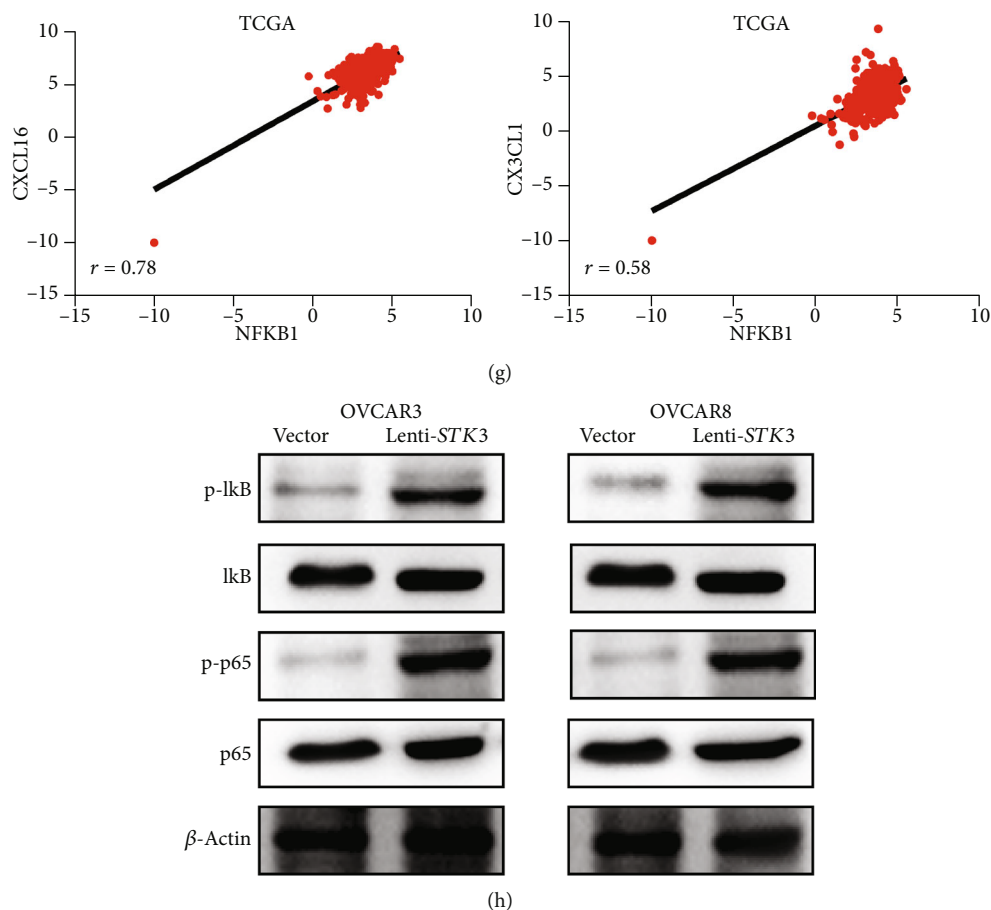


FIGURE 5: STK3 promoted release of CXCL16 and CX3CL1, migration of CD8⁺ T-cell, and activation of NF- κ B signaling. (a) Chemokine array of the conditional medium (CM) from vector and lenti-STK3 OVCAR8 cells. A. Table summarizing the relative signal intensity of indicated chemokines is presented in the lower left corner. (b) Real-time qPCR analysis of the effect of STK3 overexpression on the CXCL16 and CX3CL1 mRNA level in OVCAR3 and OVCAR8 cells (two-tailed Student's *t*-test, **P* < 0.05; ***P* < 0.01). (c) ELISA analysis of the CXCL16 and CX3CL1 level in the CM from vector and lenti-STK3 OVCAR3 and OVCAR8 cells (two-tailed Student's *t*-test, ***P* < 0.01; ****P* < 0.001). (d) Effects of rCXCL16 and rCX3CL1 on the migratory ability of human CD8⁺ T-cells. The number of cells was counted by Cellometer (two-tailed Student's *t*-test, ***P* < 0.01; ****P* < 0.001; *****P* < 0.0001). (e) Ovarian cancer cell culture supernatants were neutralized with anti-CXCL16 antibody and anti-CX3CL1 antibody and the migratory ability of CD8⁺ T-cells. The number of cells was counted by Cellometer (two-tailed Student's *t*-test, ***P* < 0.01; ****P* < 0.001; *****P* < 0.0001). (f) Correlation between STK3 and NFKB1 in the TCGA database. (g) Correlation between NFKB1 and CXCL16 or CX3CL1 in the TCGA database. (h) Western blot analysis of the effect of the STK3 overexpression on the NF- κ B pathway activity.

results of RNA-seq (Supplementary Table 1), two cytokines, CXCL16 and CX3CL1, were significantly increased in the conditional medium of lenti-STK3 cells compared with vector cells (Figure 5(a)). Real-time PCR showed that the STK3 overexpression drastically promoted the mRNA level of CXCL16 and CX3CL1 in both OVCAR8 and OVCAR3 cells (*P* value < 0.05) (Figure 5(b)). An ELISA assay confirmed the increase of CXCL16 and CX3CL1 in the conditional medium of lenti-STK3 cells (*P* value < 0.05) (Figure 5(c)). We then evaluated whether these two chemokines are responsible for CD8⁺ T-cell infiltration in vitro. Stimulation of CD8⁺ T-cells with recombinant CXCL16 (rCXCL16) and CX3CL1 (rCXCL16) showed enhanced migratory ability, and this promotive effect was largely compromised by the addition of neutralizing anti-CXCL16 and anti-CX3CL1 antibody. This indicated that

both CXCL16 and CX3CL1 contribute to CD8⁺ T-cells (*P* value < 0.05) (Figure 5(d)). Consistently, neutralization of CXCL16 and CX3CL1 in the conditional medium from OVCAR8 and OVCAR3 cells also suppressed the migratory potential of CD8⁺ T-cells (*P* value < 0.05) (Figure 5(e)).

To evaluate whether the NF- κ B pathway is responsible for the STK3-mediated CXCL16 and CX3CL1 expression, we first analyzed the correlation between the expression of STK3 and NF- κ B in TCGA. The levels of the STK3 expression were significantly positively correlated with NF- κ B (*P* value < 0.05) (Figure 5(f)). Previous study revealed that NF- κ B is the widely reported transcription factor for CXCL16 and CX3CL1. Further analyses indicated that the level of NF- κ B was also significantly positively correlated with CXCL16 and CX3CL1 (*P* value < 0.05) (Figure 5(g)). The phosphorylation level of p65 and NF- κ B inhibitor alpha

(I κ B α) in ovarian cancer regulated by STK3 was also investigated. The phosphorylation level of I κ B α and p65 was markedly increased by the overexpression of STK3 (Figure 5(h)). These data indicated that the upregulated STK3 expression could promote the NF- κ B signaling of ovarian cancer, which may further induce the expression of CXCL16 and CX3CL1.

4. Discussion

Many studies have shown that key molecules of the Hippo signal transduction pathway are important in inhibiting the occurrence and development of malignant tumors [18]. Serine/threonine kinases (STKs) are key molecules in the Hippo pathway. STKs control organ growth and reduce tumor progression by their effects on the Hippo pathway [19].

In this study, bioinformatic analysis showed that STK3 has low levels in ovarian cancer tissues, and the reduced expression of STK3 is closely related to the poor prognosis of patients suffering ovarian cancer. As an important component of the Hippo pathway, STK3 has been involved in the progression of many types of cancers. For instance, the reduced expression of STK3 was found in gastric cancer, and tumors from patients with lymph node metastasis showed minimal levels of STK3 [20]. Genetic deletion of STK3 in hepatocytes also led to the development of hepatocellular carcinoma [21]. Additionally, STK3 inhibits the proliferation of breast cancer cells and is overexpressed in breast cancer tissues [22]. Increasing evidences showing that the STK3 alterations may be caused by genetic or epigenetic changes. For example, hypermethylation of the promoter region of the STK3 gene contributes to the downregulation of the STK3 expression in soft tissue sarcoma [23], which is consistent with our result on ovarian cancer. Therefore, we believe that STK3 may be a good prognostic marker for ovarian cancer.

It is known that the overexpression of STK3 can reduce the proliferation, migration, and invasion of glioblastoma and pancreatic cancer [24, 25]. In nonsmall cell lung cancer tissues, the overexpression of STK3 can reduce the invasion and metastasis ability of lung cancer cells and promote lung cancer cell apoptosis [26]. Similarly, in the present study, we found that the overexpression of STK3 inhibits the invasion, proliferation, and metastasis of ovarian cancer cells and promotes their apoptosis. Besides STK3, other components of the Hippo pathway have roles in ovarian cancer [27]. Previous study revealed that LATS1/2 downregulation by the ubiquitin system is associated with epithelial-mesenchymal transition-like phenotypic changes in ovarian cancer cells, which trigger abnormal migration and invasion [28]. Moreover, a relationship between high levels of nuclear YAP in primary tumor tissues and inferior survival in ovarian cancer patients has also been reported [29]. In immortalized ovarian surface epithelial cells, the overexpression of YAP increased cell proliferation and migration ability and promoted anchorage-independent growth as well as contributed to the resistance to cisplatin-induced apoptosis, suggesting the oncogenic role of YAP in ovarian cancer. Our study further con-

firmed that STK3 may indirectly participate in suppressing ovarian cancer by regulating the activity of LATS1/2 and YAP.

CD8⁺ T-cells are considered to be antitumor immune cells [30]. We performed GO enrichment analysis and KEGG pathway enrichment analysis based on RNA-seq results of ovarian cancer cells in the control group and STK3 overexpression group. The results showed that STK3 and the NF- κ B signaling were related to infiltration of CD8⁺ T-cells. There is a close connection between the pathways. We also found a correlation between STK3 and CD8⁺ T-cells in the tumor microenvironment. The overexpression of STK3 can promote ovarian cancer cells to secrete CXCL16 and CX3CL1. The overexpression of STK3 can promote the migration of CD8⁺ T-cells. These results are the first correlation between the function of STK3 with CD8⁺ T-cells, and they help explain the effect of STK3 inhibition on the growth and metastasis of ovarian cancer from the perspective of the tumor microenvironment.

5. Conclusions

This study showed that upregulated serine/threonine kinase STK3 inhibits ovarian cancer aggressiveness and is correlated with CD8⁺ T-cells chemotaxis. These results provide insight into the roles of serine/threonine kinase in immune modulation. We also found that STK3 modulates intracellular NF- κ B signaling. These findings strongly suggest that the STK3/NF- κ B/CXCL16-CX3CL1/CD8⁺ T-cell axis is a potential therapeutic target in ovarian cancer.

Data Availability

The data used to support the findings of this study were supplied by Rong Zhang under license and so cannot be made freely available. Requests for access to these data should be made to Rong Zhang, rongzhang@163.com.

Conflicts of Interest

The authors declares that there is no conflict of interest regarding the publication of this paper.

Authors' Contributions

Xiangyu Wang and Fengmian Wang contributed equally to this work and should be considered co-first authors.

Acknowledgments

This study was supported by a grant from the National Natural Science Foundation of China (No.: 81472445, 81672587).

Supplementary Materials

See Supplementary Table 1 in the Supplementary Material for comprehensive transcriptome analysis in control OVCAR8 cells and STK3-overexpressing OVCAR8 cells. Transcriptome analysis in vector control and STK3-overexpressing OVCAR8 cells. Transcriptome analysis was performed on vector control and STK3-overexpressing OVCAR8 cells after extracting total

RNA. We included three biological repeats for each group in this experiment ($n = 3$). We performed paired-end sequencing using an Illumina NextSeq500 platform, and all samples were processed in the same sequencing run of the Illumina NextSeq 500 system and analyzed together with the aim to avoid the batches effect. (*Supplementary Materials*)

References

- [1] R. Barnett, "Ovarian cancer," *Lancet*, vol. 387, no. 10025, p. 1265, 2016.
- [2] P. M. Webb and S. J. Jordan, "Epidemiology of epithelial ovarian cancer," *Best Practice & Research. Clinical Obstetrics & Gynaecology*, vol. 41, pp. 3–14, 2017.
- [3] C. Allemani, H. K. Weir, H. Carreira et al., "Global surveillance of cancer survival 1995–2009: analysis of individual data for 25,676,887 patients from 279 population-based registries in 67 countries (CONCORD-2)," *Lancet*, vol. 385, no. 9972, pp. 977–1010, 2015.
- [4] B. J. Thompson and E. Sahai, "MST kinases in development and disease," *The Journal of Cell Biology*, vol. 210, no. 6, pp. 871–882, 2015.
- [5] Y. Zhang, C. Xin, J. Qiu, and Z. Wang, "Essential oil from *Pinus koraiensis* pinecones inhibits gastric cancer cells via the HIPPO/YAP signaling pathway," *Molecules*, vol. 24, no. 21, p. 3851, 2019.
- [6] D. Zhou, C. Conrad, F. Xia et al., "Mst1 and Mst2 maintain hepatocyte quiescence and suppress hepatocellular carcinoma development through inactivation of the Yap1 oncogene," *Cancer Cell*, vol. 16, no. 5, pp. 425–438, 2009.
- [7] Y. Park, J. Park, Y. Lee et al., "Mammalian MST2 kinase and human Salvador activate and reduce estrogen receptor alpha in the absence of ligand," *Journal of Molecular Medicine (Berlin, Germany)*, vol. 89, no. 2, pp. 181–191, 2011.
- [8] H. Shi, C. Liu, H. Tan et al., "Hippo kinases Mst1 and Mst2 sense and amplify IL-2R-STAT5 signaling in regulatory T cells to establish stable regulatory activity," *Immunity*, vol. 49, no. 5, pp. 899–914.e6, 2018, e6.
- [9] L. Zhang, J. R. Conejo-Garcia, D. Katsaros et al., "Intratumoral T cells, recurrence, and survival in epithelial ovarian cancer," *The New England Journal of Medicine*, vol. 348, no. 3, pp. 203–213, 2003.
- [10] S. Li, G. Zhu, Y. Yang et al., "Oxidative stress drives CD8(+) T-cell skin trafficking in patients with vitiligo through CXCL16 upregulation by activating the unfolded protein response in keratinocytes," *The Journal of Allergy and Clinical Immunology*, vol. 140, no. 1, pp. 177–189.e9, 2017, e9.
- [11] M. H. Park, J. S. Lee, and J. H. Yoon, "High expression of CX3CL1 by tumor cells correlates with a good prognosis and increased tumor-infiltrating CD8+ T cells, natural killer cells, and dendritic cells in breast carcinoma," *Journal of Surgical Oncology*, vol. 106, no. 4, pp. 386–392, 2012.
- [12] M. S. Yoon, C. T. Pham, M. T. T. Phan et al., "Irradiation of breast cancer cells enhances CXCL16 ligand expression and induces the migration of natural killer cells expressing the CXCR6 receptor," *Cytotherapy*, vol. 18, no. 12, pp. 1532–1542, 2016.
- [13] F. Zhang, W. Huang, M. Sheng, and T. Liu, "MiR-451 inhibits cell growth and invasion by targeting CXCL16 and is associated with prognosis of osteosarcoma patients," *Tumour Biology*, vol. 36, no. 3, pp. 2041–2048, 2015.
- [14] M. R. Morris, D. Gentle, M. Abdulrahman et al., "Functional epigenomics approach to identify methylated candidate tumour suppressor genes in renal cell carcinoma," *British Journal of Cancer*, vol. 98, no. 2, pp. 496–501, 2008.
- [15] J. J. Wallin, J. C. Bendell, R. Funke et al., "Atezolizumab in combination with bevacizumab enhances antigen-specific T-cell migration in metastatic renal cell carcinoma," *Nature Communications*, vol. 7, no. 1, 2016.
- [16] C. Geismann, W. Erhart, F. Grohmann et al., "TRAIL/NF- κ B/CX3CL1 mediated Onco-Immuno crosstalk leading to TRAIL resistance of pancreatic cancer cell lines," *International Journal of Molecular Sciences*, vol. 19, no. 6, p. 1661, 2018.
- [17] S. H. Jiang, L. L. Zhu, M. Zhang et al., "GABRP regulates chemokine signalling, macrophage recruitment and tumour progression in pancreatic cancer through tuning KCNN4-mediated Ca²⁺ signalling in a GABA-independent manner," *Gut*, vol. 68, no. 11, pp. 1994–2006, 2019.
- [18] F. X. Yu, B. Zhao, and K. L. Guan, "Hippo pathway in organ size control, tissue homeostasis, and Cancer," *Cell*, vol. 163, no. 4, pp. 811–828, 2015.
- [19] S. J. Rawat and J. Chernoff, "Regulation of mammalian Ste20 (Mst) kinases," *Trends in Biochemical Sciences*, vol. 40, no. 3, pp. 149–156, 2015.
- [20] F. X. Yu, Z. Meng, S. W. Plouffe, and K. L. Guan, "Hippo pathway regulation of gastrointestinal tissues," *Annual Review of Physiology*, vol. 77, no. 1, pp. 201–227, 2015.
- [21] W. Kim, S. K. Khan, J. Gvozdenovic-Jeremic et al., "Hippo signaling interactions with Wnt/ β -catenin and Notch signaling repress liver tumorigenesis," *The Journal of Clinical Investigation*, vol. 127, no. 1, pp. 137–152, 2017.
- [22] X. Zhou, S. Wang, Z. Wang et al., "Estrogen regulates hippo signaling via GPER in breast cancer," *The Journal of Clinical Investigation*, vol. 125, no. 5, pp. 2123–2135, 2015.
- [23] C. Seidel, U. Schagdarsurengin, K. Blümke et al., "Frequent hypermethylation of MST1 and MST2 in soft tissue sarcoma," *Molecular Carcinogenesis*, vol. 46, no. 10, pp. 865–871, 2007.
- [24] T. Huang, C. K. Kim, A. A. Alvarez et al., "MST4 phosphorylation of ATG4B regulates autophagic activity, Tumorigenicity, and radioresistance in glioblastoma," *Cancer Cell*, vol. 32, no. 6, pp. 840–855.e8, 2017, e8.
- [25] E. J. Childs, E. Mocchi, D. Campa et al., "Common variation at 2p13.3, 3q29, 7p13 and 17q25.1 associated with susceptibility to pancreatic cancer," *Nature Genetics*, vol. 47, no. 8, pp. 911–916, 2015.
- [26] X. L. Liu, R. Zuo, and W. B. Ou, "The hippo pathway provides novel insights into lung cancer and mesothelioma treatment," *Journal of Cancer Research and Clinical Oncology*, vol. 144, no. 11, pp. 2097–2106, 2018.
- [27] Z. Meng, T. Moroishi, and K. L. Guan, "Mechanisms of hippo pathway regulation," *Genes & Development*, vol. 30, no. 1, pp. 1–17, 2016.
- [28] H. Yagi, I. Onoyama, K. Asanoma et al., "G α 13-mediated LATS1 down-regulation contributes to epithelial-mesenchymal transition in ovarian cancer," *The FASEB Journal*, vol. 33, no. 12, pp. 13683–13694, 2019.
- [29] C. A. Hall, R. Wang, J. Miao et al., "Hippo pathway effector yap is an ovarian cancer oncogene," *Cancer Research*, vol. 70, no. 21, pp. 8517–8525, 2010.
- [30] Q. F. He, Y. Xu, J. Li, Z. M. Huang, X. H. Li, and X. Wang, "CD8+ T-cell exhaustion in cancer: mechanisms and new area for cancer immunotherapy," *Briefings in Functional Genomics*, vol. 18, no. 2, pp. 99–106, 2019.

Research Article

Effects of miR-373 Inhibition on Glioblastoma Growth by Reducing *Limk1 In Vitro*

Tao Peng,¹ Tiejun Wang,² Guohui Liu ,³ and Lixiang Zhou ¹

¹Department of Neurosurgery, The First Hospital of Jilin University, Xinmin Street 1#, Changchun 130021, China

²Division of Orthopaedic Traumatology, The First Hospital of Jilin University, Xinmin Street 1#, Changchun 130021, China

³Emergency Surgery, The First Hospital of Jilin University, Xinmin Street 1#, Changchun 130021, China

Correspondence should be addressed to Guohui Liu; zhangxx063@sina.com and Lixiang Zhou; bzclh1969@163.com

Received 25 June 2020; Accepted 4 August 2020; Published 28 September 2020

Guest Editor: Zenghui Teng

Copyright © 2020 Tao Peng et al. This is an open access article distributed under the Creative Commons Attribution License, which permits unrestricted use, distribution, and reproduction in any medium, provided the original work is properly cited.

Glioblastoma (GBM) is an aggressive brain tumor with shorter median overall survival time. It is urgent to find novel methods to enhance the therapeutic efficiency clinically. miR-373 is related to the biological development process of cancers, but there are no reports whether modulation on miR-373 could affect GBM development or modify the efficiency of chemo- or radiotherapy yet. Our current study found that the higher level of miR-373 was observed in U-251 cells. Inhibition on miR-373 could reduce the U-251 cell number by 65% and PCNA expression obviously. In addition, inhibition on miR-373 sensitized U-251 cells to chemo- or radiotherapy. The cell cycle of U-251 cells could be modulated by miR-373 knockdown, which could enhance the p21 expression and reduce the cdc2 level. Anti-miR-373 could increase the Bax/Bcl-2 ratio of U-251 cells and induce cell apoptosis significantly. These above effects of miR-373 could be reversed by *Limk1* overexpression. Thus, our experimental data confirmed the fact that miR-373 could be a new therapeutic target to enhance the efficiency of chemo- or radiotherapy for clinical GBM patients.

1. Introduction

Glioblastoma is an aggressive brain tumor with shorter median overall survival time in adults [1], although multiple therapeutic methods have been used including surgical resection and chemo- or radiotherapy [2, 3]. It has been reported that only a median survival of 15 months was obtained after radiotherapy combined with temozolomide (TMZ) [4, 5], which was the major chemotherapy drug for GBM but with resistance effects for most patients yet [6, 7]. Thus, it is urgent to find novel methods to enhance the therapeutic efficiency clinically. Recently, there are many studies that focused on the combination administration on tumor including the normal chemo- or radiotherapy and targeted gene treatment [8, 9], which could effectively reduce or block the resistance from antitumor therapy.

It is more important to find the novel targeted molecule by *in vitro* or *in vivo* experimental evidence, which could reduce the side effects and prolong the median survival time in the clinical therapy on GBM patients. miRNAs are endogenous, small (~22 nt) noncoding RNAs that were first reported in 1993. Its function was recognized by binding to the 3'-untranslational region (3'-UTR) of target mRNA [10–12]. Several miRNAs with an up- or downregulation level have been reported, and such abnormal expression was related to the biological development process of cancers, including cell apoptosis, cell cycle modulation, proliferation, invasion, and metastasis [13, 14]. The higher level of miR-221 [15] and lower level of miR-181 [16] were observed in clinical samples from GBM patients. Therefore, changing the level of above oncogenes or tumor suppressors by using molecular biological methods could provide great assistance to clinical therapy of tumor patients. In addition, some

reports showed [17–19] that the resistance of chemo- or radiotherapy on tumor clinical treatment was also related to the effects of miRNAs, such as miR-100 [20], miR-21 [21], miR-373 [22, 23], but the underlying mechanism was still unclear.

Furthermore, it has been evidenced that miR-373 may promote migration and metastasis of cancer cells *in vitro* by regulating the CD44 [24]. HIF-1 α could affect the miR-373 level in response to hypoxia [25]. As an oncogenic miRNA, miR-373 plays the key role in tumorigenesis through p53-mediated CDK effect [26]. But there are no reports whether modulation on miR-373 could affect GBM development or modify the efficiency of chemo- or radiotherapy on GBM. Further experimental evidence is needed both *in vitro* or *in vivo* to clarify the above underlying mechanism. In addition, the downstream effector or pathway related to cell proliferation, cell cycle, or apoptosis also should be explored or discussed in detail. Increasing evidence showed that Limk1 was a biomarker of squamous cell carcinoma [27], lung cancer [28], breast cancer [29], and even GBM [30, 31]. Limk1 could enhance the tumor cell proliferation and invasion by the MMP or p21-related pathway [32, 33]. But there is no study on the relationship between miR-373 and Limk1, especially in the pathological process of GBM.

The purpose of the current study was to investigate the roles of miR-373 in the biological behavior of GBM development. It is hypothesized that reducing miR-373 could change the proliferation or apoptosis of GBM cell *in vitro* and even sensitize GBM to chemo- or radiotherapy, which may provide the new therapeutic strategy for clinical patients.

2. Materials and Methods

2.1. Cell Culture. The human GBM cell line U-251 was purchased from the American Type Culture Collection (ATCC, Manassas, VA). Cells were cultured in DMEM (Gibco, Carlsbad, CA, USA) supplemented with 100 μ g/mL streptomycin, 100 U/mL penicillin, and 10% FBS, at 37°C with 5% CO₂.

For the transfection procedure, Lipofectamine™ RNAi-MAX (Thermo Fisher Scientific, IL, USA) was used as the transfection reagent [34, 35]. And anti-miR-373 (ACUCAA AAUGGGGGCGCUUCC) and the negative control were got from the company of Thermo Fisher Scientific (IL, USA). The Limk1-mutant construct was obtained from OriGene (Beijing, China). The following experiments were performed after above transfection for 48 h.

2.2. Quantitative PCR. The real-time quantitative PCR was performed to detect the miR-373 and the mRNA level of its related molecule. The TaqMan assay (ABI, Forest City, CA) was used in above experiments according to the standard protocol [36].

2.3. Western Blot. U-251 cells were cultured and collected for western blot experiments after the following different treatments. Briefly, cells were lysed as described in previous studies [37] with the following buffer including 2 mM NaF, 0.01 M Na₃VO₄, 1 μ g/mL leupeptin, 0.01 M

EDTA, 20 mM Tris-HCl, and 1% Triton X-100. Total protein was obtained after centrifugation at 12,000 rpm at 4°C for 20 min. After that, a BCA test (Pierce, Rockford, IL, USA) was used to determine the protein concentrations. Protein expression was detected by incubation with a primary antibody after the protocol of SDS-PAGE gel and transferred membranes. β -Actin was used to control and correct for above procedure.

2.4. Colony Formation Assay. U-251 cells were cultured with 6-well tissue culture plates, and the method of Giemsa stain was used to evaluate the colony formation after chemo- or radiotherapy in the presence or absence of anti-miR-373 transfection. The number of colonies was counted by light microscopy.

2.5. Chemo- and Radiotherapy on U-251 Cells. U-251 cells were cultured and received the following treatments. For the radiotherapy group, the γ -ray ionizing radiation (IR) was treated for U-251 cells by using a ⁶⁰Co source. The dose was set at 2.4 Gy/min. For the chemotherapy group, temozolomide (TMZ, Tocris) was used at 30 nM.

2.6. Cell Proliferation. Cells were seeded in a 96-well plate and used to evaluate the cell proliferation by using an MTT kit (Roche Diagnostics, Germany) after chemo- or radiotherapy in the presence or absence of anti-miR-373 transfection. Following the protocol, the 10 μ L MTT reagent and 100 μ L DMSO were added, respectively. After incubation, the absorbance was recorded by a Microplate Spectrophotometer (BioTek, USA) at 490 nm. All tests were repeated for three times. As a biomarker of cell proliferation, PCNA (proliferating cell nuclear antigen) expression in U-251 cells was observed through western blot after above treatment. The primary PCNA antibody (Cell Signaling Technology, MA, USA) was used.

2.7. Cell Cycle Analysis. The changes on cell cycle-related proteins p21 and cdc2 were tested by the western blot method after above anti-miR-373 transfection. Primary antibodies against p21 and cdc2 (Cell Signaling Technology, MA, USA) were used to evaluate protein expression.

2.8. Cell Apoptosis Analysis. Firstly, cells were seeded and used to evaluate the cell apoptosis by FACS (Flow Cytometry, Becton Dickinson, CA, USA) after chemo- or radiotherapy in the presence or absence of anti-miR-373 transfection. The analysis was performed after PI and Annexin V-FITC incubation according to the protocol. In addition, western blot was performed to assess the expression of Bax and Bcl-2 after above anti-miR-373 transfection combined with chemo- or radiotherapy. The Bax and Bcl-2 primary antibodies were obtained from Cell Signaling Technology (MA, USA).

2.9. Statistical Analysis. Student's *t*-test and ANOVA were used to analyze the difference by using GraphPad Prism and SPSS 17.0. Data were shown as the mean \pm standard error.

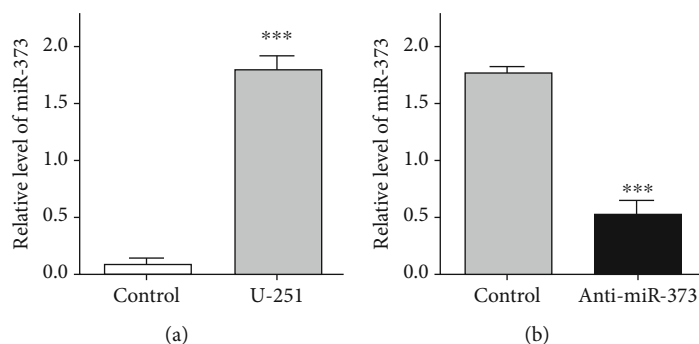


FIGURE 1: miR-373 level in U-251 cells. (a) High miR-373 level was observed by real-time quantitative PCR in U-251 cells. (b) miR-373 level was reduced obviously after anti-miR-373 transfection by real-time quantitative PCR in U-251 cells (bars indicate the standard deviation of the mean; each experiment was performed in triplicate; *** $p < 0.001$).

3. Results

3.1. Inhibition of miR-373 Reduced the U-251 Cell Proliferation. Firstly, real-time quantitative PCR was used to investigate the miR-373 level in U-251 cells after anti-miR-373 transfection. The higher level of miR-373 was obtained in U-251 cells. It was reduced obviously by at least 71% after above transfection compared with the negative control group, which may provide the effective methods for further experiments to test the effects of miR-373 knockdown on biological changes of U-251 cells *in vitro* (Figure 1).

Next, MTT assay was performed to observe the effects of miR-373 inhibition on U-251 cell proliferation by anti-miR-373 transfection. Compared with the negative control group, the number of U-251 cells was decreased significantly, reduced by 65% (Figure 2).

In addition, the western blot method was used to detect the changes on PCNA expression in the presence or absence of anti-miR-373 transfection. The results showed that PCNA expression in U-251 cells was decreased obviously by reducing the miR-373 level. In addition, the results from real-time quantitative PCR proved that the lower PCNA level was obtained after above anti-miR-373 transfection (Figure 2). It has been reported that PCNA was a typical biological marker of cancer cell proliferation. Changes on its expression level after different treatments could also provide the positive evidence for effects of its regulator [38]. Thus, our results of above experiments evidenced that miR-373 knockdown has the clear inhibition effects on U-251 cell proliferation, which may help us find the novel potential therapeutic target for the treatment of clinical GBM patients.

IR resistance was the problem for such GBM patients in clinical therapy, and a novel method or molecule was needed to reduce the resistance effects. After ionizing radiation, the cell number of U-251 cells was reduced by 60% compared with the control group. After IR combined with anti-miR-373 transfection, it was decreased by 81%, which was lower than single IR-treated U-251 cells. For the PCNA expression level, both the western blot and PCR results showed that the PCNA expression level was inhibited

after ionizing radiation, and such inhibition was also enhanced after being combined with anti-miR-373 transfection (Figure 2).

In the TMZ alone-treated group, the U-251 cell proliferation also decreased by 63%. And for the combined group, the number of U-251 cells was reduced at least by 79% after TMZ application in the presence of anti-miR-373 transfection. The result was clear that inhibition on the miR-373 level could enhance the therapeutic efficiency of TMZ on U-251 cells *in vitro*. For the expression of PCNA protein, it was reduced in the TMZ alone-treated group, and an obvious decrease was obtained after TMZ treatment combined with miR-373 knockdown. And a similar tendency was observed in the result of real-time quantitative PCR (Figure 2). Thus, above data also provided the experimental evidence that resistance of TMZ on GBM clinical therapy could be reversed or reduced by miR-373 knockdown, which may bring the higher therapeutic efficiency or lower toxicity for such patients.

3.2. Colony Formation Assay. After above experiments, colony formation assay was performed to evaluate the effects of anti-miR-373 on U-251 cells *in vitro*. Reducing the miR-373 level could decrease the colony formation of U-251 cells obviously. In the TMZ or IR alone-treated group, it was reduced significantly, but additional effects were obtained in the presence of anti-miR-373, respectively (Figure 3). Our results indicated that miR-373 knockdown may reduce the colony formation capacity of U-251 cells, and such anti-miR-373 effects could sensitize U-251 cells to chemo- or radiotherapy efficiently.

3.3. Inhibition of miR-373 Modulated the U-251 Cell Cycle. After reducing the miR-373 level in U-251 cells by anti-miR-373 transfection, the expression of cell cycle-related proteins such as p21 and cdc2 were observed by the western blot method. p21 expression was enhanced obviously in U-251 cells after anti-miR-373 transfection, but the expression of cdc2 was reduced. The results from the real-time quantitative PCR provided the same tendency that the higher p21 level, but lower cdc2 level, was obtained after reducing the miR-373 level in U-251 cells

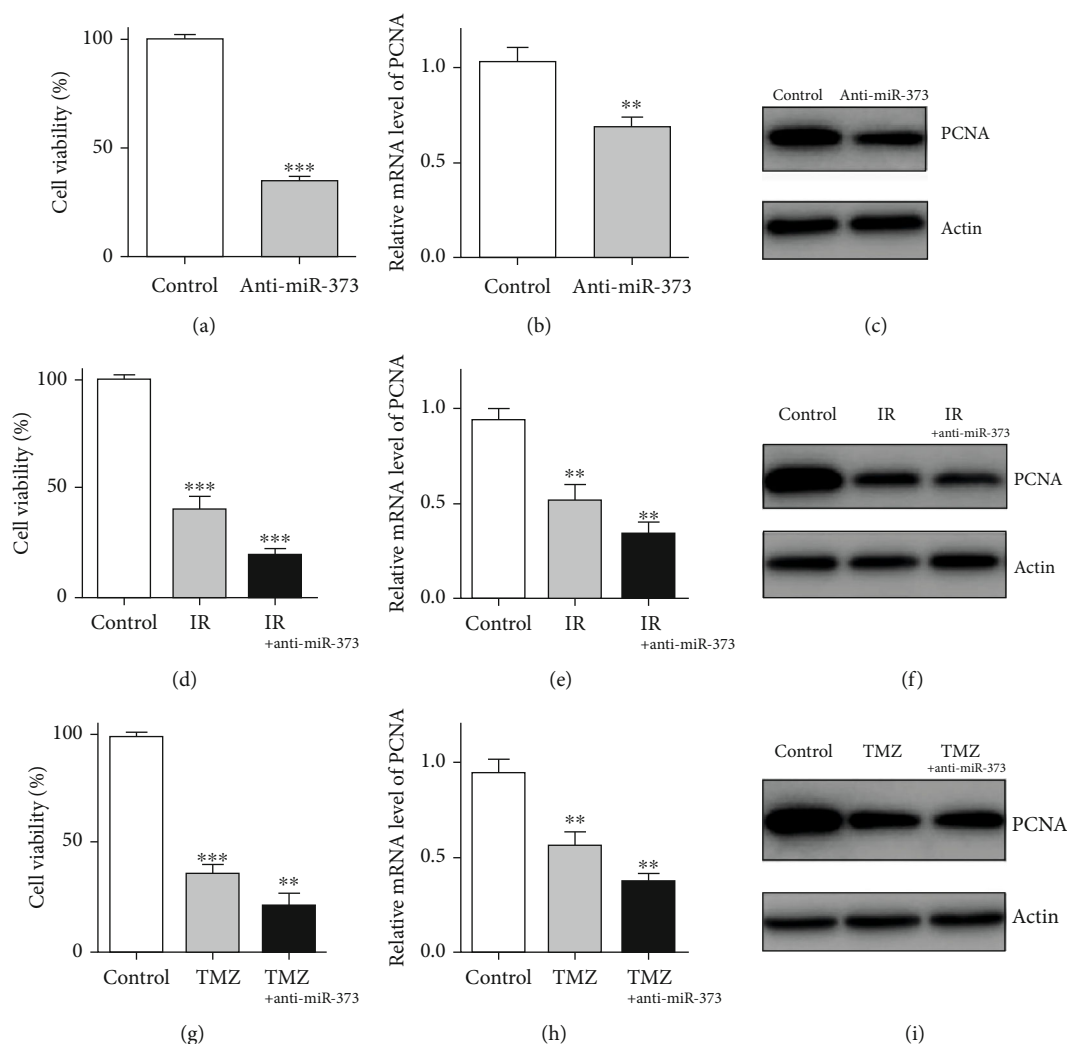


FIGURE 2: Inhibition of miR-373 reduced the U-251 cell proliferation. (a) Anti-miR-373 could reduce the U-251 cell proliferation by MTT assay. (b) PCNA mRNA level was also reduced after anti-miR-373 transfection by real-time quantitative PCR in U-251 cells. (c) Western blot results proved the lower expression of PCNA protein after anti-miR-373 transfection in U-251 cells. (d) After ionizing radiation (IR), the cell number of U-251 cells was reduced obviously by MTT assay, and additional effects were also obtained in the group of IR combined with anti-miR-373 transfection. (e) IR could also reduce the PCNA mRNA level in U-251 cells, and such inhibition was enhanced after being combined with anti-miR-373 transfection. (f) PCNA protein expression was also reduced significantly after ionizing radiation in the presence or absence of anti-miR-373 transfection. (g) After TMZ treatment, the cell number of U-251 cells was reduced obviously by MTT assay, and additional effects were also obtained in the group of TMZ treatment in the presence of anti-miR-373 transfection. (h) TMZ could also reduce the PCNA mRNA level in U-251 cells, and such inhibition was enhanced after being combined with anti-miR-373 transfection. (i) PCNA protein expression was also reduced significantly after TMZ treatment in the presence or absence of anti-miR-373 transfection (bars indicate the standard deviation of the mean; each experiment was performed in triplicate; *** $p < 0.001$; ** $p < 0.01$).

(Figure 4). Thus, these data demonstrated that inhibition of miR-373 could also modulate the U-251 cell cycle process by regulating the p21 or cdc2 level.

3.4. Inhibition of miR-373 Induced the U-251 Cell Apoptosis.

U-251 cell apoptosis was investigated after miR-373 knock-down or combined with above treatment to evaluate the effects of miR-373 on biological changes of U-251 cells. Firstly, FACS was used to analysis the apoptotic rate of U-251 cells. In the TMZ or IR alone-treated group, the percentages of apoptotic cells were $10.9 \pm 0.2\%$ and $13.2 \pm 0.6\%$, respectively. And it was $11.3 \pm 0.5\%$ in the anti-

miR-373-transfected group. In addition, in the combined group, the percentages of apoptotic cells were $17.1 \pm 0.8\%$ and $16.4 \pm 0.5\%$ after TMZ or IR treated in the presence of anti-miR-373 transfection. Above results provided the fact that cell apoptosis could be induced by miR-373 knockdown, which also enhances the effects of chemo- or radiotherapy.

Next, the apoptosis-related proteins such as Bax and Bcl-2 were detected in U-251 cells after above treatment using the western blot method. Bax expression was increased obviously after the TMZ or IR single-treated group, which was consistent with the previous reports

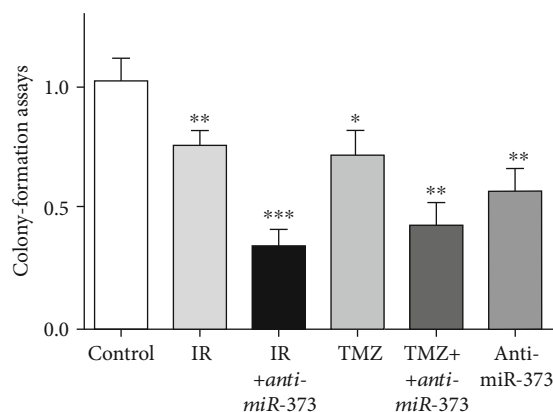


FIGURE 3: Inhibition of miR-373 reduced the U-251 cells' colony formation. Colony formation assays were performed to evaluate the effects of anti-miR-373 on U-251 cells *in vitro*. Reducing the miR-373 level, TMZ or IR treatment could decrease the colony formation of U-251 cells obviously, and additional effects were obtained in the combined groups, respectively (bars indicate the standard deviation of the mean; each experiment was performed in triplicate; *** $p < 0.001$; ** $p < 0.01$; * $p < 0.05$).

[39, 40]. After anti-miR-373 transfection, the western blot results showed that higher expression of Bax was obtained compared with the untreated group. In addition, in the combined group with anti-miR-373 and TMZ or IR treatment, Bax expression was enhanced significantly compared with the single-treated group (Figure 5). Thus, above data demonstrated that Bax was the downstream effector of the miR-373 molecule, which could affect the U-251 cell apoptosis.

At the same time, Bcl-2 expression was also observed after similar treatment. In the TMZ single-treated group, reduced expression of Bcl-2 was detected, and similar effects were obtained after using anti-miR-373 transfection or IR. And the Bcl-2 expression was decreased obviously in the TMZ- or IR-treated group in the presence of anti-miR-373 transfection (Figure 5).

3.5. Antitumor Effects of miR-373 Inhibition through Reducing *Limk1* Expression. To test the relationship between miR-373 and *Limk1*, further experiments were investigated *in vitro*. Firstly, western blot was used to test the *Limk1* expression in U-251 cells after anti-miR-373 transfection. It showed that the obvious decrease on *Limk1* expression was obtained by using anti-miR-373, while higher expression of *Limk1* was also observed in U-251 cells (Figure 6). In addition, further observation was performed by real-time quantitative PCR; the results showed that the *Limk1* level was reduced by inhibition on miR-373 in U-251 cells (Figure 6). Thus, above results provided the direct fact that miR-373 inhibition could change the *Limk1* expression in U-251 cells, which may be the downstream effector of miR-373. And the following experiments were performed to provide more details in this process.

The apoptotic rate of U-251 cells was checked again by FACS in the presence of anti-miR-373 transfection,

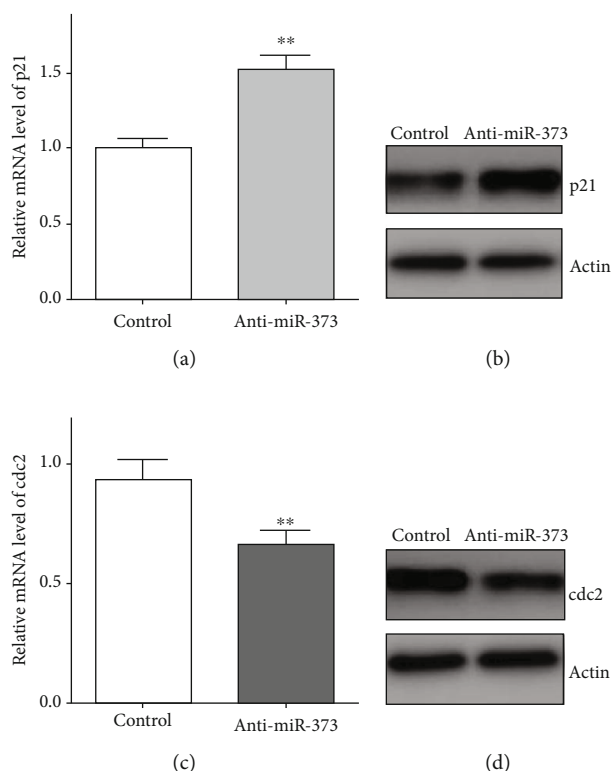


FIGURE 4: Effects of anti-miR-373 on p21 and *cdc2* expression. (a) p21 mRNA level was increased in the presence of anti-miR-373 transfection by the real-time quantitative PCR, and (b) western blot result also proved that higher p21 expression was obtained after anti-miR-373 transfection; (c) *cdc2* mRNA level was decreased in the presence of anti-miR-373 transfection by the real-time quantitative PCR, and (d) western blot result also proved that lower *cdc2* expression was obtained after anti-miR-373 transfection (bars indicate the standard deviation of the mean; each experiment was performed in triplicate; ** $p < 0.01$).

but at the same time, *Limk1* cDNA was cotransfected to test if there are different changes on the apoptotic rate in order to confirm that the above effects of anti-miR-373 might be related to its downstream effector *Limk1*. The results showed that the percentages of apoptotic cells were decreased after *Limk1* overexpression although when using anti-miR-373 transfection, it was $3.1 \pm 0.2\%$ vs. $11.3 \pm 0.5\%$, respectively, compared with the group of anti-miR-373 transfection alone. These data provided the direct information that the cell apoptosis of U-251 induced by anti-miR-373 was *Limk1* dependent, which could be reversed by *Limk1* overexpression. Next, chemo- or radiotherapy was combined to test the reversing effects of *Limk1*. After cotransfecting *Limk1* cDNA, there is no difference on the apoptotic rate of U-251 cells between the chemo- or radiotherapy single-treated group and the combined group in the presence of anti-miR-373 transfection, which means sensitization on chemo- or radiotherapy by miR-373 inhibition in U-251 cells was reversed by *Limk1* overexpression.

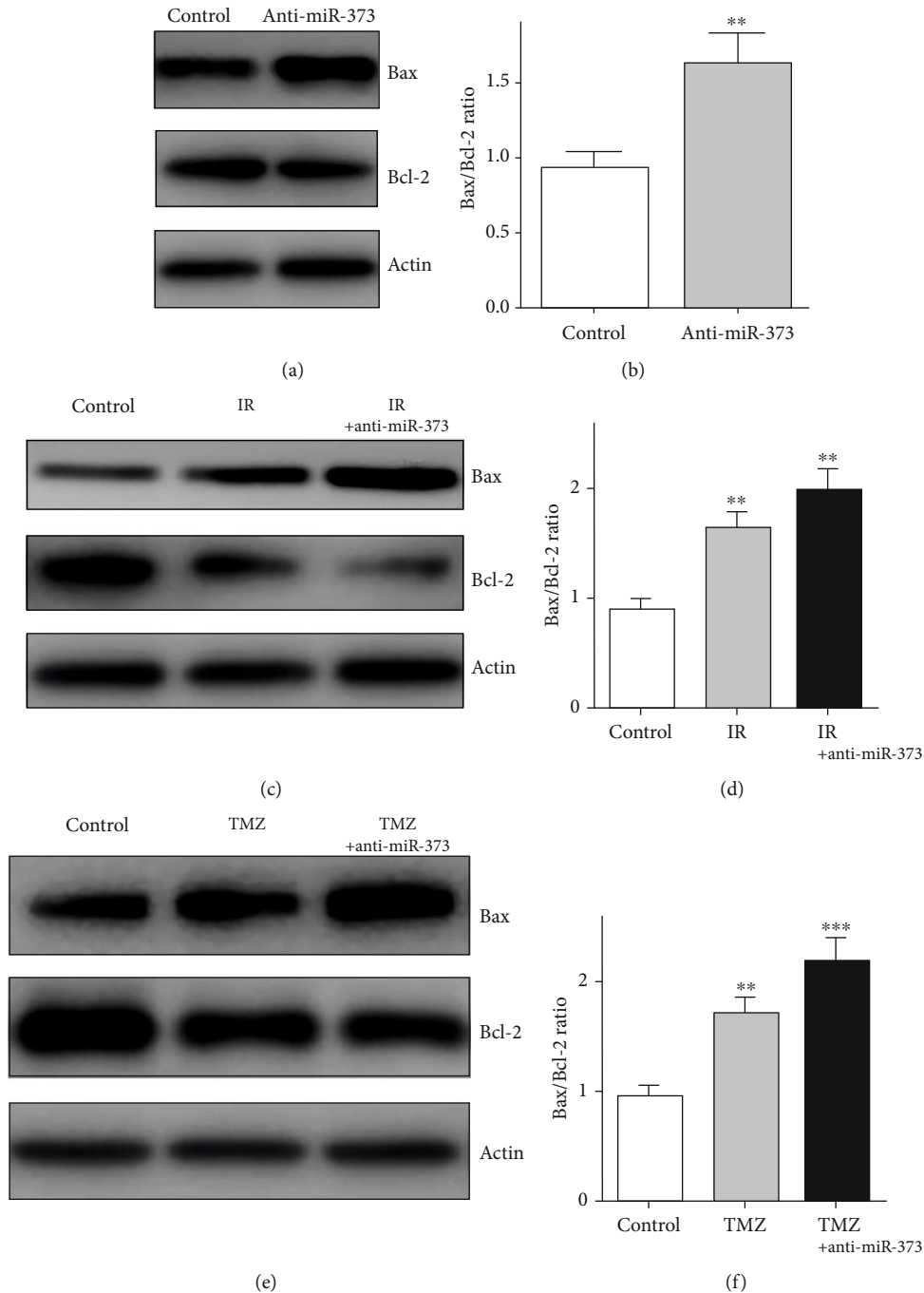


FIGURE 5: Effects of anti-miR-373 on the Bax/Bcl-2 ratio. (a, b) Anti-miR-373 could increase the Bax expression and reduce the Bcl-2 expression which resulted in the higher Bax/Bcl-2 ratio in the U-251 cells. (c, d) After ionizing radiation (IR), the Bax expression was increased combined with lower Bcl-2 expression; furthermore, the Bax/Bcl-2 ratio was also enhanced significantly after being combined with anti-miR-373 transfection. (e, f) After TMZ treatment, the Bax/Bcl-2 ratio was also increased obviously in the presence or absence of anti-miR-373 transfection, respectively (bars indicate the standard deviation of the mean; each experiment was performed in triplicate; *** $p < 0.001$; ** $p < 0.01$).

4. Discussion

Currently, for the treatment on GBM patients, surgery and chemo- or radiotherapy were the main available methods [2–4]. But the resistance to chemo- or radiotherapy was the trouble of the clinical treatment on these patients, which may reduce therapeutic efficacy or enhance the tox-

icity to normal organs by increasing the therapeutic dosage with poor long-term survival for patients [41, 42]. Temozolomide (TMZ) was the major chemotherapy drug for GBM, and surgical therapy followed with temozolomide was the standard method in the clinical treatment of glioblastoma patients currently, but most patients had the effects of temozolomide resistance that reduced the

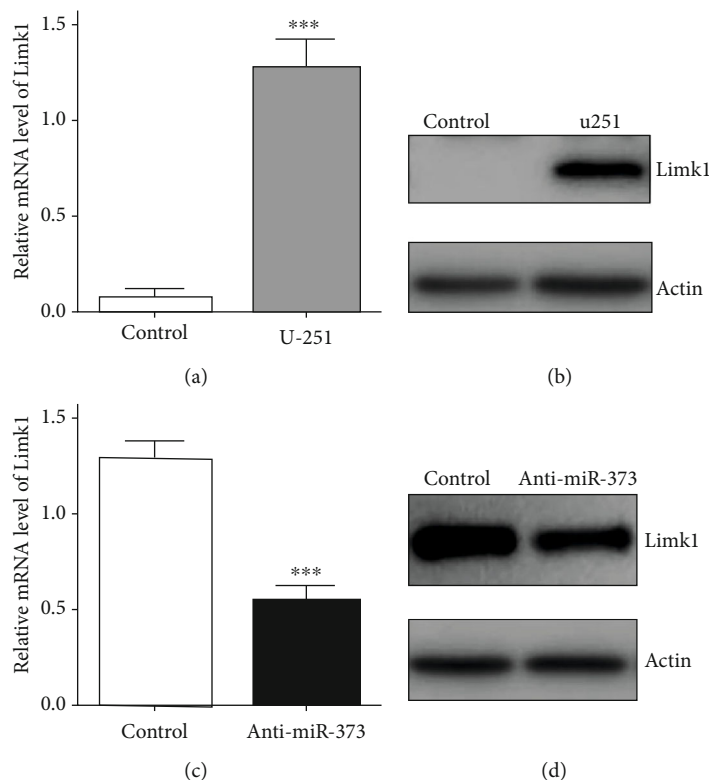


FIGURE 6: Effects of anti-miR-373 on Limk1 expression. (a) High Limk1 mRNA level was observed by the real-time quantitative PCR in U-251 cells, and (b) western blot results also proved that high Limk1 expression was obtained in U-251 cells; (c) Limk1 mRNA level was reduced by the real-time quantitative PCR in U-251 cells after anti-miR-373 transfection, and (d) lower Limk1 expression was obtained after anti-miR-373 transfection in U-251 cells (bars indicate the standard deviation of the mean; each experiment was performed in triplicate; *** $p < 0.001$).

therapeutic efficiency [43, 44]. Thus, novel methods through exploring the therapeutic target to enhance therapeutic efficacy by reducing above resistance have obtained great concerns recently.

More and more studies have provided the evidence that miRNAs were related to the cell proliferation, differentiation, and apoptosis, even in development of tumors [12, 13]. Abnormal levels of miRNAs were demonstrated in the process of carcinogenesis or progression, such as lung cancer [45] and GBM [15, 16]. It has been studied that some genes such as miR-373 [22] or miR-21 [21] play an important role in above resistance effects of cancer therapy. But there were few studies on whether inhibition on miR-373 may induce above antiresistance effects in GBM treatment and which downstream effector was involved in its process, which need to be confirmed by further experimental data or evidence. Thus, the purpose of the current experiments was to test this hypothesis and to find the possible relationships between miR-373 and its downstream effector.

Our current study provided the following novelties: (1) the higher level of miR-373 was observed in U-251 cells; (2) inhibition on miR-373 could reduce the U-251 cell proliferation; (3) inhibition on miR-373 could sensitize U-251 cells to chemo- or radiotherapy; (4) the cell cycle of U-251 cells could be modulated by miR-373 knockdown; (5) inhibition on miR-373 could induce the U-251

cell apoptosis; and (6) above effects of miR-373 could be reversed by Limk1 overexpression. Thus, these experimental data confirmed the fact that miR-373 could be a new therapeutic target to enhance the efficiency of chemo- or radiotherapy for clinical GBM patients.

For cell proliferation, as a typical biological indicator [46], PCNA expression was also tested to investigate the effects of anti-miR-373 and even to observe whether combined treatment with chemo- or radiotherapy may have the additional effects. The results confirmed the above hypothesis and showed that inhibition on miR-373 may enhance the restricted effects of chemo- or radiotherapy on cell proliferation by reducing the PCNA expression.

In addition, it has been reported that Limk1 was involved in the cancer development including tumor invasion or cell apoptosis [47]. And Limk1 knockdown induced the antitumor effects for lung cancer, breast cancer, or even GBM [28–30]. As an oncogene, it was also evidenced that Limk1 was related to the resistance of chemotherapy [48, 49]. Thus, studies on the up- or downstream effector of Limk1 may provide the details of the underlying mechanism on the pathological development of GBM and even the potent novel therapeutic target for the antitumor therapy clinically.

For the apoptosis of cancer cells, the Bax/Bcl-2 ratio could provide the development on apoptosis and reflect the changes under different modulators [50]. This Bax/Bcl-2 ratio and the percentage of apoptotic cells suggested the fact

that anti-miR-373 reduced the Limk1 expression, which may induce or enhance the apoptosis of U-251 cells.

Our results confirmed that inhibition on miR-373 may change the biological behavior of U-251 cells including cell proliferation, cell cycle, and even cell apoptosis. And these effects were related to its downstream effector Limk1, which could reverse above anti-miR-373 effects. Thus, reducing the miR-373 level may enhance the antiresistance effects on chemo- or radiotherapy in GBM treatment through negative regulation on Limk1. Based on above experimental evidence, miR-373 could be regarded as the predictive or prognostic biomarker for GBM patients. These two biological molecules may help us find the new strategy in the clinical setting by combining chemo- or radiotherapy to reduce the toxicity to normal tissues such as side effects and enhance the therapeutic efficiency.

Data Availability

The data used to support the findings of this study are included within the article.

Conflicts of Interest

All authors declare that they have no competing interests.

Authors' Contributions

Tao Peng and Tiejun Wang contributed equally to this work.

Acknowledgments

This work was supported by the Natural Science Foundation of Jilin Province (No. 20080445_2).

References

- [1] H. G. Wirsching, E. Galanis, and M. Weller, "Glioblastoma," *Handbook of Clinical Neurology*, vol. 134, pp. 381–397, 2016.
- [2] L. T. Shieh, H. R. Guo, C. H. Ho, L. C. Lin, C. H. Chang, and S. Y. Ho, "Survival of glioblastoma treated with a moderately escalated radiation dose—results of a retrospective analysis," *PLoS One*, vol. 15, no. 5, article e0233188, 2020.
- [3] A. L. Cohen and H. Colman, "Glioma biology and molecular markers," *Cancer Treatment and Research*, vol. 163, pp. 15–30, 2015.
- [4] C. Brito, A. Azevedo, S. Esteves et al., "Clinical insights gained by refining the 2016 WHO classification of diffuse gliomas with: EGFR amplification, TERT mutations, PTEN deletion and MGMT methylation," *BMC Cancer*, vol. 19, no. 1, p. 968, 2019.
- [5] J. H. Azambuja, R. S. Schuh, L. R. Michels et al., "CD73 as a target to improve temozolomide chemotherapy effect in glioblastoma preclinical model," *Cancer Chemotherapy and Pharmacology*, vol. 85, no. 6, pp. 1177–1182, 2020.
- [6] U. Herrlinger, T. Tzaridis, F. Mack et al., "Lomustine-temozolomide combination therapy versus standard temozolomide therapy in patients with newly diagnosed glioblastoma with methylated MGMT promoter (CeTeG/NOA-09): a randomised, open-label, phase 3 trial," *Lancet*, vol. 393, no. 10172, pp. 678–688, 2019.
- [7] Y. Rajesh, A. Biswas, U. Kumar et al., "Lumefantrine, an anti-malarial drug, reverses radiation and temozolomide resistance in glioblastoma," *Proceedings of the National Academy of Sciences of the United States of America*, vol. 117, no. 22, pp. 12324–12331, 2020.
- [8] G. W. Kim, D. H. Lee, S.-K. Yeon et al., "Temozolomide-resistant glioblastoma depends on HDAC6 activity through regulation of DNA mismatch repair," *Anticancer Research*, vol. 39, no. 12, pp. 6731–6741, 2019.
- [9] A. Moreau, O. Febvey, T. Moggetti, D. Frappaz, and D. Kryza, "Contribution of different positron emission tomography tracers in glioma management: focus on glioblastoma," *Frontiers in Oncology*, vol. 9, p. 1134, 2019.
- [10] R. Kalkan and E. İ. Atli, "The impacts of miRNAs in glioblastoma progression," *Critical Reviews in Eukaryotic Gene Expression*, vol. 26, no. 2, pp. 137–142, 2016.
- [11] R. Rupaimoole and F. J. Slack, "MicroRNA therapeutics: towards a new era for the management of cancer and other diseases," *Nature Reviews Drug Discovery*, vol. 16, no. 3, pp. 203–222, 2017.
- [12] L. Tutar, E. Tutar, A. Özgür, and Y. Tutar, "Therapeutic targeting of microRNAs in cancer: future perspectives," *Drug Development Research*, vol. 76, no. 7, pp. 382–388, 2015.
- [13] S. P. Nana-Sinkam and C. M. Croce, "Clinical applications for microRNAs in cancer," *Clinical Pharmacology and Therapeutics*, vol. 93, no. 1, pp. 98–104, 2012.
- [14] M. Alharbi, S. Sharma, D. Guanzon et al., "miRNA signature in small extracellular vesicles and their association with platinum resistance and cancer recurrence in ovarian cancer," *Nanomedicine*, vol. 28, p. 102207, 2020.
- [15] M. Swellam, L. Ezz el Arab, A. S. al-Posttany, and S. B. Said, "Clinical impact of circulating oncogenic miRNA-221 and miRNA-222 in glioblastoma multiform," *Journal of Neuro-Oncology*, vol. 144, no. 3, pp. 545–551, 2019.
- [16] Y. S. Liu, H. Y. Lin, S. W. Lai et al., "miR-181b modulates EGFR-dependent VCAM-1 expression and monocyte adhesion in glioblastoma," *Oncogene*, vol. 36, no. 35, pp. 5006–5022, 2017.
- [17] D. Schaeue and W. H. McBride, "Opportunities and challenges of radiotherapy for treating cancer," *Nature Reviews Clinical Oncology*, vol. 12, no. 9, pp. 527–540, 2015.
- [18] F. Wirsdörfer, S. de Leve, and V. Jendrossek, "Combining radiotherapy and immunotherapy in lung cancer: can we expect limitations due to altered normal tissue toxicity?," *International Journal of Molecular Sciences*, vol. 20, no. 1, p. 24, 2019.
- [19] B. Malla, D. M. Aebbersold, and A. Dal Pra, "Protocol for serum exosomal miRNAs analysis in prostate cancer patients treated with radiotherapy," *Journal of Translational Medicine*, vol. 16, no. 1, p. 223, 2018.
- [20] Y. Lu, X. Zhao, Q. Liu et al., "lncRNA MIR100HG-derived miR-100 and miR-125b mediate cetuximab resistance via Wnt/ β -catenin signaling," *Nature Medicine*, vol. 23, no. 11, pp. 1331–1341, 2017.
- [21] S. R. Pfeffer, C. H. Yang, and L. M. Pfeffer, "The role of miR-21 in cancer," *Drug Development Research*, vol. 76, no. 6, pp. 270–277, 2015.
- [22] M. Yeon, J. Byun, H. Kim et al., "CAGE binds to Beclin1, regulates autophagic flux and CAGE-derived peptide confers sensitivity to anti-cancer drugs in non-small cell lung cancer cells," *Frontiers in Oncology*, vol. 8, 2018.

- [23] W. Hu, Q. Liu, J. Pan, and Z. Sui, "miR-373-3p enhances the chemosensitivity of gemcitabine through cell cycle pathway by targeting CCND2 in pancreatic carcinoma cells," *Biomedicine & Pharmacotherapy*, vol. 105, pp. 887–898, 2018.
- [24] Q. Huang, K. Gumireddy, M. Schrier et al., "The microRNAs miR-373 and miR-520c promote tumour invasion and metastasis," *Nature Cell Biology*, vol. 10, no. 2, pp. 202–210, 2008.
- [25] M. E. Crosby, C. M. Devlin, P. M. Glazer, G. A. Calin, and M. Ivan, "Emerging roles of microRNAs in the molecular responses to hypoxia," *Current Pharmaceutical Design*, vol. 15, no. 33, pp. 3861–3866, 2009.
- [26] P. M. Voorhoeve, C. le Sage, M. Schrier et al., "A genetic screen implicates miRNA-372 and miRNA-373 as oncogenes in testicular germ cell tumors," *Cell*, vol. 124, no. 6, pp. 1169–1181, 2006.
- [27] E. Martín-Villar, B. Borda-d'Agua, P. Carrasco-Ramirez et al., "Podoplanin mediates ECM degradation by squamous carcinoma cells through control of invadopodia stability," *Oncogene*, vol. 34, no. 34, pp. 4531–4544, 2015.
- [28] B. C. Q. Nguyen, K. Yoshimura, S. Kumazawa, S. Tawata, and H. Maruta, "Frondoside A from sea cucumber and nymphaeols from Okinawa propolis: natural anti-cancer agents that selectively inhibit PAK1 *in vitro*," *Drug Discoveries & Therapeutics*, vol. 11, no. 2, pp. 110–114, 2017.
- [29] P. Shahi, C. Y. Wang, J. Chou et al., "GATA3 targets semaphorin 3B in mammary epithelial cells to suppress breast cancer progression and metastasis," *Oncogene*, vol. 36, no. 40, pp. 5567–5575, 2017.
- [30] J. Chen, B. Ananthanarayanan, K. S. Springer et al., "Suppression of LIM kinase 1 and LIM kinase 2 limits glioblastoma invasion," *Cancer Research*, vol. 80, no. 1, pp. 69–78, 2020.
- [31] J. B. Park, S. Agnihotri, B. Golbourn et al., "Transcriptional profiling of GBM invasion genes identifies effective inhibitors of the LIM kinase-Cofilin pathway," *Oncotarget*, vol. 5, no. 19, pp. 9382–9395, 2014.
- [32] M. Crompton, T. Purnell, H. E. Tyrer et al., "A mutation in Nischarin causes otitis media via LIMK1 and NF- κ B pathways," *PLOS Genetics*, vol. 13, no. 8, article e1006969, 2017.
- [33] E. Lagoutte, C. Villeneuve, L. Lafanechère et al., "LIMK regulates tumor-cell invasion and matrix degradation through tyrosine phosphorylation of MT1-MMP," *Scientific Reports*, vol. 6, no. 1, article 24925, 2016.
- [34] S. Koo, G. Martin, and L. G. Toussaint, "MicroRNA-145 promotes the phenotype of human glioblastoma cells selected for invasion," *Anticancer Research*, vol. 35, no. 6, pp. 3209–3215, 2015.
- [35] J. Gasparello, M. Lomazzi, C. Papi et al., "Efficient delivery of microRNA and antimicroRNA molecules using an argininoclix[4]arene macrocycle," *Molecular Therapy - Nucleic Acids*, vol. 18, pp. 748–763, 2019.
- [36] X. Meng, V. Müller, K. Milde-Langosch, F. Trillsch, K. Pantel, and H. Schwarzenbach, "Circulating cell-free miR-373, miR-200a, miR-200b and miR-200c in patients with epithelial ovarian cancer," *Advances in Experimental Medicine and Biology*, vol. 924, pp. 3–8, 2016.
- [37] O. Kargiotis, C. Chetty, C. S. Gondi et al., "Adenovirus-mediated transfer of siRNA against MMP-2 mRNA results in impaired invasion and tumor-induced angiogenesis, induces apoptosis *in vitro* and inhibits tumor growth *in vivo* in glioblastoma," *Oncogene*, vol. 27, no. 35, pp. 4830–4840, 2008.
- [38] M. Juríková, L. Danihel, Š. Polák, and I. Varga, "Ki67, PCNA, and MCM proteins: markers of proliferation in the diagnosis of breast cancer," *Acta Histochemica*, vol. 118, no. 5, pp. 544–552, 2016.
- [39] X. Xu, Z. Wang, N. Liu et al., "Association between SOX9 and CA9 in glioma, and its effects on chemosensitivity to TMZ," *International Journal of Oncology*, vol. 53, no. 1, pp. 189–202, 2018.
- [40] P. R. Gielen, Q. Aftab, N. Ma et al., "Connexin43 confers temozolomide resistance in human glioma cells by modulating the mitochondrial apoptosis pathway," *Neuropharmacology*, vol. 75, pp. 539–548, 2013.
- [41] N. Struve, Z. A. Binder, L. F. Stead et al., "EGFRvIII upregulates DNA mismatch repair resulting in increased temozolomide sensitivity of MGMT promoter methylated glioblastoma," *Oncogene*, vol. 39, no. 15, pp. 3041–3055, 2020.
- [42] A. Chandra, A. Jahangiri, W. Chen et al., "Clonal ZEB1-driven mesenchymal transition promotes targetable oncologic anti-angiogenic therapy resistance," *Cancer Research*, vol. 80, no. 7, pp. 1498–1511, 2020.
- [43] D. J. Voce, G. M. Bernal, L. Wu et al., "Temozolomide treatment induces lncRNA MALAT1 in an NF- κ B and p53 codependent manner in glioblastoma," *Cancer Research*, vol. 79, no. 10, pp. 2536–2548, 2019.
- [44] A. Karachi, F. Dastmalchi, D. A. Mitchell, and M. Rahman, "Temozolomide for immunomodulation in the treatment of glioblastoma," *Neuro-Oncology*, vol. 20, no. 12, pp. 1566–1572, 2018.
- [45] Z. S. Hashemi, S. Khalili, M. Forouzandeh Moghadam, and E. Sadroddiny, "Lung cancer and miRNAs: a possible remedy for anti-metastatic, therapeutic and diagnostic applications," *Expert Review of Respiratory Medicine*, vol. 11, no. 2, pp. 147–157, 2016.
- [46] I. Stoimenov and T. Helleday, "PCNA on the crossroad of cancer," *Biochemical Society Transactions*, vol. 37, no. 3, pp. 605–613, 2009.
- [47] K. Mardilovich, M. Gabrielsen, L. McGarry et al., "Elevated LIM kinase 1 in nonmetastatic prostate cancer reflects its role in facilitating androgen receptor nuclear translocation," *Molecular Cancer Therapeutics*, vol. 14, no. 1, pp. 246–258, 2015.
- [48] S. T. Po'uha, M. S. Y. Shum, A. Goebel, O. Bernard, and M. Kavallaris, "LIM-kinase 2, a regulator of actin dynamics, is involved in mitotic spindle integrity and sensitivity to microtubule-destabilizing drugs," *Oncogene*, vol. 29, no. 4, pp. 597–607, 2010.
- [49] Q. Yu, C. Gratzke, Y. Wang et al., "Inhibition of human prostate smooth muscle contraction by the LIM kinase inhibitors, SR7826 and LIMKi3," *British Journal of Pharmacology*, vol. 175, no. 11, pp. 2077–2096, 2018.
- [50] F. Edlich, "BCL-2 proteins and apoptosis: recent insights and unknowns," *Biochemical and Biophysical Research Communications*, vol. 500, no. 1, pp. 26–34, 2018.

Research Article

Profiling the Resident and Infiltrating Monocyte/Macrophages during Rejection following Kidney Transplantation

Jie Wang,¹ Peiling Luo,² Jingjie Zhao,³ Junhua Tan,¹ Feifan Huang,¹ Ruiying Ma,¹ Peng Huang,¹ Meiyang Huang,¹ Yuming Huang,¹ Qiuju Wei,^{4,5} Liuzhi Wei,^{4,5} Zechen Wang,⁴ and Lingzhang Meng^{ID}⁴

¹Kidney Disease of Internal, Affiliated Hospital of Youjiang Medical University for Nationalities, Baise City, Guangxi Province, China

²Graduate School of Youjiang Medical University for Nationalities, Baise City, Guangxi Province, China

³Life Science and Clinical Research Center, Affiliated Hospital of Youjiang Medical University for Nationalities, Baise City, Guangxi Province, China

⁴Center for Systemic Inflammation Research (CSIR), School of Preclinical Medicine, Youjiang Medical University for Nationalities, Baise City, Guangxi Province, China

⁵College of Pharmacy, Youjiang Medical University for Nationalities, Baise City, Guangxi Province, China

Correspondence should be addressed to Lingzhang Meng; lingzhang.meng@ymcn.edu.cn

Jie Wang, Peiling Luo, and Jingjie Zhao contributed equally to this work.

Received 25 June 2020; Revised 10 August 2020; Accepted 24 August 2020; Published 21 September 2020

Academic Editor: Jian Song

Copyright © 2020 Jie Wang et al. This is an open access article distributed under the Creative Commons Attribution License, which permits unrestricted use, distribution, and reproduction in any medium, provided the original work is properly cited.

Immune tolerance research is essential for kidney transplantation. Other than antibody and T cell-mediated immune rejection, macrophage-mediated innate immunity plays an important role in the onset phase of transplantation rejection. However, due to the complexity of the kidney environment as well as its diversity and low abundance, studies pertaining to monocyte/macrophages in kidney transplantation require further elucidation. In this study, kidney samples taken from healthy human adults and biopsy specimens from patients undergoing rejection following kidney transplantation were analysed and studied. By conducting a single-cell RNA analysis, the type and status of monocyte/macrophages in kidney transplantation were described, in which monocyte/macrophages were observed to form two different subpopulations: resident and infiltrating monocyte/macrophages. Furthermore, previously defined genes were mapped to all monocyte/macrophage types in the kidney and enriched the differential genes of the two main subpopulations using gene expression databases. Considering that various cases of rejection may be of the monocyte/macrophage type, the present data may serve as a reference for studies regarding immune tolerance following kidney transplantation.

1. Introduction

A kidney transplant's success largely depends on the degree of immune rejection [1]. Adaptive immunity in kidney transplantation is mainly comprised of T cells and B cells, which, respectively, cause T cell-mediated rejection (TCMR) and antibody-mediated rejection following kidney transplantation (antibody-mediated rejection, ABMR) [2]. Innate immunity,

however, primarily involves monocyte/macrophages, which also play an important role in initiating adaptive immunity, and is a prerequisite stage of rejection after kidney transplantation [3].

Myeloid progenitor cells in the bone marrow differentiate into monocytes; then, in the environments of inflammatory reactions and trauma, monocytes migrate and infiltrate the interstitial tissue in order to differentiate into macrophages.

However, macrophages can reside in the tissue and renew on their own, crucial for the homeostasis of tissue immunity. These resident macrophages, however, may also be replenished from the circulation in certain conditions [4]. Therefore, macrophage heterogeneity should always be considered in tissue inflammation. In the kidney, earlier studies have shown that the amount of monocyte/macrophage infiltration is closely related to kidney injury, though recent studies have demonstrated that, during the development of acute and chronic kidney disease, mononuclear/macrophage cells have both pathogenic and protective effects according to the type and state of activation. Classically activated macrophages mainly play proinflammatory and profibrotic roles, while alternatively activated macrophages are mainly anti-inflammatory and promote the repair and reconstruction of damaged tissue [5]. In fact, a certain number of resident macrophages exist in normal kidney tissue, which are less understood due to the small number of cells and lack of appropriate means or markers from which to study. The recent development of single-cell sequencing created a breakthrough in studying low abundance cells [6, 7]. Scientists have mapped kidney immune cells throughout the developmental period, from early life to adulthood, and have tried to understand how the kidney's immune system develops and matures [8]. Accordingly, they found that the earliest cells in the developing kidney were monocyte/macrophages, which engulf harmful pathogens and remain in the postnatal stage. However, the roles and characteristics of resident macrophages in the adult kidney, as well as their role during kidney transplantation, require further study.

In this study, the single-cell sequencing data of the kidney was analysed, and the transcriptome of renal resident macrophages was profiled in both healthy and transplant rejection tissue. Here, a certain number of resident monocyte/macrophages were found in normal kidney tissue, which was dramatically reduced in the kidney transplant tissue of immune rejection and replaced by infiltrating monocyte/macrophages. Correlatively, a large number of plasma cells were found in the kidney transplant rejection tissue, where nonactivated B cells disappeared. By analysing the expression profile, infiltrating monocyte/macrophages were observed to be similar to mature M1 macrophages in the common inflammatory response, whereas resident macrophages presented a series of specialized molecules. These molecules were found to be downregulated or were lost monocyte/macrophages from the transplanted rejected kidney. Research on such resident macrophage molecules may provide therapeutic insight into maintaining immune homeostasis, thus assisting in the management of renal transplantation.

2. Methods

2.1. Single-Cell mRNA Sequencing Analysis. Raw data of healthy kidney and biopsy samples of transplantation rejects were obtained from the Gene Expression Omnibus (GEO) GSE131685 and GSE109564, respectively [9, 10]. R package Seurat [11, 12] was used for data analyses, and count matrices were normalized using the SCTransform pipeline (https://satijalab.org/seurat/v3.1/sctransform_vignette.html). Samples

from both healthy and rejection tissue were integrated using reciprocal PCA (<https://satijalab.org/seurat/v3.1/integration.html>). The integrated dataset was further subjected to PCA, and the initial 15 principal components (which described almost an entire variance in the data, as indicated by elbow plot) were considered for cluster analyses. Unified manifold approximation and projection (UMAP) was used to show clustering with a resolution of 0.25, and violin plots were used to project the expression patterns of individual genes in the cluster.

2.2. Functional Enrichment Analysis. Marker genes in different clusters were then annotated for the signaling pathway using the Kyoto Encyclopedia of Genes and Genomes (KEGG) and were classified for biological processes via Gene Ontology (GO) analysis. A P value < 0.05 was considered to be statistically significant. A comparison of DEGs was performed by adopting the EnhancedVolcano method, which was illustrated using a volcano graph. DEGs were then compared using a predefined set of genes via Gene Set Enrichment Analysis (GSEA). Molecular Signatures Database (MSigDB) was used as the reference of the DEGs. Furthermore, the R package-ClusterProfiler was used to compare biological processes among the clusters [13]. The top 10 enriched signaling pathways were displayed using dot plots.

3. Results

The data for healthy kidney tissue were acquired from cells isolated in three patients that underwent radical nephrectomy, while the transplant rejection data were taken from one patient with three biopsy samples. Initially, the healthy and rejection data were integrated and corrected in order to eliminate the batch effect. At a resolution of 0.25, 12 cell clusters were generated, in which two leukocyte clusters were verified with PTPRC (CD45 gene) (Figure 1(a)). Subclustering of the leukocytes gave rise to five clusters (Figure 1(b)). Using the known gene markers, the clusters were annotated with (0) T cells (1) ,NKT cells (2, 3) ,monocyte/macrophages, and (4) B cells (Figures 1(c)–1(e)). The healthy data were first assessed (Figures 1(c)–1(e)), and despite the expression of the Igalpha/beta chain (CD79a, b), the B cell population was mainly comprised of IgM (IGHM) but not IgG1 (IGHG1), indicating the lack of plasma cells in healthy tissue (Figures 1(c) and 1(d)). CD3+ conventional T cells and NKT cells may be distinguished by their surface markers and secreted molecules (Figures 1(c) and 1(e)). In monocyte/macrophage populations, cells lack prototypical macrophage gene markers like ADGRE1 (F4/80 gene). Nevertheless, the cells can be sorted into two clusters with CD14 and MS4A7, both myeloid markers (Figure 1(e)), indicating that heterogeneity of kidney monocyte/macrophages already exists in the steady state.

When comparing the healthy and rejection data, the B cell population was removed so as to obtain a better resolution for the remaining cells. At 0.5 resolution, eight clusters were separated from the rest of the cells (Figure 2(a)). Using known gene markers, the clusters were annotated with (0) NKT cells (3) ,T cells, and five different myeloid cells (Figure 2(b)). Compared to the healthy data, the rejection

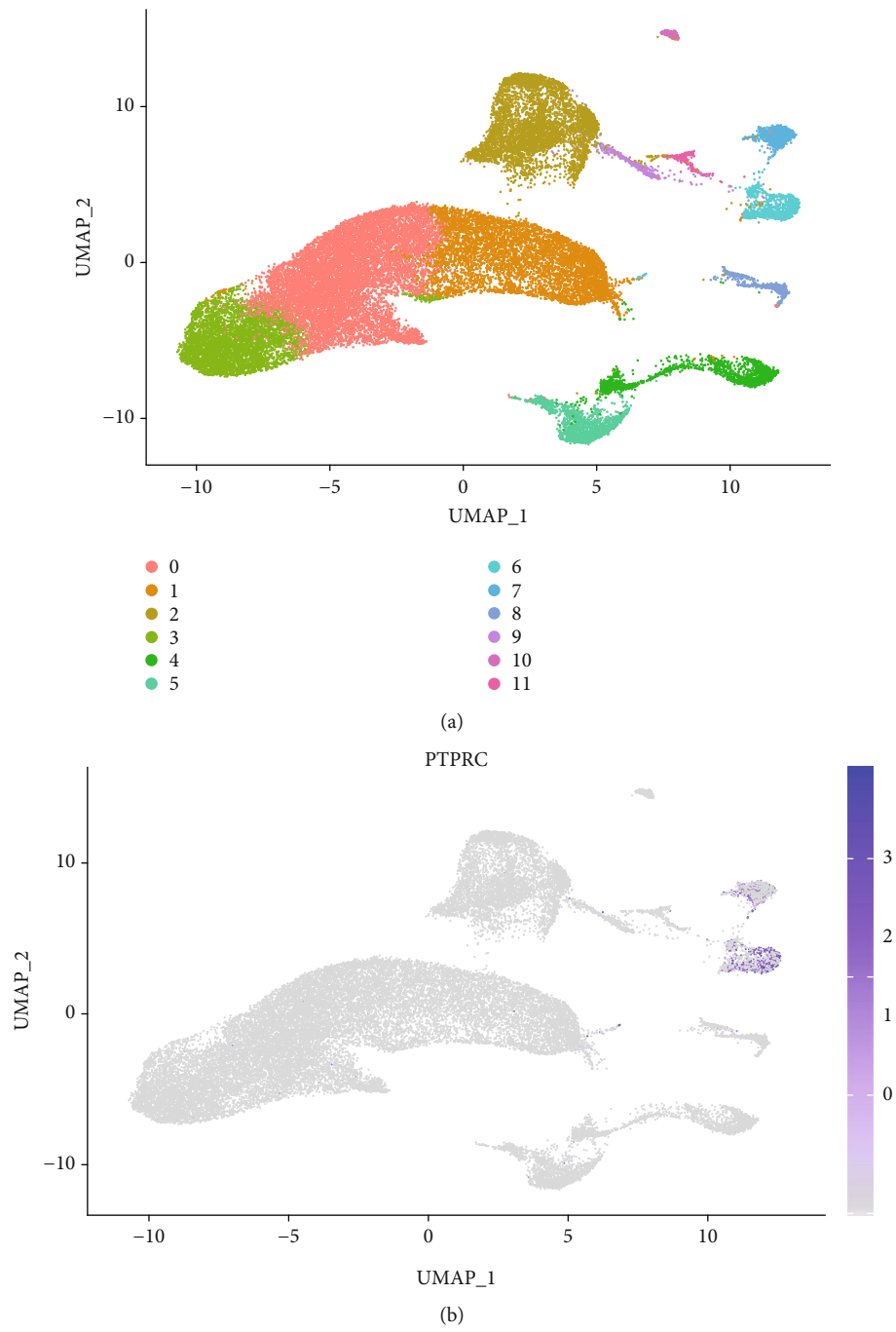


FIGURE 1: Continued.

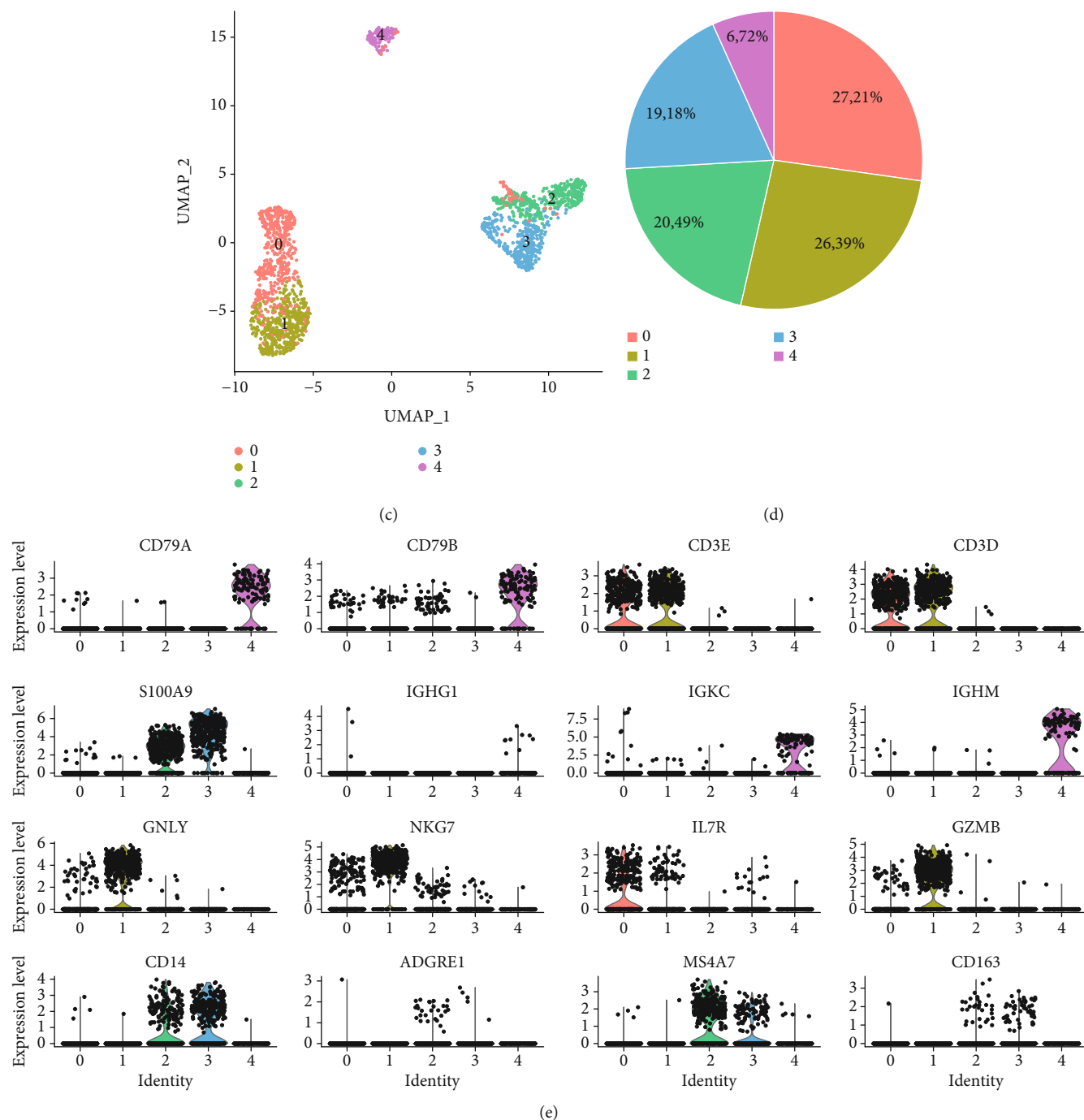


FIGURE 1: scRNA analysis of leukocytes in the kidney. (a) UMAP plot explored 12 clusters in the kidney tissue at a resolution of 0.25. (b) Gene expression of PTPRC indicated CD45+ leukocytes. (c) CD45+ leukocytes were subclustered into five clusters. (d) Pie plot shows the frequency of each cell type. (e) The subclusters were annotated with known markers for T cells (CD3), monocyte/macrophages (CD14 and MS4A7), and B cells (CD79A/B). Violin plots showed the projection of indicated genes. IGG1 refers to memory B cells or plasma cells. (e) NKT cells were shown with marker genes such as GNLY, NKG7, and GZMB. The IL7R gene refers to conventional T cells.

group demonstrated an evident rise in cluster 1 with a reduction in cluster 6 among all three samples (Figure 2(c)). In order to acquire an overview of clusters 1 and 6, their marker genes were classified via KEGG signaling pathway analysis, where cluster 1 was indeed found to be involved in allograft rejection as well as autoimmune diseases such as lupus and diabetes (Figure 2(c)). In addition, the gene in cluster 1 was

found to be relevant to IgA production and antigen presentation, indicating a close relationship to both ABMR and TCMR. However, cluster 6 genes were detected in the phagocytosis pathway (Figure 2(c)).

Furthermore, clusters 1 and 6 were compared according to the fold change and *P* value, where cluster 1 was found to possess the gene responsible for antigen presentation and

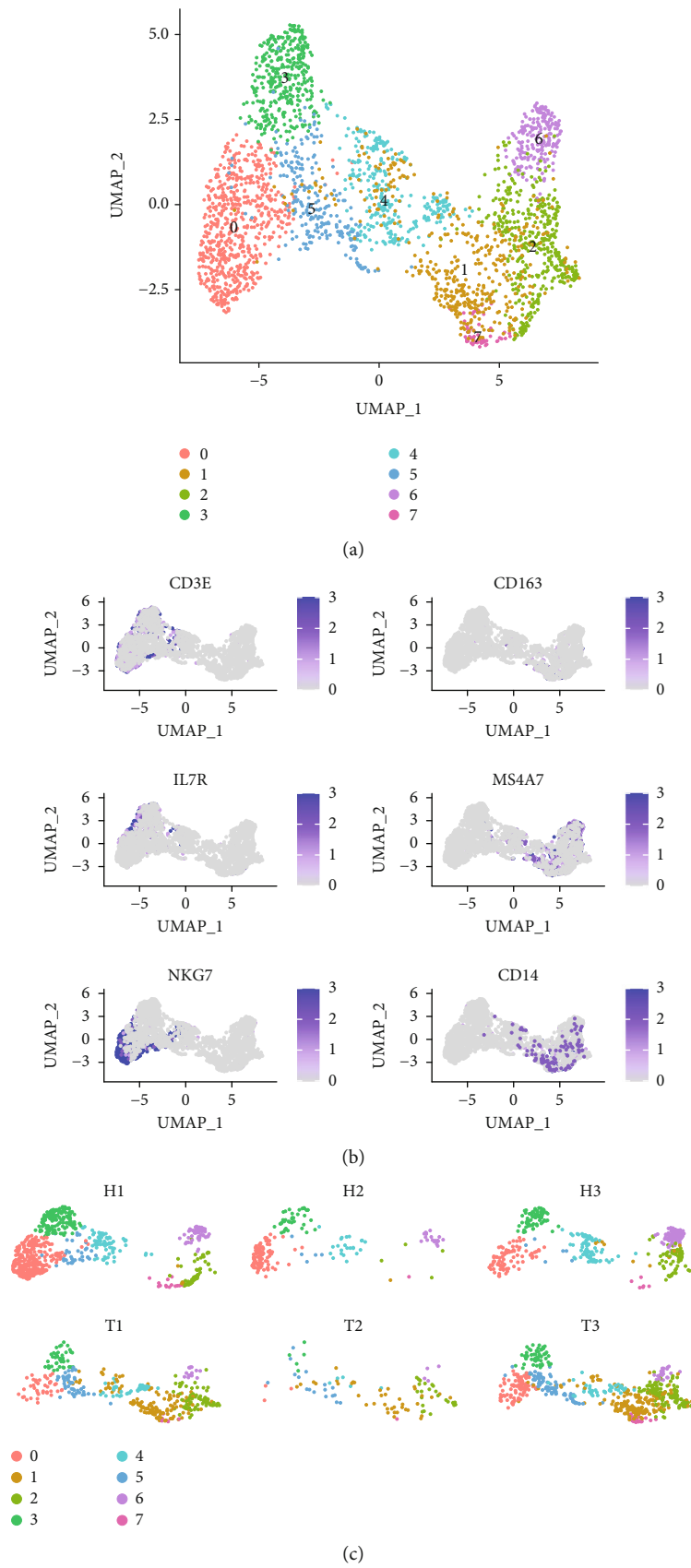
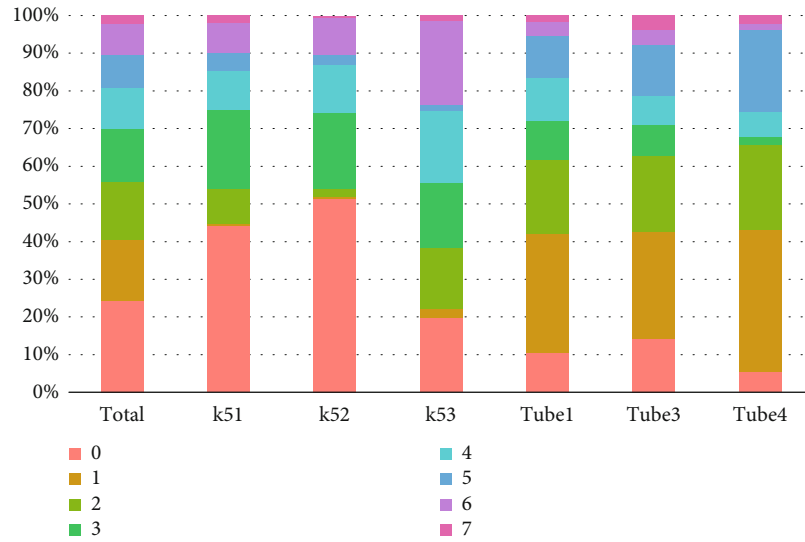
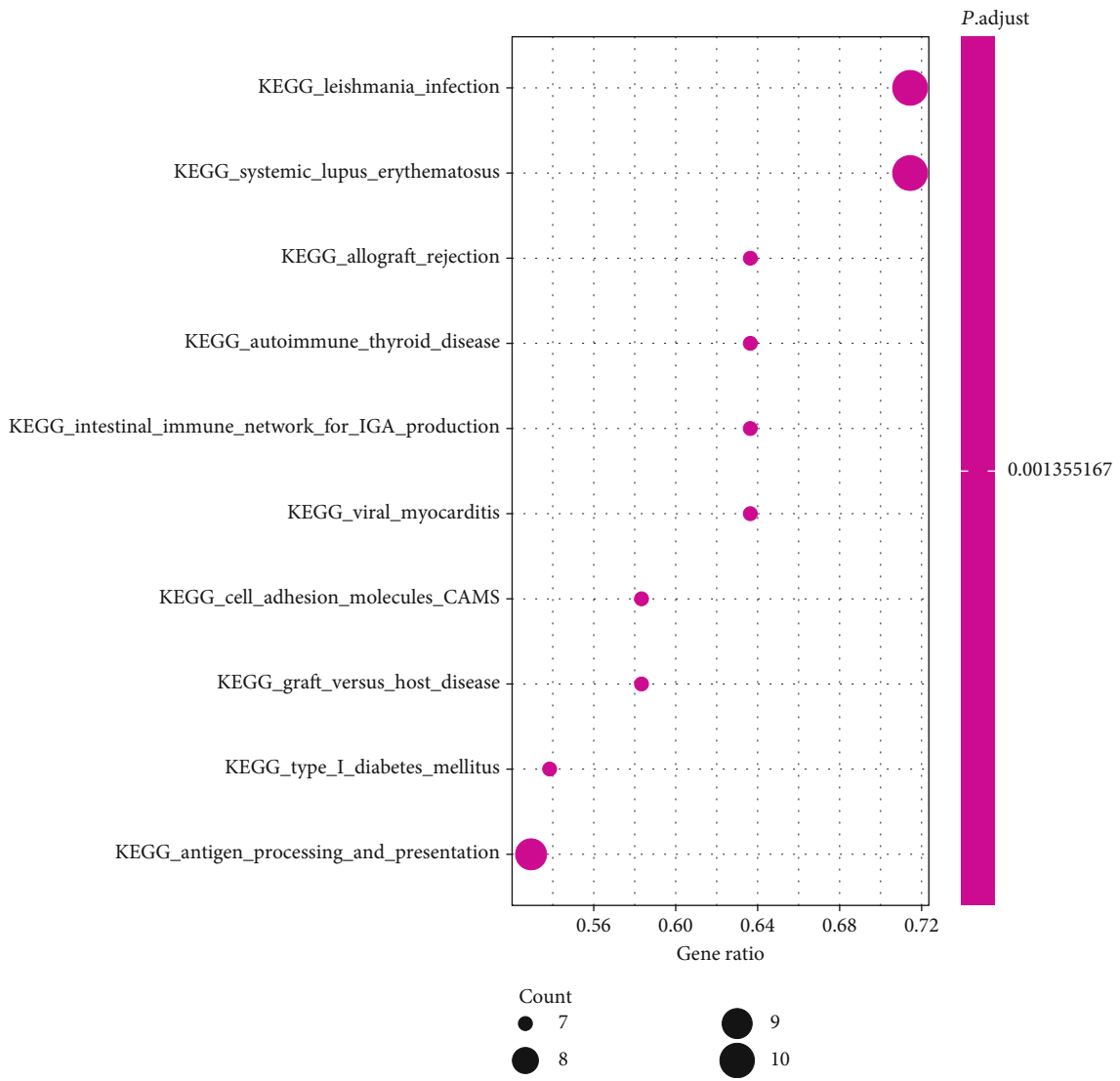


FIGURE 2: Continued.



(d)



(e)

FIGURE 2: Continued.

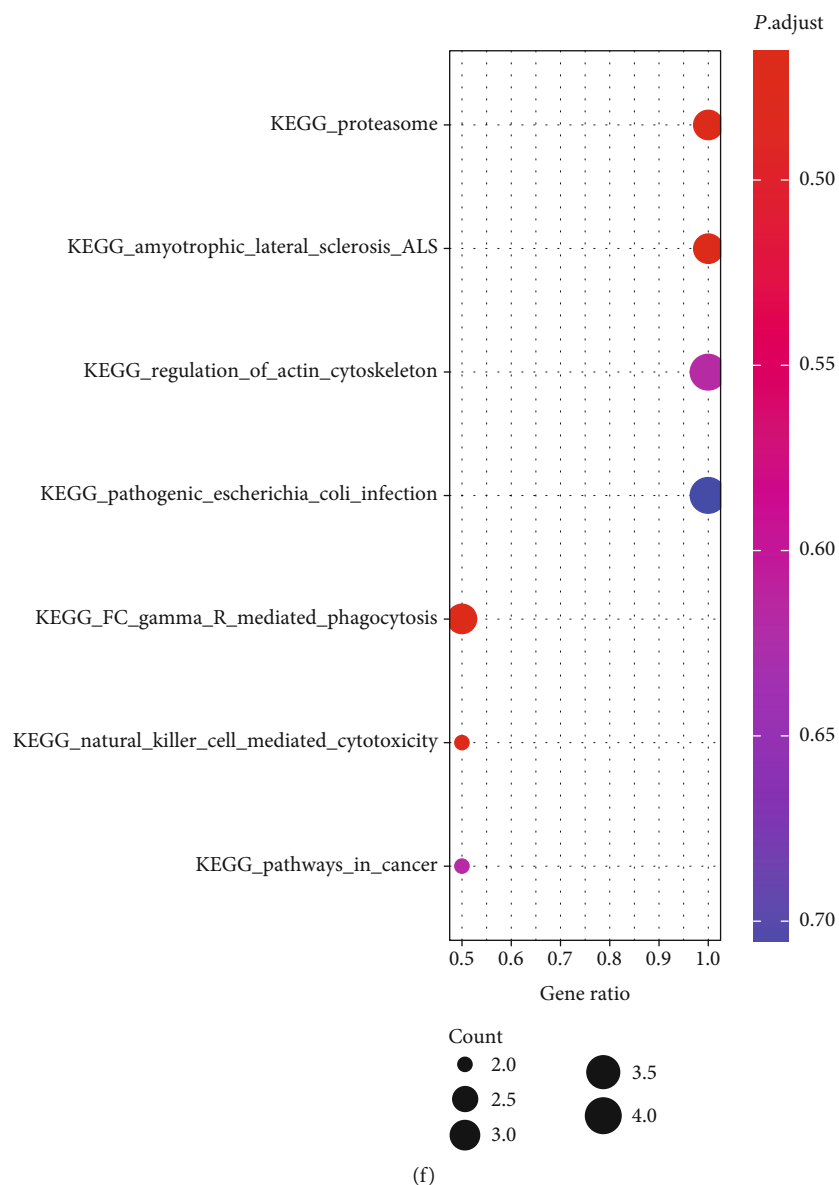


FIGURE 2: Characterizing the resident and the infiltrating monocyte/macrophage. (a) UMAP plot explored 8 clusters after the removal of B cells. (b) Clusters were annotated with known markers for T cells (3), NKT cells (0), and monocyte/macrophage cells (1, 4, and 6). (c) The cell clusters from the healthy and rejected kidney tissues were compared for individual samples. (d) Bar plot shows the frequency of each cluster of the healthy and rejection samples. The marker genes of clusters 1 (e) and 6 (f) were classified for their involvement of KEGG signaling pathways in clusters 1 and 6.

cell activation, as shown in the volcano plot (Figure 3(a)). Moreover, cluster 1 was observed to express most of the markers of the M1 macrophage, whereas cluster 6 expressed the marker of M2 or resident macrophages (Figure 3(b)). To depict the interaction of these genes, a GO enrichment analysis was carried out to illustrate the network of differentially expressed genes. Accordingly, most genes were found to be connected to the immune response; almost all cluster 1 DEGs were involved in the innate immune response (Figure 3(c)). In order to determine which signal is upregulated or downregulated in the DEGs of clusters 1 and 6, a Gene Set Enrichment Analysis (GSEA) was performed, in which the DEGs were compared to the Molecular Signatures Database (MSigDB). The GSEA again oriented the genes to the pathways similar

to the KEGG analysis. More importantly, the GSEA confirmed that the genes in cluster 1, not cluster 6, promoted autoimmune disease and allograft rejection (Figure 3(d)).

Additionally, healthy and rejection samples were compared. As cluster 1 was not detectable in the healthy group, this study focused on the comparison of cluster 6 between the rejection and healthy samples. Here, cluster 6 of the rejection samples was found to upregulate proinflammatory cytokine genes like IL1B while downregulating the expression of CD68, which has been considered a feature of kidney resident macrophages (Figure 4(a)) [14]. To depict the interaction of these genes, a GO enrichment analysis was performed to show the network of differentially expressed genes. The DEGs were mainly found to be involved in leukocyte transendothelial migration and

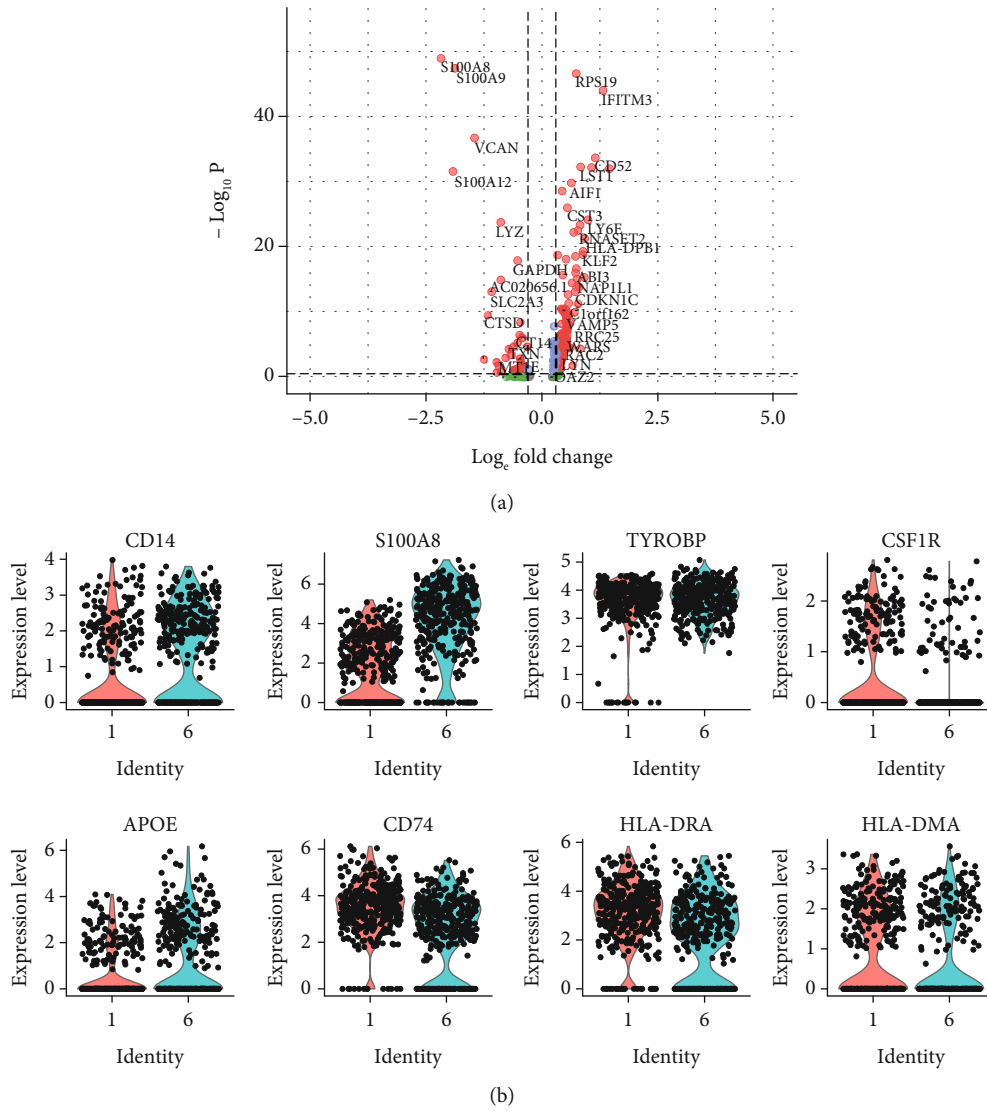
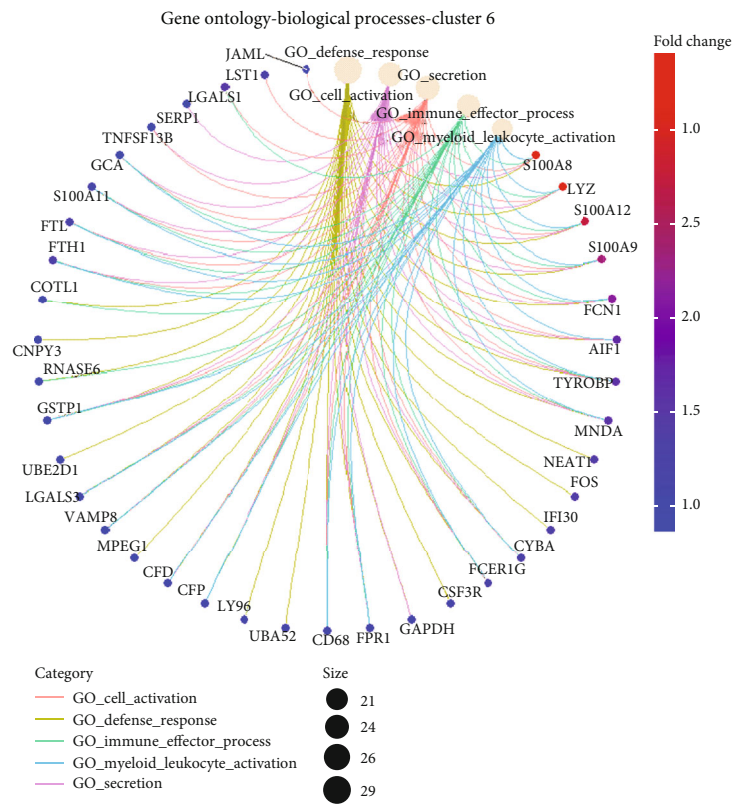
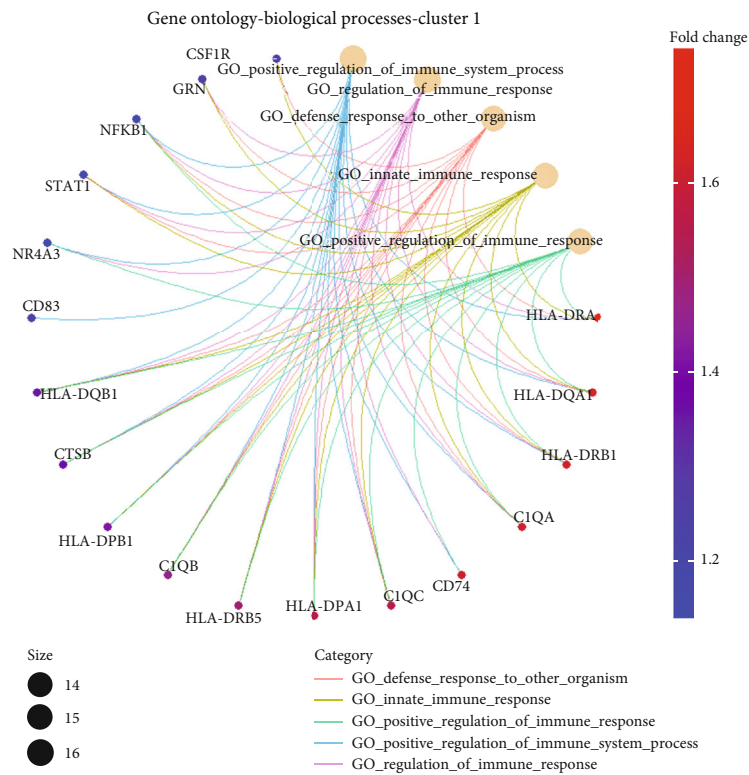
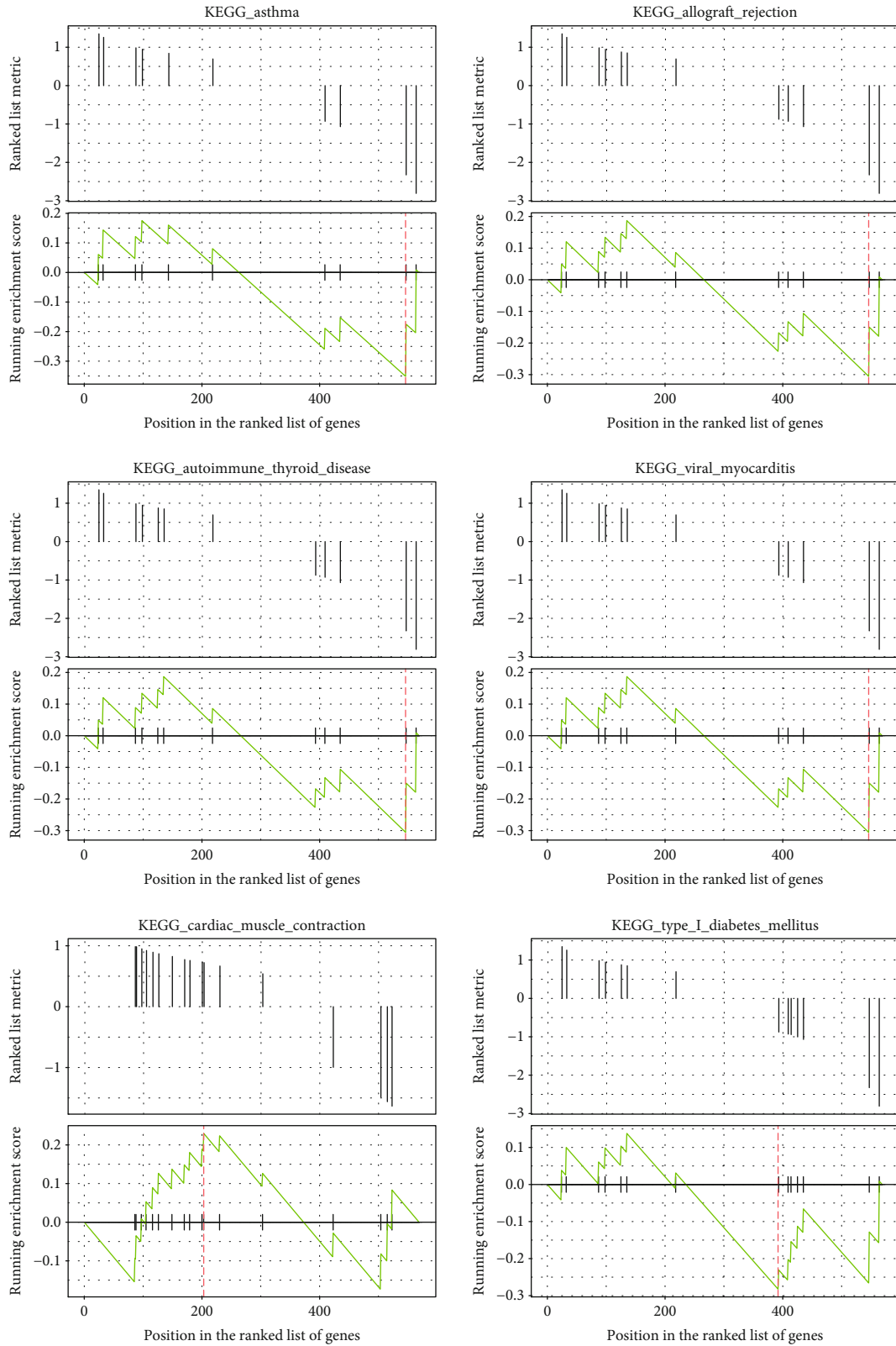


FIGURE 3: Continued.



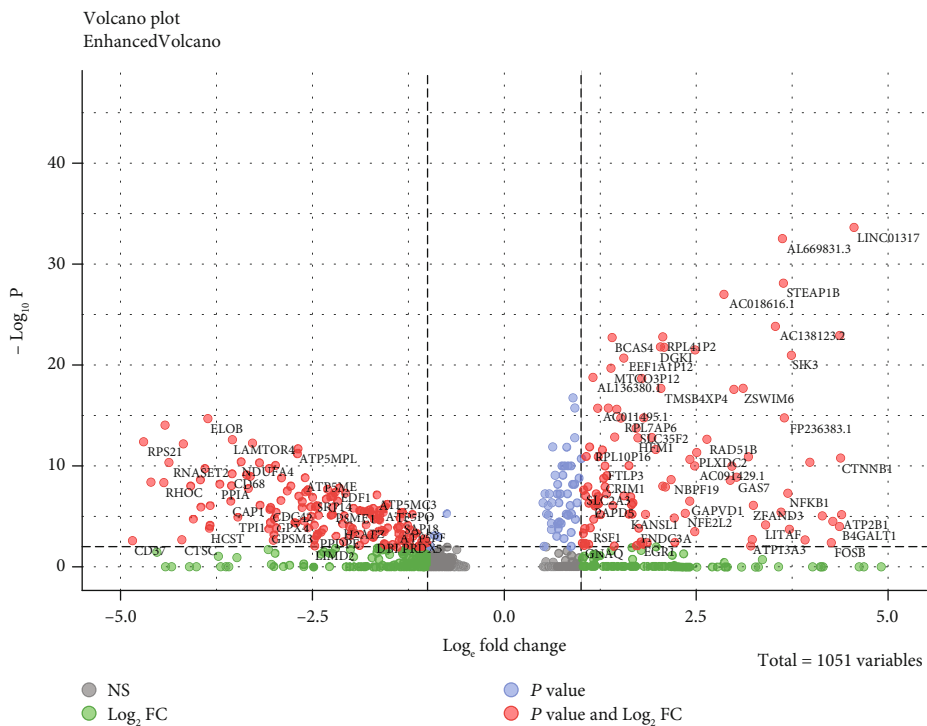
(c)

FIGURE 3: Continued.

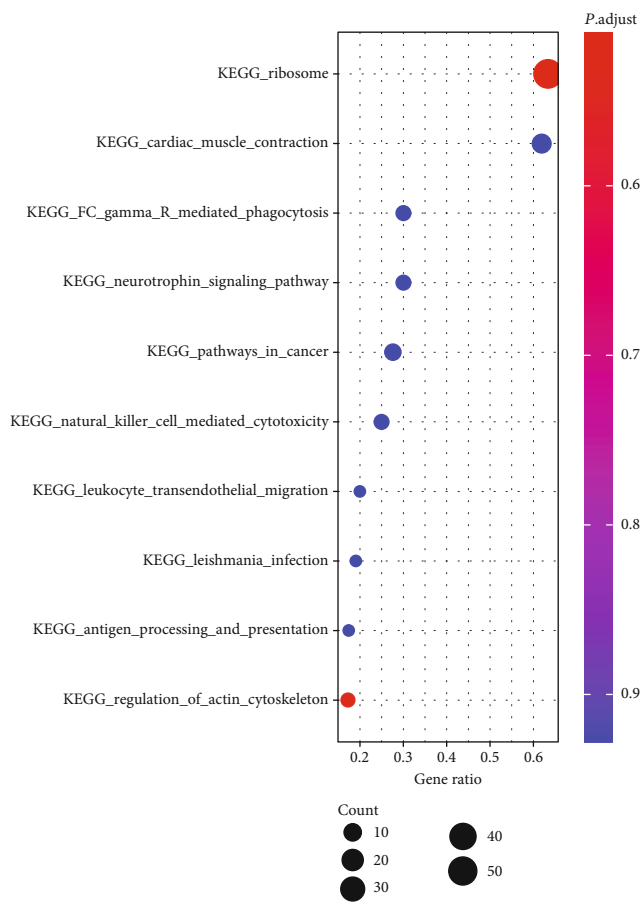


(d)

FIGURE 3: Gene enrichment analysis of the DEGs in the myeloid subsets. (a) Volcano plot demonstrated the statistical significance (P value) versus the magnitude of change (fold change) of the DEGs (1 vs. 6). (b) Violin plots showed the percentage and intensity of gene expression by clusters 1 and 6. (c) CNET plots indicated the network of DEGs in clusters 1 and 6. (d) GSEA identified the upregulated or downregulated DEGs in the indicated signaling pathway.

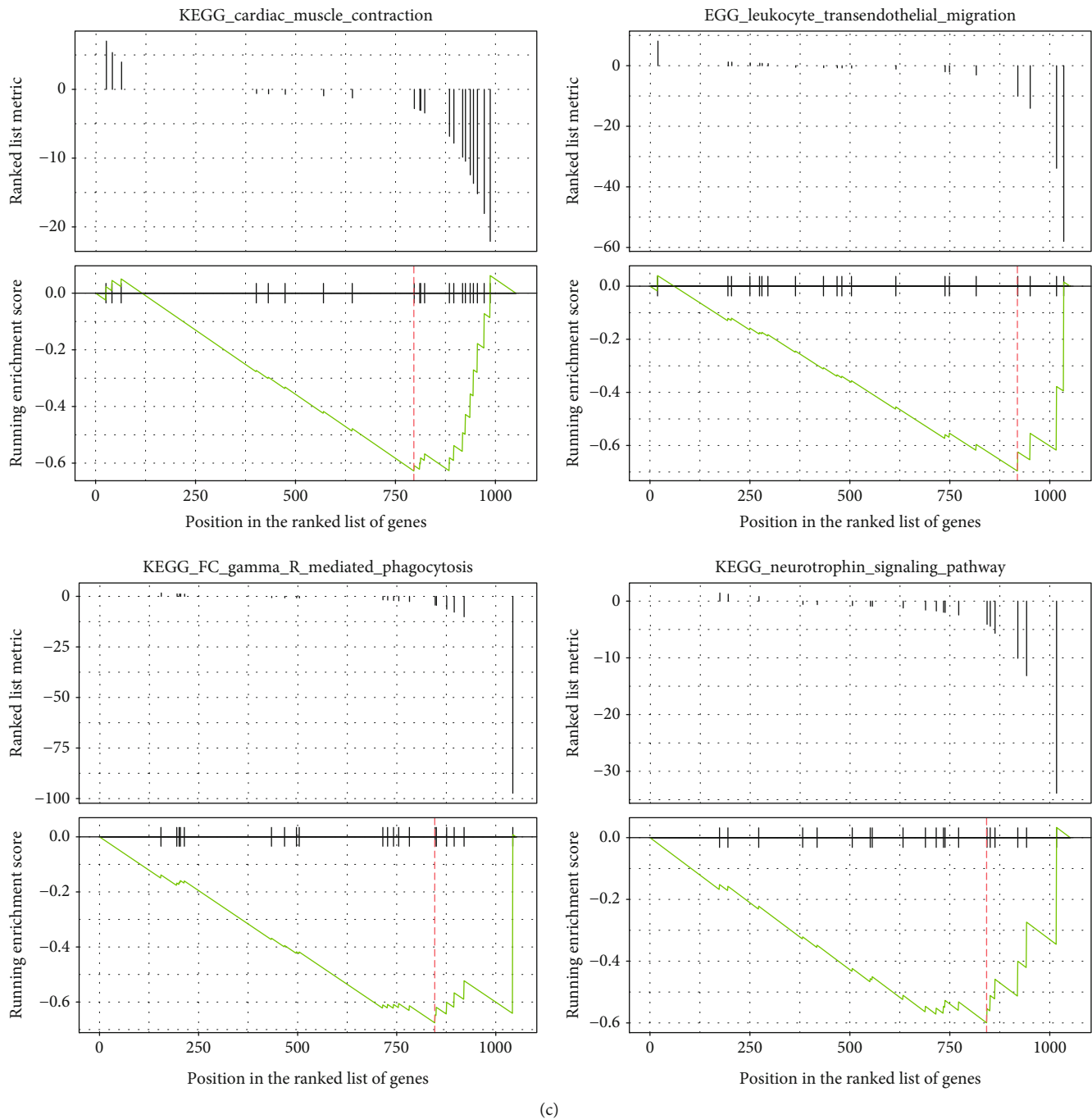


(a)



(b)

FIGURE 4: Continued.



(c)

FIGURE 4: Gene enrichment analysis of the DEGs in both the healthy and rejection kidney. (a) Volcano plot showed the statistical significance (P value) versus the magnitude of change (fold change) of the DEGs in cluster 6 (rejection vs. healthy). (b) Dot plot showed the enriched KEGG signaling pathways of the cluster 6 marker genes between the rejection and healthy samples. (c) GSEA analysis identified the upregulated or downregulated DEGs in the indicated signaling pathway (rejection vs. healthy).

Fc γ receptor-mediated phagocytosis (Figure 4(b)). The GSEA confirmed that genes in cluster 6 of the healthy group promoted transendothelial migration and phagocytosis, which were lost in the rejection samples (Figure 4(c)).

4. Discussion

The major issue of transplantation is remedying rejection following kidney transplantation and prolonging the survival

time of the recipient. In this regard, immune tolerance research may contribute to the solution. However, kidney immunity is a complex network, and the phenotype of immune cell is time and space dependent. Therefore, a comprehensive study of cell heterogeneity is required to understand renal immune homeostasis. The present study characterized the genetic expression of renal macrophages at a single-cell resolution and described the changes in resident macrophages as well as their DEGs during transplant

rejection. Using enrichment tools, the main markers of both resident and infiltrating monocyte/macrophages involved in kidney rejection were identified and classified.

Due to their high heterogeneity, monocyte/macrophages are known to have different activation states and play different roles. Classically activated M1-type macrophages promote acute kidney injury, glomerulosclerosis, and renal interstitial fibrosis by exerting proinflammatory effects, while alternatively activated M2 macrophages have an anti-inflammatory effect, promoting wound healing, reducing renal inflammatory response and fibrosis, and reducing kidney damage [15]. However, little is known about the role of resident macrophages in healthy kidneys. The present analysis demonstrated that resident macrophages share a certain similarity with M2 macrophages and decreased during the rejection response following kidney transplantation. Other than the known M2 markers, a group of characteristic molecules was also listed, which may serve as a potential target or help in finding new strategies to reduce damage and promote repair in the treatment of kidney disease.

By detecting DEGs featuring the resident macrophage, the relevant signaling pathways of these cells were investigated. In contrast to the M1 macrophage, resident macrophages have little effect in autoimmune disease and allograft rejection. While M1 cells exhibit a strong capacity in the antigen presentation, resident macrophages upregulated relevant genes during phagocytosis, similar to the phenotype of M2 macrophages [16]. Understanding the different biological functions of various monocyte/macrophages may help ascertain their role in renal inflammatory response, injury, and repair. For example, certain immune checkpoint inhibitor therapies often cause kidney damage without the detection of any infiltrating inflammatory cells [17]. One may conceive that such treatments may target and reduce the number of resident macrophages, which is crucial in maintaining the homeostasis of the kidney.

A limitation in the present analysis is that the renal rejection sample was a biopsy from a single patient. Therefore, this analysis does not represent overall chronic renal rejection and may only serve as a useful example. In this regard, additional research is needed in order to describe the immune characteristics of chronic renal rejection. However, the development and application of new technologies, such as single-cell sequencing, transcriptomics, and metabolomics, can propel kidney transplantation immune research to a new level.

Data Availability

The datasets and code generated or analysed in this study are available from the corresponding author upon reasonable request.

Conflicts of Interest

The authors declare that this research was conducted in the absence of any commercial or financial relationships that could be construed as a potential conflicts of interest.

Authors' Contributions

Jie Wang, Peiling Luo, and Jingjie Zhao contributed equally to this study.

Acknowledgments

This research was funded by the Guangxi Natural Science Foundation (#2017JJA10384, #2019JJA140059, and #2019JJA140110) and by the Youjiang Medical University for Nationalities Research Project (#yy2019bsky001).

References

- [1] J. Bedke and A. Stenzl, "Immunologic mechanisms in RCC and allogeneic renal transplant rejection," *Nature Reviews Urology*, vol. 7, no. 6, pp. 339–347, 2010.
- [2] P. F. Halloran, J. P. Reeve, A. B. Pereira, L. G. Hidalgo, and K. S. Famulski, "Antibody-mediated rejection, T cell-mediated rejection, and the injury-repair response: new insights from the Genome Canada studies of kidney transplant biopsies," *Kidney International*, vol. 85, no. 2, pp. 258–264, 2014.
- [3] D. Cucchiari, M. A. Podesta, and C. Ponticelli, "The critical role of innate immunity in kidney transplantation," *Nephron*, vol. 132, no. 3, pp. 227–237, 2016.
- [4] D. A. D. Munro and J. Hughes, "The origins and functions of tissue-resident macrophages in kidney development," *Frontiers in Physiology*, vol. 8, p. 837, 2017.
- [5] S. Gordon and F. O. Martinez, "Alternative activation of macrophages: mechanism and functions," *Immunity*, vol. 32, no. 5, pp. 593–604, 2010.
- [6] M. R. Clatworthy, "How to find a resident kidney macrophage: the single-cell sequencing solution," *Journal of the American Society of Nephrology*, vol. 30, no. 5, pp. 715–716, 2019.
- [7] A. Arazi, the Accelerating Medicines Partnership in SLE network, D. A. Rao et al., "The immune cell landscape in kidneys of patients with lupus nephritis," *Nature Immunology*, vol. 20, no. 7, pp. 902–914, 2019.
- [8] B. J. Stewart, J. R. Ferdinand, M. D. Young et al., "Spatiotemporal immune zonation of the human kidney," *Science*, vol. 365, no. 6460, pp. 1461–1466, 2019.
- [9] H. Wu, A. F. Malone, E. L. Donnelly et al., "Single-cell transcriptomics of a human kidney allograft biopsy specimen defines a diverse inflammatory response," *Journal of the American Society of Nephrology*, vol. 29, no. 8, pp. 2069–2080, 2018.
- [10] J. Liao, Z. Yu, Y. Chen et al., "Single-cell RNA sequencing of human kidney," *Scientific Data*, vol. 7, no. 1, p. 4, 2020.
- [11] A. Butler, P. Hoffman, P. Smibert, E. Papalexi, and R. Satija, "Integrating single-cell transcriptomic data across different conditions, technologies, and species," *Nature Biotechnology*, vol. 36, no. 5, pp. 411–420, 2018.
- [12] T. Stuart, A. Butler, P. Hoffman et al., "Comprehensive integration of single-cell data," *Cell*, vol. 177, no. 7, pp. 1888–1902.e21, 2019.
- [13] G. Yu, L. G. Wang, Y. Han, and Q. Y. He, "clusterProfiler: an R package for comparing biological themes among gene clusters," *OMICS: A Journal of Integrative Biology*, vol. 16, no. 5, pp. 284–287, 2012.
- [14] A. S. Puranik, I. A. Leaf, M. A. Jensen et al., "Kidney-resident macrophages promote a proangiogenic environment in the

- normal and chronically ischemic mouse kidney,” *Scientific Reports*, vol. 8, no. 1, p. 13948, 2018.
- [15] P. M. K. Tang, D. J. Nikolic-Paterson, and H. Y. Lan, “Macrophages: versatile players in renal inflammation and fibrosis,” *Nature Reviews Nephrology*, vol. 15, no. 3, pp. 144–158, 2019.
- [16] T. Chen, Q. Cao, Y. Wang, and D. C. H. Harris, “M2 macrophages in kidney disease: biology, therapies, and perspectives,” *Kidney International*, vol. 95, no. 4, pp. 760–773, 2019.
- [17] M. A. Perazella and A. C. Shirali, “Immune checkpoint inhibitor nephrotoxicity: what do we know and what should we do?,” *Kidney International*, vol. 97, no. 1, pp. 62–74, 2020.

Review Article

Immune and Inflammation in Acute Coronary Syndrome: Molecular Mechanisms and Therapeutic Implications

Haiming Wang,¹ Zifan Liu,¹ Junjie Shao,² Lejian Lin,³ Min Jiang,¹ Lin Wang,¹ Xuechun Lu,⁴ Haomin Zhang,⁴ Yundai Chen ¹, and Ran Zhang ¹

¹Department of Cardiology, The First Medical Center of Chinese PLA General Hospital & Chinese PLA Medical School, Beijing 100853, China

²The First Clinical Medical College of Inner Mongolia Medical University, Hohhot 010059, China

³Department of Cardiology, The Eighth Medical Center of Chinese PLA General Hospital, Beijing 100091, China

⁴Department of Hematology, The Second Medical Center of Chinese PLA General Hospital & Chinese PLA Medical School, Beijing 100853, China

Correspondence should be addressed to Yundai Chen; cyundai@vip.163.com and Ran Zhang; bjzhangran@126.com

Received 13 June 2020; Accepted 27 July 2020; Published 18 August 2020

Guest Editor: Jian Song

Copyright © 2020 Haiming Wang et al. This is an open access article distributed under the Creative Commons Attribution License, which permits unrestricted use, distribution, and reproduction in any medium, provided the original work is properly cited.

Acute coronary syndrome (ACS) is a major cause of acute death worldwide. Both innate and adaptive immunity regulate atherosclerosis progression, plaque stability, and thrombus formation. Immune and inflammation dysfunction have been indicated in the pathogenesis of ACS. The imbalance in the proatherogenic and antiatherogenic immune networks promotes the transition of plaques from a stable to unstable state and results in the occurrence of acute coronary events. The residual inflammatory risk (RIR) has received increasing attention in recent years, and lowering RIR has been expected to improve the outcomes of ACS patients. The CANTOS, COLCOT, and LoDoCo trials verified the benefits of reducing cardiovascular events using anti-inflammation therapies; however, most of the other studies focusing on lowering RIR produced negative or contradicting results. Therefore, restoring the balance in autoimmune regulation is essential because proatherogenic and antiatherogenic immunomodulatory effects are equally important in the complex human immune network. In this review, we summarized the recent evidence of the roles of proatherogenic and antiatherogenic immune networks in the pathogenesis of ACS and discussed how immune and inflammation contribute to atherosclerosis progression, plaque instability, and adverse cardiovascular events. We also provide a “from bench to bedside” perspective of a novel and promising personalized strategy in RIR intervention and therapeutic approaches for the treatment of ACS.

1. Introduction

Acute coronary syndrome (ACS) refers to a complex clinical syndrome that includes a spectrum of entities including unstable angina, ST segment elevation myocardial infarction (STEMI), and non-ST segment elevation myocardial infarction (NSTEMI). The accumulating evidence has implicated an inflammatory process in the pathogenesis of ACS that involves local immune cells in coronary arteries generating inflammatory factors that promote thrombus formation [1, 2]. Although nonatherosclerotic factors can also contribute to ACS, the most common cause of ACS is atherosclerotic plaque rupture or erosion with subsequent thrombus

formation. Nearly 60% of ACS patients have a high level of high-sensitivity C-reactive protein (hsCRP) (>2.0 mg/L), a biomarker of systemic inflammation and a predictive factor of high cardiovascular mortality, which is defined as the residual inflammatory risk (RIR) in these patients [3]. Atherosclerosis has been recognized as a chronic inflammatory disorder characterized by dysfunctional immune-inflammation involving interactions between immune cells (macrophages, T lymphocytes, and monocytes) and vascular cells (endothelial cells, smooth muscle cells) [4]. Systemic or local inflammation promotes coronary thrombus formation. Both innate and adaptive immune responses contribute to atherosclerosis and its thrombotic complications in ACS

through complex interactions between atherosclerosis, innate immunity, and inflammation [5]. The CANTOS trial (The Canakinumab Anti-inflammatory Thrombosis Outcomes Study) targeted interleukin-1 β (IL-1 β) innate immunity with canakinumab in patients with a history of ACS and hsCRP \geq 2.0 mg/L and reported significantly attenuated systemic inflammation indicated by hsCRP and improved clinical outcomes independent of lipid metabolism [6]. This study demonstrated that coronary RIR could be successfully treated by inhibiting IL-1 β with canakinumab and raised a potential implication of anti-inflammatory therapy in ACS patients. This article reviews recent advances in the understanding of immune-mediated inflammation in the pathogenesis of ACS and discusses its implications for ACS management strategies.

2. Current Status of Inflammatory Risk in ACS

2.1. Immune-Mediated Inflammation and the Pathogenesis of ACS. The molecular mechanisms of atherosclerosis are cholesterol deposition and immune cell aggregation in the arterial wall. Innate and adaptive immune cells with both proinflammatory and anti-inflammatory effects regulate subsequent atherosclerosis progression. The transition from stable to unstable plaques with subsequent rupture or erosion and thrombus formation contribute to ACS [2]. The link between immune-mediated inflammation and ACS is complex, and the underlying mechanisms of ACS are not fully understood. The pathogenesis of ACS can be divided into plaque rupture with systemic inflammation and red thrombus, plaque rupture with low systemic inflammation, plaque erosion with white thrombus, and ACS without epicardial coronary artery thrombus or stenosis [2]. Usually, at the sites of plaque rupture, activated macrophages and T cells secrete cytokines that trigger a self-perpetuating vicious circle reaction, eventually leading to the fragile and thin fibrous cap as well as the accumulation of a central lipid core [7, 8]. Therefore, systemic and local inflammatory responses are important causes of ACS. Plaque rupture with low systemic inflammation was characterized by no accumulation of macrophages in ruptured plaques and low-grade systemic inflammation. This kind of plaque rupture is caused by psychological stress or local vascular wall stress. Similarly, coronary plaque erosion with white thrombus is not related to macrophage-mediated inflammation, but to platelet aggregation. Although coronary plaque erosion is considered to have no explicit relationship to systemic inflammation, immune cells, and inflammatory factors have been shown to be involved in this process [2]. ACS without epicardial coronary artery thrombus or stenosis may arise from coronary vasospasm or microvascular disease.

Immune-mediated inflammatory disorders, including rheumatic diseases, inflammatory bowel disease (IBD), rheumatoid arthritis (RA), and systemic lupus erythematosus, are also closely related to acute cardiovascular events independent of traditional cardiovascular risk factors. ACS is very common in young women with IBD who often show a high level of CRP [9]. Therefore, immune-mediated inflammation but not the traditional risk factors is the main cause of these

acute cardiovascular events. However, a retrospective cohort study of 300 IBD patients without traditional risk factors in North Shore University Hospital failed to identify the relationship between IBD and acute cardiovascular events [10]. It is possible that the inflammation level is not enough to cause plaque rupture. However, the activity of inflammation is more important than the duration of inflammatory disorders. RA is associated with a higher incidence of premature cardiovascular events and a two-fold increase in the incidence of ACS [11, 12]. RA patients who respond well to anti-inflammatory medication have a decreased risk of future ACS, suggesting that inflammation induces ACS [13]. Rheumatic diseases contribute to events through specific systemic inflammation in the absence of commonly known cardiovascular risk factors. This cause-and-effect relationship is not limited to rheumatic diseases and ACS. Any disorders involving systemic inflammation may damage coronary arteries and subsequently induce ACS [14]. This immunological pathogenesis may provide a theoretical basis for potential clinical applications and interventions.

2.2. RIR: A Gap in the Management of ACS. The CANTOS trial showed that canakinumab was associated with a 15% reduction in major adverse cardiovascular events (MACEs), indicating the importance of anti-inflammatory therapy in the management of ACS residual risks [6, 15]. In the FOURIER (Further Cardiovascular Outcomes Research with PCSK9 Inhibition in Subjects With Elevated Risk) trial, patients with low-density lipoprotein cholesterol (LDL-C) $<$ 30 mg/dL but elevated hsCRP showed a higher incidence of MACE than patients with LDL-C $>$ 100 mg/dL, despite the use of proprotein convertase subtilisin-kexin type 9 (PCSK9) inhibitors [16]. In the post hoc analysis of the SPIRE (Studies of PCSK9 Inhibition and the Reduction in Vascular Events) trials, stable outpatients receiving high-intensity lipid-lowering therapies still showed a 60% increased risk of future cardiovascular events when hsCRP levels exceeded 3 mg/L [17]. This evidence suggested that RIR still exists in ACS patients who received guideline-based medication with intensive lipid-lowering therapy and lifestyle modification [3]. Therefore, the pathogenesis and management of ACS should also focus on reducing RIR beyond antiplatelet and lipid-lowering therapy in the future [3, 6].

3. Immune and Inflammation in the Pathogenesis of ACS

The accumulating evidence has demonstrated that vascular inflammation plays pivotal roles in the pathogenesis of ACS, and thus ACS is considered an inflammation-related disease. Following systemic or local inflammatory activation, endothelial cells enhance the attachment and migration of T lymphocytes and macrophages into the arterial wall via upregulated adhesion molecules. During this process, both the proatherogenic and antiatherogenic immune networks are activated (Figure 1). Once the balance is disturbed by various traditional cardiovascular risk factors, ACS occurs and develops into acute coronary events.

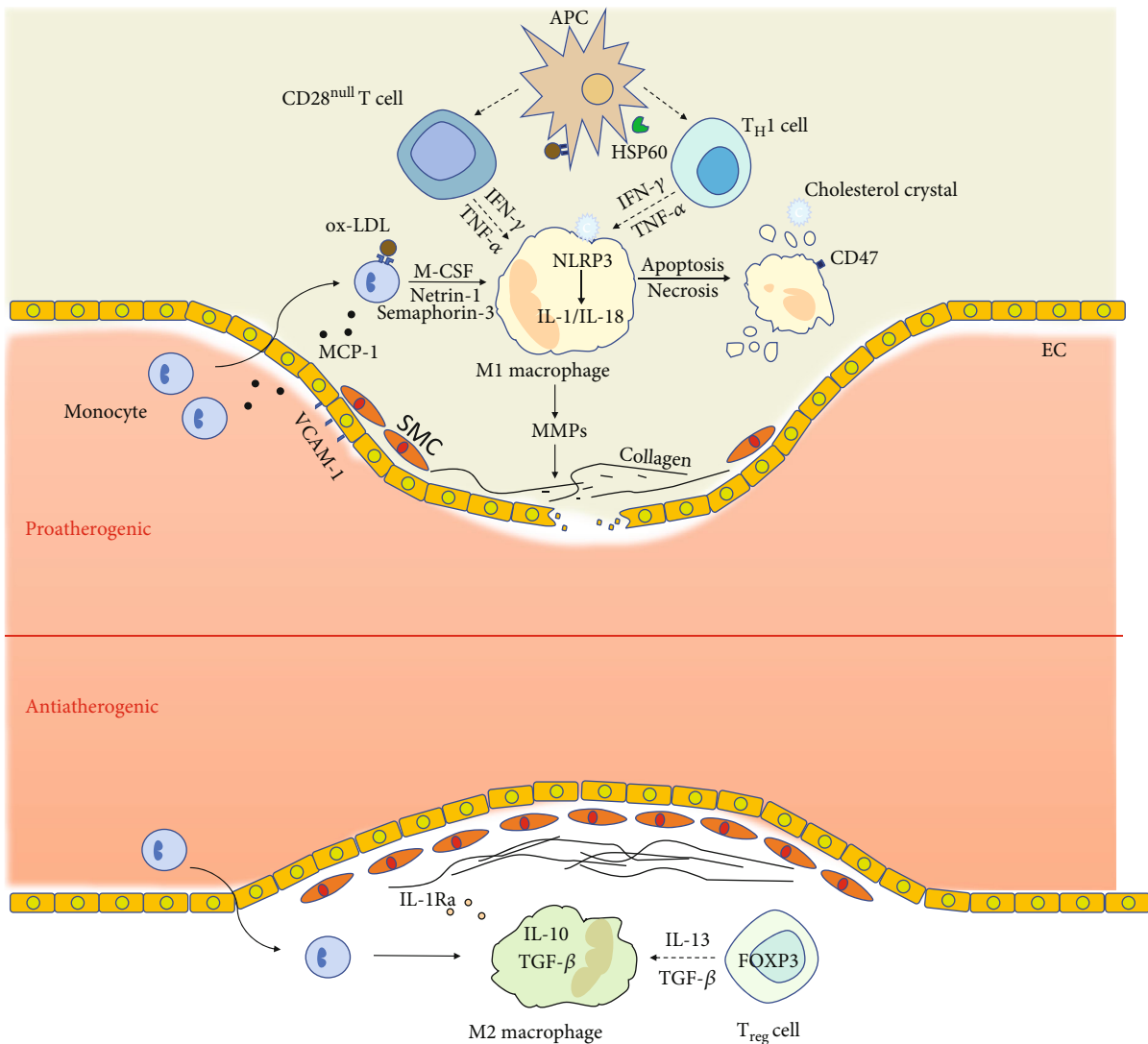


FIGURE 1: Immune and inflammation pathways in the pathogenesis of acute coronary syndrome.

3.1. Proatherogenic Immune Networks in ACS

3.1.1. Proatherogenic Roles of Innate and Adaptive Immunity in Plaque Rupture. The innate immune system is the first barrier for human self-protection that activates nonspecific immune cells to respond to pathogens [18], and immune cells are restricted to enter into the vascular endothelium under normal physiological conditions [19]. The intimal lipid particles in the artery wall promote the production of selectins, monocyte chemoattractant protein-1 (MCP-1), and vascular cell adhesion molecule-1 (VCAM-1) in endothelial cells, which provide monocytes and other inflammatory cells with specific stimuli and anchors [15, 19]. Macrophages are associated with atherosclerosis progression and plaque rupture. After recruitment, monocytes continue to propagate and differentiate into proinflammatory macrophages (M1 type) stimulated by monocyte-colony-stimulating factor (M-CSF) [8]. Platelets are not only important in thrombus formation, but also contribute to atherosclerotic inflammation [20]. Platelets can induce monocyte migration and recruitment to

form plaques and also mediate macrophage polarization to the M1 type [20]. Netrin-1 and semaphorin-3 block binding to CCL19 and CCL21 and prevent lipid-phagocytic macrophages from migrating out of diseased lesions [8, 21]. The degree of macrophage efflux increases following the intentional lowering of netrin-1 concentrations in *LDLR*^{-/-} mice [22]. Macrophages within the atherosclerotic plaque undergo apoptosis or necrosis [8] and are not effectively removed by efferocytosis [23]. CD47, an antiphagocytic signal molecule that helps evade the autoimmune system, cannot be cleared by efferocytosis [24]. CD47 is upregulated in the lipid core of atherosclerotic plaques [25] and blocks phagocytic function in plaques [26], which may be involved in the transition from stable to unstable plaques.

A thin fibrous cap is common in unstable plaques [27] and is associated with the impaired metabolism of interstitial collagens [28]. Typically, tensile interstitial collagen is resistant to degradation by a majority of proteases except for matrix metalloproteinases (MMPs) [29]. Macrophages are one of the primary sources of synthetic MMPs [30]. The

enhanced activity or abundance of MMPs promotes the breakdown of the arterial extracellular matrix [8] and plaque rupture [31]. A recent study showed that inhibiting macrophage-derived MMP-13 in mice increased the number of interstitial collagens and subsequently stabilized plaques [29].

The adaptive immune system also contributes to plaque rupture. T lymphocyte subsets with distinct effector roles have multiple inflammatory functions [7]. Both helper T (T_H) $CD4^+$ cells, especially T_{H1} cells and cytotoxic T (T_C) $CD8^+$ cells, are found in atherosclerotic plaques [7]. Stimulated by dendritic cells binding with oxidized LDL or heat shock protein (HSP) 60, T_{H1} cells promote interferon- γ (IFN- γ) production, which impairs the production of interstitial collagens in vascular smooth muscle cells (VSMCs) [19, 29, 32]. T_{H1} cells and macrophages render the thin fibrous cap susceptible to ACS. $CD28^{null}$ T cells are a subtype of T_H cells that are much more common in patients with ACS than in patients with stable angina, and they accelerate endothelial cell injury through the production of granzyme B and perforin [7, 33]. $CD28^{null}$ T cells are positively correlated with the incidence of ACS [34, 35]. As for the pathogenetic mechanism, $CD28^{null}$ T cells release excessive IFN- γ and TNF- α and resist apoptosis, which contributes to plaque vulnerability in ACS [7, 33, 35, 36]. The roles of T_C cells and other T_H cell subtypes, including T_{H2} , T_{H9} , T_{H22} , and follicular helper T (T_{FH}) cells, in ACS remain to be established [36].

The nucleotide-binding leucine-rich repeat-containing pyrin receptor 3 (NLRP3) inflammasome is a critical component of the innate immune system and triggers the immune cell release of inflammatory cytokines [19, 37]. In ACS, activated NLRP3 inflammasome produces bioactive IL-1 β and IL-18 through activated caspase 1 in patients with atherosclerosis [16]. Both IL-1 β and IL-18 destabilize the plaque by upregulating VCAM, thereby inducing T cell differentiation and promoting downstream proinflammatory reactions [19, 38]. IL-6 mobilizes hepatocytes to synthesize acute phase reactants containing fibrinogen, plasminogen activator inhibitor-1, and CRP [8, 19] and is associated with the evolution of ACS [39]. CRP interacts with Fc transport receptors and subsequently promotes proinflammatory cytokine production and aggravates the local proatherogenic state [19, 40]. In addition to interleukin-like proatherogenic cytokines, TNF- α released by macrophages induces vascular endothelial dysfunction to promote thrombosis and consistently upregulate CD47 [25, 41]. The excessive necrotic phagocytic debris stimulates Toll-like receptors (TLRs) via damage-associated molecular patterns (DAMPs) to potentiate the inflammatory elaboration [8]. Therefore, a positive feedback loop in which all proatherogenic cytokines exacerbate endothelial injury in various ways develops, and consequently, an increasing number of immune cells are attracted to the atheroma lesion [8].

3.1.2. Inflammatory Mechanism of Plaque Erosion. Unlike plaque rupture, macrophages, and T lymphocytes are seldom associated with plaque erosion [2]. Eroded lesions harbor

numerous glycosaminoglycans and proteoglycan instead of a large lipid core and interstitial collagens [2, 29]. Therefore, the molecular mechanism of plaque rupture and erosion differ in phenotypical and functional aspects, which can explain why plaque erosion is not accompanied by detectable systemic inflammation. In general, superficial plaque erosion is mainly initiated by endothelial cell damage caused by various factors, including hemodynamic disturbance, oxidative stress, and TLR activation mediated by hyaluronic acid [2, 42]. Injured endothelial cells covering the plaque progressively detach from the basement membrane. The platelets subsequently recruit to the denuded lesions and release granules to chemotactically attract a large number of neutrophils [2]. However, neutrophils do not settle on the surface of the plaque but exhibit neutrophil extracellular traps (NETs) via apoptosis, which further promotes local thrombosis [43]. Plaque erosion with thrombus shows a higher level of leukocyte myeloperoxidase in ACS postmortem specimens [2, 44].

3.2. Antiatherogenic Immune Networks in ACS. Antiatherogenic immune networks counteract the progressive proatherogenic infiltrates in the pathogenesis of ACS, which mediates a waxing and waning inflammatory environment. Some macrophages differentiate into antiatherogenic subsets (M2 type) to eliminate excessive autoimmune attacks [45]. M2 macrophages are more effective at removing necrotic cellular debris, promoting angiogenesis, and producing IL-10 and TGF- β [8, 45]. IL-10 induces more macrophages toward M2 subtype, and TGF- β controls the proliferation of immune cells, thereby restricting the proatherogenic responses [8, 46]. There are significantly more M2 macrophages in advanced plaques than M1 macrophages, which is associated with the stimulation and amplification of the proinflammatory state [8]. IL-1 β provokes a competitive reaction with IL-1 receptor antagonists (IL-1Ra) in the atheromatous plaque, leading to spontaneous arterial inflammation [19]. In ACS patients who have a higher level of IL-1Ra than those with stable CAD, IL-1Ra appears to be associated with plaque activity and elicits a potential protective effect on the impaired myocardium [19, 47].

Recently, adaptive immunosuppressed cells have received great attention. Regulatory T (T_{reg}) cells are a subtype of immunosuppressed T cells with positive FOXP3, CD20, and CTLA4 expressions that suppress antigen-presenting cells, naive and effector T cells, and natural killer (NK) cells [36]. In addition, T_{reg} cells can delay or even reverse the progression of atherosclerosis [48–50]. Once activated, T_{reg} cells release antiatherogenic cytokines, including IL-13 and TGF β , to promote plaque stabilization [51]. In addition, T_{reg} cells can remodel plaques by increasing the number of M2 macrophages, reconstructing damaged fibrous caps, and inhibiting the proliferation of proatherogenic T cells [52]. The preference of T_{reg} cell differentiation is enhanced in early hypercholesterolemia [53]. However, in advanced atherosclerotic lesions, T_{reg} cells selectively express T-bet, which changes their phenotype from an antiatherogenic inflammatory one to a proatherogenic state [54]. As the number of T_{reg} cells in plaques decreases, the self-protective antiatherogenic function gradually declines [55]. Compared with the general

population, patients with ACS have a lower number of T_{reg} cells [56, 57]. Therefore, it is reasonable to speculate that one of the possible causes of unstable plaque is the excessive consumption of T_{reg} cells and changes in the direction of T cell differentiation [36]. FOXP3, a key regulatory molecule of T_{reg} cells, is important in the pathological differentiation of T_{reg} cells [58], and T_{reg} cells are prone to exhibit proatherogenic properties in the absence of stable FOXP3 expression [36], but the detailed mechanism of this process remains unclear. Clarifying this mechanism is of great significance to understand the antiatherogenic progression of ACS through stabilizing the FOXP3 expression to inhibit the pathological differentiation of T_{reg} cells.

4. Better Attenuation of Coronary RIR Lowers the Risks of ACS

Given that a large part of ACS is a systemic inflammation-related disease in which both innate and adaptive immune systems are involved, RIR may be even common besides cholesterol risk [59]. Even in these patients who received successful percutaneous coronary intervention (PCI) to relieve myocardial ischemia, persistently high RIR was common and positively correlated with one-year MACE [60]. Although this retrospective cohort study could not exclude the risk of traditional confounding cardiovascular factors, it suggests that stratifying patients based on hsCRP levels is beneficial for the prediction of cardiovascular disease risk [60]. Currently, hybrid positron emission tomography imaging, coronary computed tomography angiography (CCTA), and biomarkers of gut microbiota have been used to stratify cardiovascular risks [15, 61]. Hybrid positron emission tomography imaging is useful in underlying cardiovascular inflammatory states [62]; however, its extensive clinical application is limited because of the prolonged exposure of patients to radiation and its expensive cost. CCTA, a common clinical noninvasive method for screening obstructive CAD, can identify morphological traits of high-risk plaques and provide indirect evidence of coronary inflammation [15, 63]. The gut microbiota can release proatherogenic metabolites and induce trimethylamine N-oxide production to induce specific inflammatory responses in epicardial adipose tissue [61, 64], which provides certain valuable information in ACS prediction. However, whether or not the intestinal microbiota can be widely used as a biomarker for RIR stratification requires further investigation.

Regarding the lack of currently available methods for RIR identification, it is difficult to identify the ACS patients that require adjuvant anti-inflammatory treatment. Therefore, it is necessary to propose a novel, efficient, and cost-effective predictive model that does not only focus on the narrow degree of the regional lumen [15]. The persistently high level of hsCRP suggests that RIR continues to drive plaque progression [19], and hsCRP is an ideal biomarker to evaluate cardiovascular events because it can reflect the active state of the inflammatory cascade [65]. A newly established risk prediction score based on hsCRP levels better identifies and stratifies high-risk ACS patients than traditional risk scores, and the detection of hsCRP is a promising approach in guid-

ing therapeutic strategies and evaluating curative effects [3]. The perivascular fat attenuation index (FAI) is an emerging biomarker of vascular inflammation based on noninvasive CCTA that can be used as a direct metric of inflammation [15]. When the plaque is in an active state of inflammation, some inflammatory factors, including IL-6 and TNF- α , promote the breakdown of PVAT [15, 66]. Clinical trials have found that patients with high FAI in the proximal right coronary artery were more prone to ACS [15, 67]. Furthermore, the combination of FAI and anatomical features of high-risk plaques in CCTA can be used to identify excessive RIR [15]. Therefore, the integration of CRP- or FAI-assisted CCTA to traditional cardiovascular risk scores provides accurate stratification, improves the predictive value for high-risk ACS, and paves the way for future precision medicine.

5. Therapeutic Approaches Targeting Immune and Inflammation in ACS

The imbalance between the proatherogenic and antiatherogenic immune networks is an essential component in the pathogenesis of ACS, although controversies regarding the contribution of inflammation to plaque erosion still exist. In addition to potent lipid-lowering manipulations, efforts to eliminate this imbalance may be a promising therapeutic strategy for ACS. Currently, although some clinical trials on anti-inflammatory treatments in ACS have obtained satisfactory endpoints; most of them have failed to complete the translation from the theoretical insight into quantifiable benefits (Table 1).

5.1. Targeting Proatherogenic Immune Modulation to Inhibit Inflammation in ACS. Given that proatherogenic immune networks dominate the pathogenesis of ACS, targeting proatherogenic immune modulation to inhibit inflammation in ACS is promising in this regard. The most successful study in targeting anti-inflammatory therapy in ACS was the CANTOS trial, which randomized 10,061 patients with previous MI and hsCRP ≥ 2.0 mg/L who were identified as having RIR [6]. Canakinumab (150 mg every 3 months), a monoclonal antibody targeting IL-1 β , significantly decreased MACE and inflammatory biomarkers independent of aggressive cholesterol control [6]. This clinical trial demonstrated the importance of neutralizing the main proatherogenic pathway involving IL-1 β to IL-6 to CRP [16]. However, immunosuppressive drugs may result in secondary infections because of their roles against the host defense system, as evidenced in the CANTOS trial in which canakinumab therapy led to an increase in infectious death [6]. Hence, early detection and effective antibiotic treatment can help counteract the risk of infection when immunosuppressive drugs are used. Methotrexate can reduce the amount of proinflammatory cytokines and limit the storage of cholesterol in macrophages [12, 19]. The Cardiovascular Inflammation Reduction (CIRT) trial is a randomized clinical trial investigating whether low-dose methotrexate can alleviate MACEs in type 2 diabetes or metabolic syndrome patients with recent ACS. The results showed a negligible effect on the level of IL-1 β and IL-6 and the number of MACE [68].

TABLE 1: Major published and ongoing clinical studies targeting inflammation therapies in coronary artery disease.

Study	Subjects	Inflammatory target	Therapeutic agent	Median follow-up duration	Primary outcome	Benefit achieved
LoDoCo	Patients with stable CAD	Broad spectrum	Colchicine	3 years	Cardiac arrest, ACS, stroke	Yes [72]
CANTOS	Post-ACS patients with high level of hsCRP	IL-1 β	Canakinumab	48 months	Cardiovascular death, nonfatal myocardial infarction or stroke	Yes [6]
CIRT	Type 2 diabetes or metabolic syndrome patients with recent ACS	Broad spectrum	Methotrexate	2.3 years	Cardiovascular death, nonfatal myocardial infarction or stroke, hospitalization for emergency revascularization	No [68]
COLCOT	Post-ACS patients	Broad spectrum	Colchicine	22.6 months	Cardiovascular death, resuscitated cardiac arrest, myocardial infarction, stroke, hospitalization for emergency revascularization	Yes [73]
CLEAR-SYNERGY	ACS patients with STEMI/SYNERGY stent	Broad spectrum	Colchicine and spironolactone	2 years	Cardiovascular death, stroke, recurrent myocardial infarction	Ongoing [75]
LoDoCo2	Patients with stable CAD	Broad spectrum	Colchicine	3 years	Cardiovascular death, ACS, stroke	Ongoing [75]
ASSAIL-MI	Patients with first STEMI	IL-6	Tocilizumab	6 months	Myocardial salvage index assessed by CMR 1 week after administration	Ongoing [70]
LATITUDE-TIMI 60	Patients with ACS	Mitogen-activated protein kinase	Losmapimod	12 weeks	Cardiovascular death, myocardial infarction, recurrent angina requiring emergency revascularization	No [80]
VCU-ART3	Patients with ACS	IL-1Ra	Anakinra	12 months	14-day changes in CRP levels, new-onset heart failure, long-term improvement of left ventricular ejection fraction	Ongoing [83]

Footnote. ACS: acute coronary syndrome; CRP: C-reactive protein; CMR: cardiovascular magnetic resonance; LoDoCo: Low-Dose Colchicine; CANTOS: Canakinumab. Anti-Inflammatory Thrombosis Outcome Study; CIRT: Cardiovascular Inflammation Reduction Trial; COLCOT: Colchicine Cardiovascular Outcomes Trial; CLEAR-SYNERGY: Colchicine and Spironolactone in Patients with STEMI/SYNERGY Stent Registry; LoDoCo2: Low Dose Colchicine After Myocardial Infarction; ASSAIL-MI: ASSESSing the Effect of Anti-IL-6 Treatment in MI; LATITUDE-TIMI 60: LosmApimod To Inhibit p38 MAP kinase as a therapeutic target and modify outcomes after an acute coronary syndrome; VCU-ART3: Virginia Commonwealth University-Anakinra Remodeling Trial-3.

Similarly, ACS patients administered with the IL-6 inhibitor tocilizumab showed a reduced level of troponin and inflammatory markers in the ASSESSing the Effect of Anti-IL-6 Treatment in MI (ASSAIL-MI) trial [16, 69, 70], which was designed to assess the effects of tocilizumab on ischemia reperfusion injury in patients with ST-elevation myocardial infarction. The neutral results in the CIRT trial suggest that future targeted inflammatory therapies should focus on the control of specific inflammatory cytokines or immune cells [16]. One potential strategy is inhibiting the main proinflammatory activation upstream of the NLRP3 inflammasome. NLRP3 inflammasome inhibitors minimized the area of myocardial infarction in animal models [71]. Colchicine, an antirheumatic drug, can cause neutrophil dysfunction and hinder NLRP3 inflammasome evolution in macrophages, resulting in the downregulated expression of the IL-1 β to IL-6 pathway [19]. The non-double-blind randomized LoDoCo (Low Dose Colchicine) trial enrolled 532 patients with CAD and investigated whether taking colchicine 0.5 mg/day could reduce the risk of cardiovascular events. The results showed that low-cost colchicine could indeed

lower the risk of ACS [72]. However, introducing colchicine for the secondary prevention of CAD is difficult because of the modest sample size and defects in trial design that did not involve the use of inflammatory markers as a reference for disease improvement. Recently, the Colchicine Cardiovascular Outcomes (COLCOT) trial showed a promising decline in the primary endpoints in ACS patients with previous myocardial infarction [73]. Although the COLCOT trial verified the potential intervention of RIR independent of aspirin and statins, there were several limitations to this study. Specifically, approximately 20% of patients failed to synchronously follow the trial for various reasons, and most importantly, a portion of the patients showed an increased risk of gastrointestinal intolerance, myelosuppression, and pneumonia following the use of colchicine [73, 74]. The ongoing Colchicine and Spironolactone in Patients with STEMI/SYNERGY Stent Registry (CLEAR-SYNERGY) and Low Dose Colchicine After Myocardial Infarction (LoDoCo2) trials may provide us with more comprehensive data supporting the overall benefit of colchicine [74, 75]. Nevertheless, the CANTOS, CIRT, and COLCOT trials that

targeted the NLRP3/IL-1 β /IL-6 pathway have provided evidence of the potential benefits of targeting proatherogenic immune networks [74].

TNF- α inhibitors are also widely used to reduce inflammation and regulate endothelial dysfunction, which may improve the outcome of chronic inflammatory diseases [12]. A systematic review and meta-analysis of 13 cohort studies on rheumatoid arthritis demonstrated that TNF- α inhibitors as adjunctive therapy, including disease-modifying antirheumatic drugs (DMARDs), reduced the risk of ACS. However, three randomized controlled trials (RCTs) failed to show any cardiovascular protective effects of TNF- α inhibitors [19, 76]. Therefore, the cardiovascular benefits of TNF- α inhibitors remain elusive, and large-scale clinical trials are needed to further verify the potential outcomes of TNF- α inhibitors in ACS patients. Agents that promote macrophage efflux or enhance efferocytosis showed promising effects on the reduction of ACS events by restricting the expression of netrin-1 and delivering nanoparticles loaded with siRNA to M1 macrophages [8]. CD47, also referred to as the “Do not-Eat-Me” signal, has received great attention in recent years and has been found to be overexpressed in most cancers [77]. CD47-blocking antibodies modified the accumulation of central lipid cores by improving the function of phagocytosis in mice with atherosclerosis [25, 78]. Therefore, the administration of CD47-blocking antibodies is a feasible anti-inflammatory strategy to mitigate the risks of ACS.

Other therapies targeting inflammation have also been investigated. The phospholipase A2 (PLA2) enzymes are key contributors to lipid metabolism and inflammatory activation and are strongly correlated with plaque burden [47, 79]. PLA2 inhibition with varespladib methyl or darapladib showed indistinctive improvements in overall cardiovascular events but rendered patients susceptible to ACS in several large clinical trials [19, 47]. A similar result was observed in large randomized trials of mitogen-activated protein kinase (MAPK) signaling cascade-related targeted therapies [47, 80]. As MAPK activation amplified inflammatory responses, MAPK inhibitors could moderate the systemic or local residual inflammation that leads to ACS [81]. Therefore, their effectiveness as a targeted therapy still needs to be explored.

5.2. Targeting Antiatherogenic Immune Modulation to Inhibit Inflammation in ACS. Due to limited atheroprotective autoimmunity, it is often difficult to prevent excessive proatherogenic immune responses. An improvement in the antiatherogenic ability is expected to affect immune homeostasis. Anakinra, an IL-1Ra antagonist, blocks endogenous IL-1 β and the downstream sequelae and has been used clinically for alleviating rheumatoid diseases. An acute, double-blind trial involving 23 patients with rheumatoid arthritis receiving anakinra (150 mg) or placebo confirmed the significant improvement in biomarkers and vascular and left ventricular function in the anakinra group [82]. Anakinra is expected to improve the outcome of atherosclerosis regarding the provocative results of the CANTOS trial. The administration of anakinra in ACS patients is progressively underway, and positive inflammation-reducing

effects have been observed [3]. The results of phase II clinical trials involving investigational drugs for ACS are expected to verify the promising clinical outcomes of anakinra [83].

Recently, T_{reg} cell-based treatments have received great attention. T_{reg} cells induced by specific antigens restored the internal immune environment and reversed atherosclerosis in mice [7, 84]. An alternative proposed strategy involving the purification of natural T_{reg} cells from subjects and their expansion *in vitro* before reinfusion has proven to be effective in the prevention of atherosclerosis progression [7]. The stability of autologous T_{reg} cells during their *in vitro* expansion and after their targeted delivery into hyperactive inflammation sites remains problematic when used for the treatment of human atherosclerosis. Although T_{reg} cell-based treatments alone might not be sufficient to prevent patients from ACS because of the persistent existence of traditional cardiovascular risk factors, optimizing T_{reg} cell-based treatments is a promising approach from a mechanistic perspective. Therefore, T_{reg} cell-based treatments may be used as a promising antiatherogenic adjuvant strategy for the management of ACS.

6. Prospective of Therapeutic Strategies Targeting Immune and Inflammation in ACS

Although several studies targeting immune and inflammation in ACS showed improved outcomes of atherosclerosis, the future in this field is full of unknowns. Certain inflammatory pathways or specific immune cells are not the perfect equivalents of systemic inflammatory responses. Fleming et al. proposed the fixed distinction between the “surrogate” and “correlate” of a disease [47, 85]. This conceptual difference indicates that inflammatory diseases may produce several biomarkers that are not the real cause of the ultimate clinical outcome. For example, PLA2 and CRP are highly expressed in ACS and positively correlated with the risk of plaque rupture, but their targeted therapies do not achieve the desired effect. Moreover, if a selected “surrogate” only targets one of the multiple proatherogenic or antiatherogenic pathways of ACS without the intervention of the other active pathways, the clinical endpoints may not be effectively modified [47]. The reason for the success of therapeutic strategies targeting the NLRP3 to IL-1 β to IL-6 pathway is that these factors serve as perfect representatives that capture abundant upstream inflammatory signals and lead directly to the magnification of the systemic or local inflammation [16]. In addition, some anti-inflammatory agents appear promising and beneficial effects in animals but not in human, such as MAPK inhibitor losmapimod and the recombinant P-selectin glycoprotein ligand-1 (PSGL-1) [47]. One of the most convincing explanations for this is related to the optimal time of drug administration. In animal experiments, these anti-inflammatory agents can be administered immediately after the established severe inflammatory stimulus, whereas it is not practical to initiate them before or when undetected ACS occurs in patients. These pose some challenges for future experimental and human investigation. The successful targeting of immune and inflammation depends not only on the discovery of a more ideal “surrogate” for inflammation

but also on the development of an experimental model more similar to humans [47].

To date, studies on targeting proatherogenic inflammation have outnumbered those targeting antiatherogenic inflammation. The clinical benefits observed in most trials investigating the regulation of proatherogenic mechanisms alone were suboptimal. Furthermore, the overwhelming suppression of proatherogenic immunomodulatory effects attenuates systemic immunocompetence and results in multiple infections and malignant tumors [7, 16]. Accumulating evidence indicates that proatherogenic and antiatherogenic immunomodulatory effects are equally important in the complex human immune network, and promising attempts have been made to reinforce antiatherogenic T lymphocyte subsets and other anti-inflammatory cytokines to restore the balance of autoimmune regulation in the treatment of autoimmune diseases, cancer, and allogeneic transplantation [7]. Therefore, efforts should focus on antiatherogenic adjuvant agents in the future development of immunotherapies for ACS.

7. Conclusions

ACS has been referred to as an inflammation-related disease regarding its pathogenesis. Understanding the mechanisms of immune and inflammation in ACS will transform risk evaluations and treatment paradigms. The management of RIR beyond traditional guideline-based therapy leads to positive cardiovascular outcomes. Efforts targeting the immune system and inflammation to alleviate the ACS burden have provided promising results. Although they are still being developed, therapies based on anti-inflammation and immune modulation will promote a personalized medicine in the future. Finally, cooperation among cardiologists, oncologists, and rheumatologists is needed to achieve precise prevention and therapy for ACS patients.

Conflicts of Interest

The authors declare that they have no conflict of interest regarding the publication of this article.

Authors' Contributions

Haiming Wang and Zifan Liu contributed equally to this work.

Acknowledgments

We thank Birth Defect Intervention and Rescue Foundation of China for professional advice on project design. This work was supported by the National Natural Science Foundation of China (81871516, 81571841) and Open Research Fund of National Clinical Research Center for Geriatric Diseases (NCRCG-PLAGH-2018001).

References

- [1] P. Libby, G. Pasterkamp, F. Crea, and I. K. Jang, "Reassessing the mechanisms of acute coronary syndromes," *Circulation Research*, vol. 124, no. 1, pp. 150–160, 2019.
- [2] F. Crea and P. Libby, "Acute coronary syndromes: the way forward from mechanisms to precision treatment," *Circulation*, vol. 136, no. 12, pp. 1155–1166, 2017.
- [3] P. R. Lawler, D. L. Bhatt, L. C. Godoy et al., "Targeting cardiovascular inflammation: next steps in clinical translation," *European Heart Journal*, 2020.
- [4] R. Spirig, J. Tsui, and S. Shaw, "The emerging role of TLR and innate immunity in cardiovascular disease," *Cardiology Research and Practice*, vol. 2012, Article ID 181394, 12 pages, 2012.
- [5] P. Libby and G. K. Hansson, "From focal lipid storage to systemic inflammation: JACC review topic of the week," *Journal of the American College of Cardiology*, vol. 74, no. 12, pp. 1594–1607, 2019.
- [6] P. M. Ridker, B. M. Everett, T. Thuren et al., "Antiinflammatory therapy with canakinumab for atherosclerotic disease," *The New England Journal of Medicine*, vol. 377, no. 12, pp. 1119–1131, 2017.
- [7] J. Bullenkamp, S. Dinkla, J. C. Kaski, and I. E. Dumitriu, "Targeting T cells to treat atherosclerosis: odyssey from bench to bedside," *European Heart Journal - Cardiovascular Pharmacotherapy*, vol. 2, no. 3, pp. 194–199, 2016.
- [8] P. Libby, I. Tabas, G. Fredman, and E. A. Fisher, "Inflammation and its resolution as determinants of acute coronary syndromes," *Circulation Research*, vol. 114, no. 12, pp. 1867–1879, 2014.
- [9] S. Singh, I. J. Kullo, D. S. Pardi, and E. V. Loftus Jr., "Epidemiology, risk factors and management of cardiovascular diseases in IBD," *Nature Reviews Gastroenterology & Hepatology*, vol. 12, no. 1, pp. 26–35, 2015.
- [10] P. Ruisi, J. N. Makaryus, M. Ruisi, and A. N. Makaryus, "Inflammatory bowel disease as a risk factor for premature coronary artery disease," *Journal of Clinical Medicine Research*, vol. 7, no. 4, pp. 257–261, 2015.
- [11] R. López-Mejías, S. Castañeda, C. González-Juanatey et al., "Cardiovascular risk assessment in patients with rheumatoid arthritis: the relevance of clinical, genetic and serological markers," *Autoimmunity Reviews*, vol. 15, no. 11, pp. 1013–1030, 2016.
- [12] J. C. Mason and P. Libby, "Cardiovascular disease in patients with chronic inflammation: mechanisms underlying premature cardiovascular events in rheumatologic conditions," *European Heart Journal*, vol. 36, no. 8, pp. 482–489, 2015.
- [13] W. G. Dixon, K. D. Watson, M. Lunt et al., "Reduction in the incidence of myocardial infarction in patients with rheumatoid arthritis who respond to anti-tumor necrosis factor α therapy: results from the British Society for Rheumatology Biologics Register," *Arthritis and Rheumatism*, vol. 56, no. 9, pp. 2905–2912, 2007.
- [14] S. N. Lee, D. Moon, K. W. Moon, and K. D. Yoo, "The Glasgow prognostic score as a significant predictor of clinical outcomes in patients with acute coronary syndrome," *Journal of Cardiology*, vol. 74, no. 2, pp. 130–135, 2019.
- [15] C. Antoniadou, A. S. Antonopoulos, and J. Deanfield, "Imaging residual inflammatory cardiovascular risk," *European Heart Journal*, vol. 41, no. 6, pp. 748–758, 2020.

- [16] P. M. Ridker, "Anticytokine agents: targeting interleukin signaling pathways for the treatment of atherothrombosis," *Circulation Research*, vol. 124, no. 3, pp. 437–450, 2019.
- [17] A. D. Pradhan, A. W. Aday, L. M. Rose, and P. M. Ridker, "Residual inflammatory risk on treatment with PCSK9 inhibition and statin therapy," *Circulation*, vol. 138, no. 2, pp. 141–149, 2018.
- [18] J. Y. Noh, S. R. Yoon, T. D. Kim, I. Choi, and H. Jung, "Toll-like receptors in natural killer cells and their application for immunotherapy," *Journal of Immunology Research*, vol. 2020, Article ID 2045860, 9 pages, 2020.
- [19] J. Khambhati, M. Engels, M. Allard-Ratick, P. B. Sandesara, A. A. Quyyumi, and L. Sperling, "Immunotherapy for the prevention of atherosclerotic cardiovascular disease: promise and possibilities," *Atherosclerosis*, vol. 276, pp. 1–9, 2018.
- [20] T. J. Barrett, M. Schlegel, F. Zhou et al., "Platelet regulation of myeloid suppressor of cytokine signaling 3 accelerates atherosclerosis," *Science Translational Medicine*, vol. 11, no. 517, article eaax0481, 2019.
- [21] F. K. Swirski, M. Nahrendorf, and P. Libby, "The ins and outs of inflammatory cells in atheromata," *Cell Metabolism*, vol. 15, no. 2, pp. 135–136, 2012.
- [22] J. M. van Gils, M. C. Derby, L. R. Fernandes et al., "The neuroimmune guidance cue netrin-1 promotes atherosclerosis by inhibiting the emigration of macrophages from plaques," *Nature Immunology*, vol. 13, no. 2, pp. 136–143, 2012.
- [23] E. Thorp, M. Subramanian, and I. Tabas, "The role of macrophages and dendritic cells in the clearance of apoptotic cells in advanced atherosclerosis," *European Journal of Immunology*, vol. 41, no. 9, pp. 2515–2518, 2011.
- [24] M. E. W. Logtenberg, F. A. Scheeren, and T. N. Schumacher, "The CD47-SIRP α immune checkpoint," *Immunity*, vol. 52, no. 5, pp. 742–752, 2020.
- [25] Y. Kojima, J. P. Volkmer, K. McKenna et al., "CD47-blocking antibodies restore phagocytosis and prevent atherosclerosis," *Nature*, vol. 536, no. 7614, pp. 86–90, 2016.
- [26] A. R. Jalil, J. C. Andrechak, and D. E. Discher, "Macrophage checkpoint blockade: results from initial clinical trials, binding analyses, and CD47-SIRP α structure-function," *Antibody Therapeutics*, vol. 3, no. 2, pp. 80–94, 2020.
- [27] G. Sun, H. Song, and S. Wu, "miR-19a promotes vascular smooth muscle cell proliferation, migration and invasion through regulation of Ras homolog family member B," *International Journal of Molecular Medicine*, vol. 44, no. 6, pp. 1991–2002, 2019.
- [28] J. J. DiNicolantonio and J. H. O'Keefe, "The benefits of Omega-3 fats for stabilizing and remodeling atherosclerosis," *Missouri Medicine*, vol. 117, no. 1, pp. 65–69, 2020.
- [29] P. Libby, "Mechanisms of acute coronary syndromes and their implications for therapy," *The New England Journal of Medicine*, vol. 368, no. 21, pp. 2004–2013, 2013.
- [30] B. C. Meneghini, E. R. Tavares, M. C. Guido et al., "Lipid core nanoparticles as vehicle for docetaxel reduces atherosclerotic lesion, inflammation, cell death and proliferation in an atherosclerosis rabbit model," *Vascular Pharmacology*, vol. 115, pp. 46–54, 2019.
- [31] L. Lahdentausta, J. Leskelä, A. Winkelmann et al., "Serum MMP-9 diagnostics, prognostics, and activation in acute coronary syndrome and its recurrence," *Journal of Cardiovascular Translational Research*, vol. 11, no. 3, pp. 210–220, 2018.
- [32] P. Libby, "Collagenases and cracks in the plaque," *The Journal of Clinical Investigation*, vol. 123, no. 8, pp. 3201–3203, 2013.
- [33] I. E. Dumitriu, P. Baruah, C. J. Finlayson et al., "High levels of costimulatory receptors OX40 and 4-1BB characterize CD4⁺CD28^{null} T cells in patients with acute coronary syndrome," *Circulation Research*, vol. 110, no. 6, pp. 857–869, 2012.
- [34] G. Liuzzo, L. M. Biasucci, G. Trotta et al., "Unusual CD4⁺CD28^{null} T lymphocytes and recurrence of acute coronary events," *Journal of the American College of Cardiology*, vol. 50, no. 15, pp. 1450–1458, 2007.
- [35] E. Kovalcsik, R. F. Antunes, P. Baruah, J. C. Kaski, and I. E. Dumitriu, "Proteasome-mediated reduction in proapoptotic molecule Bim renders CD4⁺CD28^{null} T cells resistant to apoptosis in acute coronary syndrome," *Circulation*, vol. 131, no. 8, pp. 709–720, 2015.
- [36] R. Saigusa, H. Winkels, and K. Ley, "T cell subsets and functions in atherosclerosis," *Nature Reviews Cardiology*, vol. 17, no. 7, pp. 387–401, 2020.
- [37] S. Toldo and A. Abbate, "The NLRP3 inflammasome in acute myocardial infarction," *Nature Reviews Cardiology*, vol. 15, no. 4, pp. 203–214, 2018.
- [38] J. Deng, X. Q. Yu, and P. H. Wang, "Inflammasome activation and Th17 responses," *Molecular Immunology*, vol. 107, pp. 142–164, 2019.
- [39] IL6R Genetics Consortium Emerging Risk Factors Collaboration, "Interleukin-6 receptor pathways in coronary heart disease: a collaborative meta-analysis of 82 studies," *The Lancet*, vol. 379, no. 9822, pp. 1205–1213, 2012.
- [40] V. Aas, K. L. Sand, H. C. Asheim, H. B. Benestad, and J. G. Iversen, "C-reactive protein triggers calcium signalling in human neutrophilic granulocytes via Fc γ RIIa in an allele-specific way," *Scandinavian Journal of Immunology*, vol. 77, no. 6, pp. 442–451, 2013.
- [41] B. Wang, R. Chen, H. Gao et al., "A comparative study unraveling the effects of TNF- α stimulation on endothelial cells between 2D and 3D culture," *Biomedical Materials*, 2020.
- [42] M. Tomaniak, Y. Katagiri, R. Modolo et al., "Vulnerable plaques and patients: state-of-the-art," *European Heart Journal*, 2020.
- [43] E. J. Folco, T. L. Mawson, A. Vromman et al., "Neutrophil extracellular traps induce endothelial cell activation and tissue factor production through interleukin-1 α and cathepsin G," *Arteriosclerosis, Thrombosis, and Vascular Biology*, vol. 38, no. 8, pp. 1901–1912, 2018.
- [44] G. Ferrante, M. Nakano, F. Prati et al., "High levels of systemic myeloperoxidase are associated with coronary plaque erosion in patients with acute coronary syndromes: a clinicopathological study," *Circulation*, vol. 122, no. 24, pp. 2505–2513, 2010.
- [45] A. Tajbakhsh, M. Rezaee, P. T. Kovanen, and A. Sahebkar, "Efferocytosis in atherosclerotic lesions: malfunctioning regulatory pathways and control mechanisms," *Pharmacology & Therapeutics*, vol. 188, pp. 12–25, 2018.
- [46] T. Bauer, A. Zagórska, J. Jurkin et al., "Identification of Axl as a downstream effector of TGF- β 1 during Langerhans cell differentiation and epidermal homeostasis," *The Journal of Experimental Medicine*, vol. 209, no. 11, pp. 2033–2047, 2012.
- [47] J. A. Rymer and L. K. Newby, "Failure to launch: targeting inflammation in acute coronary syndromes," *JACC: Basic to Translational Science*, vol. 2, no. 4, pp. 484–497, 2017.

- [48] H. Ait-Oufella, B. L. Salomon, S. Potteaux et al., "Natural regulatory T cells control the development of atherosclerosis in mice," *Nature Medicine*, vol. 12, no. 2, pp. 178–180, 2006.
- [49] H. von Boehmer, "Mechanisms of suppression by suppressor T cells," *Nature Immunology*, vol. 6, no. 4, pp. 338–344, 2005.
- [50] R. Klingenberg, N. Gerdes, R. M. Badeau et al., "Depletion of FOXP3⁺ regulatory T cells promotes hypercholesterolemia and atherosclerosis," *The Journal of Clinical Investigation*, vol. 123, no. 3, pp. 1323–1334, 2013.
- [51] A. K. L. Robertson, M. Rudling, X. Zhou, L. Gorelik, R. A. Flavell, and G. K. Hansson, "Disruption of TGF- β signaling in T cells accelerates atherosclerosis," *The Journal of Clinical Investigation*, vol. 112, no. 9, pp. 1342–1350, 2003.
- [52] M. Sharma, M. P. Schlegel, M. S. Afonso et al., "Regulatory T cells license macrophage pro-resolving functions during atherosclerosis regression," *Circulation Research*, vol. 127, no. 3, pp. 335–353, 2020.
- [53] R. K. W. Mailer, A. Gisterå, K. A. Polyzos, D. F. J. Ketelhuth, and G. K. Hansson, "Hypercholesterolemia induces differentiation of regulatory T cells in the liver," *Circulation Research*, vol. 120, no. 11, pp. 1740–1753, 2017.
- [54] D. E. Gaddis, L. E. Padgett, R. Wu et al., "Apolipoprotein AI prevents regulatory to follicular helper T cell switching during atherosclerosis," *Nature Communications*, vol. 9, no. 1, article 1095, 2018.
- [55] E. Maganto-García, M. L. Tarrío, N. Grabie, D. X. Bu, and A. H. Lichtman, "Dynamic changes in regulatory T cells are linked to levels of diet-induced hypercholesterolemia," *Circulation*, vol. 124, no. 2, pp. 185–195, 2011.
- [56] A. Mor, G. Luboshits, D. Planer, G. Keren, and J. George, "Altered status of CD4(+)CD25(+) regulatory T cells in patients with acute coronary syndromes," *European Heart Journal*, vol. 27, no. 21, pp. 2530–2537, 2006.
- [57] J. George, S. Schwartzberg, D. Medvedovsky et al., "Regulatory T cells and IL-10 levels are reduced in patients with vulnerable coronary plaques," *Atherosclerosis*, vol. 222, no. 2, pp. 519–523, 2012.
- [58] S. L. Bailey-Bucktrout, M. Martinez-Llordella, X. Zhou et al., "Self-antigen-driven activation induces instability of regulatory T cells during an inflammatory autoimmune response," *Immunity*, vol. 39, no. 5, pp. 949–962, 2013.
- [59] P. M. Ridker, "Clinician's guide to reducing inflammation to reduce atherothrombotic risk: JACC review topic of the week," *Journal of the American College of Cardiology*, vol. 72, no. 25, pp. 3320–3331, 2018.
- [60] D. N. Kalkman, M. Aquino, B. E. Claessen et al., "Residual inflammatory risk and the impact on clinical outcomes in patients after percutaneous coronary interventions," *European Heart Journal*, vol. 39, no. 46, pp. 4101–4108, 2018.
- [61] D. Pedicino, A. Severino, S. Ucci et al., "Epicardial adipose tissue microbial colonization and inflammasome activation in acute coronary syndrome," *International Journal of Cardiology*, vol. 236, pp. 95–99, 2017.
- [62] A. S. Reddy, D. E. Uceda, M. Al Najafi, A. K. Dey, and N. N. Mehta, "PET scan with fludeoxyglucose/computed tomography in low-grade vascular inflammation," *PET Clinics*, vol. 15, no. 2, pp. 207–213, 2020.
- [63] P. Maurovich-Horvat, M. Ferencik, S. Voros, B. Merkely, and U. Hoffmann, "Comprehensive plaque assessment by coronary CT angiography," *Nature Reviews Cardiology*, vol. 11, no. 7, pp. 390–402, 2014.
- [64] X. S. Li, S. Obeid, R. Klingenberg et al., "Gut microbiota-dependent trimethylamine N-oxide in acute coronary syndromes: a prognostic marker for incident cardiovascular events beyond traditional risk factors," *European Heart Journal*, vol. 38, no. 11, pp. 814–824, 2017.
- [65] S. M. Grundy, N. J. Stone, A. L. Bailey et al., "2018 AHA/ACC/AACVPR/AAPA/ABC/ACPM/ADA/AGS/APHA/ASPC/NLA/PCNA guideline on the management of blood cholesterol: a report of the American College of Cardiology/American Heart Association task force on clinical practice guidelines," *Circulation*, vol. 139, no. 25, pp. e1082–e1143, 2019.
- [66] A. S. Antonopoulos, F. Sanna, N. Sabharwal et al., "Detecting human coronary inflammation by imaging perivascular fat," *Science Translational Medicine*, vol. 9, no. 398, article eaal2658, 2017.
- [67] E. K. Oikonomou, M. Marwan, M. Y. Desai et al., "Non-invasive detection of coronary inflammation using computed tomography and prediction of residual cardiovascular risk (the CRISP CT study): a post-hoc analysis of prospective outcome data," *Lancet*, vol. 392, no. 10151, pp. 929–939, 2018.
- [68] P. M. Ridker, B. M. Everett, A. Pradhan et al., "Low-dose methotrexate for the prevention of atherosclerotic events," *The New England Journal of Medicine*, vol. 380, no. 8, pp. 752–762, 2019.
- [69] T. Cai, Y. Zhang, Y. L. Ho et al., "Association of Interleukin 6 receptor variant with cardiovascular disease effects of interleukin 6 receptor blocking therapy: a phenome-wide association study," *JAMA Cardiology*, vol. 3, no. 9, pp. 849–857, 2018.
- [70] A. K. Anstensrud, S. Woxholt, K. Sharma et al., "Rationale for the ASSAIL-MI-trial: a randomised controlled trial designed to assess the effect of tocilizumab on myocardial salvage in patients with acute ST-elevation myocardial infarction (STEMI)," *Open Heart*, vol. 6, no. 2, article e001108, 2019.
- [71] G. P. J. van Hout, L. Bosch, G. H. J. M. Ellenbroek et al., "The selective NLRP3-inflammasome inhibitor MCC950 reduces infarct size and preserves cardiac function in a pig model of myocardial infarction," *European Heart Journal*, vol. 38, no. 11, pp. 828–836, 2016.
- [72] S. M. Nidorf, J. W. Eikelboom, C. A. Budgeon, and P. L. Thompson, "Low-dose colchicine for secondary prevention of cardiovascular disease," *Journal of the American College of Cardiology*, vol. 61, no. 4, pp. 404–410, 2013.
- [73] J. C. Tardif, S. Kouz, D. D. Waters et al., "Efficacy and safety of low-dose colchicine after myocardial infarction," *The New England Journal of Medicine*, vol. 381, no. 26, pp. 2497–2505, 2019.
- [74] P. M. Ridker, "From CANTOS to CIRT to COLCOT to clinic: will all atherosclerosis patients soon be treated with combination lipid-lowering and inflammation-inhibiting agents," *Circulation*, vol. 141, no. 10, pp. 787–789, 2020.
- [75] M. T. Nguyen, S. Fernando, N. Schwarz, J. T. M. Tan, C. A. Bursill, and P. J. Psaltis, "Inflammation as a therapeutic target in atherosclerosis," *Journal of Clinical Medicine*, vol. 8, no. 8, article 1109, 2019.
- [76] C. Barnabe, B. J. Martin, and W. A. Ghali, "Systematic review and meta-analysis: anti-tumor necrosis factor α therapy and cardiovascular events in rheumatoid arthritis," *Arthritis Care & Research*, vol. 63, no. 4, pp. 522–529, 2011.
- [77] Y. Zhou, Y. Yao, Y. Deng, and A. Shao, "Regulation of efferocytosis as a novel cancer therapy," *Cell Communication and Signaling: CCS*, vol. 18, no. 1, p. 71, 2020.

- [78] D. Engelbertsen, A. Autio, R. A. F. Verwilligen et al., "Increased lymphocyte activation and atherosclerosis in CD47-deficient mice," *Scientific Reports*, vol. 9, no. 1, article 10608, 2019.
- [79] F. Yang, L. Ma, L. Zhang et al., "Association between serum lipoprotein-associated phospholipase A2, ischemic modified albumin and acute coronary syndrome: a cross-sectional study," *Heart and Vessels*, vol. 34, no. 10, pp. 1608–1614, 2019.
- [80] M. L. O'Donoghue, R. Glaser, M. A. Cavender et al., "Effect of losmapimod on cardiovascular outcomes in patients hospitalized with acute myocardial infarction: a randomized clinical trial," *JAMA*, vol. 315, no. 15, pp. 1591–1599, 2016.
- [81] M. Fisk, P. R. Gajendragadkar, K. M. Mäki-Petäjä, I. B. Wilkinson, and J. Cheriyan, "Therapeutic potential of p38 MAP kinase inhibition in the management of cardiovascular disease," *American Journal of Cardiovascular Drugs*, vol. 14, no. 3, pp. 155–165, 2014.
- [82] I. Ikonomidis, J. P. Lekakis, M. Nikolaou et al., "Inhibition of interleukin-1 by anakinra improves vascular and left ventricular function in patients with rheumatoid arthritis," *Circulation*, vol. 117, no. 20, pp. 2662–2669, 2008.
- [83] A. Rout, A. Sukhi, R. Chaudhary, K. P. Bliden, U. S. Tantry, and P. A. Gurbel, "Investigational drugs in phase II clinical trials for acute coronary syndromes," *Expert Opinion on Investigational Drugs*, vol. 29, no. 1, pp. 33–47, 2020.
- [84] J. Zhang, C. Chen, H. Fu et al., "MicroRNA-125a-loaded polymeric nanoparticles alleviate systemic lupus erythematosus by restoring effector/regulatory T cells balance," *ACS Nano*, vol. 14, no. 4, pp. 4414–4429, 2020.
- [85] T. R. Fleming and D. L. DeMets, "Surrogate end points in clinical trials: are we being misled," *Annals of Internal Medicine*, vol. 125, no. 7, pp. 605–613, 1996.

Research Article

MPC1 Deficiency Promotes CRC Liver Metastasis via Facilitating Nuclear Translocation of β -Catenin

Guang-Ang Tian,^{1,2} Chun-Jie Xu,³ Kai-Xia Zhou,² Zhi-Gang Zhang^{1,2}, Jian-Ren Gu,^{1,2} Xue-Li Zhang^{1,2}, and Ya-Hui Wang^{1,2}

¹Shanghai Medical College of Fudan University, Shanghai 200032, China

²State Key Laboratory of Oncogenes and Related Genes, Shanghai Cancer Institute, Renji Hospital, School of Medicine, Shanghai Jiao Tong University, Shanghai 200240, China

³Department of Gastrointestinal Surgery, Renji Hospital, School of Medicine, Shanghai Jiao Tong University, Shanghai 200127, China

Correspondence should be addressed to Xue-Li Zhang; xlzhang@shsci.org and Ya-Hui Wang; yhwang@shsci.org

Received 4 May 2020; Revised 9 July 2020; Accepted 17 July 2020; Published 8 August 2020

Guest Editor: Zenghui Teng

Copyright © 2020 Guang-Ang Tian et al. This is an open access article distributed under the Creative Commons Attribution License, which permits unrestricted use, distribution, and reproduction in any medium, provided the original work is properly cited.

Accumulating evidence has pointed out that metastasis is the leading cause of death in several malignant tumor, including CRC. During CRC, metastatic capacity is closely correlated with reprogrammed energy metabolism. Mitochondrial Pyruvate Carrier 1 (MPC1), as the carrier of transporting pyruvate into mitochondria, linked the glycolysis and TCA cycle, which would affect the energy production. However, the specific role of MPC1 on tumor metastasis in CRC remains unexplored. Here, by data mining of genes involved in pyruvate metabolism using the TCGA dataset, we found that MPC1 was significantly downregulated in CRC compared to nontumor tissues. Similar MPC1 expression pattern was also found in multiple GEO datasets. IHC staining in both human sample and AOM/DSS induced mouse CRC model revealed significant downregulation of MPC1. What is more, we found that MPC1 expression was gradually decreased in normal tissue, primary CRC, and metastasis CRC. Additionally, poor prognosis emerged in the MPC1 low expression patients, especially in patients with metastasis. Following, functional tests showed that MPC1 overexpression inhibited the motility of CRC cells *in vitro* and MPC1 silencing enhanced liver metastases *in vivo*. Furthermore, we uncovered that decreased MPC1 activated the Wnt/ β -catenin pathway by promoting nuclear translocation of β -catenin to mediate the expression of MMP7, E-cadherin, Snail1, and myc. Collectively, our data suggest that MPC1 has the potential to be served as a promising biomarker for diagnosis and a therapeutic target in CRC.

1. Introduction

Colorectal carcinoma (CRC), as one of the most common gastrointestinal malignancies, has developed the world's fourth most deadly cancer with a high rate of incidence and mortality [1, 2]. Liver metastasis, which is the most common form for CRC metastasis, is the leading cause of high mortality for this severe malignancy [2]. However, few clinical prevention and treatment measures could be available for tumor metastasis. Therefore, it is really urgent to develop new biomarkers and explore the underlying mechanism for CRC metastasis, and eventually develop new therapeutic strategies for CRC patients.

During cancer progression, metabolic reprogramming with increasing glucose utilization is termed as Warburg effect, which is accompanied by altered pyruvate and mitochondrial metabolism [3]. The fate of pyruvate is the core manifestation to distinguish normal cells and tumor cells through metabolism. In normal cells, pyruvate was used for efficient ATP production directly into mitochondria. However, pyruvate was converted into lactate in cytosol despite of normoxic and hypoxic conditions in cancer cells [4]. This may be due to the impaired process of pyruvate from the cytosol into the mitochondrial matrix, which is a critical metabolic step linking glycolysis and mitochondrial oxidative phosphorylation. The Mitochondrial Pyruvate Carrier (MPC), a

multimeric complex containing two distinct proteins MPC1 and MPC2, which is located in the inner mitochondrial membrane, is responsible for efficient mitochondrial pyruvate uptake [5]. Loss of MPC expression or activity blocks pyruvate entry into the TCA cycle, which results in a metabolism switch to increase glycolysis and the compensatory usage of glutamine [6, 7].

Existed studies have reported that MPC1 was related with immunoregulation, stemness, metabolism, cellular morphology, etc. [3, 8–10]. Currently, the important role of MPC1 was uncovered in several tumors. In CRC and esophageal squamous cell carcinoma, decreased MPC1 results in accelerated aerobic glycolysis and malignant progression [11, 12]. In lung adenocarcinoma, MPC1 deficiency accelerates lung adenocarcinoma progression through the STAT3 pathway [13]. In prostate cancer, MPC1 was reported to be involved in stemness and metabolism which regulated by COUPTFII [14, 15]. In renal cell carcinoma, hypoxia-induced loss of MPC1 enhanced the expression of MMP7 and MMP9 to promote cell invasion [16]. Collectively, these data suggested that MPC1 maybe serves as a suppressor to disrupt tumor malignancy. However, whether MPC1 is involved in CRC metastasis and the underlying mechanisms remain to be illustrated.

In the present study, we figured out the relationship between the MPC1 expression and CRC liver metastasis. We identified that decreased MPC1 was closely correlated with patient's metastasis, as well as led to poor prognosis. Functionally, MPC1 overexpression could attenuate the migration and invasion capacities of CRC cells both *in vitro* and *in vivo*. Mechanically, MPC1 suppressed CRC metastasis through mediating the Wnt/ β -catenin signaling. Thus, our finding firstly revealed a critical role of MPC1 in CRC liver metastasis.

2. Materials and Methods

2.1. Data Mining. Seven GEO datasets (GSE21510, GSE5206, GSE20916, GSE9348, GSE89393, GSE67675, and GSE4183) and TCGA were used to analyze the MPC1 expression pattern in CRC. The primary data for TCGA datasets were downloaded <https://www.cancer.gov/>. The primary data for GEO datasets were downloaded at <https://www.ncbi.nlm.nih.gov/geo>. The OncoLnc database (<http://www.oncolnc.org/>) was used to detect the prognostic value of MPC1 in the TCGA cohort.

2.2. Patients and Clinical Specimens. In our study, a total of 392 patients containing paired CRC tissues and adjacent nontumor tissues were enrolled from the Department of Gastrointestinal Surgery, Renji Hospital, School of Medicine, Shanghai Jiao Tong University. Among them, 30 cases of liver metastases were collected. And only 225 cases were available with complete follow-up data for survival analysis. Informed consents were signed by all patients. The research was approved by the Research Ethics Committee of Renji Hospital and carried out in accordance with ethical standards as formulated in the Helsinki Declaration.

TABLE 1: Sequences of primers used for real-time PCR.

Primer	Sequence 5'-3'
MMP7 forward	GAGTGAGCTACAGTGGGAACA
MMP7 reverse	CTATGACGCGGGAGTTTAACAT
E-cadherin forward	ATGAGTGTCCCCGGTATCTTC
E-cadherin reverse	ACGAGCAGAGAATCATAAGGCG
Snail1 forward	GTATCCAGAGCTGTTTGGGA
Snail1 reverse	AACATTTTCTCCCAGGCC
Myc forward	ATCACAGCCCTCACTCAC
Myc reverse	ACAGATTCCACAAGGTGC
GAPDH forward	CTGGGCTACACTGAGCACC
GAPDH reverse	AAGTGGTCGTTGAGGGCAATG

2.3. Cell Culture and Cell Transduction. Human CRC cell lines (HCT116, HT29, SW620, RKO, SW480, and Lovo) and mouse CRC cell line MC38 were gained from the Cell Bank of the Chinese Academy of Sciences (Shanghai, China). All cells were cultured in DMEM medium supplemented with 10% fetal bovine serum and 1% antibiotics at 37°C in a humidified incubator with 5% CO₂.

MC38 cells were transfected with lentivirus containing a luciferase reporter plasmid. Stable transfection cells were screened with 5 μ g/ml blasticidin for 14 days, which termed MC38-Luc. In addition, one short hairpin RNA (shRNA) sequence against MPC1 was packaged as lentivirus and transfected into MC38-luc cells. Lovo and SW480 were transfected with lentivirus containing full-length human MPC1 cDNA or empty vehicle control. Stable transfection cells were screened under 2 μ g/ml puromycin for 14 days and verified by western blot. In those assays, all lentiviral transfections were performed in the presence of 6 μ g/ml polybrene.

2.4. Immunohistochemical (IHC). The protocol of this assay and quantify the MPC1 protein expression level were performed according to previously reported [17]. Primary antibodies used as follows: MMP7 (YT2663, Immunoway), E-cadherin (14472, CST), Snail1 (ab53519, Abcam), and MYC (YP0861, Immunoway).

2.5. Cellular Immunofluorescence. Assays were performed according to the previous description [18]. Briefly, cells were incubated with antibodies against β -catenin (ab32572, Abcam) and incubated with Alexa 488-conjugated secondary antibody (1:200). The nuclei were stained with 4',6-diamidino-2-phenylindole (DAPI).

2.6. Western Blotting. Whole-cell lysates or nuclear protein was extracted using a protein extraction buffer (Beyotime, Shanghai, China) or nucleoprotein extraction kit (Sangon Biotech, C500009), respectively. Proteins were resolved by SDS-PAGE and transferred onto nitrocellulose (NC) membranes using standard methods. Primary antibodies used as follows: MPC1 (ab74871, Abcam), β -catenin (ab32572, Abcam), lamin A/C (ab8984, Abcam), and GAPDH (ab9485, Abcam). Species-specific secondary antibodies used

TABLE 2: Related enzyme and carrier of pyruvate analyzed in this study.

Gene	Description	Location
PDHA1	Pyruvate dehydrogenase (lipoamide) alpha 1	Mitochondrion matrix.
PDHB	Pyruvate dehydrogenase (lipoamide) beta	Mitochondrion matrix.
PDK4	Pyruvate dehydrogenase kinase, isozyme 4	Mitochondrion matrix.
PDHX	Pyruvate dehydrogenase complex, component X	Mitochondrion matrix.
MPC2	Mitochondrial pyruvate carrier 2	Mitochondrion inner membrane
PDK2	Pyruvate dehydrogenase kinase, isozyme 2	Mitochondrion matrix.
PDK1	Pyruvate dehydrogenase kinase, isozyme 1	Mitochondrion matrix.
PDK3	Pyruvate dehydrogenase kinase, isozyme 3	Mitochondrion matrix.
MPC1	Mitochondrial pyruvate carrier 1	Mitochondrion inner membrane
PC	Pyruvate carboxylase	Mitochondrion matrix.
PDP1	Pyruvate dehydrogenase phosphatase catalytic subunit 1	Mitochondrion matrix.
P DPR	Pyruvate dehydrogenase phosphatase regulatory subunit	Mitochondrion matrix.
PDHA2	Pyruvate dehydrogenase (lipoamide) alpha 2	Mitochondrion matrix.
PDP2	Pyruvate dehydrogenase phosphatase catalytic subunit 2	Mitochondrion matrix.
PKLR	Pyruvate kinase, liver and RBC	Mitochondrion

as follows: IRDye 680 Goat anti-Mouse IgG (LI-COR) and IRDye 800 Goat anti-rabbit IgG (LI-COR).

2.7. Real-Time PCR. Total RNA was extracted using Trizol (Takara) according to the manufacturer's instructions. cDNA was synthesized using the PrimeScript reverse transcription-polymerase chain reaction (RT-PCR) kit (Takara). The qPCR was performed using SYBR Green Master Mix (Roche). The $2^{-\Delta\Delta CT}$ method was used to analyze the data and GAPDH was used as a loading control. The primer sequences are listed in Table 1.

2.8. Liver Metastasis Model. This study was performed in accordance with the recommendations in the Guide for the Care and Use of Laboratory Animals and relevant Chinese laws and regulations. The protocol was approved by the Institutional Animal Care and Use Committee (IACUC) of Shanghai Jiao Tong University. The MC38 cells transplanting luciferase-expressing were injected into the spleens of C57BL/6N mice ($n = 5$) with a concentration of 10^6 cells/mouse. Two weeks later, the mice were killed and the liver metastasis tissues were harvested.

2.9. Luciferase Reporter Assay. The protocols of this assay were operated in accordance with previous reported [18]. 100 ng TOP reporter plasmid (Wnt/ β -catenin signaling) or 100 ng FOP reporter plasmid (negative control of Wnt/ β -catenin signaling) and 10 ng Renilla were mixed and transfected into CRC cells using Lipofectamine 2000. Dual-luciferase reporter assay system (Promega) was used to detect the firefly and Renilla luciferase activities.

3. Statistical Analyses

Data are shown as means \pm SD. SPSS 20.0 (Chicago, IL, USA) and GraphPad Prism 5 software were used to manipulate statistical analyses. Kaplan-Meier method was used to calculate cumulative survival time. The chi-square test or Student's

t-test was used for comparison between groups. $P < 0.05$ was considered as statistically significant.

4. Results

4.1. MPC1 Expression Was Aberrantly Decreased in CRC. Pyruvate is a pivotal intermediate in the process of cell metabolism, which connects glycolysis and the TCA cycle. To determine the potential maladjustment genes involved in pyruvate metabolism, which is located in mitochondria, as shown in Table 2, we analyzed the TCGA dataset containing 50 CRC and their normal counterparts. The results showed that multiple genes are significantly upregulated or downregulated in CRC (T) tissues compared to normal colon (N). Notably, MPC1 had a log₂ (fold change) less than -1 (Figures 1(a) and 1(b)). As known to us, pyruvate translocation from the cytoplasm to the mitochondria is the first step into the TCA cycle, which needs MPC1/MPC2 heterodimer. In the analysis, no significant change was found in MPC2. Therefore, MPC1 was selected for further study. The expression pattern of MPC1 was further analyzed in five independent GEO datasets (GSE21510, GSE5206, GSE20916, GSE9348, and GSE4183). Consistently, we found that MPC1 was downregulated with statistical difference in CRC tissues (Figure 1(c)) and inflammatory tissue (Supplementary Figure 1) in comparison to their normal counterparts. Meanwhile, we found decreased MPC1 expression in human CRC tissues compared to their normal counterparts (Figure 1(d)). In addition, a similar phenomenon was revealed in AOM/DSS induced mouse CRC models (Figure 1(e)). Then, we evaluated the protein level of MPC1 used a tissue microarray containing 392 matching cancer and corresponding adjacent nontumor tissues which subjected IHC staining. The expression of MPC1 was scored as “-, +, ++, +++” based on the staining area and intensity (Figure 1(f)). We found that more lower MPC1 expression (score as “-” and “+”) was presented in CRC

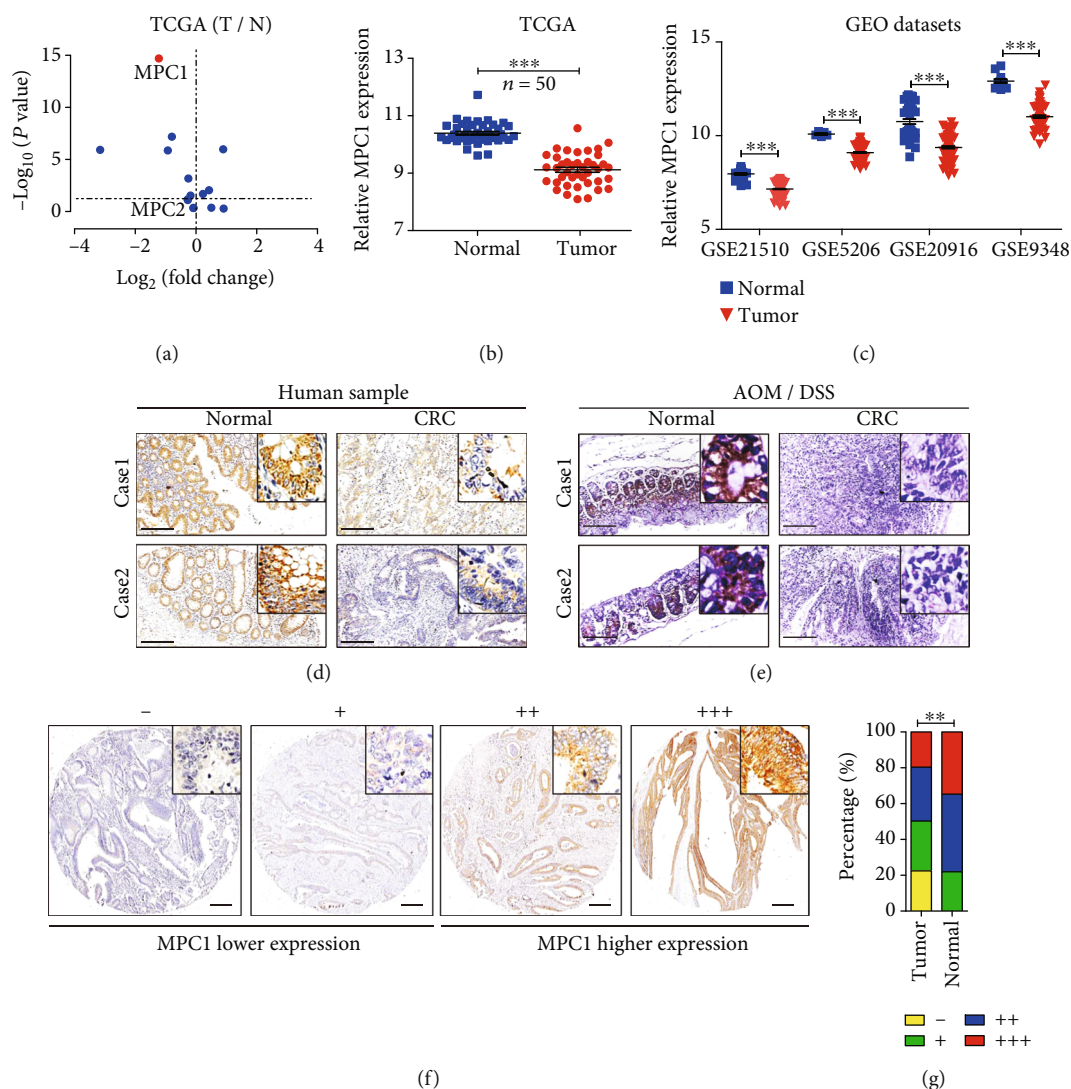


FIGURE 1: Expression pattern of MPC1 in CRC. (a) Volcano plot showed fold changes (x -axis) and corresponding P values (\log_{10} , y -axis) of pyruvate metabolism-related genes located in mitochondria analyzed in the TCGA dataset between paired normal and CRC samples (Student's t -test). (b) The comparison of MPC1 expression in tumor and matched normal tissues using the TCGA dataset (Student's t -test, $***P < 0.001$). (c) Expression analysis of MPC1 in tumors and corresponding normal tissue using four independent GEO datasets (GSE21510, GSE5206, GSE20916, and GSE9348) (Student's t -test, $***P < 0.001$). (d) IHC staining of MPC1 expression in matched CRC tumor and nontumor tissues (Scale bar: $200 \mu\text{m}$). (e) IHC staining of MPC1 expression in the AOM/DSS induced CRC mouse models and control animal (Scale bar: $200 \mu\text{m}$). (f) Representative IHC staining of MPC1 expression in tissue microarray from the Ren Ji cohort which contained CRC patients and paired adjacent normal tissue ($n = 392$), the tumor tissues were divided into two groups based on the expression level which scored as "-", "+", "++", "+++" (Scale bar: $500 \mu\text{m}$). (g) The percentage of tissue displaying different expression level of MPC1 in CRC tumor and adjacent nontumor tissues (Fisher's exact test, $**P < 0.01$).

tissues (Figure 1(g)). Overall, these results revealed that MPC1 was disrupted during CRC.

4.2. Decreased MPC1 Enhanced Tumor Metastasis Capability and Predicated Poor Prognosis in CRC. It is well known that CRC is one of the most malignant tumors given its strong metastasis ability, so we tried to figure out whether the MPC1 expression was correlated with metastasis. We found that lower MPC1 expression was closely correlated with metastasis ($P = 0.009$), lymph node invasion ($P = 0.003$), and TNM stage ($P = 0.001$), which revealed by the analysis between the clinical significance and MPC1 expression in

CRC (Table 3). Next, to illuminate the expression pattern of MPC1 in different process of CRC, data mining was carried out by two independent GEO datasets (GSE21510 and GSE89393), which contained normal tissue, primary CRC, and metastatic lesion in the liver (M-CRC). As shown in Figures 2(a) and 2(b), MPC1 expression was gradually down-regulated in patients with an increase in metastasis ability. A similar result was found in mice cells CT26 with high liver metastasis (HM-CT26) or poor liver metastasis (PM-CT26) (Figure 2(c)), which isolated by in vivo selection in an orthotopic mouse model of colon cancer metastasis to the liver. Further analysis showed that MPC1 protein expression was

TABLE 3: Clinicopathological correlation of MPC1 expression in the Ren Ji CRC cohort.

Clinicopathological feature	Expression of MPC1		P value (χ^2 test)
	Low	High	
Age (years)			
<60	95	96	0.766
≥60	103	98	
Gender			
Male	112	120	0.287
Female	86	74	
Metastasis			
Yes	52	30	0.009
No	146	164	
Lymph node invasion			
Yes	106	75	0.003
No	91	119	
Tumor size			
<5 cm	99	108	0.388
≥5 cm	94	86	
TNM stage			
I	15	20	0.001
II	58	92	
III	74	52	
IV	51	30	
KRAS mutation			
Mutation	33	40	0.246
No mutation	51	43	

gradually downregulated in normal tissue, primary CRC, and liver metastasis CRC (CRLM) tissues (Figure 2(d)). Furthermore, survival analysis showed that patients with lower MPC1 expression had a worse outcome compared to the patients with higher MPC1 expression using the TCGA cohort (Figure 2(e)) and Ren Ji cohort (Figure 2(f)). Additionally, among patients with metastasis, worse prognosis was emerged in the MPC1 low cases (Figure 2(g)), while no significant association was observed in patients without metastasis (Figure 2(h)).

4.3. MPC1 Overexpression Impaired CRC Cells Motility Both In Vitro and In Vivo. To evaluate the role of MPC1 on the motility of CRC cells, the transwell assay was performed. Firstly, we examined low MPC1 protein expression in human and high MPC1 protein expression in mouse MC38 CRC cells by western blot (Figure 3(a)). MPC1-overexpressing stable cell lines were established using a lentivirus carrying the MPC1 gene in Lovo and SW480 cells. And the overexpression efficiency was confirmed by immunoblots (Figure 3(b)). MPC1 knockdown in Luc-MC38 cells were established and verified by WB (Figure 3(c)). MPC1 overexpression exhibited significantly weaker migration and invasion ability than the control cells in both Lovo (Figure 3(d)) and SW480 (Figure 3(e)) cells. Following, the liver metastasis

model of CRC was established by spleen orthotopically injecting MC38 cells transplanting luciferase-expressing, which would simulate MC38 metastasis to the liver through splenic vein-portal vein. The results revealed that the MPC1 knockdown promoted MC38 cells metastasis to the liver through detecting the luminescence intensity monitored by bioluminescence imaging (Figure 3(f)). Notably, the number of metastatic liver nodules in the MPC1 silencing group was smaller than that in the control group (Figure 3(g)). Histological examination also proved that MPC1 knockdown decreased the metastatic potential of CRC *in vivo* (Figure 3(g)).

4.4. Decreased MPC1 Activated the Wnt/ β -Catenin Pathway by Promoting Nuclear Translocation of β -Catenin. To further explore the underlying mechanism of MPC1-mediated inhibition of CRC metastasis, the TCGA database was used to perform GSEA analysis. The results indicated that MPC1 was involved in the Wnt/ β -catenin signaling when set the mRNA expression median as a cutoff (Figure 4(a)). And dual-luciferase reporter gene assay revealed that MPC1 overexpression obviously inhibited the activity of Wnt/ β -catenin pathway (Figure 4(b)), which confirmed the result above. We then tested the distribution changes of β -catenin in nuclear and cytoplasmic, which was a crucial step in Wnt/ β -catenin pathway. As shown in Figure 4(c), no significant difference was emerged in the total amount of β -catenin between MPC1 overexpression cells and the control cells (Figure 4(c)). However, obviously decreased distribution of nuclear β -catenin was presented in MPC1 overexpression cells compared to that in the control cells, as revealed by the stronger gray corresponding to β -catenin (Figures 4(c) and 4(d)). Consistently, immunofluorescence (IF) staining showed that MPC1 overexpression weakened nuclear β -catenin localization in both Lovo and SW480 cells when compared to control cells (Figures 4(e) and 4(f)). A similar phenomenon was observed in mouse liver metastasis tissues by IHC (Figure 4(g)). Following, qPCR analyses displayed some downstream target genes of β -catenin, such as MMP7, E-cadherin, Snail1, and MYC. Obviously increased in E-cadherin and decreased in MMP7, Snail1, and MYC were observed after the MPC1 overexpression in both Lovo and SW480 cells compared to that in the control cells (Figures 4(h) and 4(i)). Meanwhile, the opposite trend was observed in MC38 cell after MPC1 knockdown (Figure 4(j)), and similar results were observed in mouse liver tissue detected by IHC (Figures 4(k)–4(n)). Taken together, the data above indicated that MPC1 mediated CRC cell metastasis through the Wnt/ β -catenin pathway.

5. Discussion

Accumulating evidences have shown that reprogrammed energy metabolism conduces to the tumor malignant properties, including enhanced CRC liver metastatic capacity [19–21]. Mitochondria, as the primary site of energy production, regulate the pyruvate metabolism under both physiologic and pathologic conditions. The first step of the TCA cycle is mediated by MPC, which transports pyruvate into

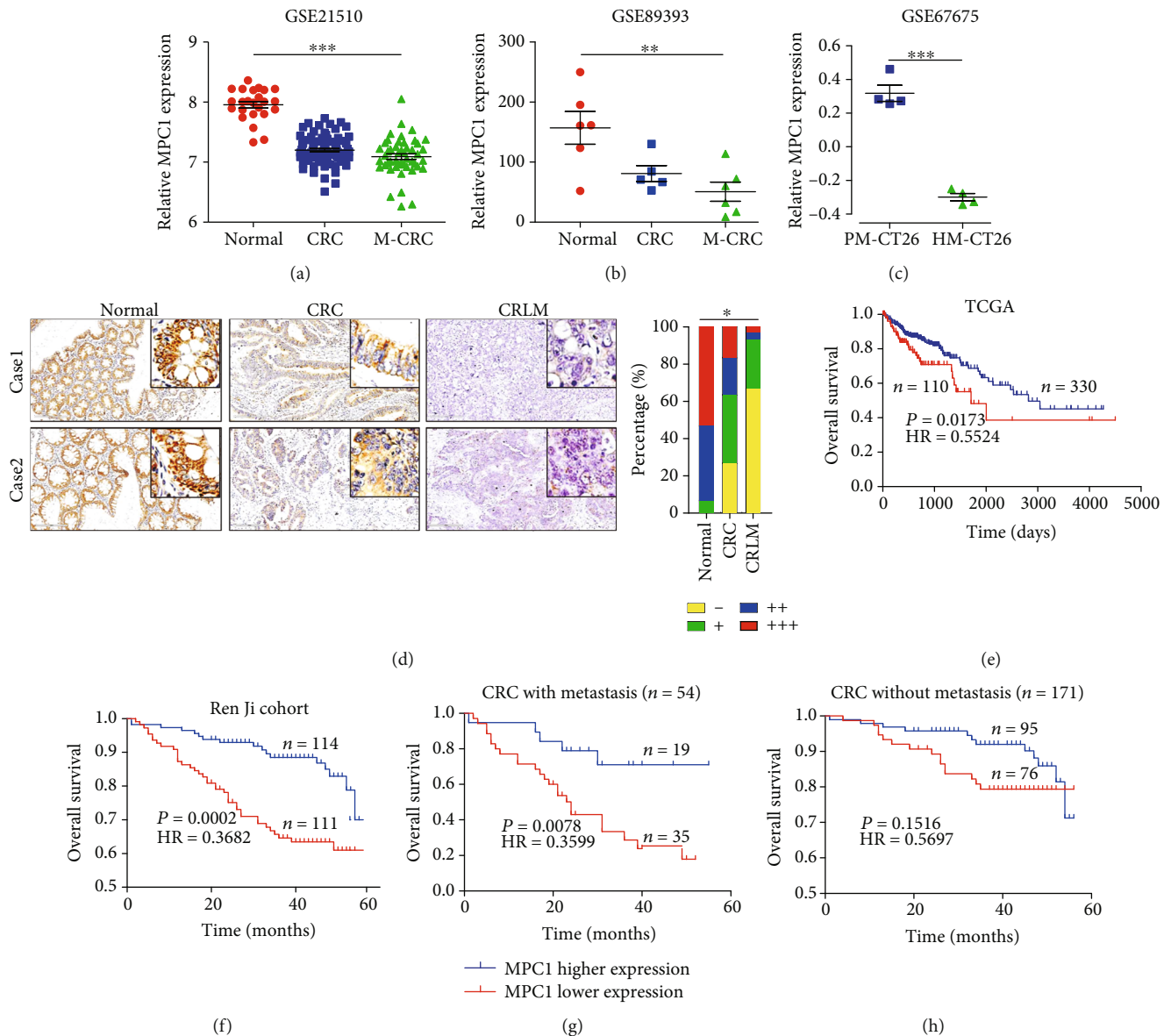


FIGURE 2: Decreased MPC1 enhances tumor metastasis and predicts poor prognosis in CRC. (a, b) Data mining showed MPC1 expression was gradually decreased in normal tissue, primary CRC, and liver lesion of metastatic CRC (M-CRC) from two independent GEO datasets (One-way ANOVA, A, GSE21510, $***P < 0.001$; B, GSE89393, $**P < 0.01$). (c) Data from GSE67675 revealed that MPC1 expression was lower in high liver metastasis CT26 cells (HM-CT26) than that in poor liver metastasis CT26 cells (PM-CT26) (Student's *t*-test, $***P < 0.001$). (d) Gradually decreased MPC1 expression was presented in normal tissue, primary CRC, and liver metastasis CRC (CRLM) tissue (Scale bar: $200\ \mu\text{m}$) ($n = 30$, Fisher's exact test, $*P < 0.05$). (e) Kaplan-Meier overall survival (OS) curves in the TCGA dataset of CRC patients according to the mRNA expression of MPC1, the lower quartile value of expression was utilized as a cut-off (log-rank test, $P = 0.0173$). (f) Kaplan-Meier OS curve for the MPC1 expression in the Ren Ji cohort (log-rank test, $P = 0.0033$). (g) Kaplan-Meier OS curve for the MPC1 expression in patients with metastasis (log-rank test, $P = 0.0078$). (h) Kaplan-Meier OS curve for the MPC1 expression in patients without metastasis (log-rank test, $P = 0.1516$).

mitochondrial from cytoplasm [3]. In the beginning, TCGA was used to analyze the relative genes involved in pyruvate metabolism, which is located in mitochondria. The results revealed that MPC1 expression was significantly downregulated in CRC tissues. Meanwhile, the GEO datasets analysis, as well as, IHC staining on CRC patients' tissue and mouse models confirmed this trend. These phenomena may indicate that loss of MPC activity enhanced tumorigenic glucose

utilization by blocking mitochondrial pyruvate uptake and oxidation. Interestingly, in the course of data analysis, we found that the expression of MPC1 was decreased at the stage of intestinal inflammation, which was not different from that in tumor tissue. MPC1 has been reported to be involved in immune regulation of peripheral T cell homeostasis through metabolic regulation [8]. And a decrease in MPC1 was found at the earliest stages of CRC [22]. Hence,

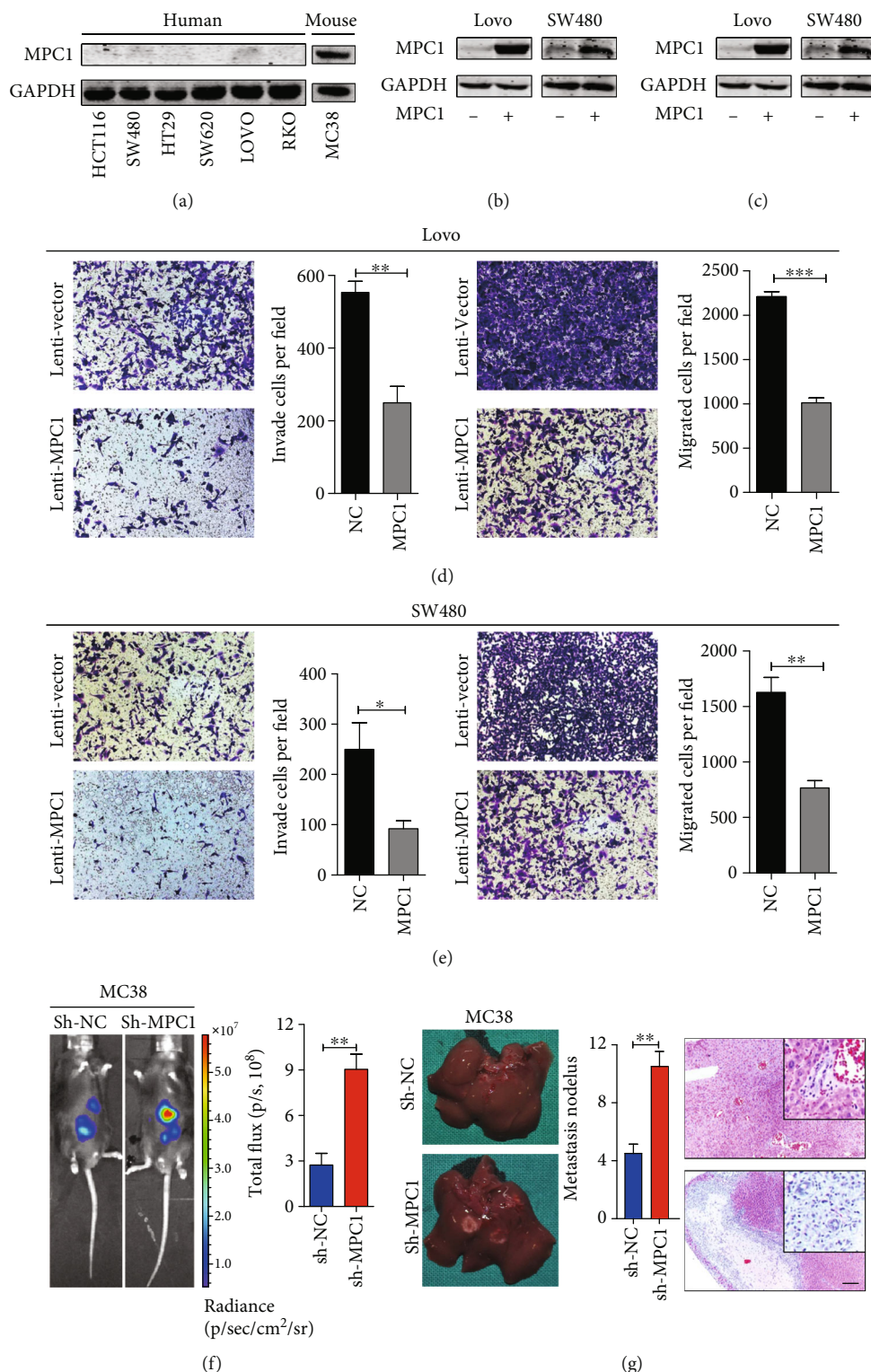


FIGURE 3: MPC1 overexpression inhibits the motility of CRC cells *in vitro* and *in vivo*. (a) MPC1 expression in human and mouse CRC cell lines examined by western blot. GAPDH serves as loading control. (b) MPC1 overexpression in Lovo and SW480 cells. (c) MPC1 silencing by sh-RNA-MPC1 in mouse MC38 cells. (d, e) Transwell assays showed that upregulated MPC1 suppressed the invasion and migration ability of Lovo (d) and SW480 (e) cells. Quantification of invaded and migrated cells was performed for five randomly selected fields, values are means \pm SD. (f) Representative bioluminescence photograph of mice spleen implanted with luciferase-expressing MC38 cells treated with sh-MPC1 or control vector, total flux was quantified by the IVIS system to verify the ability of liver metastasis. (g) Representative image of liver metastases and quantified by the nodules in mice inoculated with MC38 cells treated with sh-MPC1 or control vector, as well as representative images of H&E staining of the liver metastatic lesions. Scale bar: 100 μ m. Student's *t*-test, **P* < 0.05, ***P* < 0.01, ****P* < 0.001.

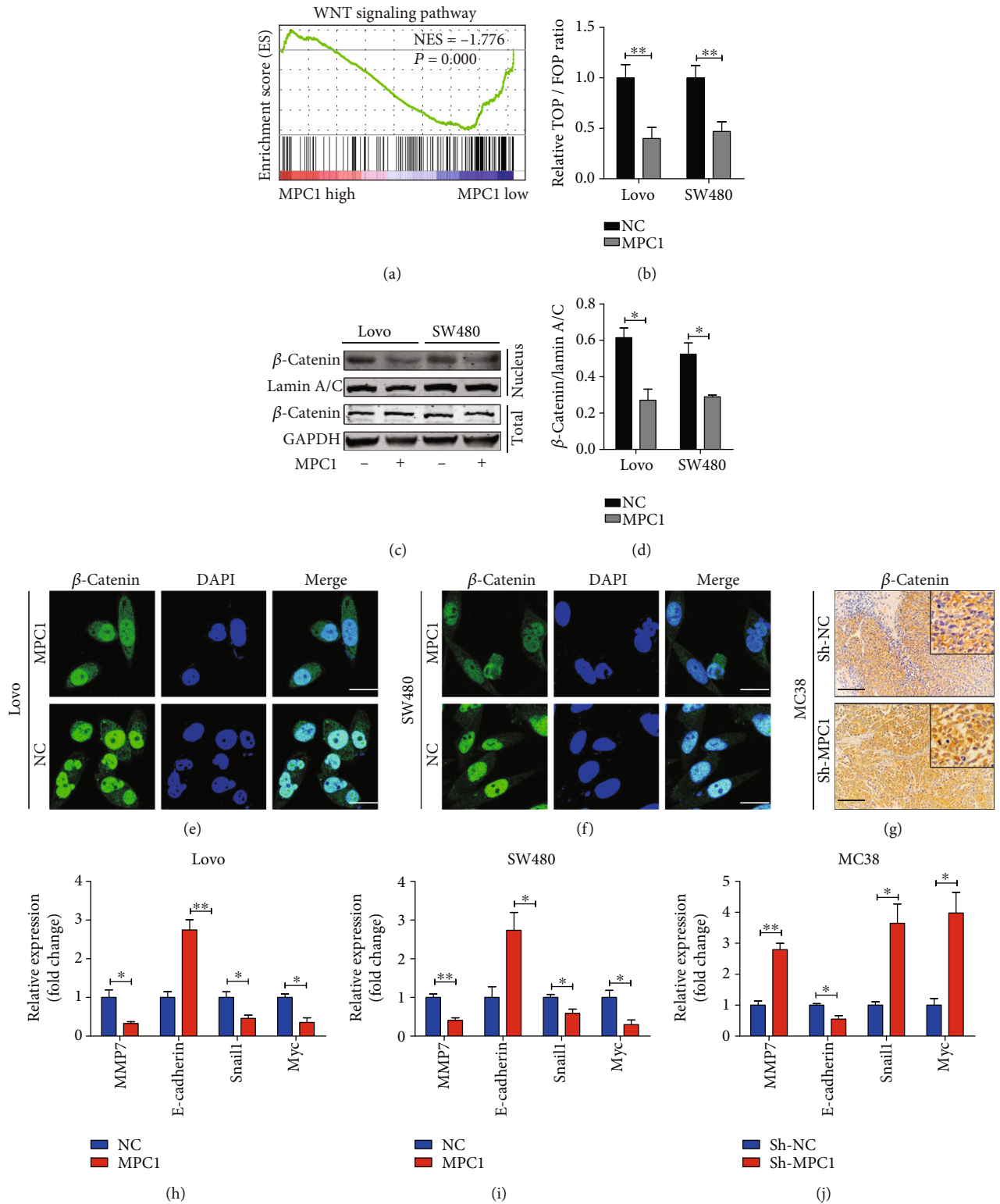


FIGURE 4: Continued.

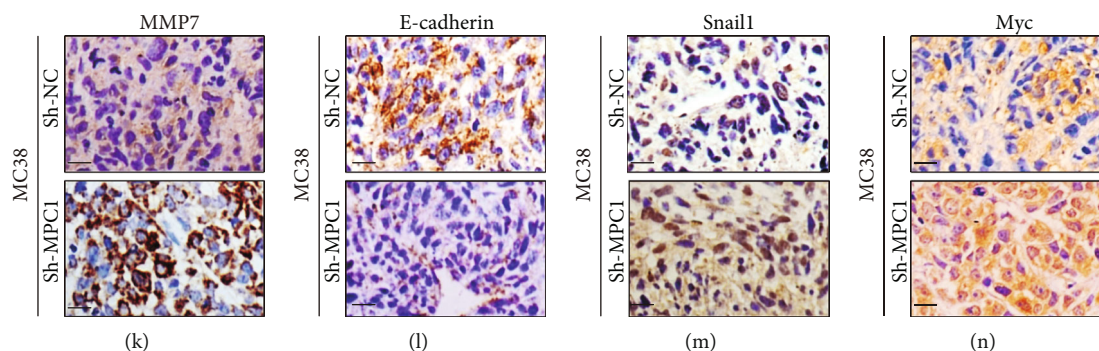


FIGURE 4: Decreased MPC1 activates the WNT/ β -catenin pathway by promoting nuclear translocation of β -catenin. (a) GSEA analysis of MPC1 expression in CRC using the TCGA dataset. NES: Normalized Enrichment Score. (b) Luciferase reporter gene assay of CRC cells treated with MPC1 overexpression or not. (c) The expression of total β -catenin and nuclear β -catenin was detected in control and MPC1-overexpression CRC cells, respectively. GAPDH and lamin A/C were used as the loading control of total and nuclear protein, respectively. (d) The gray value analysis of nuclear β -catenin in MPC1-overexpression cells and control cells. (e, f) MPC1 overexpression could inhibit the nuclear translocation of β -catenin in CRC cells. Scale bar: 100 μ m. (g) IHC staining of β -catenin in mouse liver metastatic lesions inoculated with MC38 cells treatment with sh-MPC1 or control vector. Scale bar: 200 μ m. (h, i) Relative mRNA expression level of β -catenin target genes in CRC cells with MPC1 overexpression or control vector. (j) Relative mRNA expression level of β -catenin target genes in MC38 cells with sh-MPC1 or control vector. (k–n) Relative protein expression level of β -catenin target genes in mouse liver tissue detected by IHC. Scale bar: 50 μ m. Student's *t*-test, * $P < 0.05$, ** $P < 0.01$.

we suspect that MPC1 is involved in bowel inflammation to tumorigenesis. And more studies need to be devised to illustrate this process.

Following, in the analysis between the clinical significance and MPC1 expression in CRC, we found that MPC1 expression was especially correlated with metastasis. Inspired by this, we detected the MPC1 expression pattern in normal tissue, primary CRC, and metastasis CRC by GEO datasets and patients' tissue. All results revealed that gradually down-regulated MPC1 was in patients with an increase in metastasis ability. Survival analysis indicated that worse outcome was presented in patients with lower MPC1 expression, especially in patients with metastasis. Additionally, function assays verified that MPC1 overexpression could attenuate the migration and invasion capacities of CRC cells *in vitro* and MPC1 knockdown could enhance the metastasis capacity *in vivo*. And existing studies have revealed that the MPC1 was participated in metastatic dissemination of PGC1 α -transduced cholangiocarcinoma through elevating reactive oxygen species (ROS) production [10]. Besides, MPC inhibitor UK5099 treatment could trigger strong invasive capacity through blocking pyruvate translocation into the mitochondria so as to attenuate mitochondrial oxidative phosphorylation and trigger aerobic glycolysis [12]. These phenomena together with our results indicate that MPC1 could act as a tumor suppressor through inhibiting tumor metastasis. And existing studies have shown that MPC1 could alter the maintenance and fate of stem cells through regulating cancer metabolism in CRC [11]. However, the relationship between the metabolism and tumor metastasis regulated by MPC1 was not being mentioned. Thus, further evidence should be received to confirm this.

Subsequently, the underlying mechanism of MPC1 in regulating metastasis was explored. For this purpose, GSEA analysis was performed. The results indicated that MPC1 was involved in the Wnt/ β -catenin signaling. The next series of experiments also confirmed that MPC1 could mediate the

WNT/ β -catenin pathway by redistribution of β -catenin. Previous reports showed that cytoplasmic β -catenin phosphorylated in N-terminally localized to sites of cell-cell contact is associated with E-cadherin and was required for intact cell-cell adhesions, without any change detected in the levels of total β -catenin [23–25]. Simultaneously, cell–cell adhesion based on cadherin binding with β -catenin limited Wnt signals [24]. In addition, β -catenin was reported to interact with USP9x to inhibit the degradation of β -catenin through the deubiquitination of β -catenin in breast cancer [26]. A constitutive IRS1 and β -catenin protein interaction activated MYC expression in Acute Lymphoblastic Leukemia Cells [27]. In HCC, β -catenin was reported to interact with Yap1 to lead to rapid tumorigenesis [28]. Hence, it is reasonable to guess that accumulated cytoplasmic β -catenin maybe crosstalk with other genes or involved in other biological processes. What is more, some downstream target genes of β -catenin, such as MMP7, E-cadherin, Snail1, and myc, were changed in expression. As known to us, MMP-7 is a member of the proteolytic enzyme family, which promotes the invasion and metastasis of tumor cells by degrading the basement membrane and extracellular matrix [29]. And previous studies had evidenced for involvement of MMP-7 activation in colorectal cancer liver metastases [30, 31]. E-cadherin and Snail1 were considered as the epithelial-mesenchymal transition (EMT) marker, which was involved in metastasis of malignant tumor [32]. Moreover, E-cadherin was reported to be involved in cell-cell junction to regulate cancer invasion and metastasis [33, 34]. And the GSEA analysis also revealed that MPC1 could affect the cell-cell contacts (data not shown). As described previously, MMP-7 could facilitate morphological transition by cleaving E-cadherin [35]. The communication between the cells is disrupted when E-cadherin was shredded, leading to destructed cell adhesion and induction of EMT, followed by increased cell migration [36]. Inspired by this, we assumed that MPC1 could mediate tumor cell motility through affecting MMP7 activity, cell-cell

contacts, and EMT. However, further studies need to be performed to clarify the detailed underlying mechanisms.

6. Conclusions

In conclusion, we firstly demonstrated that decreased MPC1 was closely correlated with patient's metastasis, as well as led to poor outcome. Moreover, MPC1-driven nuclear translocation of β -catenin contributed to CRC cell motility. This means that MPC1 has the potential to be a diagnostic biomarker and therapeutic target for metastasis patients.

Abbreviations

CRC: Colorectal carcinoma
MPC: Mitochondrial pyruvate carrier
EMT: Epithelial-mesenchymal transition
GSEA: Gene set enrichment analysis.

Data Availability

The data used to support the findings of this study are available from the corresponding author upon request.

Conflicts of Interest

All authors declare no conflicts of interest.

Authors' Contributions

Ya-Hui Wang and Guang-Ang Tian conceived and designed the study. Chun-Jie Xu and Kai-Xia Zhou obtained and organized the data. Guang-Ang Tian analyzed the data. Zhi-Gang Zhang and Jian-Ren Gu contributed reagents/materials/analysis tools. Xue-Li Zhang and Guang-Ang Tian wrote the manuscript. Guang-Ang Tian, Chun-Jie Xu, and Kai-Xia Zhou contributed equally to this work.

Acknowledgments

This work was supported by the National Natural Science Foundation of China (No. 81672358 to Zhi-Gang Zhang) and the Natural Science Foundation of Shanghai (No. 18ZR1436900 to Xueli-Li Zhang).

Supplementary Materials

"Supplementary Figure 1: expression analysis of MPC1 in normal, IBD, and tumor tissues using the GSE4183 dataset. One-way ANOVA was used to analyze the statistical differences between IBD, adenoma, and CRC tissues. ns: No significance. Student's *t*-test, ****P* < 0.001, ***P* < 0.01, **P* < 0.05." (Supplementary Materials)

References

- [1] H. Brody, "Colorectal cancer," *Nature*, vol. 521, no. 7551, 2015.
- [2] R. L. Siegel, K. D. Miller, S. A. Fedewa et al., "Colorectal cancer statistics, 2017," *CA: A Cancer Journal for Clinicians*, vol. 67, no. 3, pp. 177–193, 2017.
- [3] A. J. Rauckhorst and E. B. Taylor, "Mitochondrial pyruvate carrier function and cancer metabolism," *Current Opinion in Genetics & Development*, vol. 38, pp. 102–109, 2016.
- [4] M. G. Vander Heiden, L. C. Cantley, and C. B. Thompson, "Understanding the Warburg effect: the metabolic requirements of cell proliferation," *Science*, vol. 324, no. 5930, pp. 1029–1033, 2009.
- [5] S. Herzig, E. Raemy, S. Montessuit et al., "Identification and functional expression of the mitochondrial pyruvate carrier," *Science*, vol. 337, no. 6090, pp. 93–96, 2012.
- [6] C. Yang, B. Ko, C. T. Hensley et al., "Glutamine oxidation maintains the TCA cycle and cell survival during impaired mitochondrial pyruvate transport," *Molecular Cell*, vol. 56, no. 3, pp. 414–424, 2014.
- [7] T. Bender, G. Pena, and J. C. Martinou, "Regulation of mitochondrial pyruvate uptake by alternative pyruvate carrier complexes," *The EMBO Journal*, vol. 34, no. 7, pp. 911–924, 2015.
- [8] A. G. Ramstead, J. A. Wallace, S.-H. Lee et al., "Mitochondrial pyruvate carrier 1 promotes peripheral T cell homeostasis through metabolic regulation of thymic development," *Cell Reports*, vol. 30, no. 9, pp. 2889–2899.e6, 2020.
- [9] X. Zhou, Z. J. Xiong, S. M. Xiao et al., "Overexpression of MPC1 inhibits the proliferation, migration, invasion, and stem cell-like properties of gastric cancer cells," *Oncotargets and Therapy*, vol. 10, pp. 5151–5163, 2017.
- [10] D. Li, C. Wang, P. Ma et al., "PGC1 α promotes cholangiocarcinoma metastasis by upregulating PDHA1 and MPC1 expression to reverse the Warburg effect," *Cell Death & Disease*, vol. 9, no. 5, 2018.
- [11] J. C. Schell, K. A. Olson, L. Jiang et al., "A role for the mitochondrial pyruvate carrier as a repressor of the Warburg effect and colon cancer cell growth," *Molecular Cell*, vol. 56, no. 3, pp. 400–413, 2014.
- [12] Y. Li, X. Li, Q. Kan et al., "Mitochondrial pyruvate carrier function is negatively linked to Warburg phenotype *in vitro* and malignant features in esophageal squamous cell carcinomas," *Oncotarget*, vol. 8, no. 1, pp. 1058–1073, 2017.
- [13] H. Zou, Q. Chen, A. Zhang et al., "MPC1 deficiency accelerates lung adenocarcinoma progression through the STAT3 pathway," *Cell Death & Disease*, vol. 10, no. 3, 2019.
- [14] L. Wang, M. Xu, J. Qin et al., "MPC1, a key gene in cancer metabolism, is regulated by COUPTFII in human prostate cancer," *Oncotarget*, vol. 7, no. 12, pp. 14673–14683, 2016.
- [15] Y. Zhong, X. Li, D. Yu et al., "Application of mitochondrial pyruvate carrier blocker UK5099 creates metabolic reprogram and greater stem-like properties in LnCap prostate cancer cells *in vitro*," *Oncotarget*, vol. 6, no. 35, pp. 37758–37769, 2015.
- [16] X. P. Tang, Q. Chen, Y. Li et al., "Mitochondrial pyruvate carrier 1 functions as a tumor suppressor and predicts the prognosis of human renal cell carcinoma," *Laboratory Investigation*, vol. 99, no. 2, pp. 191–199, 2019.
- [17] G. A. Tian, C. C. Zhu, X. X. Zhang et al., "CCBE1 promotes GIST development through enhancing angiogenesis and mediating resistance to imatinib," *Scientific Reports*, vol. 6, no. 1, article 31071, 2016.
- [18] C. Xu, G. Tian, C. Jiang et al., "NPTX2 promotes colorectal cancer growth and liver metastasis by the activation of the canonical Wnt/ β -catenin pathway via FZD6," *Cell Death & Disease*, vol. 10, no. 3, 2019.
- [19] C. Soydal, N. O. Kucuk, D. Balci, E. Gecim, S. Bilgic, and A. H. Elhan, "Prognostic importance of the presence of early

- metabolic response and absence of extrahepatic metastasis after selective internal radiation therapy in colorectal cancer liver metastasis,” *Cancer Biotherapy & Radiopharmaceuticals*, vol. 31, no. 9, pp. 342–346, 2016.
- [20] Z. Wu, D. Wei, W. Gao et al., “TPO-induced metabolic reprogramming drives liver metastasis of colorectal cancer CD110+ tumor-initiating cells,” *Cell Stem Cell*, vol. 17, no. 1, pp. 47–59, 2015.
- [21] Q. He, H. Zhang, S. Yao et al., “A study on relationship between metabolic syndrome and colorectal cancer,” *Journal of BUON*, vol. 23, no. 5, pp. 1362–1368, 2018.
- [22] C. L. Bensard, D. R. Wisidagama, K. A. Olson et al., “Regulation of tumor initiation by the mitochondrial pyruvate carrier,” *Cell Metabolism*, vol. 31, no. 2, pp. 284–300.e7, 2020.
- [23] M. C. Faux, J. L. Coates, N. J. Kershaw, M. J. Layton, and A. W. Burgess, “Independent interactions of phosphorylated β -catenin with E-cadherin at cell-cell contacts and APC at cell protrusions,” *PLoS One*, vol. 5, no. 11, article e14127, 2010.
- [24] M. T. Maher, A. S. Flozak, A. M. Stocker, A. Chenn, and C. J. Gottardi, “Activity of the β -catenin phosphodestruction complex at cell–cell contacts is enhanced by cadherin-based adhesion,” *The Journal of Cell Biology*, vol. 186, no. 2, pp. 219–228, 2009.
- [25] S. Roura, S. Miravet, J. Piedra, A. García de Herreros, and M. Duñach, “Regulation of E-cadherin/catenin association by tyrosine phosphorylation,” *Journal of Biological Chemistry*, vol. 274, no. 51, pp. 36734–36740, 1999.
- [26] W. Ouyang, S. Zhang, B. Yang et al., “ β -catenin is regulated by USP9x and mediates resistance to TRAIL-induced apoptosis in breast cancer,” *Oncology Reports*, vol. 35, no. 2, pp. 717–724, 2016.
- [27] J. C. Fernandes, A. P. N. Rodrigues Alves, J. A. Machado-Neto et al., “IRS1/ β -catenin axis is activated and induces MYC expression in acute lymphoblastic leukemia cells,” *Journal of Cellular Biochemist*, vol. 118, no. 7, pp. 1774–1781, 2017.
- [28] J. Tao, D. F. Calvisi, S. Ranganathan et al., “Activation of β -catenin and Yap1 in human hepatoblastoma and induction of hepatocarcinogenesis in mice,” *Gastroenterology*, vol. 147, no. 3, pp. 690–701, 2014.
- [29] C. Gialeli, A. D. Theocharis, and N. K. Karamanos, “Roles of matrix metalloproteinases in cancer progression and their pharmacological targeting,” *The FEBS Journal*, vol. 278, no. 1, pp. 16–27, 2011.
- [30] Z. S. Zeng, W. P. Shu, A. M. Cohen, and J. G. Guillem, “Matrix metalloproteinase-7 expression in colorectal cancer liver metastases: evidence for involvement of MMP-7 activation in human cancer metastases,” *Clinical Cancer Research*, vol. 8, no. 1, pp. 144–148, 2002.
- [31] Y. J. Fang, Z. H. Lu, G. Q. Wang et al., “Elevated expressions of MMP7, TROP2, and survivin are associated with survival, disease recurrence, and liver metastasis of colon cancer,” *International Journal of Colorectal Disease*, vol. 24, no. 8, pp. 875–884, 2009.
- [32] M. Saitoh, “Involvement of partial EMT in cancer progression,” *Journal of Biochemistry*, vol. 164, no. 4, pp. 257–264, 2018.
- [33] W. K. Kim, Y. Kwon, M. Jang et al., “ β -catenin activation down-regulates cell-cell junction-related genes and induces epithelial-to-mesenchymal transition in colorectal cancers,” *Scientific Reports*, vol. 9, no. 1, article 18440, 2019.
- [34] M. Canel, A. Serrels, M. C. Frame, and V. G. Brunton, “E-cadherin-integrin crosstalk in cancer invasion and metastasis,” *Journal of Cell Science*, vol. 126, no. 2, pp. 393–401, 2013.
- [35] V. Noe, B. Fingleton, K. Jacobs et al., “Release of an invasion promoter E-cadherin fragment by matrilysin and stromelysin-1,” *Journal of Cell Science*, vol. 114, Part 1, pp. 111–118, 2001.
- [36] T. Maretzky, K. Reiss, A. Ludwig et al., “ADAM10 mediates E-cadherin shedding and regulates epithelial cell-cell adhesion, migration, and beta-catenin translocation,” *Proceedings of the National Academy of Sciences of the United States of America*, vol. 102, no. 26, pp. 9182–9187, 2005.

Research Article

Single-Cell Transcriptome Analysis Profile of Meniscal Tissue Macrophages in Human Osteoarthritis

Jingbin Zhou ^{1,2}, Zhihong Zhao ³, Chen He,² Feng Gao,² Yu Guo,³ Feng Qu,⁴
and Yujie Liu ¹

¹Medical School of Chinese PLA, Beijing 100853, China

²Chinese National Institute of Sports Medicine, Beijing 100061, China

³Department of Orthopedics, Beijing Second Hospital, Beijing 100031, China

⁴Department of Foot and Ankle Surgery, Beijing Tongren Hospital Affiliated to Capital Medical University, Beijing 100730, China

Correspondence should be addressed to Yujie Liu; liuyujie301@163.com

Received 5 May 2020; Revised 8 June 2020; Accepted 16 June 2020; Published 28 July 2020

Guest Editor: Zenghui Teng

Copyright © 2020 Jingbin Zhou et al. This is an open access article distributed under the Creative Commons Attribution License, which permits unrestricted use, distribution, and reproduction in any medium, provided the original work is properly cited.

Osteoarthritis (OA) has long been considered as a degenerative disease, but growing evidence suggests that inflammation plays a vital role in its pathogenesis. Unlike rheumatoid arthritis and other autoimmune diseases, inflammation in OA is chronic and, in relatively low grade, mainly mediated by the innate immune system, especially macrophages. However, due to its low abundance, there is a lack of systematic studies on macrophages in the OA condition. Here, we have used single-cell RNA sequencing analysis to gain insight into the heterogeneity and functional specialization of human knee macrophages. We also compared the gene expression profiles of macrophages in healthy people and OA patients and found the characteristic changes of special macrophages in the OA knee. We believe that this in-depth understanding of the basis of OA inflammation will bring hope for the development of new therapies.

1. Introduction

Osteoarthritis (OA) is a common joint degenerative disease, characterized by the progressive destruction of articular cartilage, involving the subchondral bone and the synovium. However, the pathological process of OA, especially the molecular mechanism, still needs to be understood [1]. Traditionally, OA has been considered as a noninflammatory disease [2]. With the deepening of research, more and more studies have shown that the immune system plays an important role in the progress of OA and is closely related with the pathological changes of articular cartilage and synovium [3, 4], which began to define OA as a low-grade inflammation state and explores the pathogenesis of OA from a perspective of the immune system [5, 6]. Therefore, a comprehensive study of its related immune cells and subtypes is required.

The knee is the most common site of OA and believed to be the price that humans pay for walking upright. The knee OA is initiated with the wear and tear of articular cartilage and the inevitable inflammation [7, 8], so the focus of research should be on the inflammation regression and the process of tissue repair. In these processes, tissue macrophages in the knee are crucial [9]. With strong plasticity, macrophages can be divided into M1 subgroups that trigger inflammation and release a large number of proinflammatory factors or M2 subgroups that suppress inflammation, reshape tissues, and release anti-inflammatory factors and growth factors [4, 10]. However, recent studies show that M1 and M2 subpopulations may only be two extreme types of differentiation and macrophages may be reprogrammed according to their microenvironment [11]. The latest animal experiments have found a special type of macrophage that

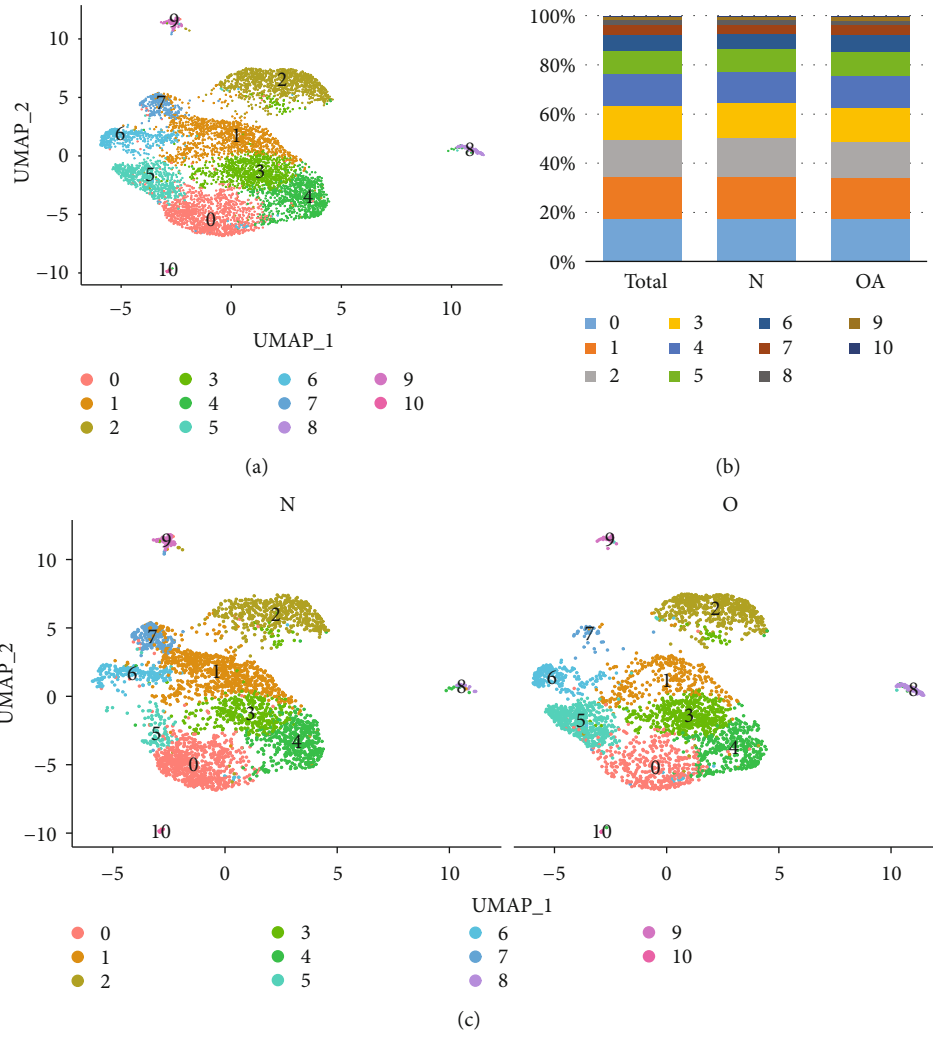


FIGURE 1: Continued.

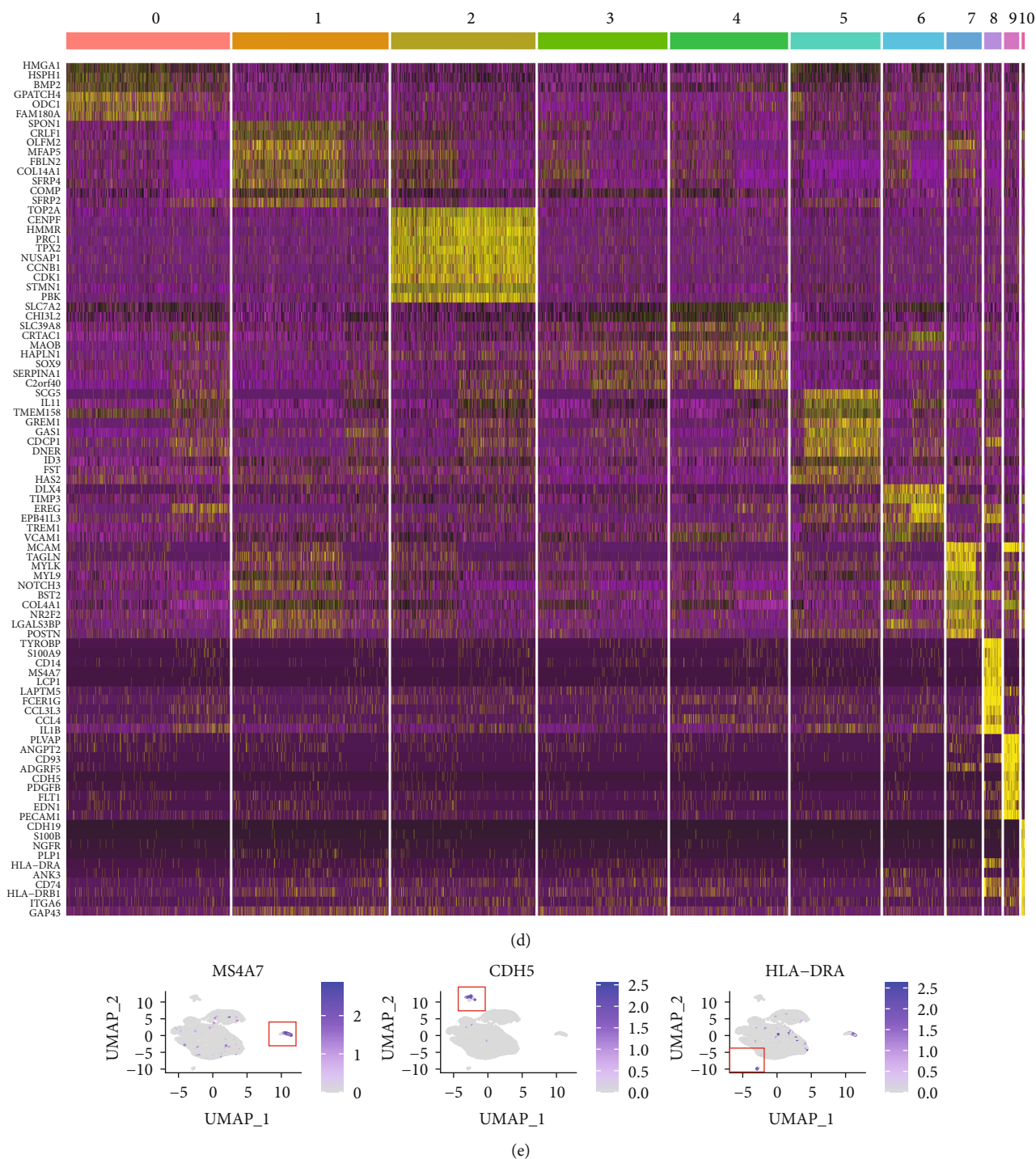


FIGURE 1: Single-cell RNA-seq analysis of cell types in the knee of healthy and OA patients. (a) UMAP plot of 6833 single cells from the human knee depicting 11 major cell types. Colours correspond to the clusters 0 to 10. (b) Bar plot shows frequency of each cell type in total, healthy, and OA groups. (c) Split UMAP plot depicting the clusters from healthy (N) and OA patients (O). (d) Heat map indicates the top 10 marker genes for each cell type. (e) Expression distribution of the top marker genes for the nonchondrocytes projected onto the UMAP plot: macrophages (MS4A7), endothelial cells (CDH5), and monocytes (HLA-DRA).

exists in healthy knee joints, which not only forms a structural barrier but can also digest and remove neutrophils in rheumatoid arthritis to form joint immune barrier [12]. However, the dynamic changes of macrophages in the

human OA are unclear, and their gene expression characteristics need further investigation.

In this study, we use the newly released single-cell sequencing data of knee tissues from healthy people and

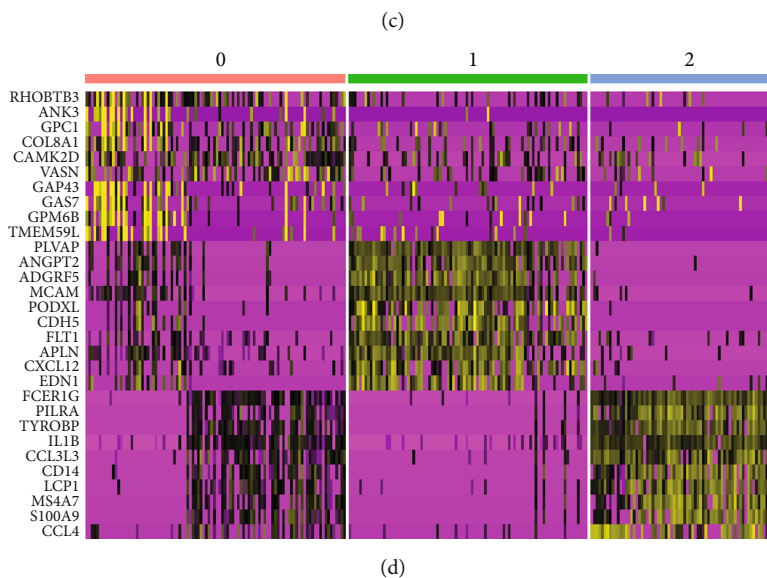
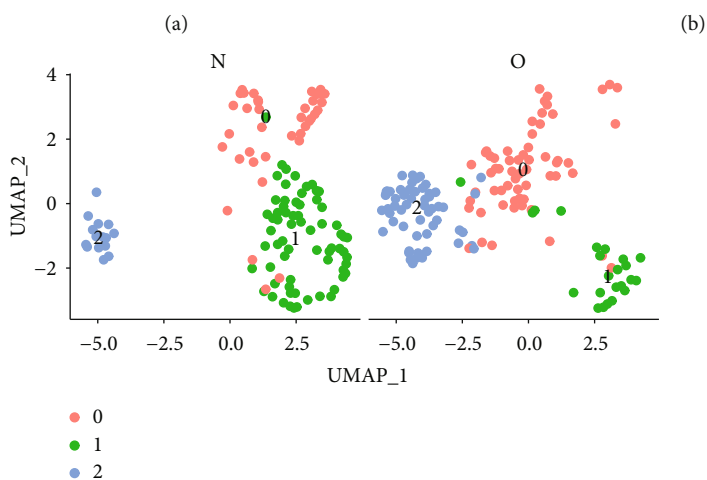
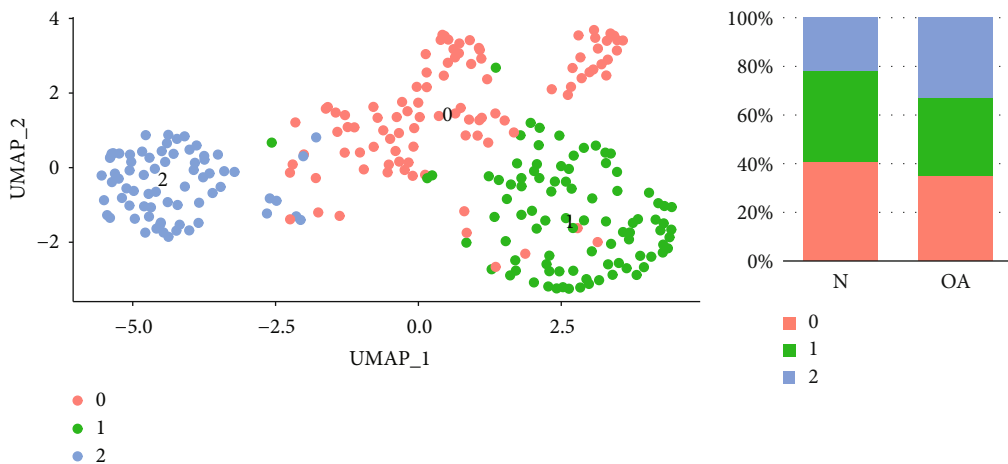
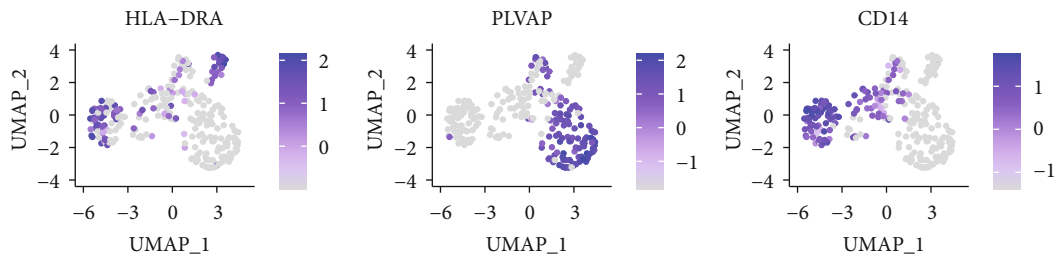
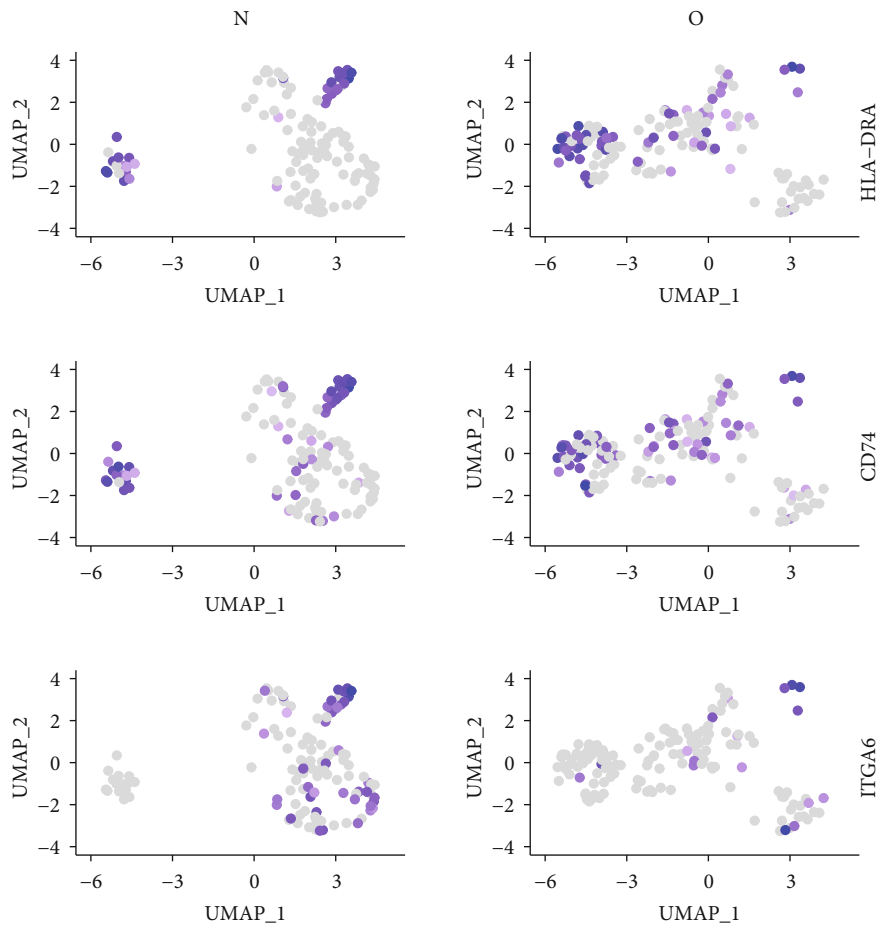


FIGURE 2: Continued.



(e)



(f)

FIGURE 2: Continued.

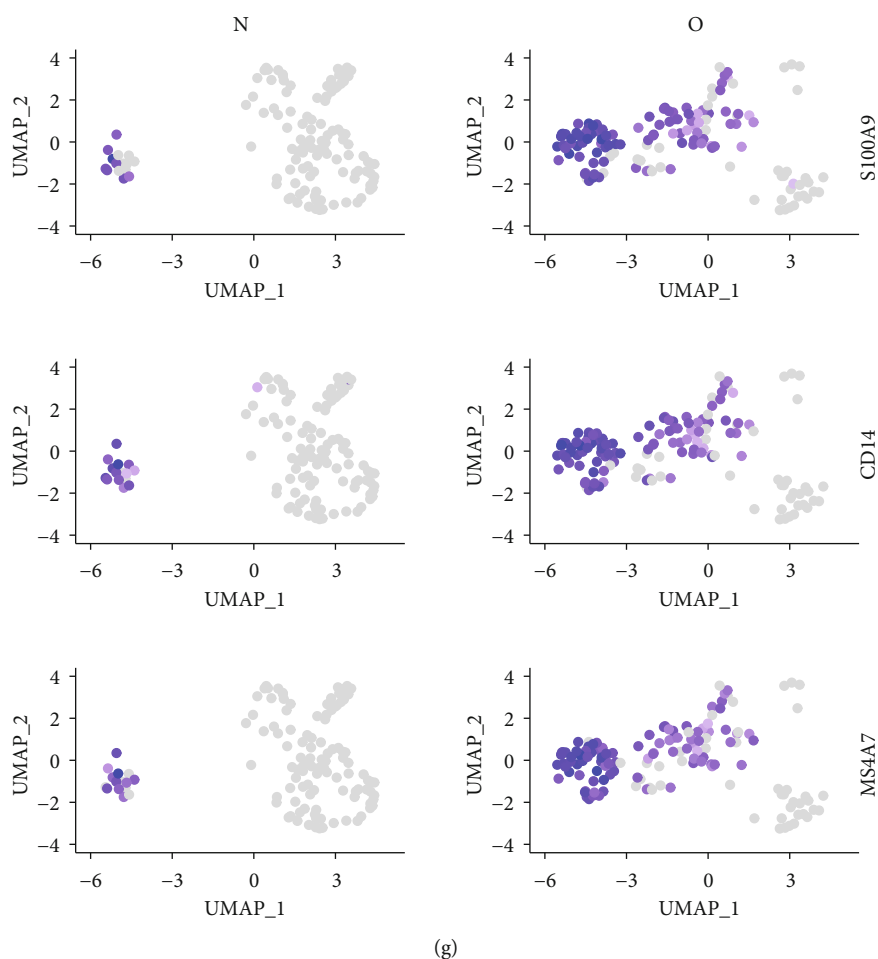


FIGURE 2: Single-cell RNA-seq analysis of nonchondrocytes from healthy and OA patients. (a) UMAP plot of 259 single cells from the human knee depicting 3 nonchondrocyte cell types. (b) Bar plot shows frequency of each cell type in the healthy and OA groups. (c) Split UMAP plot depicting the nonchondrocyte clusters from healthy (N) and OA patients (O). (d) Heat map indicates the top 10 marker genes for each cell type. (e) Expression distribution of the top marker genes for the nonchondrocytes projected onto the UMAP plot. (f) Expression distribution of top markers in the monocyte cluster. (g) Expression distribution of top markers in the macrophage cluster.

OA patients to identify macrophage subsets and characterize the differential gene expression involved in the OA pathogenesis. Our data show the diversified characteristics of specific cell types and explore the potential transition process of macrophages in the healthy and OA knee.

2. Methods

2.1. Single-Cell mRNA Sequencing Data. Data from Sun et al. [13] are downloaded from the Gene Expression Omnibus (GEO) dataset and are accessed at GSE133449. These scRNA data were from the cells isolated from the meniscus with the synovium specifically removed. Of the total 6833 cells, 3577 cells were obtained from people without OA, and the other 3256 cells were obtained from patients with OA.

2.2. Single-Cell mRNA Sequencing Analysis Tool. The volcano plots for the differential gene expression (DEG) study were drawn using the R package ggplot2. Other plots were drawn using the tools in the R package Seurat.

2.3. Single-Cell mRNA Sequencing Analysis. Using Seurat, we determined 15 principal components (PC) and performed dimensionality reduction and cluster analysis with a resolution parameter of 0.5. A differential expression analysis was performed on each cluster, and the results were visualized using Uniform Manifold Approximation and Projection (UMAP). Nonchondrocyte clusters were subclustered, and Feature plot was used to define the gene expression patterns in the clusters. A heat map was employed to characterize the top 10 genes in the clusters. Dot plots were used to demonstrate the expression pattern and level of expression of specific genes. The enhanced volcano plots displayed the DEG between two clusters of cells, in which we enter the normalized gene count converted by Log_2 to obtain DEG. For DEG testing, the value is <0.01 and is considered DEG.

3. Results

After strict quality control and data collation, 3577 cells from healthy people and 3256 cells from OA patients were retained for subsequent analysis. In order to solve the heterogeneity

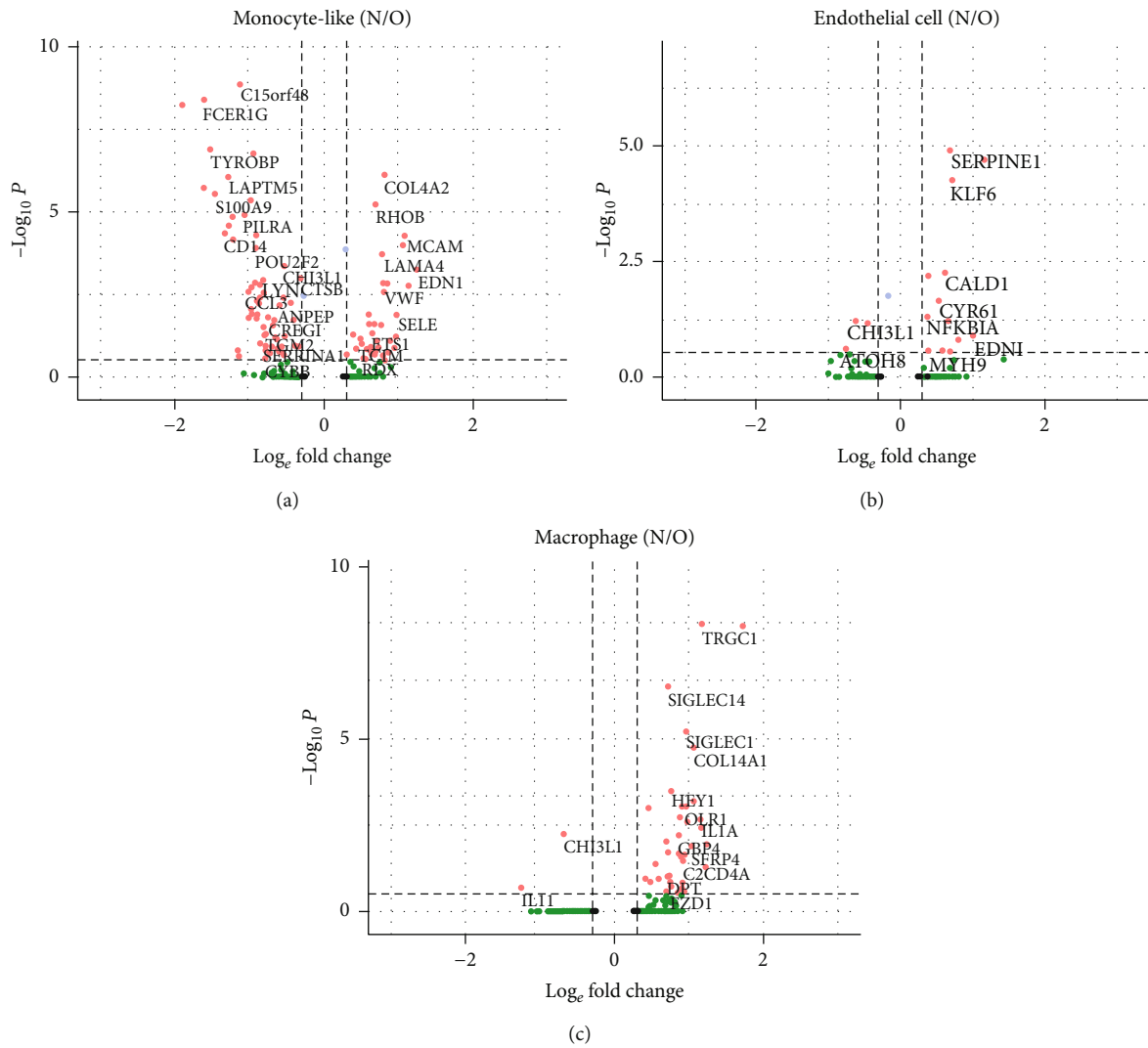
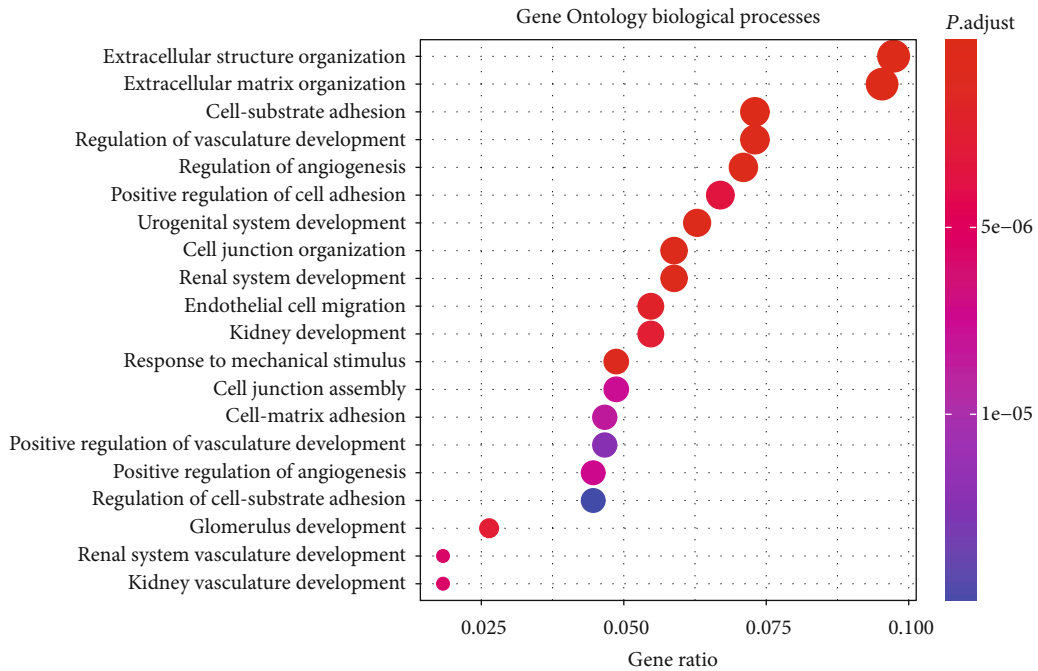
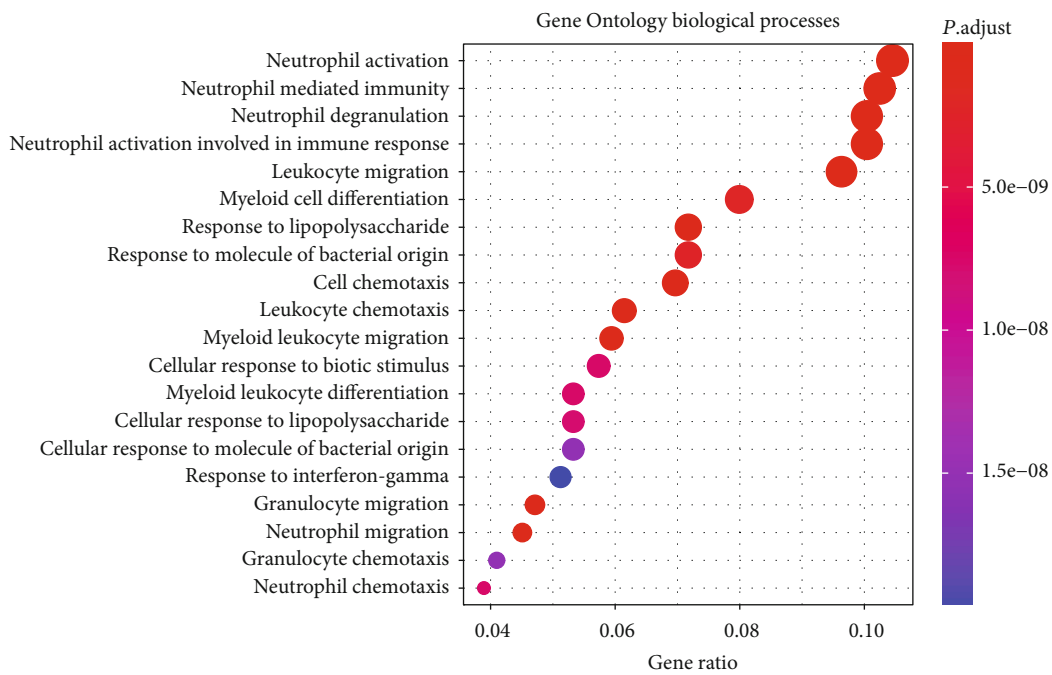


FIGURE 3: Continued.



(d)



(e)

FIGURE 3: Continued.

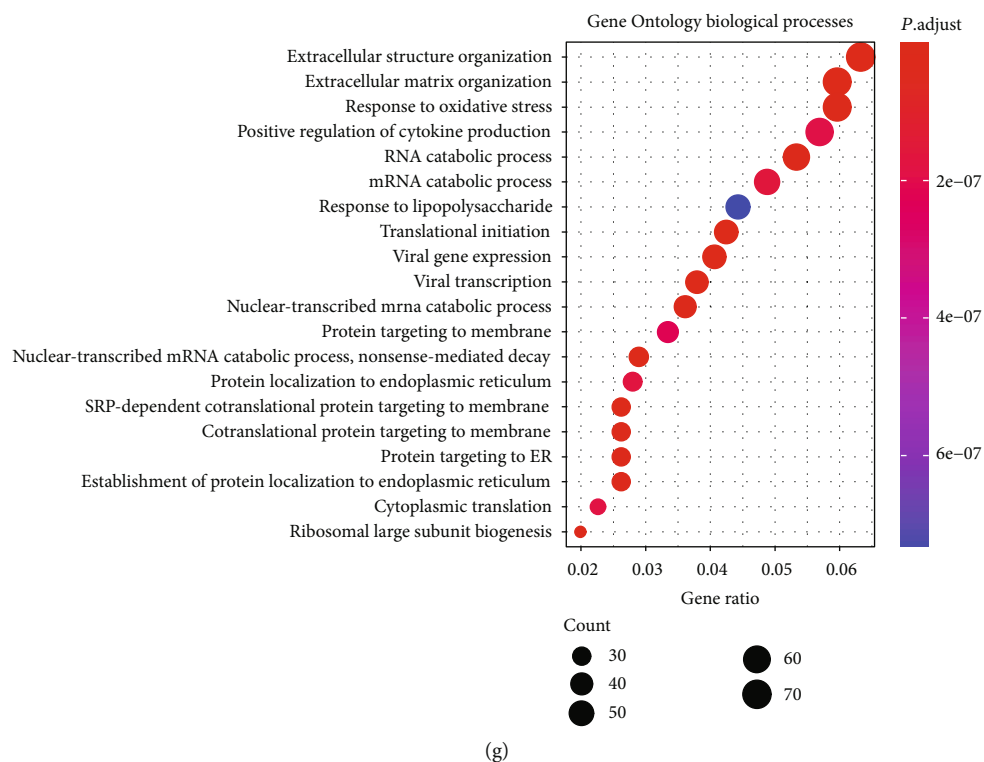
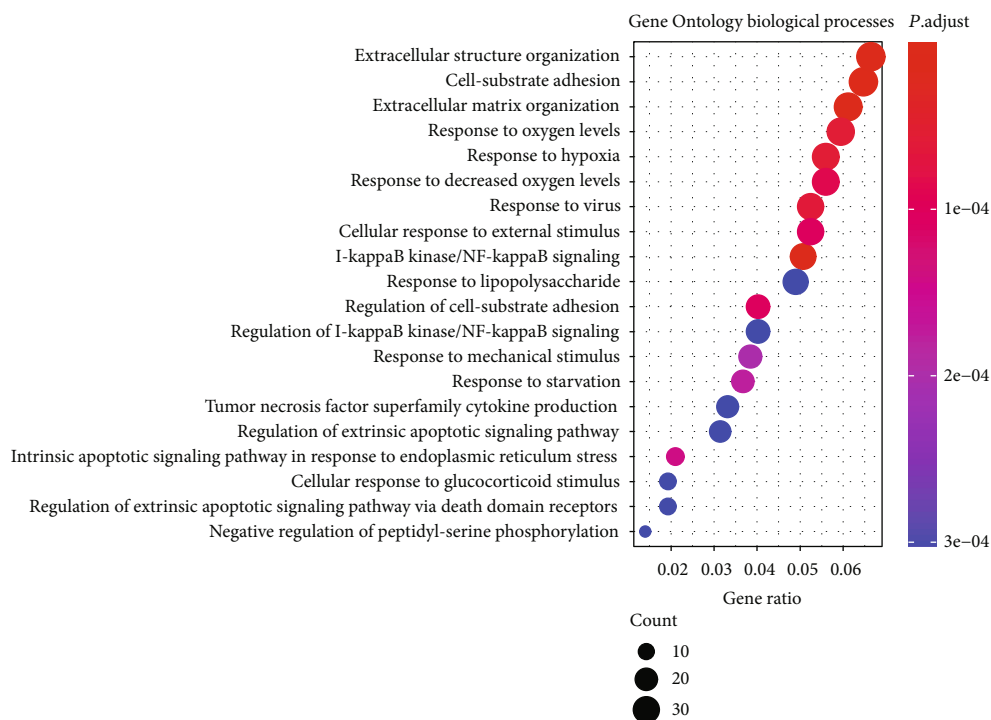


FIGURE 3: Comparison of DEG of the nonchondrocyte cluster from healthy and OA patients. (a) Volcano plot comparing the gene expression between healthy and OA monocyte clusters. (b) Volcano plot comparing the gene expression between healthy and OA endothelial cell clusters. (c) Volcano plot comparing the gene expression between healthy and OA macrophage clusters. Each plot represents one gene. Threshold of Log_2 fold change has been set as 0.3. (d) Dot plot showing the enrichment of Gene Ontology biological processes in the upregulated monocyte DEG between healthy and OA tissues. (e) Dot plot showing the enrichment of Gene Ontology biological processes in the downregulated monocyte DEG between healthy and OA tissues. (f) Dot plot showing the enrichment of Gene Ontology biological processes in the upregulated endothelial cell DEG between healthy and OA tissues. (g) Dot plot showing the enrichment of Gene Ontology biological processes in the upregulated macrophage DEG between healthy and OA tissues.

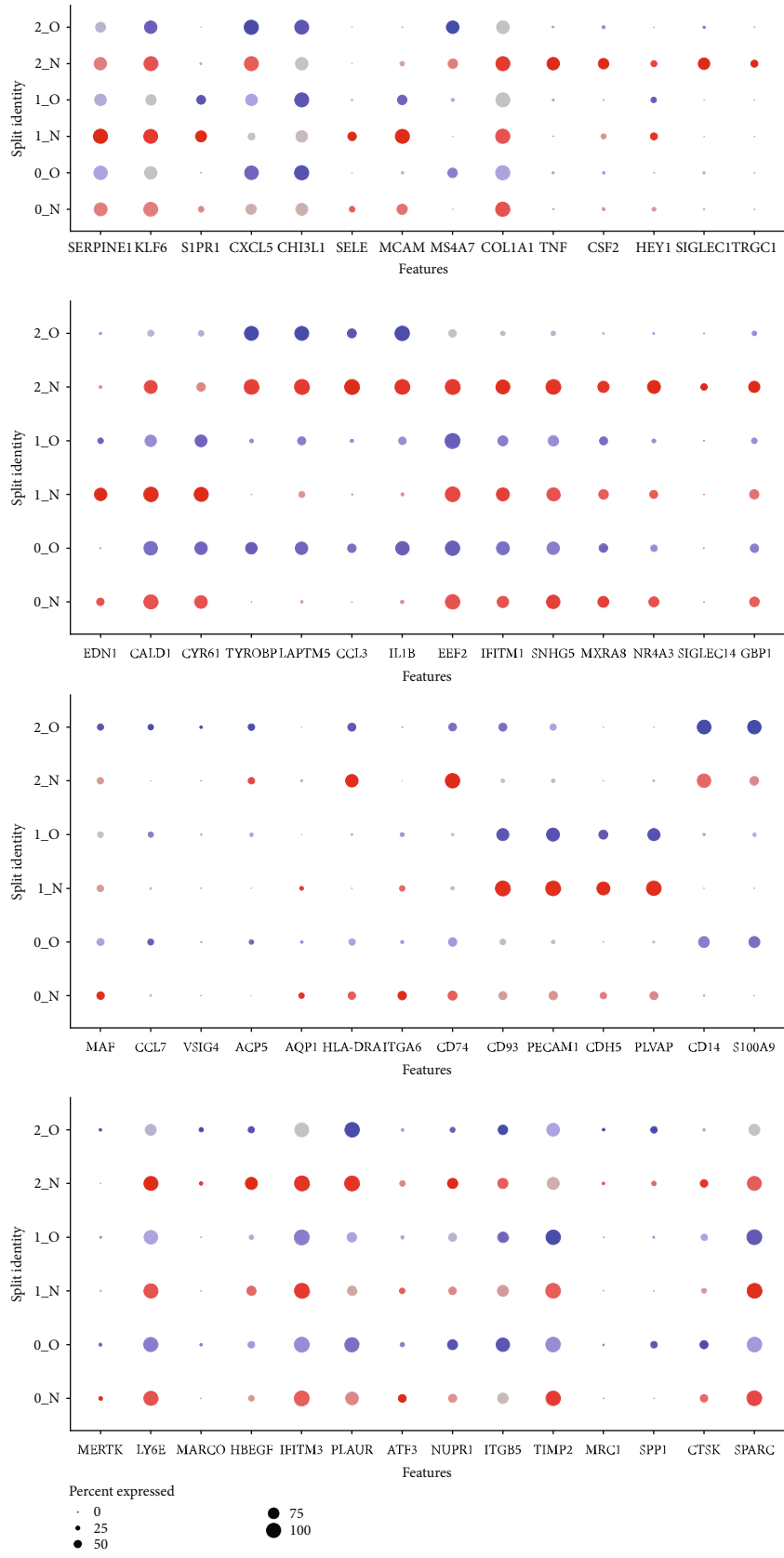


FIGURE 4: Continued.

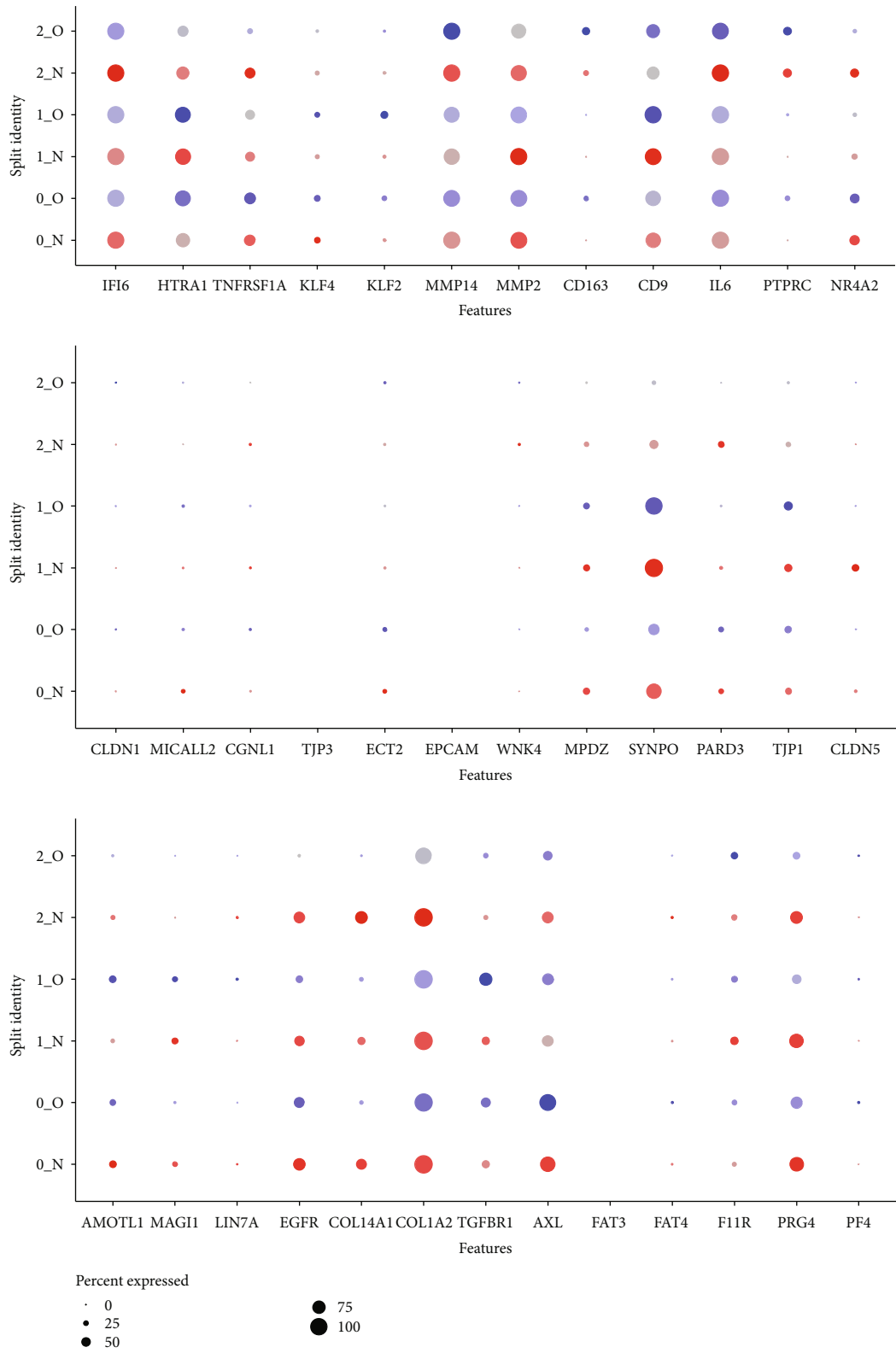


FIGURE 4: Continued.

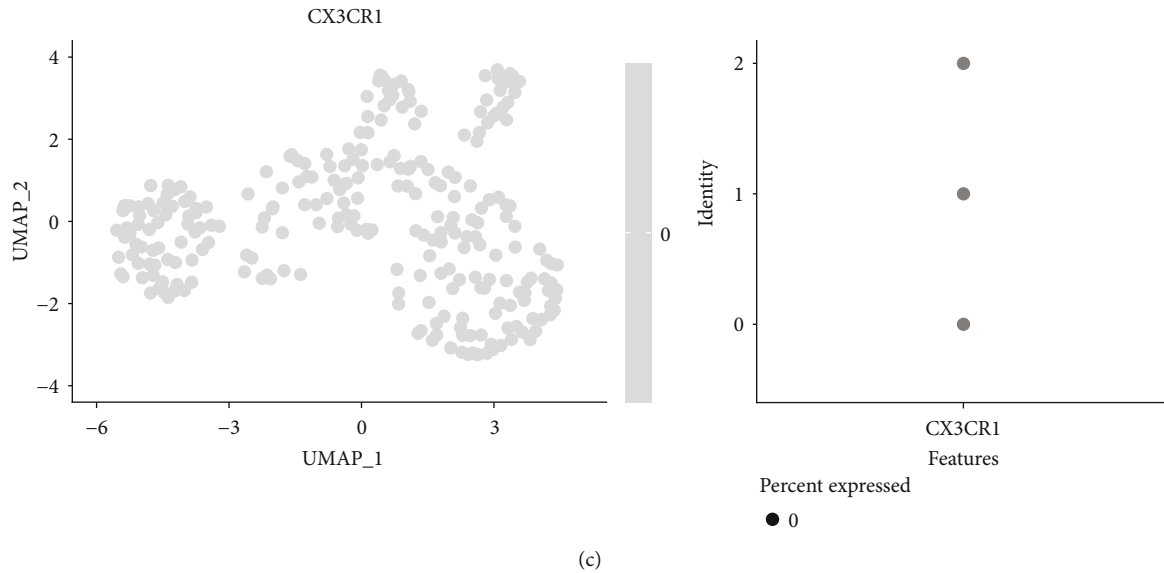


FIGURE 4: Special features of barrier macrophages in the OA tissue. (a) Dot plots demonstrating the expression pattern and level of expression of M1 or M2 genes. Colour intensities show the expression level of the indicated gene. (b) Dot plots demonstrating the expression pattern and level of expression of barrier macrophages. (c) CX3CR1 expression.

between the healthy and OA cells and remove the batch effect in between, we used the SCTransform method [14] to integrate and correct the data from the healthy and OA groups before the principal component analysis (PCA).

To study the heterogeneity of knee cells, we used the selected PC load as input and clustered cells with UMAP. After PCA clustering with a resolution of 0.5, a total of eleven hypothetical cell clusters were generated, including 8 chondrocyte-based populations and 3 non-chondrocyte-based populations (Figure 1(a)). The clusters in the healthy and OA groups are comparable, although the proportions differ (Figures 1(b) and 1(c)). Each cell type has been successfully annotated with known marker genes (Figures 1(d) and 1(e)). As the chondrocyte populations have been analysed in previous articles, we are interested here in three nonchondrocyte populations, namely, MS4A7+ macrophages (8), VE-cadherin+ (CDH5) endothelial cells (9), and HLA-DRA+ monocytes (10).

To further examine the molecular characteristics of non-chondrocytes at the single-cell level, we conducted population analysis of these cells in the healthy group and the OA group (Figure 2(a)). 120 nonchondrocytes from healthy people and 139 nonchondrocytes from OA patients were analysed. In nonchondrocytes, the number of macrophages in the OA group was much higher than that in the healthy group (Figures 2(b) and 2(c)). Macrophages (2), endothelial cells (1), and monocytes (0) are also reannotated with known marker genes (Figures 2(d) and 2(e)). The OA group showed less HLA-DRA-, CD74-, and ITGA6-expressing monocytes compared to the healthy group (Figure 2(f)), while there were much higher proportions of S100A9-, CD14-, and MS4A7-positive cells in the healthy group (Figure 2(g)).

To study the changes of nonchondrocytes in the OA state systematically, we compared the gene expression differences between the three cell types in healthy and OA states, including monocytes (Figure 3(a)), endothelial

cells (Figure 3(b)), and macrophages (Figure 3(c)). It is clear that monocytes in the OA group tend to express activation markers such as IL1beta, CXCL5, and TYROBP, while the macrophages in the OA downregulate both M1 marker such as SIGLEC1 and M2 marker such as CSF2, indicating that macrophages in the OA state polarize towards directions other than the M1/M2 division. To further analyse the up- or downregulated gene expression in the monocytes, endothelia, and macrophages between healthy and OA tissues, we classified the DEGs using GO enrichment and focused on the biological processes of those genes (Figures 3(d)–3(g)).

In order to clearly analyse the differences in gene expression profile, we use dot plots to show the proportions and intensities of different cells in different states (Figure 4(a)). Unexpectedly, macrophages in the OA state are more inclined to express the M2 markers, which is contrary to the concept that M2 macrophages promote the process of tissue repair [15].

Recent studies have shown a special kind of barrier macrophages in the outer layer of healthy knee synovium [11, 12]. These macrophages express certain characteristic molecules of epithelial cells, which not only form a tightly connected structural barrier but also digest and remove neutrophils in rheumatoid arthritis, forming an immune barrier in the synovium of the joint. However, the dynamic changes of these macrophages in the human OA remain unknown. Therefore, we compared the gene expression differences of barrier macrophage characteristic genes between the healthy and OA macrophages (Figure 4(b)). The tight junction genes of barrier macrophages are not unexpectedly expressed on endothelial cells. However, the expression of CX3CR1 is missing in the meniscal tissue macrophages (Figure 4(c)). As the murine barrier-forming synovial macrophages have been identified as CX3CR1+, this suggests a

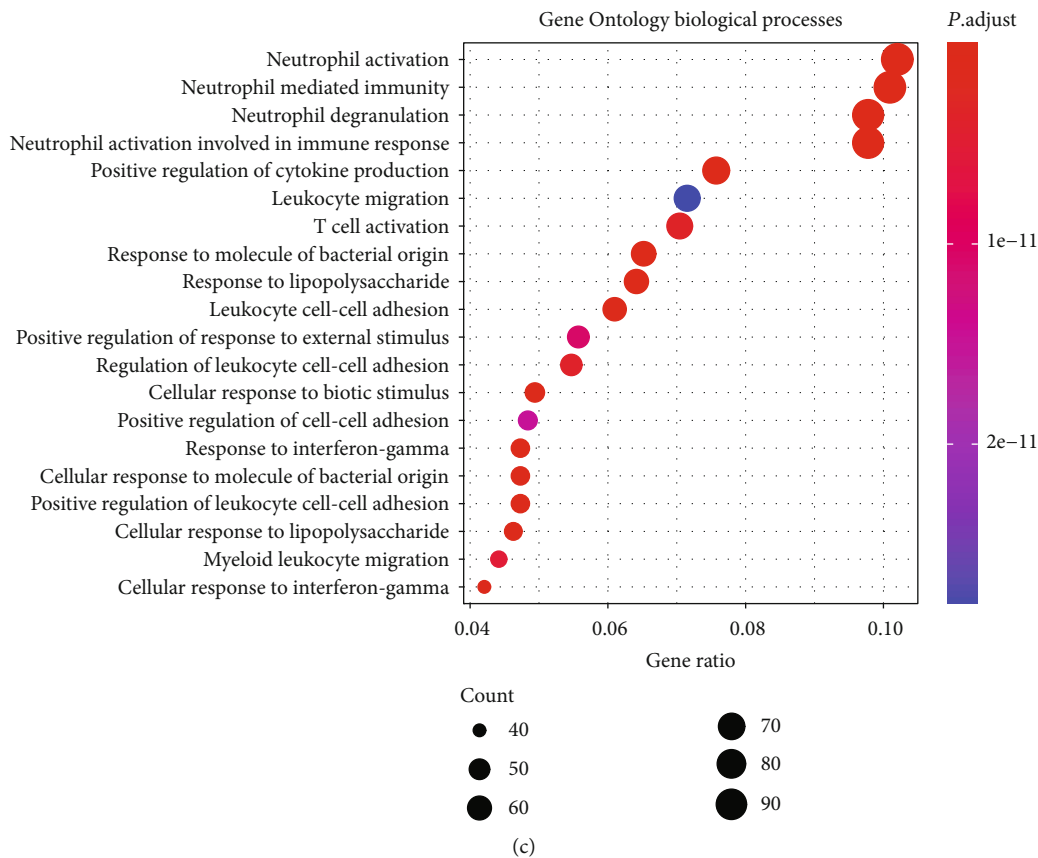
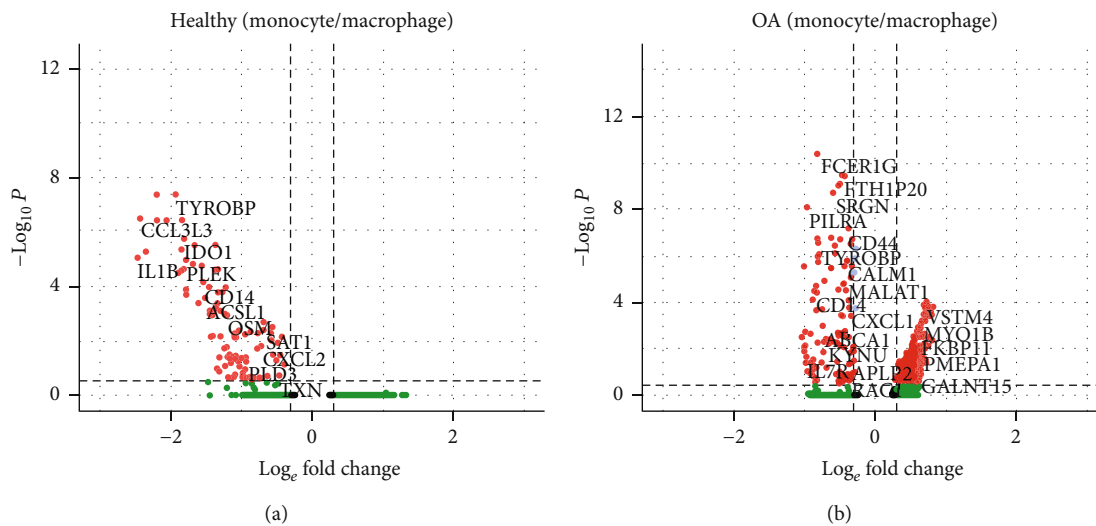


FIGURE 5: Continued.

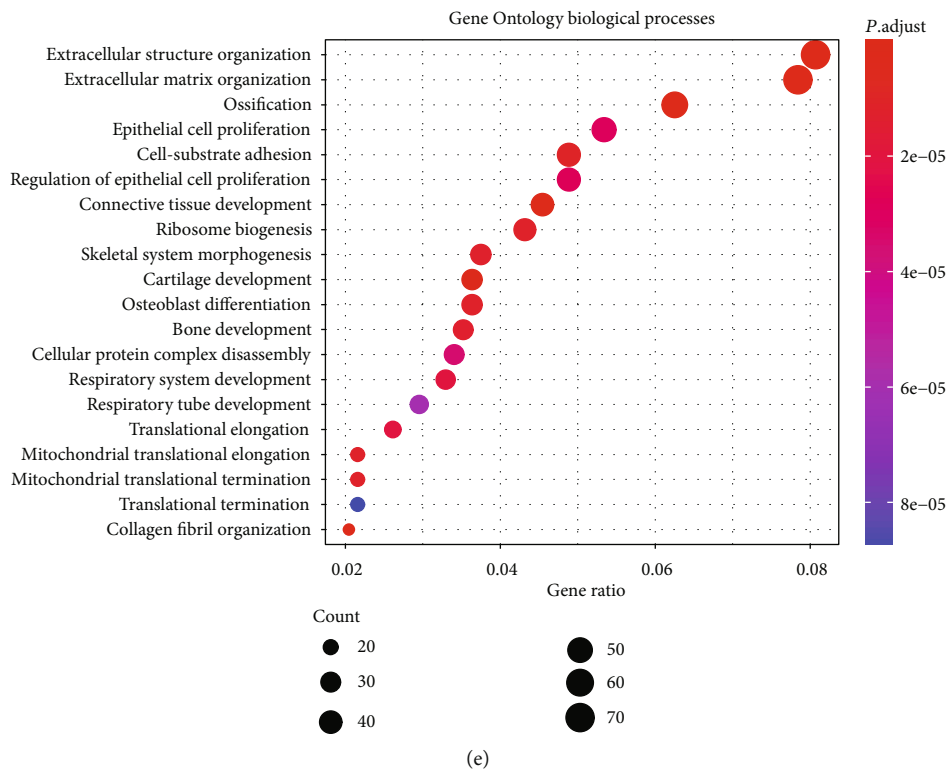
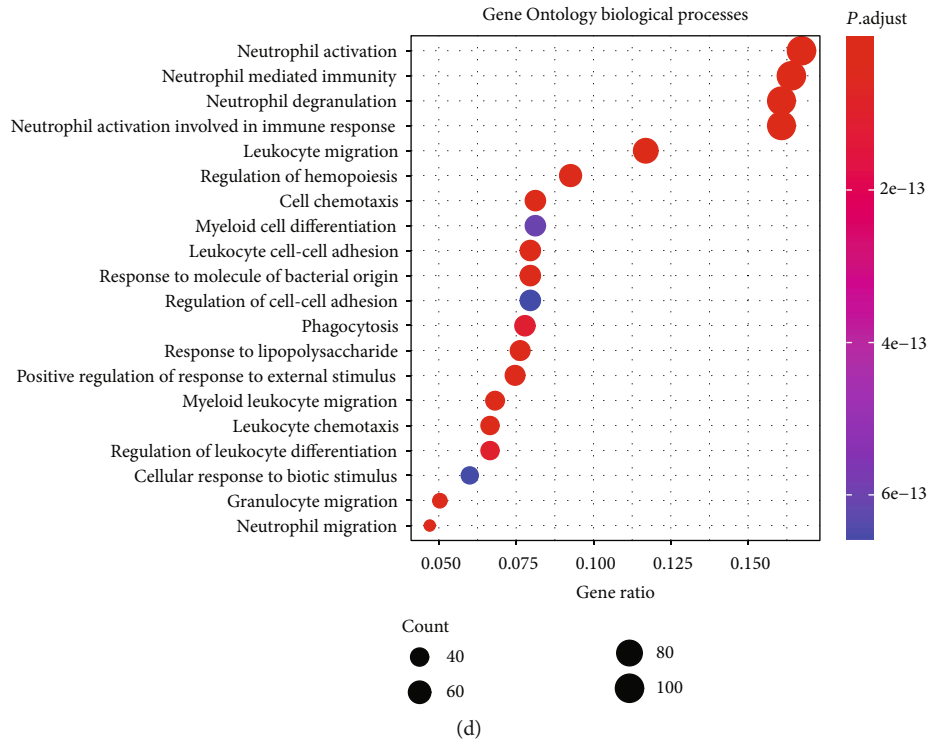


FIGURE 5: Gene expression comparison between monocytes and macrophages in the OA tissue. (a) Volcano plot comparing the gene expression between monocytes and macrophages in the healthy tissue. (b) Volcano plot comparing the gene expression between monocytes and macrophages in the OA tissue. (c) Dot plot showing the enrichment of Gene Ontology biological processes in the downregulated DEG between monocyte-like cell and macrophage in the healthy tissue. (d) Dot plot showing the enrichment of Gene Ontology biological processes in the downregulated DEG between monocyte-like cell and macrophage in the OA tissue. (e) Dot plot showing the enrichment of Gene Ontology biological processes in the upregulated DEG between monocyte-like cell and macrophage in the OA tissue.

different feature in the meniscus. Nevertheless, the expression of these genes on macrophages of healthy tissues is much higher when compared to that of the OA tissues, indicating a correlation of these macrophages to the human OA pathogenesis.

In addition, we also compared the gene expression differences between monocytes and macrophages. In healthy tissues, macrophages demonstrate the typical genes of macrophages as well as the feature genes of monocytes, suggesting that monocytes might be present as the potential precursors of macrophages. In the OA cells, monocytes upregulate even more activation genes, such as CD44, CXCL1, and TYROBP, indicating a transformation of these monocytes in OA (Figures 5(a) and 5(b)). The DEGs have been classified with GO enrichment (Figures 5(c)–5(e)).

4. Discussion

Our research reveals the single-cell gene expression characteristics and transition process of meniscal resident macrophages in the knee and describes the transcriptional dynamics of macrophages during the OA process. Our data found that resident macrophages exhibit special characteristics that differ from the M1/M2 subtypes and adapt to their immune niche.

Macrophages in joints are normally under the steady state. When joint injury or aging stress leads to cell apoptosis, DAMP produced by the breakdown of chondrocytes and extracellular matrix can activate and differentiate macrophages into the M1 subpopulation through the canonical pathway [16], which upregulate the release of inflammatory factors and aggravate OA. In contrast, the use of rapamycin to inhibit mTORC1 or specific deficiency of mTORC1 in macrophages can polarize the cells to M2 macrophages, which engulf dead cells, accelerate the repair process, and inhibit synovial inflammation [9]. One might expect that M2 or wound healing macrophages might be more predominant in OA-damaged meniscus. However, these gene expression studies were based on a large number of RNA samples and only provide a virtual average of the cell mixture. Our current single-cell study can provide molecular differentiation of all cell types within a complex composition, which helps to improve the understanding of homogeneity and discover the complexity and transitional nature of macrophages in the OA joints.

The latest animal studies have shown that healthy knee macrophages express certain characteristic molecules of epithelial cells, forming a structural barrier with tight junctions. In a mouse model of rheumatoid arthritis, the barrier layer undergoes functional remodelling, which loses the barrier function of macrophages [12]. Using single-cell sequencing technology, they analysed specific genes of barrier macrophages in mice. The macrophages/monocytes in this study were from the meniscus and not the synovium. Current data indicate that although some specific genes expressed by barrier macrophages can be found, meniscal tissue macrophages display different characteristics from murine barrier-forming synovial macrophages. These features have undergone tremendous changes under OA conditions.

Different from the bulk-seq method, single-cell transcriptional research can make a molecular distinction between all cell types, which helps to improve the understanding of histological identity and decipher why adjacent cells make different differentiation decisions during development [17]. Here, we focus on the presence of macrophages in the joints and provide their connection with OA pathogenesis, which may provide potential targets and pathways for OA treatment.

Data Availability

Data from Sun et al. (13) are downloaded from the Gene Expression Omnibus (GEO) dataset and are accessed at GSE133449. All other data supporting the findings are available from the corresponding author on reasonable request.

Conflicts of Interest

The authors declare that they have no conflicts of interest.

Authors' Contributions

Jingbin Zhou and Zhihong Zhao have equal contribution.









References

- [1] S. J. Rice, F. Beier, D. A. Young, and J. Loughlin, "Interplay between genetics and epigenetics in osteoarthritis," *Nature reviews. Rheumatology*, vol. 16, no. 5, pp. 268–281, 2020.
- [2] N. Zhang, Q. Shi, and X. Zhang, "An epidemiological study of knee osteoarthritis," *Zhonghua Nei Ke Za Zhi*, vol. 34, no. 2, pp. 84–87, 1995.
- [3] J.-H. Kim, J. Jeon, M. Shin et al., "Regulation of the catabolic cascade in osteoarthritis by the zinc-ZIP8-MTF1 axis," *Cell*, vol. 156, no. 4, pp. 730–743, 2014.
- [4] L. Utomo, Y. M. Bastiaansen-Jenniskens, J. A. N. Verhaar, and G. J. V. M. van Osch, "Cartilage inflammation and degeneration is enhanced by pro-inflammatory (M1) macrophages *in vitro*, but not inhibited directly by anti-inflammatory (M2) macrophages," *Osteoarthritis and Cartilage*, vol. 24, no. 12, pp. 2162–2170, 2016.
- [5] F. W. Roemer, A. Guermazi, D. T. Felson et al., "Presence of MRI-detected joint effusion and synovitis increases the risk of cartilage loss in knees without osteoarthritis at 30-month follow-up: the MOST study," *Annals of the Rheumatic Diseases*, vol. 70, no. 10, pp. 1804–1809, 2011.
- [6] W. H. Robinson, C. M. Lopus, Q. Wang et al., "Low-grade inflammation as a key mediator of the pathogenesis of osteoarthritis," *Nature reviews. Rheumatology*, vol. 12, no. 10, pp. 580–592, 2016.
- [7] A. B. Blom, P. L. van Lent, S. Libregts et al., "Crucial role of macrophages in matrix metalloproteinase-mediated cartilage destruction during experimental osteoarthritis: involvement of matrix metalloproteinase 3," *Arthritis and Rheumatism*, vol. 56, no. 1, pp. 147–157, 2007.
- [8] B. D. Furman, K. A. Kimmerling, R. D. Zura et al., "Articular ankle fracture results in increased synovitis, synovial macrophage infiltration, and synovial fluid concentrations of inflammatory cytokines and chemokines," *Arthritis & rheumatology*, vol. 67, no. 5, pp. 1234–1239, 2015.

- [9] D. M. Mosser and J. P. Edwards, “Exploring the full spectrum of macrophage activation,” *Nature Reviews. Immunology*, vol. 8, no. 12, pp. 958–969, 2008.
- [10] H. Zhang, C. Lin, C. Zeng et al., “Synovial macrophage M1 polarisation exacerbates experimental osteoarthritis partially through R-spondin-2,” *Annals of the Rheumatic Diseases*, vol. 77, no. 10, pp. 1524–1534, 2018.
- [11] F. Zhang, K. Wei, K. Slowikowski et al., “Defining inflammatory cell states in rheumatoid arthritis joint synovial tissues by integrating single-cell transcriptomics and mass cytometry,” *Nature immunology*, vol. 20, no. 7, pp. 928–942, 2019.
- [12] S. Culemann, A. Gruneboom, J. A. Nicolas-Avila et al., “Locally renewing resident synovial macrophages provide a protective barrier for the joint,” *Nature*, vol. 572, no. 7771, pp. 670–675, 2019.
- [13] H. Sun, X. Wen, H. Li et al., “Single-cell RNA-seq analysis identifies meniscus progenitors and reveals the progression of meniscus degeneration,” *Annals of the Rheumatic Diseases*, vol. 79, no. 3, pp. 408–417, 2020.
- [14] A. Butler, P. Hoffman, P. Smibert, E. Papalexi, and R. Satija, “Integrating single-cell transcriptomic data across different conditions, technologies, and species,” *Nature Biotechnology*, vol. 36, no. 5, pp. 411–420, 2018.
- [15] K. Y. Gerrick, E. R. Gerrick, A. Gupta, S. J. Wheelan, S. Yegnasubramanian, and E. M. Jaffee, “Transcriptional profiling identifies novel regulators of macrophage polarization,” *PLoS One*, vol. 13, no. 12, article e0208602, 2018.
- [16] E. W. Orlovsky and V. B. Kraus, “The role of innate immunity in osteoarthritis: when our first line of defense goes on the offensive,” *The Journal of Rheumatology*, vol. 42, no. 3, pp. 363–371, 2015.
- [17] Q. Ji, Y. Zheng, G. Zhang et al., “Single-cell RNA-seq analysis reveals the progression of human osteoarthritis,” *Annals of the Rheumatic Diseases*, vol. 78, no. 1, pp. 100–110, 2018.

Research Article

miR-24-3p/KLF8 Signaling Axis Contributes to LUAD Metastasis by Regulating EMT

Pengyu Jing ¹, Nianlin Xie ¹, Nan Zhao ², Ximing Zhu ¹, Pei Li ¹, Guizhou Gao ¹,
Haizhou Dang ¹ and Zhongping Gu ¹

¹Department of Thoracic Surgery, The Second Affiliated Hospital, Air Force Medical University, Xi'an 710038, China

²Department of Public Health, Xi'an Medical University, Xi'an 710021, China

Correspondence should be addressed to Pengyu Jing; jingpengyu163@163.com, Nianlin Xie; xienianlin@126.com, Nan Zhao; zhaonanxiyi@163.com, and Zhongping Gu; gu-zhong-ping@163.com

Received 4 February 2020; Accepted 6 April 2020; Published 28 April 2020

Guest Editor: Zenghui Teng

Copyright © 2020 Pengyu Jing et al. This is an open access article distributed under the Creative Commons Attribution License, which permits unrestricted use, distribution, and reproduction in any medium, provided the original work is properly cited.

Reprogramming of the tumor immune microenvironment is a salient feature during metastasis in LUAD. miR-24-3p and KLF8, which are key regulators of the tumor immune microenvironment, had been proved to show metastasis-promoting property in LUAD. However, whether miR-24-3p could regulate LUAD metastasis by targeting KLF8 remains unclear. This study explored the functions and mechanisms of miR-24-3p/KLF8 signaling in advanced LUAD. The expression level of miR-24-3p and KLF8 were tested in LUAD patients, and the correlation of miR-24-3p and KLF8 was evaluated. The interaction of miR-24-3p and KLF8 was demonstrated by luciferase reporter activity assay, *in vitro* migration and invasion studies, and *in vivo* metastatic studies. miR-24-3p level was downregulated in LUAD and negatively associated with KLF8 mRNA expression. miR-24-3p controls LUAD metastasis by directly targeting KLF8 and inducing Snail and E-cadherin expressions. Targeting the miR-24-3p/KLF8/EMT axis might be of great therapeutic value to advanced LUAD patients.

1. Introduction

Lung cancer ranks one of the most fearsome malignancies globally due to the foremost cause of mortality worldwide [1, 2]. Lung adenocarcinoma (LUAD) contributes to the major histologic type of lung cancer with an unfavorable 5-year survival rate of only 15% [3–5]. Metastasis is the leading cause of cancer-related death for advanced LUAD [1, 2, 4–6]. However, a full understanding of the underlying mechanisms controlling LUAD metastasis is still largely insufficient. Mounting evidences have confirmed that reprogramming the tumor immune microenvironment is a major process that drives LUAD metastasis by EMT activation and provided multiple targetable checkpoint molecules for advanced LUAD [7, 8]. The dysregulation of microRNAs (miRNAs) is broadly participated in the pathogenesis of LUAD and functionally act as a key contributor to cancer cell metastasis [9, 10]. Yet, the key dysregulated miRNAs and the exact mechanisms in LUAD metastasis remain unrevealed.

miR-24-3p is one of the most frequently dysregulated EMT-associated miRNAs in carcinogenesis, which is best known for its role in regulating cancer cell metastasis, including human breast adenocarcinoma, hepatocellular carcinoma, gastric cancer, prostate carcinoma, and lung cancer [11–15]. Importantly, miR-24-3p has been reported to be involved in LUAD metastasis by targeting fibroblast growth factor receptor 3 (FGFR3), inhibitor of growth 5 (ING5), and sex-determining region Y-box 7 (SOX7) [11, 15, 16], indicating that miR-24-3p plays a pivotal role in LUAD metastasis. Despite the significant role of miR-24-3p in metastatic LUAD, the potential mechanisms of miR-24-3p in regulating cell invasion and migration of LUAD are not fully clear yet.

Krüppel-like transcription factor 8 (KLF8) belongs to the Krüppel-like C2H2 zinc-finger transcription factor family, which is involved in multiple cellular biological processes, such as cell proliferation, differentiation, and migration [17, 18]. KLF8 has been reported to maintain the invasive

capacity of cancer cells by inducing epithelial-to-mesenchymal transition (EMT) [17–19]. Of importance, KLF8 has been implicated to be regulated by miRNAs in metastatic progression of lung cancer. miR-1236-3p and miR-135a could inhibit the metastatic procedure of lung cancer by targeting KLF8 [20, 21]. However, whether miR-24-3p could regulate LUAD metastasis by targeting KLF8 remains unclear.

This study demonstrated that miR-24-3p level was down-regulated in LUAD and negatively associated with KLF8 mRNA expression. miR-24-3p controls LUAD metastasis by directly targeting KLF8 and inducing EMT activation. Targeting the miR-24-3p/KLF8/EMT axis might be of great therapeutic value to advanced LUAD patients.

2. Materials and Methods

2.1. Tissues, Cell Lines, and Reagents. Surgical specimens, which contain 18 pairs of tumor tissues and nontumor tissues of LUAD, were collected from Tangdu Hospital according to the Medical Ethics Committee's guidelines. Tissue RNA was extracted for real-time PCR evaluation, and tissue protein was collected and analyzed by Western blot. A549 and H1299 human cell lines of LUAD were ordered from the Cell bank of Chinese Academy of Sciences (Shanghai, China) after being tested for mycoplasma contamination. All cells were cultured in complete DMEM (plus 10% FBS and 100 U/ml penicillin sodium and 100 µg/ml streptomycin) in 37°C incubator with 5% CO₂. Primary antibodies used in Western blot study were as follows: KLF8 (Abcam, ab168527, 1: 1000), Snail (Cell Signaling Technology, #3879, 1: 1000), E-cadherin (Cell Signaling Technology, #3195, 1: 1000), and β-actin (Cell Signaling Technology, #3700, 1: 5000). HRP-conjugated secondary antibodies and the HRP substrate kit were ordered from the Merck Company. Lipofectamine™ was purchased from Invitrogen Company.

2.2. RNA Extraction and qRT-PCR. RNA isolation was carried out by using TRIzol (Life Technologies) according to previous reports [11]. Total 3 µg/RT reaction of RNA from the LUAD cells or tissues was used for analysis of the mRNA level of the target gene by real-time quantitative PCR on the Light Cycler 480II (Roche). The primer sequences information is listed as follows: miR-24-3p F: TGGCTCACATCAGCAGGAACA; U6 F: GGAACGATACAGAGAAGATAGC, U6 R: TGGAACGCTTCACGAATTTGCG; KLF8 F: GCTCACCGCAGAATCCATACA, KLF8 R: GTGCACCGAAAAGGCTTGAT; and β-actin F: CATGTACGTTGCTATCCAGGC, β-actin R: CTCCTTAATGTCACGCACGAT.

2.3. Protein Collection and Western Blots. Proteins of cells were extracted with a lysis buffer (containing RIPA, protease inhibitors, and phosphatase inhibitors). 20 µg of each protein was used for SDS-PAGE. Then, the proteins were transferred onto membranes and incubated with primary antibodies overnight. After incubation with HRP-conjugated secondary antibodies, membranes were visualized using Immobilon™ Western.

2.4. Luciferase Reporter Activity Assay. Plasmids containing the wild-type (WT) KLF8-3'-UTR sequence and a mutant KLF8-3'-UTR sequence were synthesized by GeneCopoeia (Shanghai, China). Cells were transfected with the plasmids and harvested and lysed for luciferase assay by using a Dual Luciferase Assay kit (GeneCopoeia) according to the manufacturer's instructions as described previously [11, 22].

2.5. In Vitro Functional Studies. *In vitro* migration and invasion assays were performed by using transwell chambers according to the manufacturer's instructions. For migration assay, 5 × 10⁴ cells were seeded in a serum-free medium in the upper chamber. For invasion assay, the chambers were covered with Matrigel previously and dried overnight. 1 × 10⁵ cells were seeded in DMEM with 1% FBS in the upper chamber. A medium supplemented with 20% FBS was added into the lower chamber. Cells remaining on the upper membrane after 24-hour incubation were removed, and cells on the lower surface of the membrane were fixed, stained, and counted. For wound healing assay, cells were seeded in 6-well plates until reaching confluence. Then, wounds were scratched by using sterile tips, and wound closure was recorded every 12 hours by using a microscope.

2.6. In Vivo Animal Experiments. All of the mouse studies were approved by Animal Care and Use Committee of the Ethics Committee of Tangdu Hospital. Nude mice (BALB/C strain, 6-week old, male) were used as the metastatic model. 3 × 10⁶ cells were injected through the tail veins for 5 weeks. D-luciferin (Roche) was injected intraperitoneally in the mice at week 2 and week 5, and the bioluminescence images were gained with an IVIS 100 Imaging System (Xenogen).

3. Statistical Analysis

All statistical analyses for this study were assessed by using SPSS 20.0 software (SPSS Inc., USA). Student's *t*-test was used to evaluate the quantitative data between groups. Kaplan-Meier analyses, as well as the log-rank test, were used to estimate the overall survival. Pearson's correlation coefficients were used to evaluate the correlation between two indices in clinical samples. A difference at *p* < 0.05 was considered statistically significant.

4. Results

4.1. miR-24-3p Was Negatively Associated with KLF8 mRNA Expression and Was Closely Related to EMT Markers in LUAD. We initially analyzed the expression of miR-24-3p and KLF8 in 18 pairs of tumor tissues and nontumor tissues of LUAD by qRT-PCR and found that the expression levels of miR-24-3p declined in LUAD tissues than those in adjacent nontumor tissues (Figure 1(a)), while KLF8 mRNA expression was increased in LUAD tissues than that in adjacent nontumor tissues (Figure 1(b)). What is more, we found that miR-24-3p expression level was negatively associated with KLF8 mRNA expression level (Figure 1(c)). Together, these data indicated that miR-24-3p involved in LUAD progression may be associated with KLF8. To further confirm

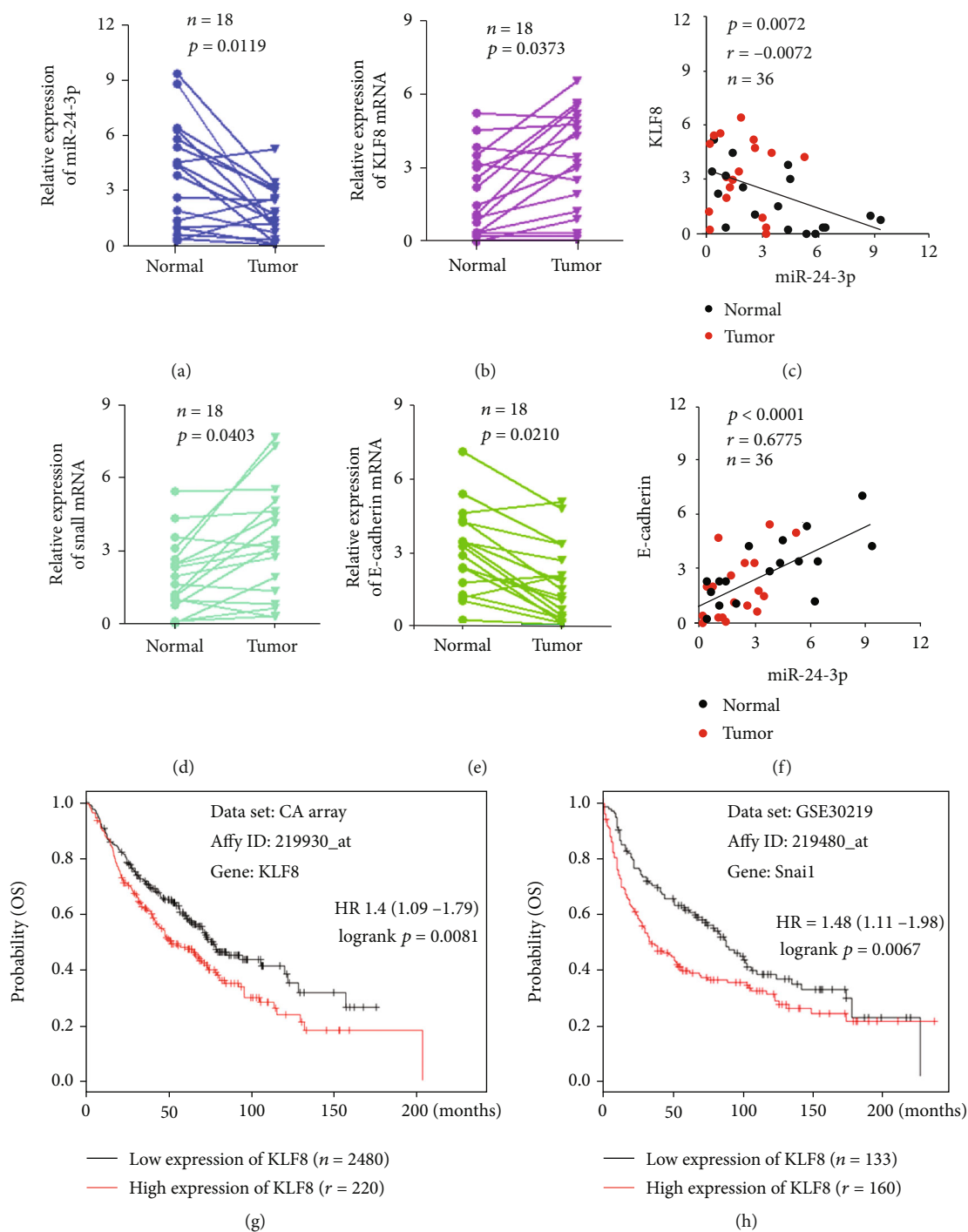


FIGURE 1: miR-24-3p was negatively associated with KLF8 mRNA expression and was closely related to EMT markers (Snail and E-cadherin mRNA). (a) miR-24-3p expression in lung adenocarcinoma was less than that in normal tissues. (b) KLF8 mRNA expression in lung adenocarcinoma was higher than that in normal tissues. (c) Regression analysis comparing miR-24-3p and KLF8 mRNA expressions in lung adenocarcinoma tissues and the corresponding normal tissues. (d) Snail mRNA expression in lung adenocarcinoma tissues was higher than that in normal tissues. (e) E-cadherin mRNA expression in lung adenocarcinoma was less than that in normal tissues. (f) Regression analysis comparing miR-24-3p and E-cadherin mRNA expressions in lung adenocarcinoma tissues and the corresponding normal tissues. (g, h) Kaplan-Meier estimates of the cumulative survival rate based on the Kaplan-Meier plotter database. The higher KLF8 and Snail mRNA expression were closely related to poor prognosis in lung adenocarcinoma.

whether the dysregulation of miR-24-3p in LUAD was associated with EMT, we analyzed the mRNA levels of key EMT markers, Snail and E-cadherin, and revealed that the Snail

mRNA level was increased, while the E-cadherin mRNA level was decreased in LUAD (Figures 1(d) and 1(e)). In addition, regression analysis comparing miR-24-3p and E-cadherin

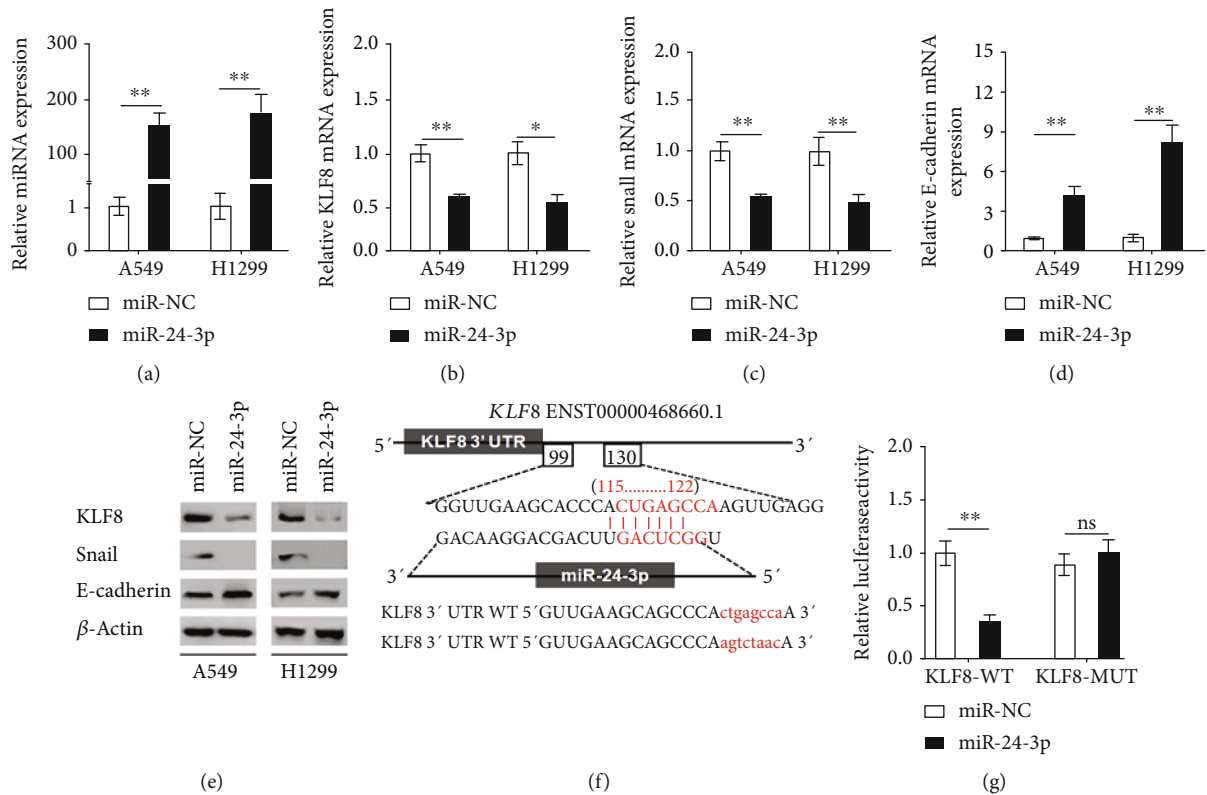


FIGURE 2: miR-24-3p regulated KLF8, Snail, and E-cadherin expressions in lung adenocarcinoma cells, and KLF8 was a direct target of miR-24-3p. (a) qRT-PCR analysis of miR-24-3p expression in A549 and H1299 cells transfected with either miR-NC or miR-24-3p mimics. (b–d) mRNA expression of KLF8 (b), Snail (c), and E-cadherin (d) in A549 and H1299 cells transfected with either miR-NC or miR-24-3p mimics was detected by qRT-PCR. (e) Expression of KLF8, Snail, and E-cadherin in A549 and H1299 cells transfected with either miR-NC or miR-24-3p mimics was detected by Western blot. (f) miR-24-3p binding sites in 3'-UTR of KLF8 were predicted by TargetScan. The seed region of miR-24-3p and the recognition site in the KLF8 3'-UTR are shown in red. The sequences of the WT and MUT KLF8 3'-UTR were used for the dual luciferase reporter construct. (g) The pMIR-REPORT vector and either KLF8-WT or KLF8-MUT plasmids were cotransfected with miR-24-3p or miR-NC mimics in H1299 cells, and the relative luciferase activity was detected. Data are mean \pm SD. * $p < 0.05$, ** $p < 0.01$.

mRNA expressions revealed that miR-24-3p levels were closely associated with E-cadherin (Figure 1(f)), suggesting that miR-24-3p involved in LUAD progression may be associated with EMT. Further analysis by Kaplan-Meier plotter database implicated that both KLF8 and Snail mRNA expression levels were closely related to poor clinical outcomes of LUAD, manifesting that KLF8 and Snail are critical in the progression of LUAD (Figures 1(g) and 1(h)).

4.2. miR-24-3p Regulates KLF8, Snail, and E-Cadherin Expressions and Directly Targets KLF8. To further confirm the regulator role of miR-24-3p for KLF8, Snail, and E-cadherin, we overexpressed miR-24-3p in A549 and H1299 cells (Figure 2(a)). KLF8 and Snail mRNA levels were significantly downregulated, while E-cadherin mRNA level was significantly upregulated when the cells overexpressed miR-24-3p (Figures 2(b)–2(d)). Western blot assay also showed that the protein levels were correspondingly changed after the cells overexpressed miR-24-3p (Figure 2(e)). The wild-type (WT) KLF8 3'-UTR sequence and a mutant KLF8 3'-UTR sequence were inserted into a luciferase reporter

vector to further validate whether miR-24-3p regulated the expression of KLF8 by binding to its 3'-UTR (Figure 2(f)). As determined by luciferase activity assay, miR-24-3p conspicuously suppressed the relative luciferase activity in presence of WT reporter construct of KLF8 3'-UTR, while there was no significant differences of relative luciferase activity when the mutant-type reporter construct of KLF8 3'-UTR was constructed (Figure 2(g)), suggesting that miR-24-3p could directly target KLF8.

4.3. KLF8 Promoted LUAD Cell Metastasis In Vitro and In Vivo. The metastatic role of KLF8 in LUAD was further tested in A549 cells *in vitro* and *in vivo*. Wound healing assay showed that KLF8 overexpression strengthened the migration capacity of A549 cell after 48 hours of induction (Figure 3(a)). Consistently, transwell analysis demonstrated that KLF8 overexpression enhanced the migration and invasion ability in A549 cells. What is more, the enhanced migration and invasion capacity induced by KLF8 overexpression could significantly reverse after the cells cotransfected with miR-24-3p, suggesting that miR-24-3p could control LUAD

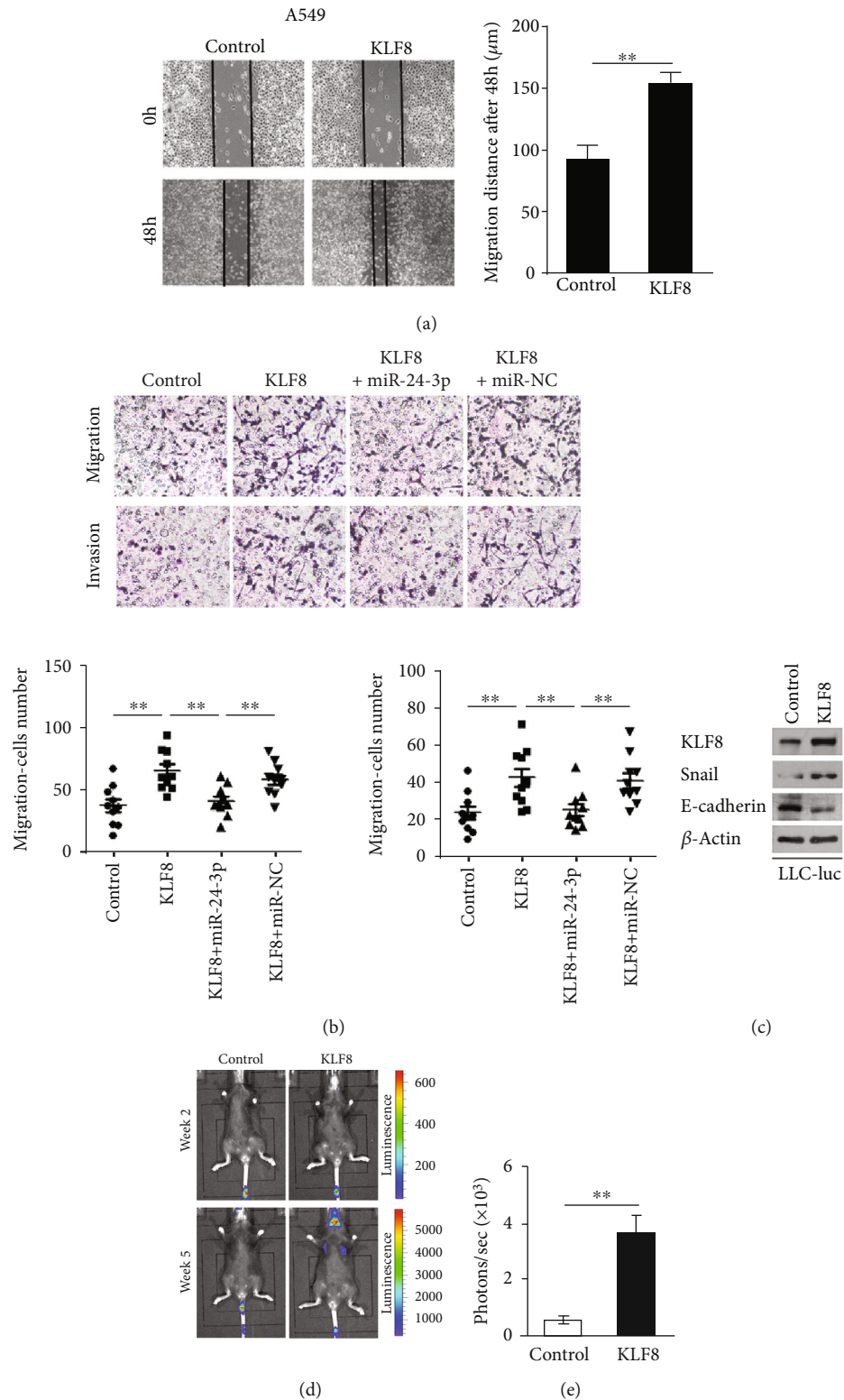


FIGURE 3: KLF8 promoted lung adenocarcinoma cell metastasis in vitro and in vivo. (a) The wound healing assay ($n = 5$) demonstrated that KLF8 overexpression strengthened the migration of A549 cell. (b) The migration and invasion potentials of the A549 cell as indicated were evaluated using transwell assay, and the numbers of migrated and invaded cells are shown ($n = 10$). (c) Protein expression of KLF8, Snail, and E-cadherin in LLC-luc-Control or LLC-luc-KLF8 cells was detected by Western blot. (d) LLC-luc-Control or LLC-luc-KLF8 cells were injected IV into C57BL/6 mice, and tumor growth and metastasis were monitored by in vivo imaging. (e) Intensities of luciferase signal in lungs of LLC-luc-KLF8 mice were higher than that in lungs of LLC-luc-Control mice. Data are mean \pm SD. $**p < 0.01$.

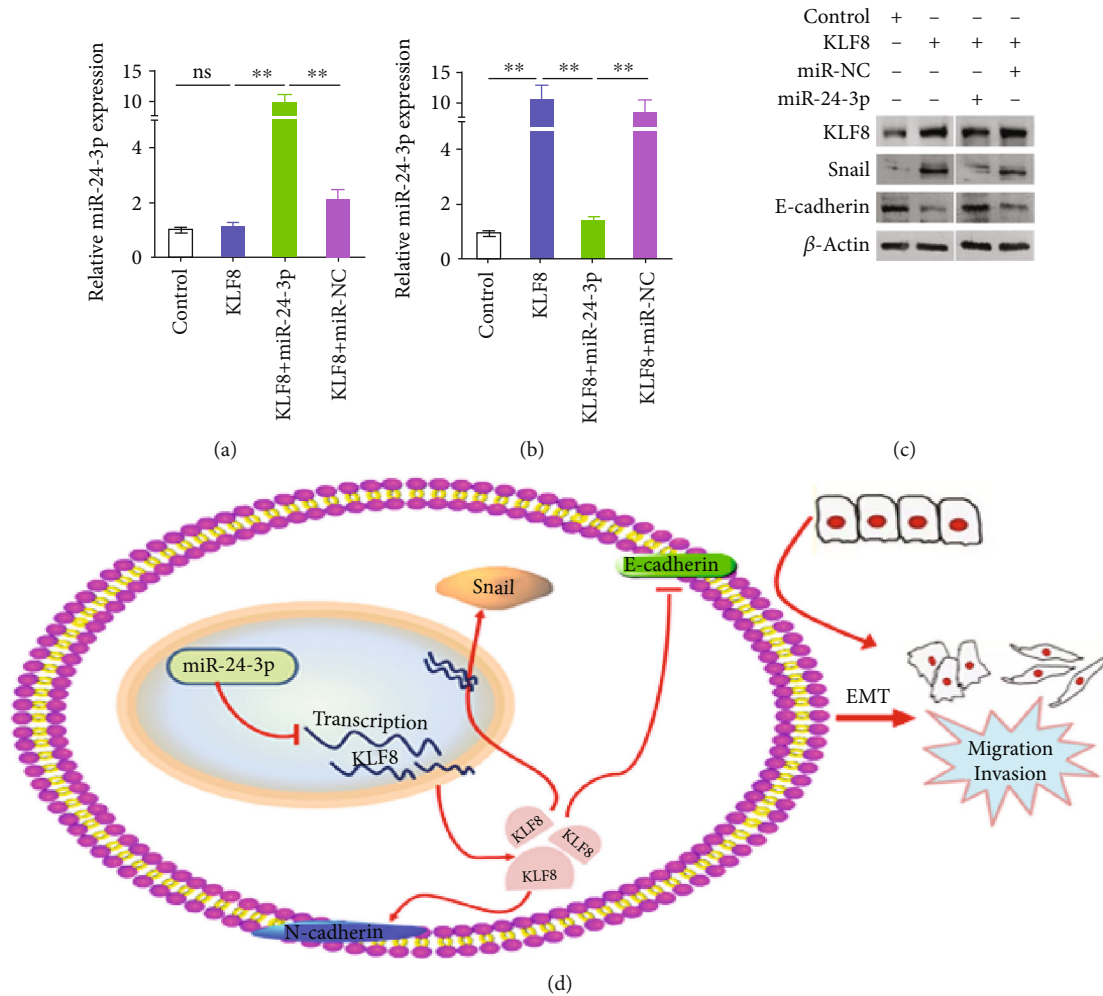


FIGURE 4: miR-24-3p regulated EMT through KLF8. (a, b) Expression of miR-24-3p (a) and KLF8 (b) mRNAs in the cell as indicated was detected by qPCR. Transfection of miR-24-3p mimics in A549 cells with KLF8 overexpression increased miR-24-3p expression and also decreased KLF8 mRNA expression. (c) Expression of KLF8, Snail, and E-cadherin in A549 cells with overexpression of KLF8, miR-24-3p, or their corresponding genes. (d) A schematic diagram for roles of miR-24-3p in lung adenocarcinoma and interactions with KLF8 and EMT programs. miR-24-3p suppressed KLF8 transcription directly, and the reduced KLF8 levels resulted in a decrease in Snail expression and an increase in E-cadherin expression, which in turn promoted EMT program and ultimately lead to enhanced metastasis of lung adenocarcinoma. Data are mean \pm SD. ** $p < 0.01$.

metastasis at least partly depending on targeting of KLF8 (Figure 3(b)). As expected, KLF8 overexpression further lead to an increase of Snail protein level, while the E-cadherin protein level was suppressed after KLF8 overexpression, suggesting that KLF8 could regulate EMT in LUAD (Figure 3(c)). *In vivo* metastasis model showed that KLF8 overexpression increased the metastasis of A549 cells as evidenced by bioluminescence images (Figures 3(d) and 3(e)). All the above data confessed that KLF8 promoted LUAD cell metastasis.

4.4. miR-24-3p Regulated EMT through KLF8. Further, we found that cotransfection of miR-24-3p mimics in A549 cells with KLF8 overexpression increased miR-24-3p expression and also decreased KLF8 mRNA expression as determined by qRT-PCR (Figures 4(a) and 4(b)). The protein expression of Snail and E-cadherin was also reversed when cotrans-

ected with miR-24-3p mimics in A549 cells with KLF8 (Figure 4(c)). These results indicate that miR-24-3p could regulate EMT through KLF8, thus promoting LUAD metastasis.

5. Discussion

In this study, we found that miR-24-3p was frequently silenced in LUAD patients and controls LUAD metastasis by directly targeting KLF8 and inducing EMT, which broaden the understanding of the miR-24-3p/KLF8/EMT axis in the pathogenesis of LUAD and provided therapeutic indications to advanced LUAD patients.

It is well known that miRNAs, especially metastatic-related miRNAs, such as miR-1236-3p, miR-24-3p, and miR-135a, which usually regulates EMT-related genes to control metastasis, is often dysregulated during the pathogenesis

of LUAD [21, 23]. The miR-24-3p expression level has been reported to be silenced in LUAD and contributed to LUAD metastasis by regulating multiple targets, including FGFR3, ING5, and SOX7 [11, 15, 16]. Therefore, miR-24-3p was selected to be the most researched miRNA in LUAD. In this study, we first studied the expression status of miR-24-3p in LUAD patients and presented that miR-24-3p showed a lower expression level in LUAD tissues than in adjacent nontumor tissues as previously described [11, 16, 24]. In addition, regression analysis revealed that miR-24-3p levels were closely associated with E-cadherin in LUAD, suggesting that miR-24-3p involved in LUAD progression may be associated with EMT. It is well known that microRNAs are known for its role in posttranscriptionally regulating target genes by binding to its 3'-UTR. Therefore, to confirm whether the miR-24-3p is an upstream regulator of KLF8, we overexpressed miR-24-3p in LUAD cell lines and explored the interaction of KLF8 and miR-24-3p in LUAD cells; using Western blot assay and luciferase reporter assay, we demonstrated that KLF8 was a direct target of miR-24-3p and that the downregulation of miR-24-3p could affect KLF8 protein expression in LUAD.

As a KLF family member, KLF8 is often aberrantly expressed in many types of cancer and its overexpression is significantly correlated with oncogenic transformation. Also, KLF8 is known for its ability of inducing EMT and drug resistance in tumor progression [25–28]. KLF8 has been proved to be regulated by miR-1236-3p and miR-135a in metastatic progression of lung cancer [20, 21]. Our study confirmed that KLF8 expression in LUAD was higher than that in nontumor tissues. Using the public prediction database, we found that KLF8 mRNA expression level was positively correlated to poor overall survival of LUAD. *In vitro* and *in vivo* functional studies also revealed that KLF8 promoted LUAD cell metastasis and invasion, manifesting that KLF8 is critical in the progression of LUAD. However, the role of miR-24-3p in regulating KLF8 expression is still unclear. Therefore, we wondered whether miR-24-3p is responsible for LUAD metastasis via interacting with KLF8. Here, we reported that miR-24-3p could directly target KLF8 by binding to its 3'-UTR, which contributed to further EMT in LUAD. Thus, the miR-24-3p/KLF8/EMT axis may be responsible for the aggressive behaviors of LUAD, paving the way for developing novel targeted drugs and designing new therapeutic strategy. As a kind of easy-to-metastasized cancer, tumor immune microenvironment played a significant role in LUAD by EMT activation [29]. EMT might contribute to immune escape through multiple routes. Our data suggested that the miR-24-3p/KLF8 axis is responsible for EMT activation, which provides new insights into immunotherapy focused on the miR-24-3p/KLF8 axis.

6. Conclusions

In conclusion, we found that miR-24-3p and KLF8 played an important role in EMT of LUAD. Importantly, we demonstrated that miR-24-3p could directly target KLF8. We believed that the currently identified miR-24-3p/KLF8/EMT axis could provide a novel insight into the molecular basis of

advanced LUAD and represent potential therapeutic targets for the treatment of metastatic LUAD.

Abbreviations

LUAD:	Lung adenocarcinoma
miRNAs:	MicroRNAs
BC:	Breast cancer
FGFR3:	Fibroblast growth factor receptor 3
SOX7:	Sex-determining region Y-box 7
SOX18:	Sex-determining region Y-box 18
KLF8:	Krüppel-like transcription factor 8
EMT:	Epithelial-to-mesenchymal transition
WT:	Wild type.

Data Availability

The data used to support the findings of this study are available from the corresponding author upon request.

Conflicts of Interest

All authors declare that they have no competing interests in this study.

Authors' Contributions

Pengyu Jing, Nianlin Xie, and Nan Zhao contributed equally to this work.

Acknowledgments

This work was supported by the National Natural Science Foundation of China under Grant Nos. 81372510, 81171922, and 81972166.

References

- [1] R. L. Siegel, K. D. Miller, and A. Jemal, "Cancer statistics, 2019," *CA: a Cancer Journal for Clinicians*, vol. 69, no. 1, pp. 7–34, 2019.
- [2] F. Bray, J. Ferlay, I. Soerjomataram, R. L. Siegel, L. A. Torre, and A. Jemal, "Global cancer statistics 2018: GLOBOCAN estimates of incidence and mortality worldwide for 36 cancers in 185 countries," *CA: a Cancer Journal for Clinicians*, vol. 68, no. 6, pp. 394–424, 2018.
- [3] J. Ferlay, M. Colombet, I. Soerjomataram et al., "Estimating the global cancer incidence and mortality in 2018: GLOBOCAN sources and methods," *International Journal of Cancer*, vol. 144, no. 8, pp. 1941–1953, 2019.
- [4] Network Cancer Genome Atlas Research, "Author Correction: Comprehensive molecular profiling of lung adenocarcinoma," *Nature*, vol. 559, no. 7715, article E12, 2018.
- [5] Network Cancer Genome Atlas Research, "Comprehensive molecular profiling of lung adenocarcinoma," *Nature*, vol. 511, no. 7511, pp. 543–550, 2014.
- [6] B. Pang, N. Wu, R. Guan et al., "Overexpression of RCC2 enhances cell motility and promotes tumor metastasis in lung adenocarcinoma by inducing epithelial-mesenchymal transition," *Clinical Cancer Research*, vol. 23, no. 18, pp. 5598–5610, 2017.

- [7] Q. Zhang, Y. Zhang, Y. Chen, J. Qian, X. Zhang, and K. Yu, "A novel mTORC1/2 inhibitor (MTI-31) inhibits tumor growth, epithelial-mesenchymal transition, metastases, and improves antitumor immunity in preclinical models of lung cancer," *Clinical Cancer Research*, vol. 25, no. 12, pp. 3630-3642, 2019.
- [8] Y. Lou, L. Diao, E. R. Cuentas et al., "Epithelial-mesenchymal transition is associated with a distinct tumor microenvironment including elevation of inflammatory signals and multiple immune checkpoints in lung adenocarcinoma," *Clinical Cancer Research*, vol. 22, no. 14, pp. 3630-3642, 2016.
- [9] L. Li, M. Peng, W. Xue et al., "Integrated analysis of dysregulated long non-coding RNAs/microRNAs/mRNAs in metastasis of lung adenocarcinoma," *Journal of Translational Medicine*, vol. 16, no. 1, p. 372, 2018.
- [10] X. Ge, G. Y. Li, L. Jiang et al., "Long noncoding RNA CAR10 promotes lung adenocarcinoma metastasis via miR-203/30/SNAI axis," *Oncogene*, vol. 38, no. 16, pp. 3061-3076, 2019.
- [11] P. Jing, N. Zhao, N. Xie et al., "miR-24-3p/FGFR3 Signaling as a Novel axis is involved in epithelial-mesenchymal transition and regulates lung adenocarcinoma progression," *Journal of Immunology Research*, vol. 2018, Article ID 2834109, 13 pages, 2018.
- [12] J. Gabler, J. Wittmann, M. Porstner et al., "Contribution of microRNA 24-3p and Erk 1/2 to interleukin-6-mediated plasma cell survival," *European Journal of Immunology*, vol. 43, no. 11, pp. 3028-3037, 2013.
- [13] Y. Duan, L. Hu, B. Liu et al., "Tumor suppressor miR-24 restrains gastric cancer progression by downregulating RegIV," *Molecular Cancer*, vol. 13, no. 1, p. 127, 2014.
- [14] F. L. Meng, W. Wang, and W. D. Jia, "Diagnostic and prognostic significance of serum miR-24-3p in HBV-related hepatocellular carcinoma," *Medical Oncology*, vol. 31, no. 9, p. 177, 2014.
- [15] S. Cui, X. Liao, C. Ye et al., "ING5 suppresses breast cancer progression and is regulated by miR-24," *Molecular Cancer*, vol. 16, no. 1, p. 89, 2017.
- [16] L. Yan, J. Ma, Y. Zhu et al., "miR-24-3p promotes cell migration and proliferation in lung cancer by targeting SOX7," *Journal of Cellular Biochemistry*, vol. 119, no. 5, pp. 3989-3998, 2018.
- [17] X. Li, C. Ma, L. Zhang et al., "LncRNAAC132217.4, a KLF8-regulated long non-coding RNA, facilitates oral squamous cell carcinoma metastasis by upregulating IGF2 expression," *Cancer Letters*, vol. 407, pp. 45-56, 2017.
- [18] X. Wang, H. Lu, A. M. Urvalek et al., "KLF8 promotes human breast cancer cell invasion and metastasis by transcriptional activation of MMP9," *Oncogene*, vol. 30, no. 16, pp. 1901-1911, 2011.
- [19] F. Lin, Z. Shen, L. N. Tang et al., "KLF8 knockdown suppresses proliferation and invasion in human osteosarcoma cells," *Molecular Medicine Reports*, vol. 9, no. 5, pp. 1613-1617, 2014.
- [20] Y. Zheng, B. Zheng, X. Meng, Y. Yan, J. He, and Y. Liu, "LncRNA DANCR promotes the proliferation, migration, and invasion of tongue squamous cell carcinoma cells through miR-135a-5p/KLF8 axis," *Cancer Cell International*, vol. 19, no. 1, p. 302, 2019.
- [21] T. Bian, D. Jiang, J. Liu et al., "miR-1236-3p suppresses the migration and invasion by targeting KLF8 in lung adenocarcinoma A549 cells," *Biochemical and Biophysical Research Communications*, vol. 492, no. 3, pp. 461-467, 2017.
- [22] P. Jing, N. Zhao, M. Ye et al., "Protein arginine methyltransferase 5 promotes lung cancer metastasis via the epigenetic regulation of miR-99 family/FGFR3 signaling," *Cancer Letters*, vol. 427, pp. 38-48, 2018.
- [23] H. Shi, Y. Ji, D. Zhang, Y. Liu, and P. Fang, "MiR-135a inhibits migration and invasion and regulates EMT-related marker genes by targeting KLF8 in lung cancer cells," *Biochemical and Biophysical Research Communications*, vol. 465, no. 1, pp. 125-130, 2015.
- [24] M. Olbromski, A. Rzechonek, J. Grzegorzolka et al., "Influence of miR-7a and miR-24-3p on the SOX18 transcript in lung adenocarcinoma," *Oncology Reports*, vol. 39, no. 1, pp. 201-208, 2018.
- [25] X. Yi, H. Zai, X. Long, X. Wang, W. Li, and Y. Li, "Krüppel-like factor 8 induces epithelial-to-mesenchymal transition and promotes invasion of pancreatic cancer cells through transcriptional activation of four and a half LIM-only protein 2," *Oncology Letters*, vol. 14, no. 4, pp. 4883-4889, 2017.
- [26] Y. N. Shen, H. G. He, Y. Shi et al., "Krüppel-like factor 8 promotes cancer stem cell-like traits in hepatocellular carcinoma through Wnt/ β -catenin signaling," *Molecular Carcinogenesis*, vol. 56, no. 2, pp. 751-760, 2017.
- [27] H. Zhang, L. Liu, Y. Wang et al., "KLF8 involves in TGF-beta-induced EMT and promotes invasion and migration in gastric cancer cells," *Journal of Cancer Research and Clinical Oncology*, vol. 139, no. 6, pp. 1033-1042, 2013.
- [28] G. Yu, F. Wu, and E. Wang, "KLF8 promotes temozolomide resistance in glioma cells via β -Catenin activation," *Cellular Physiology and Biochemistry*, vol. 38, no. 4, pp. 1596-1604, 2016.
- [29] S. Terry, P. Savagner, S. Ortiz-Cuaran et al., "New insights into the role of EMT in tumor immune escape," *Molecular Oncology*, vol. 11, no. 7, pp. 824-846, 2017.

Research Article

Assessing the Changes of Mumps Characteristics with Different Vaccination Strategies Using Surveillance Data: Importance to Introduce the 2-Dose Schedule in Quzhou of China

Chunting Zhou,¹ Wei Song ¹, Zhiying Yin ², Sheng Li ¹, Xiaoying Gong,² Quanjun Fang,² and Shuangqing Wang²

¹Women & Children Health Care Hospital of Quzhou, Quzhou, 324000 Zhejiang, China

²Department of Immunization, Quzhou Center for Disease Control and Prevention, Quzhou, 324000 Zhejiang, China

Correspondence should be addressed to Zhiying Yin; zyz1815@sohu.com and Sheng Li; zjqzyr@126.com

Received 19 December 2019; Revised 20 February 2020; Accepted 3 March 2020; Published 27 March 2020

Guest Editor: Zenghui Teng

Copyright © 2020 Chunting Zhou et al. This is an open access article distributed under the Creative Commons Attribution License, which permits unrestricted use, distribution, and reproduction in any medium, provided the original work is properly cited.

Background. From 2005 to 2016, the prevention and control of mumps in China have undergone three stages of transition. These include the use of MuCV as a self-supported vaccine, the introduction of one-dose MMR to the Expanded Program on Immunization (EPI), and the administration of two-dose MuCV following supplementary immunization activities (SIAs) using MM. Here, using surveillance data, we assessed the epidemiology of mumps during the three stages. **Methods.** Children in Quzhou of China born from 2005 to 2016 and registered in the Zhejiang Provincial Immunization Information System (ZJIS) were included. We analyzed the epidemic data and calculated incidence and MuCV coverage via birth cohorts. **Results.** The average incidence of mumps in 2005-2006, 2007-2010, and 2011-2016 was 51.57, 41.02, and 12.53 per 100,000 individuals, respectively. The highest incidence was in children aged 6-14 years from 2005-2016, of which the majority were school students (67.84%). Approximately 90% of the reported outbreaks occurred in school children (primary school/middle school). The seasonal characteristics of mumps were less obvious from 2011 to 2016. The coverage of one-dose MMR in the 2005 birth cohort was 71.38%. For the 2006-2010 birth cohort, the coverage of one-dose MuCV was 96.82% and the coverage of two-dose MuCV was 17.68%. The children born from 2011 to 2016 were only free vaccinated with MMR; the coverage of one-dose MuCV was 99.10%. The mumps incidence in the three birth cohorts significantly declined ($X^2 = 805.90$, $P < 0.001$ for trend). Except the children less than two years old, the mumps incidence for the children born from 2006 to 2010 was higher than that for the children born from 2011 to 2016. **Conclusion.** The mumps incidence significantly declined following the introduction of one-dose MMR. The SIA using MM led to a rapid reduction of mumps cases. Therefore, we recommend a two-dose MuCV routine immunization schedule and improved vaccination coverage.

1. Introduction

Mumps is a contagious disease caused by the mumps virus. It typically starts with fever, headache, muscle ache, tiredness, and loss of appetite. The majority of sufferers also develop swelling of the salivary glands [1]. In China, mumps was a national statutory C infectious disease in 1990, and all mumps cases have been mandatorily reported via the National Notifiable Disease Reporting System (NNDRS) since 2004, a web-based computerized reporting system. Reported incidence rates are approximately 22 per 100,000

within the total population but have reached as high as 89.91 per 100,000 in 2009 in one province. The number of reported mumps outbreaks was 436, 327, and 194 for 2008, 2009, and 2010, respectively [2]. Due to the outbreaks and high incidence rates, mumps prevention in China needs to be strengthened and improved.

Mumps vaccine (MuV) is the most effective strategy for mumps protection. In 1990, the China Food and Drug Administration licensed a live, attenuated mumps vaccine that was produced using the S79 vaccine strain, derived through attenuation of the Jeryl Lynn strain used in the

U.S.-licensed vaccine [3]. Mumps vaccination was initiated in Quzhou since 1998 using two mumps-containing vaccines (MuCV) including the monovalent mumps vaccine (S79 strain) and the measles-mumps-rubella (MMR) vaccine developed by Merk (Jery1-Lynn vaccine strain). Monovalent mumps vaccines were replaced with the measles-mumps (MM) vaccine (S79 strain) since 2000. However, MuVs were not included in the Expanded Program on Immunization (EPI), meaning parents were forced to pay sums for the MuV. In 2007, domestic MMR (S79 strain) was introduced into the EPI for children born after the 1st January 2006 and replaced the second routine dose of measles vaccine, targeting children aged 18–24 months. Since the first dose of measles-containing vaccine is administered as the measles-rubella (MR) vaccine, the EPI system supports only one-dose mumps vaccination strategy [4]. Though MMR was introduced into the EPI for routine use with high vaccination coverage, over 1,839 mumps cases were reported in 2009 in Quzhou. The majority of outbreaks occurred amongst school-age children [5]. Outbreaks have been reported amongst highly vaccinated populations in numerous countries [6–8]. In September 2010, supplementary immunization activities (SIAs) using MM were performed, targeting children aged 8 months to 4 years of age. The Zhejiang Provincial Immunization Information System (ZJIIS), also known as the immunization registries, is a computerized population-based system containing demographic and vaccination data for all children aged less than 15 years living in the Zhejiang Province since 2004 [9]. We analyzed mumps epidemiology and MuCV coverage of Quzhou using the NNDRS and ZJIIS from 2005 to 2016 in this study.

2. Material and Methods

2.1. Setting. Quzhou is a medium city of Zhejiang Province in the East of China and includes 2 districts and 4 counties. Based on the annual census data from the Quzhou municipal Bureau of Statistics, its population increased from 2,456,000 in 2005 to 2,649,000 in 2016 (7.86% increase), with an annual birth cohort of approximately 24,000. Quzhou is served by 108 vaccination clinics, which are responsible for vaccinating all children residing in the catchment areas, regardless of whether they were locally born or migrated to Quzhou. Since 2005, all children, including migrant (nonlocally born), were registered in ZJIIS during their first contact with the immunization clinic during which they were administered a unique identification number. The system contains children's demographic information, historical immunization data, and current immunization.

2.2. Case and Outbreak Definitions. For surveillance purposes, mumps is defined as a clinically diagnosed illness. According to the diagnostic criteria for mumps approved by the Ministry of Health of China in 2007 [10], we defined a mumps case as a person with acute onset of unilateral or bilateral swelling of the parotid gland or other salivary glands characterized by any of the following, which could not be explained by another more likely diagnosis: (1) fever, headache, weakness, and loss of appetite; (2) orchitis; (3) pancre-

atitis; (4) encephalitis and/or aseptic meningitis. In Quzhou, a mumps outbreak is defined as the occurrence of ≥ 10 mumps cases in a community, school, company, or other settings within a seven-day period.

2.3. Mumps and Vaccination. Data for patients diagnosed with mumps in Quzhou from 2005 to 2016 were extracted from the NNDRS on 30 March 2017. Data on MuCV vaccination coverage were obtained from the ZJIIS. We defined the birth cohorts from 2005 to 2016 by the number of children enrolled in ZJIIS. We calculated MuCV vaccination coverage using the cumulative number of children who had received the MuCV until the end of each year, divided by the total number of children in the corresponding birth cohort.

2.4. Statistical Analyses. We described the epidemic characteristics of mumps occurring from 2005–2016, and MuCV coverage and incidence of mumps by birth cohorts from 2005 to 2016, using the life table method. Data were collected using Microsoft Office Excel (version 2007) and analyzed using SPSS for Windows, version 17.0 (SPSS Inc., USA). Differences amongst incidence periods were calculated using the trend Chi-square test. Differences according to median age were calculated using the Kruskal-Wallis H test. All comparisons were 2-tailed, and a P value < 0.05 was considered significant.

2.5. Ethical Considerations. This study was determined to be exempt from ethical review by the Quzhou CDC institutional review board. Data were anonymous and exported from ZJIIS. Confidentiality without individual identifiers was maintained throughout.

3. Results

3.1. Mumps Cases and Incidence. The average annual reported incidence of mumps was 28.67 per 100,000 of the population from 2005 to 2016, the overall incidence of which decreased by 86.24% from the maximum 73.91 per 100,000 of the population in 2009 to the minimum 10.17 per 100,000 of the population in 2015. The average incidence of mumps in 2005–2006, 2007–2010, and 2011–2016 was 51.57, 41.02, and 12.53 per 100,000 people, respectively, which declined across the three periods ($X^2 = 552.551$, $P < 0.001$ for trend).

3.2. Demographic Characteristics of Mumps Cases. In the three assessment periods, mumps incidence was highest amongst children aged 6–14 years and lowest amongst adults aged ≥ 20 years. The incidence amongst children aged less than 2 years did not significantly change ($X^2 = 0.062$, $P = 0.969$). The incidence amongst children aged 6–14 years declined across the three periods (Table 1).

The median age of mumps cases was almost nine from 2005 to 2009, eight from 2010 to 2014, seven in 2015, and ten in 2016, which significantly differed ($X^2 = 138.001$, $P < 0.001$). The interquartile range (IQR) changed from five to seven and ranged from 5 years to 12 years (Figure 1).

TABLE 1: The incidence of mumps amongst age groups in the three assessment periods.

Age group	2005-2006		2007-2010		2011-2016		X^2	P
	No.	Incidence (1/100,000)	No.	Incidence (1/100,000)	No.	Incidence (1/100,000)		
<2 y	12	12.63	24	12.30	38	11.74	0.062	0.969
2-5 y	289	131.92	700	179.72	506	84.97	171.775	<0.001
6-14 y	1947	352.82	2932	281.21	1141	76.50	2035.562	<0.001
15-19 y	144	39.78	220	30.96	90	10.83	112.646	<0.001
≥20 y	141	3.83	197	2.60	144	1.19	110.152	<0.001

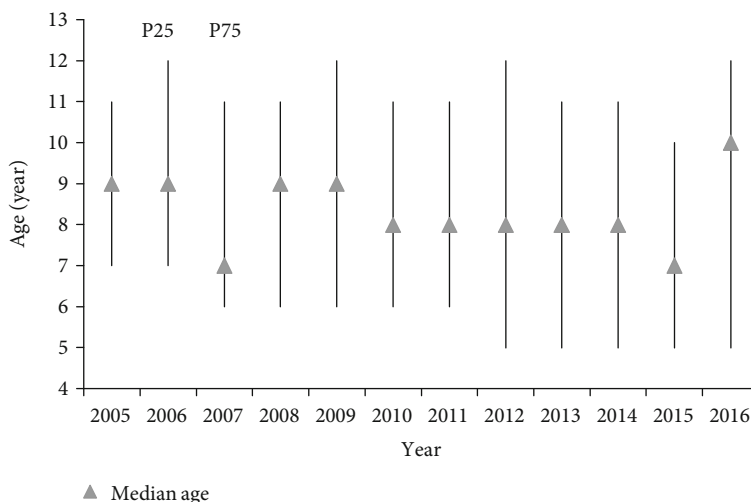


FIGURE 1: Median age and interquartile range (IQR) of mumps cases from 2005 to 2016.

Of the 8,525 cases, 5,214 (61.16%) were male. The majority of cases (67.84%) were school students, and 1,646 (19.31%) of cases were childcare children in kindergartens. The proportion of students steadily decreased from 79.94% in 2005 to 64.18% in 2016, and the proportion in childcare gradually increased from 13.34% in 2005 to 22.09% in 2016.

3.3. Seasonal Characteristics of Mumps Cases. Mumps cases were reported throughout all 12 months of the year. No obvious seasonal patterns were observed despite its reported seasonal occurrence. Most mumps cases occurred between March and July, with small peaks also occurring in December and January in 2005-2006 and in 2007-2010. With the decreased number of mumps cases in 2011-2016, the two epidemic peaks were less obvious than those observed from the other study periods (Figure 2).

3.4. Outbreaks. From 2005 to 2016, a total of 21 outbreaks with 919 cases were reported. Approximately 90% of the reported outbreaks occurred in school children (primary school/middle school), which accounted for the majority (approximately 95%) of outbreak-related cases. Since 2008, no outbreaks in kindergartens had been reported. Since 2010, no outbreak in primary schools had been reported. From 2011 to 2016, no mumps outbreaks were reported (Table 2).

3.5. Incidence of Mumps Cases by Birth Cohort. The children born in 2005 vaccinated MuCV must pay sums, the coverage

of one-dose MuCV was 71.38%, and the incidence of mumps was 138.56 per 100,000 person-years. The children born from 2006 to 2010 were free vaccinated with MMR and boost immunity using MM, and the coverage of one-dose MuCV and two-dose MuCV was 96.82% and 17.68%, respectively. The children born from 2011 to 2016 were only free vaccinated with MMR, and the coverage of one-dose MuCV was 99.10%. The incidence of mumps in the three birth cohorts significantly declined ($X^2 = 805.90$, $P < 0.001$ for trend) (Table 3).

The incidence of mumps in children born in 2005 had two peaks: the one was 4-5 years old and the other was 11-12 years old. Except the children less than two years old, the incidence of mumps for children born from 2006 to 2010 was higher than that for children born from 2011 to 2016 by age (Figure 3).

4. Discussion

Mumps is a vaccine-preventable disease. Since the prevaccination era, a 99% decrease in mumps cases has been observed in the United States [1]. In 2015, amongst the 194 World Health Organization (WHO) countries, 121 (62%) had incorporated MuV into their national immunization program, the majority of which used the MMR vaccine [11]. From 2005 to 2016, the prevention and control of mumps has gone through three periods in Quzhou. The first occurred in 2005-2006 in which MuCV was used as a self-supported vaccine. The second was from 2007 to 2010 in which one-

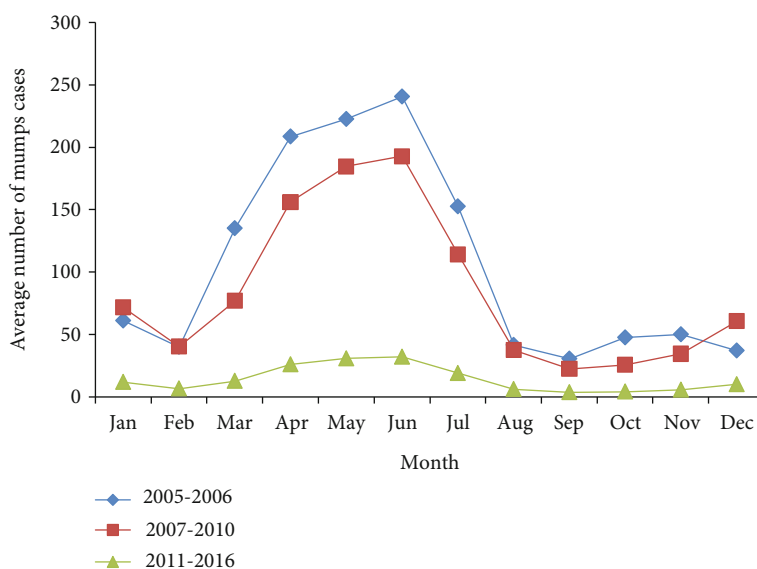


FIGURE 2: Average number of mumps cases in Quzhou per month during the three assessment periods.

TABLE 2: No. of mumps outbreaks and outbreak-related cases from 2005 to 2016.

Period	Kindergarten		Primary school		Middle school		Total	
	No. of outbreaks	No. of cases	No. of outbreaks	No. of cases	No. of outbreaks	No. of cases	No. of outbreaks	No. of cases
2005-2006	1	12	7	346	0	0	8	358
2007-2010	1	35	10	483	2	43	13	561
2011-2016	0	0	0	0	0	0	0	0
Total	2	47	17	829	2	43	21	919

TABLE 3: Incidence of mumps and coverage of MuCV in different birth cohorts.

Birth cohort	No. of children	Coverage of one-dose MuCV (%)	Coverage of two-dose MuCV (%)	No. of cases	Cumulative exposure (person-year)	Incidence (/100,000 person-years)
2005	23824	71.38	0	377	272079.5	138.56
2006-2010	123157	96.82	17.68	804	1035725.5	77.63
2011-2016	149827	99.10	0	201	446128	45.05

dose MMR was introduced into the EPI for children aged 18–24 months. The third was from 2011 to 2016 in which some children were administered two-dose MuCV, including one-dose MM of SIAs and one-dose MMR of EPI. Our studies have shown that 8,525 mumps cases with an average annual incidence of 28.67 per 100,000 of the population were reported in Quzhou in 2005–2016. This was higher than that of Beijing and Jiangsu province [12, 13]. The average mumps incidence from 2007-2010 modestly decreased compared to 2005-2006, due to the short timeframe of MMR vaccine introduction and the susceptible population with a low mumps vaccination coverage. However, these values drastically declined from 2011 to 2016 ($X^2 = 552.551$, $P < 0.001$). A single dose of the MMR vaccine used in the UK, which contains the Jeryl Lynn mumps strain, has been reported to confer between 61 and 91% protection [14].

Mumps is a common childhood infection in unimmunized individuals, but in highly vaccinated populations, the disease affects mainly adolescents and young adults [15–18].

From 2005 to 2016, the age distributions for mumps cases also deviated. In children aged less than 2 years and adults aged ≥ 20 years, no obvious changes were evident since these did not represent the susceptible or target population of EPI. However, the number of mumps cases amongst adults increased in some provinces [19]. From 2005-2010, only some of the children aged 2–5 years were the target population of EPI, and thus, the incidence was volatile. The inclusion of all children as the target EPI population since 2011 has led to the incidence significantly declining. The susceptible population of mumps infection was mainly comprised of children aged 6–14 years, who had not received the mumps vaccination from 2005-2010. In 2016, the incidence amongst those aged 15–19 years significantly increased, suggesting that mumps is not simply a childhood disease. The most afflicted age groups were teenagers, adolescents, and young adults, similar to those previously reported [20]. A Korean study also identified the need to strengthen surveillance in adolescents, in addition to younger aged children [21].

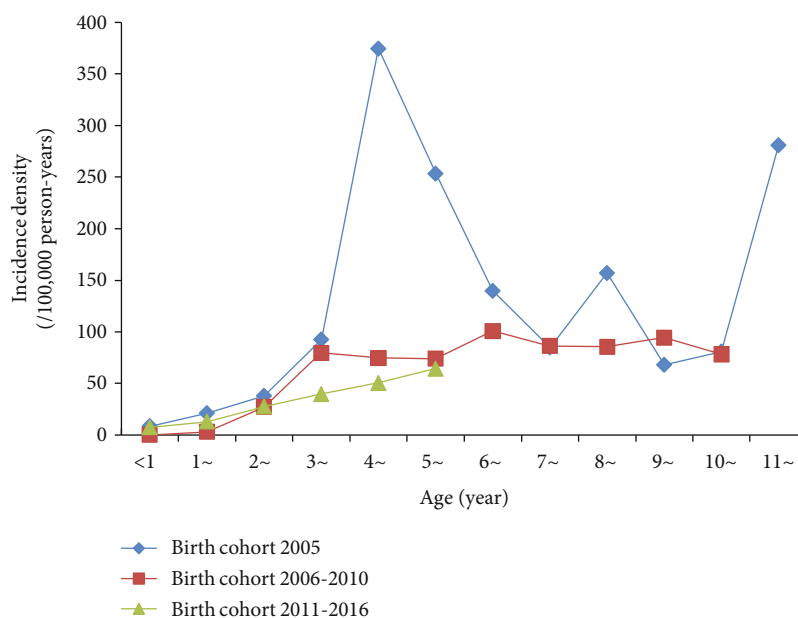


FIGURE 3: Incidence of mumps amongst different birth cohorts by age.

According to the median age of mumps from 2005-2016, the highest incidence rates occurred in children aged 6–14 years. The other birth cohorts excluding 2006 and 2008 had low mumps vaccination coverage as the MuCV was only introduced into the EPI for children born after 1 January 2006, and the time after vaccination with MuCV was assessed in the future. The issue of the growing risk of developing mumps at increasing postvaccination has been addressed [22, 23]. Studies suggested that humoral immunity induced by live vaccines at childhood, including measles and mumps antibodies, does not provide lifelong immunity but can rapidly decline to extremely low levels by adolescence and young adulthood. This situation is particularly apparent in populations lacking boosters derived from natural infections [24]. During the epidemic season, the two epidemic peaks were less obvious in 2011–2016 than in the other two periods.

Of all the mumps cases assessed, 61.16% were male, and 67.84% were students in schools. These values may be attributable to sex-based immune responses and hormonal influences in addition to genetic and epigenetic factors [25, 26]. The accumulation of susceptible young persons who are brought together in high-density settings can lead to high levels of infection and an increased risk of exposure [27, 28]. Mumps outbreaks were recently reported in the US and in Europe, both with high MMR vaccine coverage [27, 29]. From 2005 to 2016, 21 mumps outbreaks were reported, and primary school students accounted for 90.21% of the outbreak-related cases. No mumps outbreaks were reported from 2011 to 2016. Both factors are consistent with the observation that the mumps outbreak primarily affected students [15, 30–32]. Compared to the 2005-2006 and 2007-2010 periods, the mumps epidemiological characteristics remained unchanged from 2011-2016. There were three possibilities for the changes. Firstly, the susceptible populations decreased due to the mumps infection. Secondly, children with MuCV vaccination had accumulated. Thirdly, the SIAs

using MM could reduce the number of individuals who failed immunization with MuCV and increased the doses of MuCV immunizations. Studies also revealed the importance of waning immunity and the assessment of the time since vaccination [33]. Thus, continuing epidemic surveillance for mumps is necessary to understand whether the inclusion of MuCV will break the natural epidemic cycle of mumps in Quzhou and help maintain low incidence levels.

We also observed that the incidence of mumps cases assessed by birth cohort was connected to the coverage of MuCV and the doses of MuCV administered. The coverage of one-dose MuCV in the 2005 birth cohort was 71.38%. The coverage of one-dose MuCV and two-dose MuCV in 2006-2010 birth cohorts was 96.82% and 17.68%, respectively. The coverage of one-dose MuCV in 2011-2016 birth cohorts was 99.10%. The incidence of mumps in the three birth cohorts significantly declined ($X^2 = 805.90$, $P < 0.001$ for trend). The WHO reported that the MuCV coverage should reach 90% to prevent a mumps outbreak [34]. Studies performed in a French cohort concluded that the effectiveness of the MuV decreases with time and therefore proposed the introduction of a targeted third dose in an outbreak setting, for individuals whose last dose was longer than 10 years earlier [35]. It has been shown that valid and invalid vaccination rates influence the spread of mumps, but vaccine coverage and the transition to two doses of MMR vaccine were made freely available in China [36]. Our analysis concludes that the preventive effects of one-dose MuCV above a 90% coverage were limited and that a routine immunization schedule of two-dose MuCV for children is urgently required.

There were several limitations to this study: (1) all mumps cases were clinically diagnosed without laboratory confirmation. Mumps virus infection can result in symptomatic or asymptomatic infections [37], and the estimated 20–30% of asymptomatic cases were not possible to identify [3]. Mumps incidence in this study may therefore be

underestimated or overestimated. (2) The immunization status of each mumps case was unknown, and we were unable to calculate the effectiveness of various vaccine doses as the NNDRS and ZJIS data were disconnected. (3) MuCV vaccination coverage may have been underestimated since children with prior mumps infections were not excluded from the study cohort.

In conclusion, the coverage of one-dose MMR has reached approximately 90% since its introduction into the EPI in Quzhou, and the incidence of mumps in target children has significantly declined. Due to the short time of EPI initiation, mumps-susceptible individuals with no MuCV immunization history increased the mumps incidence, and the SIAs using MuCV can improve mumps antibody levels in the target population over a short timeframe, which led to a rapid reduction in mumps cases. A further decrease in mumps incidence could be achieved through the introduction of two doses of MuCV and by improving 2-dose MuCV vaccination coverage. However, determining the optimal age and adjustment of the schedule will require a further consideration of laboratory and serological survey results [20].

Data Availability

The data used to support the findings of this study are available from the corresponding author by email (zyz1815@sohu.com).

Conflicts of Interest

The authors declare no conflict of interest.

Authors' Contributions

Zhiying Yin and Chunting Zhou conceived and designed the study. Sheng Li, Xiaoying Gong, and Quanjun Fang obtained and organized the data. Wei Song and Shuangqing Wang analyzed the data. Wei Song contributed reagents/materials/analysis tools. Zhiying Yin and Chunting Zhou wrote the manuscript. Chunting Zhou and Wei Song contributed equally to this work.

Acknowledgments

This work was supported by the Science and Technology Bureau of Quzhou, Zhejiang, China (Project No. 20172090), and by the Immune Programming of Zhejiang Preventive Medicine Association, China (Project No. 2017YF03).

References

- [1] Centers for Disease Control Prevention, "Mumps vaccination," in *Encyclopedia of Public Health*, W. Kirch, Ed., Springer, Dordrecht, 2008, February 2018, <https://www.cdc.gov/mumps/vaccination.html>.
- [2] H. Wang, Y. Hu, G. Zhang, J. Zheng, L. Li, and Z. An, "Meta-analysis of vaccine effectiveness of mumps-containing vaccine under different immunization strategies in China," *Vaccine*, vol. 32, no. 37, pp. 4806–4812, 2014.
- [3] C. Ma, Y. Liu, J. Tang et al., "Assessment of mumps-containing vaccine effectiveness during an outbreak: importance to introduce the 2-dose schedule for China," *Human Vaccines & Immunotherapeutics*, vol. 14, no. 6, pp. 1392–1397, 2018.
- [4] H. Q. He, B. Zhang, R. Yan et al., "Economic evaluation on different two-dose-vaccination-strategies related to measles, mumps and rubella combined attenuated live vaccine," *Zhonghua Liu Xing Bing Xue Za Zhi*, vol. 37, no. 8, pp. 1121–1126, 2016.
- [5] Z. Y. Yin, X. Y. Gong, S. Q. Wang et al., "Epidemiological characteristics of mumps before and after introduction of mumps vaccine in Quzhou city, Zhejiang province," *Chinese Journal of Vaccines and Immunization*, vol. 23, no. 6, pp. 672–677, 2017.
- [6] A. E. Barskey, C. Schulte, J. B. Rosen et al., "Mumps outbreak in Orthodox Jewish communities in the United States," *The New England Journal of Medicine*, vol. 367, no. 18, pp. 1704–1713, 2012.
- [7] L. Kenny, E. O'Kelly, J. Connell, C. De Gascun, and J. Hassan, "Mumps outbreaks in a highly vaccinated population: investigation of a neutralization titre against the current circulating wildtype genotype G5 mumps virus," *Journal of Clinical Virology*, vol. 74, pp. 8–12, 2016.
- [8] J. P. Albertson, W. J. Clegg, H. D. Reid et al., "Mumps outbreak at a university and recommendation for a third dose of measles-mumps-rubella vaccine — Illinois, 2015–2016," *Morbidity and Mortality Weekly Report*, vol. 65, no. 29, pp. 731–734, 2016.
- [9] Y. Hu, Y. Chen, B. Zhang, and Q. Li, "An evaluation of voluntary varicella vaccination coverage in Zhejiang Province, East China," *International Journal of Environmental Research and Public Health*, vol. 13, no. 6, p. 560, 2016.
- [10] *Diagnostic criteria for mumps (WS270-2007)*, National Health and Family Planning Commission of the People's Republic of China, <http://www.nhfpc.gov.cn/zhuz/s9491/200704/38797/files/4b993dfd62834ccda16b8240ab078a00.pdf>.
- [11] A. Cui, Z. Zhu, Y. Hu et al., "Mumps epidemiology and mumps virus genotypes circulating in mainland China during 2013–2015," *PLoS One*, vol. 12, no. 1, article e0169561, 2017.
- [12] R. Ma, L. Lu, T. Zhou, J. Pan, M. Chen, and X. Pang, "Mumps disease in Beijing in the era of two-dose vaccination policy, 2005–2016," *Vaccine*, vol. 36, no. 19, pp. 2589–2595, 2018.
- [13] Y. Liu, Y. Hu, X. Deng et al., "Seroepidemiology of mumps in the general population of Jiangsu province, China after introduction of a one-dose measles-mumps-rubella vaccine," *Scientific Reports*, vol. 5, no. 1, article 14660, 2015.
- [14] UK Departments of Health, "Immunisation against infectious disease," <https://www.gov.uk/government/collections/immunisation-against-infectious-disease-the-green-book>.
- [15] S. Jussi, S. Gouma, M. Koopmans et al., "Epidemic of mumps among vaccinated persons, The Netherlands, 2009–2012," *Emerging Infectious Diseases*, vol. 20, no. 4, pp. 643–648, 2014.
- [16] C. Stein-Zamir, H. Shoob, N. Abramson, E. Tallen-Gozani, I. Sokolov, and G. Zentner, "Mumps outbreak in Jerusalem affecting mainly male adolescents," *Eurosurveillance*, vol. 14, p. 3, 2009.
- [17] W. Otto, A. Mankertz, S. Santibanez et al., "Ongoing outbreak of mumps affecting adolescents and young adults in Bavaria, Germany, August to October 2010," *Eurosurveillance*, vol. 15, p. 4, 2010.

- [18] M. O. Vareil, G. Rouibi, S. Kassab et al., "Épidémie de formes compliquées d'oreillons chez de jeunes adultes vaccinés dans le Sud-Ouest de la France et revue de la littérature," *Médecine et Maladies Infectieuses*, vol. 44, no. 11-12, pp. 502–508, 2014.
- [19] Q. R. Su, J. Liu, C. Ma et al., "Epidemic profile of mumps in China during 2004 - 2013," *Zhonghua Yu Fang Yi Xue Za Zhi*, vol. 50, p. 4, 2016.
- [20] H. Orliková, M. Malý, P. Lexová et al., "Protective effect of vaccination against mumps complications, Czech Republic, 2007–2012," *BMC Public Health*, vol. 16, no. 1, article 293, 2016.
- [21] Y. J. Choe, Y. H. Lee, and S. I. Cho, "Increasing mumps incidence rates among children and adolescents in the Republic of Korea: age-period-cohort analysis," *International Journal of Infectious Diseases*, vol. 57, pp. 92–97, 2017.
- [22] M. M. Cortese, H. T. Jordan, A. T. Curns et al., "Mumps vaccine performance among university students during a mumps outbreak," *Clinical Infectious Diseases*, vol. 46, no. 8, pp. 1172–1180, 2008.
- [23] J. Castilla, M. Garcia Cenoz, M. Arriazu et al., "Effectiveness of Jeryl Lynn-containing vaccine in Spanish children," *Vaccine*, vol. 27, no. 15, pp. 2089–2093, 2009.
- [24] Y. H. Ho, C. C. Tsai, Y. W. Tsai et al., "Humoral immunity to mumps in a highly vaccinated population in Taiwan," *Journal of Microbiology, Immunology and Infection*, vol. 52, no. 3, pp. 379–385, 2017.
- [25] S. L. Klein, I. Marriott, and E. N. Fish, "Sex-based differences in immune function and responses to vaccination," *Transactions of the Royal Society of Tropical Medicine and Hygiene*, vol. 109, no. 1, pp. 9–15, 2015.
- [26] I. F. Cook, "Sexual dimorphism of humoral immunity with human vaccines," *Vaccine*, vol. 26, no. 29-30, pp. 3551–3555, 2008.
- [27] A. E. Barskey, J. W. Glasser, and C. W. LeBaron, "Mumps resurgences in the United States: a historical perspective on unexpected elements," *Vaccine*, vol. 27, no. 44, pp. 6186–6195, 2009.
- [28] S. Rubin, R. Kennedy, and G. Poland, "Emerging mumps infection," *The Pediatric Infectious Disease Journal*, vol. 35, no. 7, pp. 799–801, 2016.
- [29] M. Sabbe and C. Vandermeulen, "The resurgence of mumps and pertussis," *Human Vaccines & Immunotherapeutics*, vol. 12, no. 4, pp. 955–959, 2016.
- [30] S. Hahné, J. Whelan, R. van Binnendijk et al., "Mumps vaccine effectiveness against orchitis," *Emerging Infectious Diseases*, vol. 18, no. 1, pp. 191–193, 2012.
- [31] S. Gouma, T. M. Schurink-van't Klooster, H. E. de Melker et al., "Mumps serum antibody levels before and after an outbreak to assess infection and immunity in vaccinated students," *Open Forum Infectious Diseases*, vol. 1, no. 3, article ofu101, 2014.
- [32] E. Santacruz-Sanmartin, D. Hincapié-Palacio, M. C. Ospina et al., "Seroprevalence of mumps in an epidemic period in Medellín, Colombia," *Vaccine*, vol. 33, no. 42, pp. 5606–5612, 2015.
- [33] C. V. Cardemil, R. M. Dahl, L. James et al., "Effectiveness of a third dose of MMR vaccine for mumps outbreak control," *The New England Journal of Medicine*, vol. 377, no. 10, pp. 947–956, 2017.
- [34] Organization WH, "Mumps virus vaccines: WHO position paper," *Weekly Epidemiological Record*, vol. 82, p. 51, 2007.
- [35] S. Vygen, A. Fischer, L. Meurice et al., "Waning immunity against mumps in vaccinated young adults, France 2013," *Eurosurveillance*, vol. 21, no. 10, p. 8, 2016.
- [36] Q. Qu, C. Fang, L. Zhang, W. Jia, J. Weng, and Y. Li, "A mumps model with seasonality in China," *Infectious Disease Modelling*, vol. 2, no. 1, pp. 1–11, 2017.
- [37] S. Hahne, T. Schurink, J. Wallinga et al., "Mumps transmission in social networks: a cohort study," *BMC Infectious Diseases*, vol. 17, no. 1, p. 56, 2017.